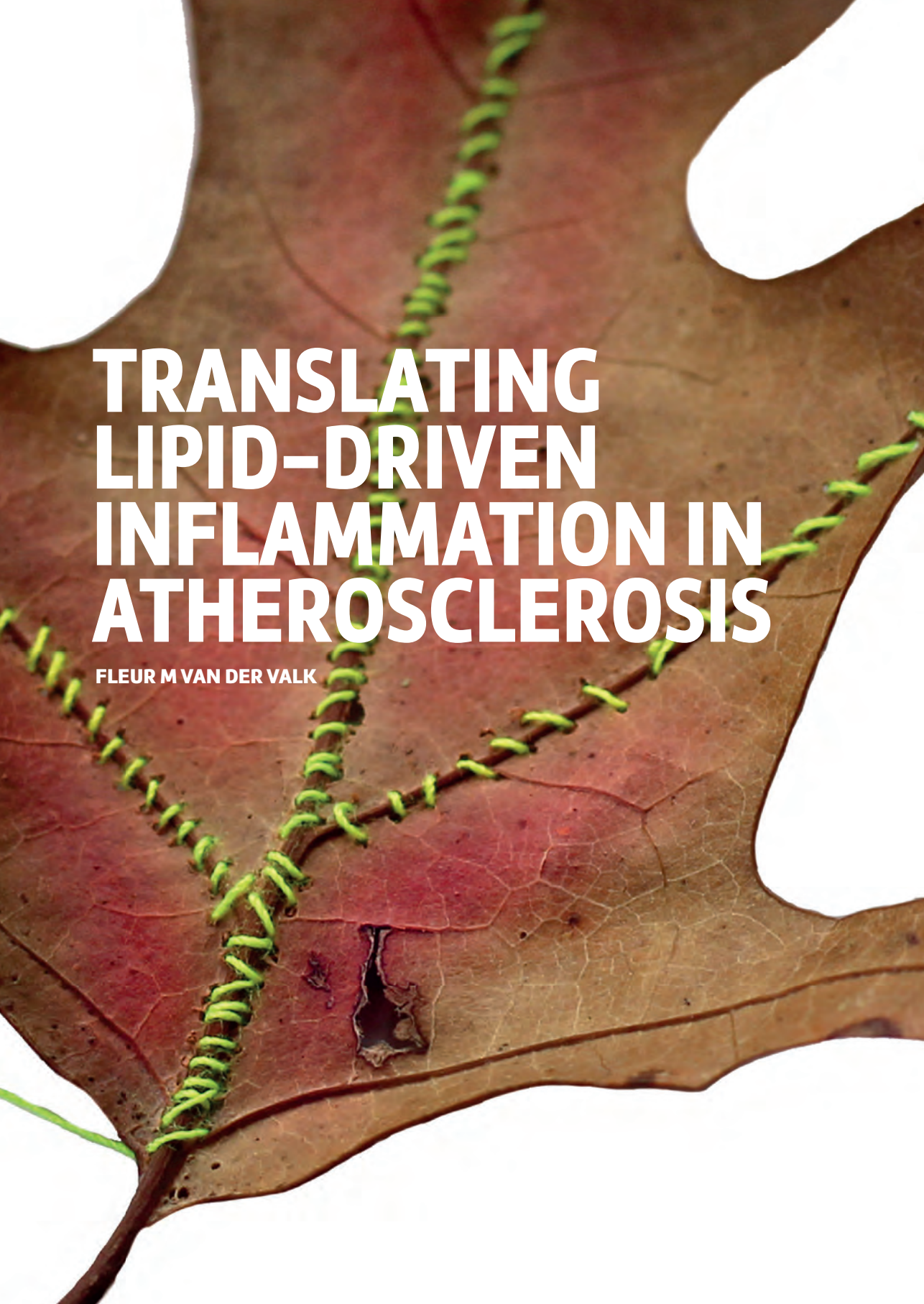

TRANSLATING LIPID-DRIVEN INFLAMMATION IN ATHEROSCLEROSIS

FLEUR M VAN DER VALK

TRANSLATING LIPID-DRIVEN INFLAMMATION IN ATHEROSCLEROSIS

Fleur van der Valk

Colofon

Author: Fleur van der Valk

Cover: Carolien Koopman

Layout: Iliana Boshoven-Gkini (AgileColor.com)

Printing: Ridderprint BV (Ridderprint.nl)

ISBN: 978-94-6299-418-8

The research described in this thesis was supported by a grant of the Dutch Heart Foundation (DHF-2010B284). Financial support by the Dutch Heart Foundation, Stichting Steun Promovendi Vasculaire Geneeskunde, Stichting Wetenschappelijk Onderzoek Interne Geneeskunde OLVG, Medcon, Sanofi, Chip Soft, AMSTOL Stichting, Amgen, Bayer, Astellas and Novo Nordisk for the publication of this thesis is gratefully acknowledged.

TRANSLATING LIPID-DRIVEN INFLAMMATION IN ATHEROSCLEROSIS

ACADEMISCH PROEFSCHRIFT

ter verkrijging van de graad van doctor
aan de Universiteit van Amsterdam
op gezag van de Rector Magnificus
prof. dr. ir. K.I.J. Maex
ten overstaan van een door het College voor Promoties ingestelde commissie,
in het openbaar te verdedigen in de Agnietenkapel
op dinsdag 4 oktober 2016, te 14:00 uur

door

Fleurtje Marieke van der Valk
geboren te Dinxperlo

Promotiecommissie

Promotores:	Prof. dr. E.S.G. Stroes	Universiteit van Amsterdam
	Prof. dr. M. Nieuwdorp	Universiteit van Amsterdam
Copromotor:	Dr. ir. A.J. Nederveen	Universiteit van Amsterdam
Overige leden:	Prof. dr. J. Booij	Universiteit van Amsterdam
	Prof. dr. H.R. Büller	Universiteit van Amsterdam
	Prof. dr. M.M. Levi	Universiteit van Amsterdam
	Prof. dr. M.G. Netea	Radboud Universiteit Nijmegen
	Prof. dr. T. van der Poll	Universiteit van Amsterdam
	Dr. J.H.F. Rudd	University of Cambridge

Faculteit der Geneeskunde

TABLE OF CONTENTS

CHAPTER 1

GENERAL INTRODUCTION AND OUTLINE OF THE THESIS

Van der Valk FM

Published in part in *Current Opinion Lipidology* 2015 and *The Lancet* 2015

GENERAL INTRODUCTION

"To say that atherosclerosis is an inflammatory disease is almost tautologic. Of course it is."
Steinberg 2005

The clinical and societal need for atherosclerosis research

Atherosclerosis is a lipid-driven inflammatory disease affecting the arterial wall, and underlies the majority of cardiovascular diseases such as myocardial infarction and stroke. Worldwide, cardiovascular diseases are the leading cause of death and loss of productive life years[1]. Taking it closer to home, in the Netherlands, one hundred individuals die of cardiovascular disease, every day. Whereas its mortality rate has been steadily declining the past three decades, the prevalence of atherosclerotic disease in the Netherlands keeps rising. We are expecting 840.000 patients in 2030, predominantly driven by the concomitant rise in population growth and life expectancies. As such, atherosclerosis also carries a large public health and economic burden; in fact, it is one of the most expensive medical conditions in the Netherlands, comprising 8.3 billion euro in 2011[2].

Current prevention strategies almost exclusively rely on the recognition and management of traditional risk factors, such as smoking, blood pressure and lipids. Yet, this risk-based paradigm fails to accurately identify high-risk patients. More than 75% of the atherosclerotic ischemic events occur in individuals classified as having low or intermediate risk[3]. Next to primary prevention, traditional risk factor profiling is also suboptimal in the setting of secondary prevention. Current management still allows 66% of the recurrent cardiovascular events to occur[4].

In aggregate, there is a strong impetus to better understand *who* is at risk, *what* is driving it and *how* to attenuate this risk in patients with atherosclerosis.

The evolving concepts of atherosclerosis

Beginning with the pioneer Anitschkow in 1913, who describes that a cholesterol-fed rabbit develops atherosclerosis[5], the 20th century is the era in which the atherogenic role of lipids becomes firmly established[6]. Epidemiological studies reveal higher atherosclerotic disease rates in subjects with increased low-density-lipoprotein cholesterol (LDL-c)[7]. In addition, the advent of hydroxymethyl glutaryl coenzyme A reductase inhibitors (collectively known as statins) enables a series of randomized clinical trials consistently showing the beneficial impact of LDL-c lowering on cardiovascular outcome[8]. At that time, atherosclerosis is predominantly conceived as a lipid storage disease.

As with many modern concepts in medicine, the roots of inflammation's key role in atherogenesis stretch far back in time. The Roman Celsus is the first to describe and define cardinal signs of inflammation[9]. It is Virchow in the 19th century to recognize the inflammatory nature of atherosclerosis; describing plaques as an active product of inflammation[10]. However, it will take more than a century for elements of Virchow's concept of atherogenesis to be embraced.

Meanwhile, Mechnikov and Ehrlich pave the way for modern immunology, sharing the Nobel Prize in 1908 for their studies on immunity and host defense[11]. Finally, at the turn of the century research on inflammation in atherosclerosis really takes off, following the late Russell Ross' landmark paper in 1999 entitled: "Atherosclerosis - an inflammatory disease"[12].

The contemporary view of atherosclerosis' pathophysiology proposes that early lesions arise when, amongst other atherogenic risk factors, lipid particles induce endothelial dysfunction at susceptible arterial sites[13]. The latter allows for lipid accumulation in the intimal space followed by modification into its oxidized forms. In parallel, inflammatory cells, of which monocytes are the most abundant, are recruited into the subintimal space. Upon extravasation these cells transform into macrophages, and subsequently foam cells after taking up the oxidized lipid moieties[14]. What may in essence begin as a protective mechanism, results in lipid-rich inflammation; the first signs of an atherosclerotic lesion, called the fatty streak[15]. Over time, these early lesions progress into advanced atherosclerotic plaques, predominantly driven by inflammatory responses[16].

The scientific efforts in the field of atherosclerosis research are shown in **Figure 1**; illustrating that the initial focus on lipids in atherosclerosis (blue) is now overtaken by inflammation (red). Yet, this figure also illustrates that the knowledge revolution of inflammation in atherosclerosis almost exclusively happened in the preclinical realm. Therefore, this thesis aims to contribute to the clinical translation of inflammatory mechanisms in human atherogenesis, by addressing the following objectives:

1. The inflammatory burden in multiple compartments in patients with atherosclerosis;
2. The impact of atherogenic lipoproteins on this inflammatory activity in patients; and
3. The therapeutic potential of targeted anti-inflammatory drugs in patients with atherosclerosis.

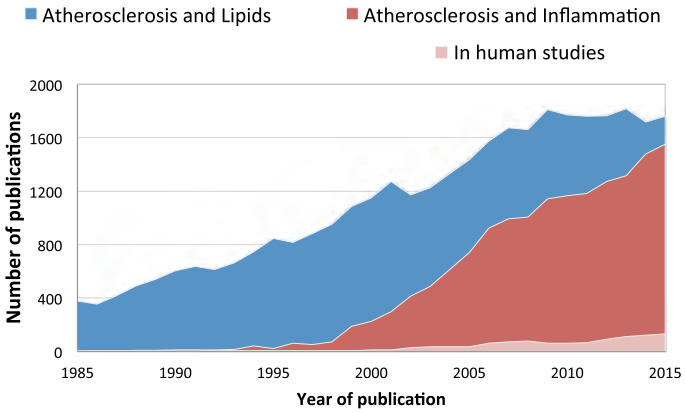

FIGURE 1. Atherosclerosis publications

Graph figure illustrating that the initial focus on lipids in atherosclerosis (blue) is now overtaken by inflammation (red), of which only a few concern in human studies (pink).

Ultimately, such advances will also provide guidance for the previously mentioned pending "who, what and how" issues.

OUTLINE OF THIS THESIS

Past years, imaging techniques have facilitated the clinical validation of inflammatory mechanisms involved atherogenesis. In analogy, **Part I** of this thesis innovates our understanding on the inflammatory strain in multiple compartments of patients with atherosclerosis, by means of functional imaging. **Chapter 2** describes the inflammatory activity of the arterial wall in several patient populations, using ^{18}fluorodeoxyglucose positron emission tomographic (^{18}F-FDG PET) imaging. In addition, **chapter 3** details a single-photon emission computed tomographic (SPECT) imaging approach to traffic circulating immune cells to atherosclerotic plaques in patients. In view of the key contribution of immune cells in atherosclerosis, **chapter 4** comprises a translational approach to describe the activity of their production sites in patients with atherosclerotic disease, as assessed with ^{18}F-FDG PET and hematopoietic cell assays.

Fueled by the observed correlations between inflammatory measures and (oxidized) lipids in the first part of this thesis, **Part II** integrates functional imaging with immunological assays to deal with the impact of atherogenic lipoproteins on inflammation. **Chapter 5** is an intervention study in patients suffering from familial hypercholesterolemia (FH) to evaluate the effect of LDL-c lowering by means of lipoprotein apheresis on arterial wall inflammation, as assessed with ^{18}F-FDG PET. Going from plaque to plasma, **chapter 6** studies the function and phenotype of circulating monocytes in FH patients, also addressing the effect of lipid lowering through either statins or proprotein convertase subtilisin/kexin type 9 (PCSK9) antibodies. Using multimodal imaging, **chapter 7** draws renewed interest in lipoprotein (a) [Lp(a)], a causal risk factor for atherosclerosis, by describing the inflammatory activity in the arterial wall, as well as the effect of Lp(a) on circulating monocytes.

Recognizing the increased inflammatory activity in atherosclerosis, as repeatedly illustrated in the previous parts of this thesis, **Part III** discusses its potential as a therapeutic target to further reduce atherosclerotic disease risk in patients. **Chapter 8** reviews both traditional as novel drugs with anti-inflammatory properties in atherosclerosis, with a cautionary note on its feared complication, immunosuppression, in case of systemic and long-term use. In an attempt to overcome such drawbacks, **chapter 9** details a series of clinical studies on the first anti-inflammatory nanomedicine in atherosclerosis; assessing the local delivery and efficacy of liposomal prednisolone in patients with atherosclerosis. In follow-up, **chapter 10** describes the experimental work aiming to dissect the mechanisms by which prednisolone adversely affects atherosclerosis. To provide an improved estimate of the expected drug effect on plaque macrophages, **chapter 11** provides an *in vitro* approach to assess the overall performance of several high potential anti-atherosclerotic drug candidates on macrophage function and phenotype.

Finally, **chapter 12** summarizes the most important findings of this thesis and elaborates on its future directions. A Dutch summary is provided in **chapter 13**.

REFERENCES

1. Roth GA et al. Demographic and Epidemiologic Drivers of Global Cardiovascular Mortality. N Engl J Med. 2015;372:1333–1341.
2. Vaartjes I et al. Hart- en vaatziekten in Nederland 2013. Den Haag: Hartstichting; 2013.
3. Lauer MS et al. Primary prevention of atherosclerotic cardiovascular disease: the high public burden of low individual risk. JAMA. 2007;297:1376–8.
4. Libby P. The forgotten majority: unfinished business in cardiovascular risk reduction. J Am Coll Cardiol 2005;46:1225–8.
5. Anitschkow N. Über die veränderungen der kaninchenaorta bei experimenteller cholesterinsteatose. Beitr Pathol Anat. 1913;56:379–404.
6. Steinberg D. The cholesterol controversy is over. Circulation. 1989;80:1070–1079.
7. Grundy SM et al. The Cholesterol Facts. A summary of the evidence realting dietary fats, serum cholesterol and coronary heart disease. Circulation. 1990;81:1721–33.
8. LaRosa JC et al. Effect of Statins on Risk of Coronary Disease. JAMA. 1999;282:2340.
9. Celsus A. De Medicina.
10. Virchow R. Cellular Pathology. London, United Kingdom: John Churchill; 1858.
11. The Nobel lectures in immunology. The Nobel prize for physiology or medicine, awarded to Elie Metchnikoff & Paul Ehrlich "in recognition of their work on immunity.". 1908.
12. Ross R. Atherosclerosis - an inflammatory disease. N Engl J Med. 1999;340:115–126.
13. Steinberg D. Atherogenesis in perspective: hypercholesterolemia and inflammation as partners in crime. Nat Med. 2002;8:1211–1217.
14. Moore KJ et al. Macrophages in the pathogenesis of atherosclerosis. Cell. 2011;145:341–55.
15. Libby P et al. Progress and challenges in translating the biology of atherosclerosis. Nature. 2011;473:317–25.
16. Viola J et al. Atherosclerosis – A matter of unresolved inflammation. Semin Immunol. 2015;1–10.

PART I

IMAGING INFLAMMATORY
NETWORKS IN ATHEROSCLEROSIS

CHAPTER 2

THRESHOLD VALUES FOR ARTERIAL WALL INFLAMMATION QUANTIFIED BY ^{18}F-FLUORODEOXYGLUCOSE POSITRON EMISSION TOMOGRAPHIC IMAGING: IMPLICATIONS FOR VASCULAR INTERVENTIONAL STUDIES

Van der Valk FM, Verweij SL, Zwinderman AH, Strang AC, Kaiser Y, Marquering HA, Nederveen AJ, Stroes ESG, Verberne HJ, Rudd JHF

Accepted in JACC Cardiovasc Imaging, 2016

ABSTRACT

Rationale: ^{18}F-FDG positron emission tomography (PET) can identify plaque inflammation as a surrogate endpoint for vascular interventional drug trials. However, an overview of ^{18}F-FDG uptake metrics, threshold values and reproducibility in healthy compared with diseased subjects is not available. Here, we assessed five frequently applied arterial ^{18}fluorodeoxyglucose (^{18}F-FDG) uptake metrics in healthy control subjects, those with risk factors and patients with cardiovascular disease (CVD), to derive uptake thresholds in each subject group. Additionally, we tested the reproducibility of these measures, and produced recommended sample sizes for interventional drug studies.

Methods and Results: ^{18}F-FDG PET/CT of the carotid arteries and ascending aorta was performed in 83 subjects (61±8 years) comprising three groups; 25 healthy controls, 23 patients at increased CVD risk and 35 patients with known CVD. We quantified ^{18}F-FDG uptake across the whole artery, the most diseased segment, and within all active segments over several pre-defined cut-offs. We report these data with and without background corrections. Finally, we determined measurement reproducibility and recommended sample sizes for future drug studies based on these results.

All ^{18}F-FDG uptake metrics were significantly different between healthy and diseased subjects for both the carotids and aorta. Thresholds of physiological ^{18}F-FDG uptake were derived from healthy controls using the 90th percentile of their TBR value; whole artery TBR_{max} 1.84 for the carotids and 2.68 in the aorta. These were exceeded by >52% of risk factor patients and >67% of CVD patients. Reproducibility was excellent in all study groups (ICC>0.95). Using carotid TBR_{max} as primary endpoint resulted in sample size estimates approximately 20% lower than aorta.

Conclusion: We report thresholds for physiological ^{18}F-FDG uptake in the arterial wall in healthy subjects, which are exceeded by the majority of CVD patients. This remains true, independent of readout vessel, signal quantification method or the use of background correction. We also confirm the high reproducibility of ^{18}F-FDG PET measures of inflammation. Nevertheless, because of overlap between subject categories and the relatively small population studied, these data have limited generalizability until substantiated in larger, prospective event-driven studies.

INTRODUCTION

Atherosclerosis is a chronic, low-grade inflammatory disease of the arterial wall that can cause myocardial infarction and stroke[1]. Despite aggressive primary and secondary prevention strategies, long-term disability and death from cardiovascular disease continue to increase[2]. Arterial inflammation is strongly related to the risk of atherosclerotic plaque rupture. Quantification of inflammation may improve patient risk-stratification and allow new drug therapies to be tested[1].

Non-invasive imaging, in particular with ^{18}F-fluordeoxyglucose positron emission tomography (^{18}F-FDG PET), has been used in this way[3,4]. Arterial wall ^{18}F-FDG uptake mirrors inflammatory activity in atherosclerosis[5-7]; inflammatory cells consume large amounts of glucose in comparison with other plaque cells. This results in ^{18}F-FDG accumulation. In addition, arterial ^{18}F-FDG uptake is higher in morphologically unstable plaques, and also predicts future vascular events[8-13].

^{18}F-FDG PET can assess the efficacy (or futility) of treatments designed to lower plaque inflammation[14-27]. As shown in Table S1, the number of vascular intervention trials using ^{18}F-FDG PET as a surrogate marker of inflammation is growing, with half being published in the past 2 years. Several of these studies enriched their study populations by excluding subjects with ^{18}F-FDG uptake below pre-defined thresholds. However, a consensus regarding the most appropriate thresholds is lacking[28-31], primarily because healthy subjects, presumably without pathological arterial inflammation have not been systematically imaged, and large-scaled prospective outcome studies are awaited[32-33]. Without these data, it is challenging to enroll patients with sufficient arterial inflammation to need therapy, and to avoid randomizing those unlikely to respond.

In this study we assessed five frequently applied arterial ^{18}F-FDG uptake metrics in three distinct groups; healthy control subjects, those with risk factors for CVD, and a group with established CVD. Considering ^{18}F-FDG uptake in the arterial wall of healthy control subjects as physiological, we determined the 90th percentile for arterial wall inflammatory activity using several commonly reported PET endpoints. Finally, we determined the reproducibility of published measures of ^{18}F-FDG uptake and derived optimal sample sizes for drug studies based on our results.

METHODS

Study population

We recruited subjects into three groups; (i) healthy control subjects, (ii) patients at increased CVD risk (Framingham risk score >10%) and (iii) patients with known CVD (experienced myocardial infarction, transient ischemic attack, stroke or carotid artery atherosclerosis >12 months before PET imaging). Healthy control subjects were recruited via advertisements in newspapers and screened to exclude those with a history of cardiovascular disease, cardiovascular risk factors or medication use. All healthy control subjects had a value of zero for coronary artery calcium score. Exclusion criteria for all subjects were age <40 years, diabetes mellitus or inflammatory or malignant disease. ^{18}F-FDG PET/CT imaging was performed at the Academic Medical Center, Amsterdam, The Netherlands. Ten subjects underwent repeated imaging after 3 weeks to assess interscan reproducibility. All subjects provided written informed consent. The study was approved by the local institutional review board and conducted according to the principles of the International Conference on Harmonization–Good Clinical Practice.

Biometric and biochemical measurements

Presence of cardiovascular risk factors and use of medication were assessed by questionnaire. EDTA plasma was obtained to measure total cholesterol (TChol), high-density lipoprotein cholesterol (HDL-c), triglycerides (TG), C-reactive protein (CRP), glucose, creatinine, leukocyte and monocyte counts, using commercially available enzymatic methods. Low-density lipoprotein cholesterol (LDL-c) levels were calculated using the Friedewald equation.

^{18}F-FDG PET/CT imaging ad analysis

^{18}F-FDG PET/CT imaging was performed on a PET/CT scanner (Philips, Best, The Netherlands). Subjects fasted for >6 hours prior to infusion of 200 MBq of ^{18}F-FDG (5.5 mCi). PET imaging was initiated with a low-dose, non-contrast enhanced CT for attenuation correction and anatomic co-registration (slice thickness 3mm), 90 minutes after ^{18}F-FDG administration. Additionally, CT scans were used for coronary artery calcium scoring (please see Supplementary Methods). Images were analyzed using OsiriX software (Geneva, Switzerland; http://www.osirix-viewer.com/).

Please also see Figure 1 for an overview of the ^{18}F-FDG uptake analysis and metrics.^{18}F-FDG uptake was assessed (1) in the carotids starting from 1 slice caudal to the carotid bifurcation downwards, and (2) in the aorta from 1 slice cranial to the pulmonary arteries upwards, per standard methods[34]. From each region of interest (ROI), standardized uptake values (SUVs) were read. SUV represents ^{18}F-FDG activity adjusted for ^{18}F-FDG dose, corrected for decay and divided

by body weight. To correct for background ^{18}F-FDG, whole artery SUV was either subtracted or divided (target to background ratio, TBR) by background SUV obtained from venous or remote arterial blood. After whole artery metrics, most diseased segment TBR (TBR_{mds}) was recorded as the mean of 3 adjacent slices with the highest arterial value of SUV_{max}. In the active segment analysis, slices with TBR_{max} values above a pre-defined cut-off level (either ≥1.60, ≥1.80 or ≥2.00 for the carotid arteries, and ≥2.40, ≥2.60 or ≥2.80 for the aorta) were considered active, whereas non-inflamed segments were excluded. Using this approach, the percentage of those having at least 1 active slice, the $TBR_{active\ slices}$ and the percentage of active slices ($\%_{active\ slices}$) were assessed.

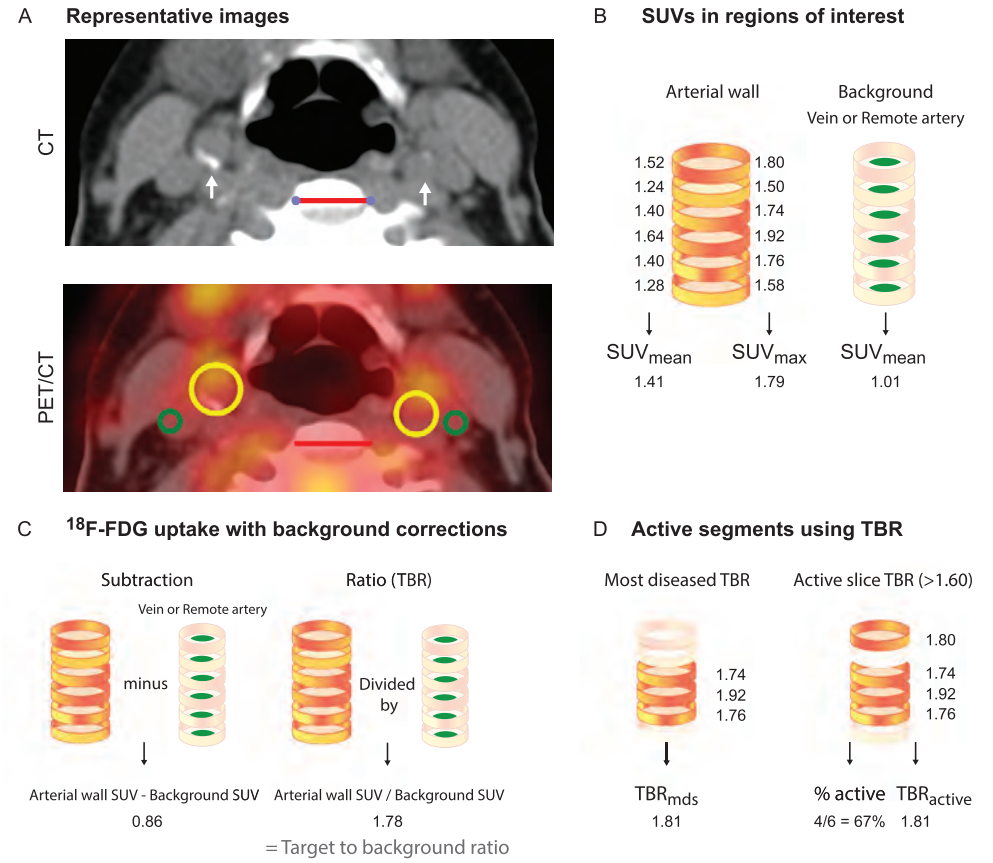

FIGURE 1. Arterial PET/CT images and analysis methods

(**A**) Representative CT and ^{18}F-FDG PET/CT images of the carotid arteries (white arrow, yellow regions of interest, ROIs) and jugular veins (green ROIs) in a patient with cardiovascular disease. Red scale bars indicate 2cm. (**B-D**) Schematics showing (**B**) standardized uptake values (SUVs) in the whole artery and the background, (**C**) background corrections and (**D**) active segment analysis with corresponding imaging parameters. A similar analysis is performed for the aortic segment. *^{18}F-FDG indicates ^{18}fluorodeoxyglucose; CT, computed tomography; MDS, most-diseased segment; PET, positron emission tomography; ROI, regions of interest; TBR, target to background ratio.*

Statistical analysis

Continuous variables are expressed as mean ± standard deviation (SD) or median and interquartile range (IQR), unless otherwise specified. Differences in ^{18}F-FDG uptake between the different groups were assessed using a multivariate model to account for age, gender, hypertension (SBP >140 mmHg, DBP >90 mmHg or use of antihypertensive medication), BMI, smoking, drugs usage (statins, ezetimibe, ace inhibitors, acetylsalicylic acid, beta blockers), lipid profile and glucose. We estimated SUV and TBR upper threshold values based on the tolerance interval[35] using the 95th and 90th percentile of log-normal SUV and TBR in the healthy control subjects. Power analyses to detect the superiority of a test over a control in SUV and TBR were based on a 2-sample unpaired t test (2-sided) and performed with 80% power and an alpha of 5%. The agreement between scans and analyses were assessed using intraclass correlation coefficients (ICC, r) and Bland-Altman plots. The SD of the paired differences (SDpd) and the coefficient of variation (COV) between the initial and repeat scans were calculated. COV was calculated by dividing the SDpd by the mean value of the population for each parameter. P values <0.05 were considered statistically significant. Data were analyzed using SPSS version 19.0 (SPSS Inc., Chicago, Illinois).

RESULTS

Clinical characteristics

In total, 83 participants (aged 61±8 years) were imaged, comprising 25 healthy control subjects, 23 patients at increased CVD risk (median Framingham score 14% [IQR 4]), and 35 patients with a history of CVD documented as significant carotid artery stenosis (n=13), transient ischemic attack (n=9), stroke (n=9), and/or myocardial infarction (n=25). Subject demographics are listed in Table 1.

Whole artery ^{18}F-FDG uptake

Whole artery ^{18}F-FDG in the carotids and aorta, expressed as SUV_{max}, showed a gradual increase from healthy to diseased subjects (Table 2). The mean difference in SUV_{max} between healthy control subjects and those at increased CVD risk was 0.30±0.08 for the carotids, and 0.36±0.09 for the aorta. The mean difference in SUV_{max} between patients at increased CVD risk and patients with known CVD was 0.10±0.08 for the carotids and 0.28±0.10 for the aorta.

TABLE 1. Clinical characteristics of study subjects

Characteristic	Healthy control subjects (n=25)	Patients at increased CVD risk (n=23)	Patients with known CVD (n=35)	P-value #	P-value ^
Age, y	60 ± 11	59 ± 6	63 ± 7	ns	ns
Gender, %male (n)	60 (15)	74 (17)	77 (27)	ns	ns
BMI, kg/m^2	25 ± 3	26 ± 3	27 ± 4	ns	ns
SBP, mmHg	134 ± 16	135 ± 9	133 ± 8	ns	ns
DBP, mmHg	81 ± 10	82 ± 8	81 ± 7	ns	ns
Smoking,%active(n)	0 (0)	0 (0)	14 (5)	0.026	0.012
Lipid lowering drugs, %yes	0 (0)	83 (19)	100 (35)	<0.001	ns
Statin use (%)	0 (0)	83 (19)	86 (30)	<0.001	ns
Ezetimibe use (%)	0 (0)	0 (0)	14 (5)	<0.001	<0.001
ACE-inhibitor use (%)	0 (0)	91 (21)	100 (35)	<0.001	ns
Acetylsalicylic acid use (%)	0 (0)	70 (16)	100 (35)	<0.001	ns
B-blocker use, %yes	0 (0)	74 (17)	100 (35)	<0.001	ns
TChol, mmol/L	5.32 ± 0.96	7.33 ± 2.81	5.99 ± 3.16	0.040	ns
LDL-c, mmol/L	3.24 ± 0.97	5.42 ± 2.63	4.18 ± 3.11	0.011	ns
HDL-c, mmol/L	1.65 ± 0.37	1.21 ± 0.25	1.24 ± 0.37	<0.001	ns
TG, mmol/L	0.89 [0.84]	1.57 [0.99]	1.42 [0.91]	0.001	ns
Glucose, mmol/L	5.04 ± 0.33	5.40 ±0.75	5.41 ± 1.19	ns	ns
Creatinine, µmol/L	79 [16]	80 [17]	82 [17]	ns	ns
Leukocytes, 10^9/L	6.10 ± 1.74	6.30 ± 2.54	6.29 ± 1.52	ns	ns
Monocytes, 10^9/L	0.45 ± 0.13	0.51 ± 0.16	0.54 ± 0.20	ns	ns
CRP, mg/L	1.30 [1.35]	1.20 [2.00]	2.30 [3.30]	ns	ns
CACscores*	0 (0)	303 (110)	691 (372)	<0.001	<0.001

Data are expressed as mean±SD, percentage (number) or median[IQR]. # P value between all groups. ^ P value between patients at increased CVD risk and patients with known disease. * Agatston score. *BMI indicates body mass index; CAC score, coronary artery calcium score; CRP, C-reactive protein; DBP, diastolic blood pressure; HDL-c, high-density lipoprotein cholesterol; LDL-c, low-density lipoprotein cholesterol; SBP, systolic blood pressure; TChol, total cholesterol; TG, triglycerides.*

TABLE 2. Whole artery and active segment based ^{18}F-FDG uptake in study groups

	Healthy control subjects	Patients at increased CVD risk	Patients with known CVD	P-value*
Whole artery SUV_{max}				
Carotid arteries	1.49 ± 0.28	1.79 ± 0.27	1.99 ± 0.37	<0.001
Ascending aorta	1.98 ± 0.31	2.34 ± 0.31	2.63 ± 0.63	<0.001
Venous background SUV_{mean}				
Jugular veins	0.84 ± 0.13	0.92 ± 0.14	0.93 ± 0.18	ns
Superior vena cava	0.96 ± 0.11	0.84 ± 0.16	0.90 ± 0.20	ns
Arterial SUV – venous SUV_{mean}				
Carotid arteries	0.53 ± 0.20	0.86 ± 0.22	0.96 ± 0.28	<0.001
Ascending aorta	1.14 ± 0.22	1.49 ± 0.23	1.73 ± 0.54	<0.001
Whole artery TBR_{max} §				
Carotid arteries	1.55 ± 0.23	1.94 ± 0.27	2.13 ± 0.30	<0.001
Ascending aorta	2.36 ± 0.25	2.80 ± 0.31	2.97 ± 0.59	<0.001
Active segment approach				
Carotid arteries (active ≥1.60)	48% of subjects	96% of patients	100% of patients	
$\%_{active\ slices}$	32 ± 40%	80 ± 31%	90 ± 19%	0.020
$TBR_{active\ slices}$	1.79 ± 0.12	2.00 ± 0.29	2.09 ± 0.32	0.044
Ascending aorta (active ≥2.40)	88% of subjects	96% of patients	97% of patients	
$\%_{active\ slices}$	74±30%	88±25%	91±18%	ns
$TBR_{active\ slices}$	2.70±0.21	2.97±0.40	3.00±0.49	ns

Multivariate analysis adjusted for age, gender, hypertension, smoking, body mass index, drug usage, lipid profile and glucose. § TBR = Arterial wall SUV_{max} / Venous background SUV_{mean}. *TBR indicates target to background ratio; CVD, cardiovascular disease.*

Prior to calculating subtraction or ratio metrics, we demonstrated that both venous and arterial blood ^{18}F-FDG background values were comparable between groups (Table 2 and Table S2). In line with this observation, ^{18}F-FDG background corrections of the SUV values with either subtraction or ratio (TBR) did not affect the significance between groups (Table 2 and Table S2).

Active segment approach

We also examined the TBR of the most diseased segment (TBR_{mds}, Table S2). In addition, an active segment analysis was performed using several pre-defined cut-offs. Using a cutoff of TBR ≥1.60 for the carotids, 48% of the healthy control subjects had at least 1 active slice compared with 96% and 100% of the patients at increased risk for or with known CVD, respectively (Table 2). The percentage of active slices was 32±40% in healthy control subjects, 80±31% in patients at risk for CVD and 90±19% in known CVD patients (p=0.020). The corresponding $TBR_{active\ slices}$ values were also distinct between groups (p=0.044; Table 2). With cutoffs of ≥1.80 or ≥2.00,

the number of healthy control subjects with at least 1 active slice in the carotids decreased substantially (Table S3). Whereas the $\%_{active\ slices}$ remained significantly different between groups, the $TBR_{active\ slices}$ did not (Table S3).

In contrast to the carotids, a much larger proportion of the subjects had active aortic walls. With a cutoff of ≥2.40, 88% of the healthy control subjects had at least 1 active slice, however, the $TBR_{active\ slices}$ and $\%_{active\ slices}$ were not distinct between groups (Table 2). With the active-definition at ≥2.60 or ≥2.80, still more than half of the healthy control subjects had active segments (Table S3). For the highest cutoff, $TBR_{active\ slices}$ was significantly different between groups (p=0.015).

Thresholds

The TBR thresholds based on the tolerance interval in healthy control subjects are listed in Table 3. Based on the 90th percentile of this interval, the threshold for SUV_{max} was 1.85 for the carotids and 2.38 for the aorta. For TBR_{max} this threshold was set at 1.84 for the carotids and 2.68 for the aorta. Figure 2 illustrates both the SUV_{max} and TBR_{max} values per group, with corresponding thresholds (red dashed lines). For SUV_{max}, 39-43% of those at increased CVD risk versus 66% of the CVD patients exceeded these thresholds. For TBR_{max} these numbers were in general larger; 52-57% of those at increased CVD risk and 67-74% of CVD patients. In Table S4, we also provide the thresholds using the 95th percentile values.

TABLE 3. ^{18}F-FDG uptake threshold values

Artery	Metric	Threshold*	Percentage above threshold	
			Patients at increased CVD risk	Patients with known CVD
Carotid	SUV_{max}	> 1.85	39%	66%
	TBR_{max}	> 1.84	52%	74%
Aorta	SUV_{max}	> 2.38	43%	66%
	TBR_{max}	> 2.68	57%	67%

* Thresholds were determined using the 90th percentile value observed in the healthy control subjects. *TBR indicates target to background ratio; CVD, cardiovascular disease.*

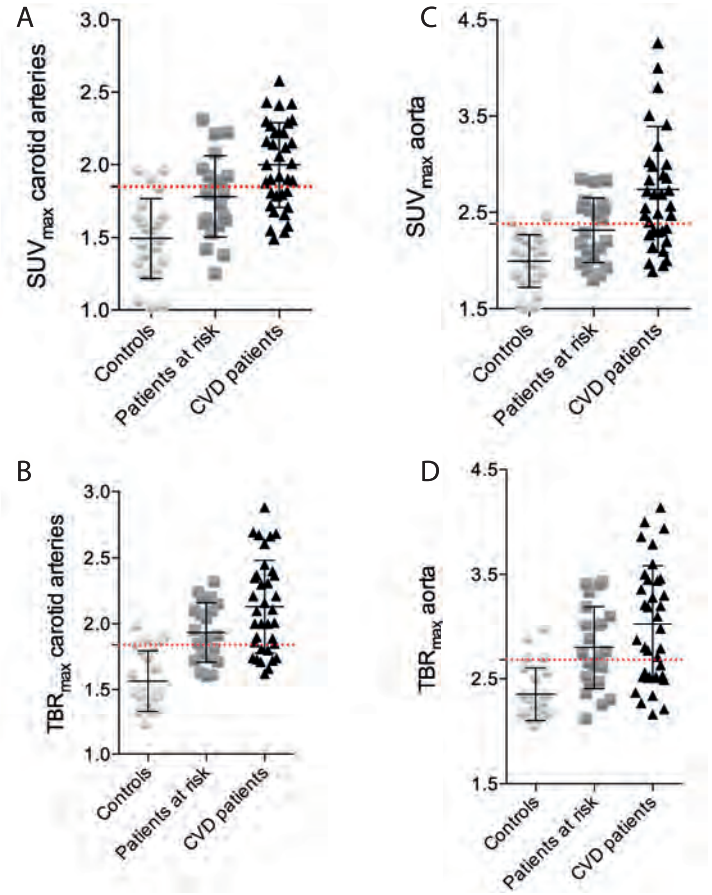

FIGURE 2. Gradual increase of TBR_{max} in the carotids and aorta between groups

Scatterplots showing the gradual increase in SUV_{max} and TBR_{max} for the carotids (**A,B**) and aorta (**C,D**) in healthy control subjects, patients at CVD risk and patients with known CVD. The red dashed line represents the 90th percentile value in healthy control subjects. *CVD indicates cardiovascular disease; TBR, target to background ratio.*

Sample sizes

Based on the TBR_{max} values in the present study, Figure 3 depicts the sample sizes required for an estimated drug effect; ranging from 5 to 20%, as has been observed in previous drug trials (Table S1). Carotid TBR as primary endpoint requires approximately 20% fewer subjects compared with the aorta. Of note, sample sizes based upon SUV_{max} values necessitate approximately 20 to 45% more subjects compared with TBR_{max} (Figure S1).

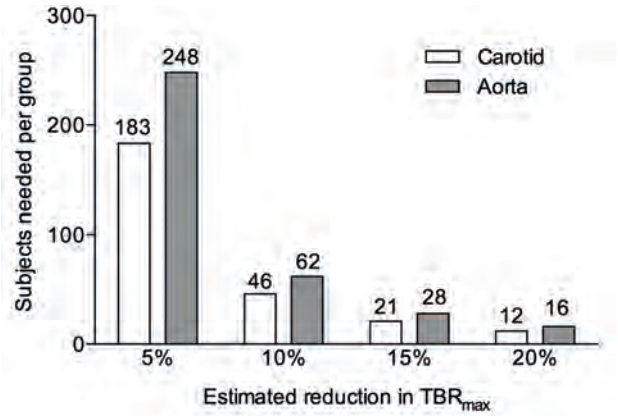

FIGURE 3. Estimated sample sizes for intervention studies

Sample sizes required for studies using TBR_{max} as the primary endpoint. These are dependent on the estimated drug effect (ranging between 5 and 20%) and target vessel for imaging (carotid artery or aorta). *TBR indicates target to background ratio.*

Reproducibility

The intra- and inter-observer, and interscan agreement within 3 weeks was excellent for TBR_{max} as indicated by (i) ICC values of >0.95 with narrow 95% confidence intervals, and (ii) the absence of fixed or proportional bias in the Bland-Altman plots (Figure S2). In addition, agreement for all ^{18}F-FDG metrics was also excellent in healthy control subjects (Table S4,5).

DISCUSSION

In the present work, we tested five frequently applied approaches to quantify ^{18}F-FDG uptake in the arterial wall of healthy controls, patients at risk and patients with known CVD. Whole artery SUV_{max} was significantly different between groups, and ^{18}F-FDG venous blood background values were similar. As such, ^{18}F-FDG uptake metrics with background corrections, such as the subtraction or ratio method (TBR), remained significantly different. Moreover, the TBR and active slice methods accentuated differences between the groups. Based on the above, we determined threshold values for arterial wall inflammation and found that >39% of patients at risk for and >66% with known CVD had inflamed arterial walls, highlighting a potential therapeutic window for additional anti-inflammatory strategies. Nevertheless, due to the substantial overlap between healthy controls and patients, the value of ^{18}F-FDG PET for individual risk assessment is limited.

Here, we assessed the most commonly reported ^{18}F-FDG endpoints: (i) whole artery SUV, (ii) background subtraction, (iii) background ratio (TBR), (iv) most diseased segment, and finally

(v) active segments. These different approaches highlight the ability of a single PET scan to measure multiple aspects of artery's inflammatory status. However, by the same token, the use of multiple endpoints in drug studies is statistically less robust than a single readout[31].

As shown in Table 2, differences in background ^{18}F-FDG activity between groups exist, but are not significantly different. Both background correction methods show smaller variations compared with SUV; in patients with established CVD the carotid SUV standard deviation is 0.37 versus 0.28-0.30 after background correction. Consequently, the sample size based on TBR as read-out is smaller than SUV. In addition, in drug studies with repeat imaging, the use of a ratio, such as TBR, limits the effect on signal quantification where variation between scans exists (e.g. weight change, ^{18}F-FDG dose change, ^{18}F-FDG circulation time change)[36]. For these reasons, we favor the use of TBR, as also endorsed in the recent EANM position paper on vascular PET imaging[36].

With respect to the active segment approach, a substantial bias is induced by eliminating (a potentially large number of) included subjects and imaged slices (e.g. 48% of healthy subjects included in the carotid analysis). Consequently, the $TBR_{active\ slice}$ loses much of its power to differentiate between healthy and diseased subjects. Hence, this approach should be interpreted with caution, and might be better suited for changes within one individual[20,26].

The validation of ^{18}F-FDG as a marker of plaque inflammation originates from histology[5-7] and gene expression studies[37,38] performed on human carotid plaque material. Over time, quantification of ^{18}F-FDG uptake in the aorta became adopted, supported by, amongst other, the histological work in rabbit models[39,40], and the incremental value in cardiovascular risk stratification[11]. The present study was not designed to investigate the nature of ^{18}F-FDG vascular uptake, but nevertheless showed that SUVs and TBRs were consistently higher in the aorta compared with the carotids. This is relevant when applying an "index vessel approach" to drug trials, since in ~80% of subjects, the index vessel will originate from the aorta[31]. This might be sub-optimal, as we also demonstrated that aortic TBR as endpoint requires a larger sample size to detect drug efficacy[37]. Taking into account that the published drug-induced TBR changes have been relatively small (ranging between 5 to 15%, Table S1), the optimal choice of endpoint vessel is important. The use of the carotid artery as a readout vessel holds the strongest biological validation linking the ^{18}F-FDG signal and inflammation to recommend it [5-7,13,37,38]. Therefore, we suggest that if the index vessel approach is not used, the carotid artery is best validated as primary readout vessel, as highlighted by Gholami et al[31].

Previously, histological carotid plaque studies demonstrated the correlation between plaque rupture and inflammation[41-43]; macrophage-rich areas in carotid plaques were higher in symptomatic patients (18±10%) compared with asymptomatic patients (11±4%)[42]. Tawakol et al[6] were the first to link plaque macrophages *ex vivo* to plaque inflammation *in vivo*; demonstrating a linear relation between macrophage content and ^{18}F-FDG uptake in plaques of 17 patients scheduled for carotid endarterectomy. Carotid plaques with a macrophage area

of <5% had low TBR values, whereas inflamed carotid plaques with macrophage areas >5% had carotid TBRs between 1.80 and 2.40 (25th and 75th percentiles)[6].

Instead of histology-based approaches, here we classified arterial wall inflammation using population-based data, by regarding the 90th percentile of ^{18}F-FDG uptake metrics in healthy controls as a natural threshold. Reassuringly, our healthy control data are consistent with ^{18}F-FDG uptake values reported in prior studies[22,44-46]. In addition, our carotid uptake values are comparable to those reported in histology-based[6,41,42,47] and epidemiology-based[46] studies, further supporting the validity of our data.

In line with previous studies[34,48], we report excellent reproducibility of PET atherosclerosis imaging in patients at risk and with known CVD, and extended the findings into healthy control subjects. We derived ICCs for interobserver variability of >0.95, similar to values reported previously[34,48]. Further, we document low inter-scan TBR changes (<3.5% over a 3 week period), which is in line with previous placebo-controlled intervention studies revealing small variations during a 3 to 6 month timeframe[19,23]. This makes PET/CT a highly reproducible and sensitive tool suitable for identifying patients for anti-inflammatory interventions and for determining their effectiveness.

Several limitations merit further consideration. First, this limited observational study does not address the predictive value of arterial PET imaging. Using the present population-based approach substantial overlap in ^{18}F-FDG metrics between healthy and diseased subjects exists. Therefore, ^{18}F-FDG metrics should be correlated by outcome data to enable the assessment of "true" pathological ^{18}F-FDG reference ranges in humans. For this, the results of larger, long-term prospective studies (BioImage[32] and PESA[33]) are awaited. Second, despite the published recommendations on PET imaging protocols[34,48], substantial variation in patient preparation (e.g. glucose levels, time of fasting), PET image protocol (e.g. time and areas of scanning) and technology (e.g. acquisition, reconstruction)[28-31.] As such, extrapolation of our thresholds is limited to studies using similar imaging and analysis protocols. Third, with respect to the population-based approach with a relative small group size, it must be stressed that clinical characteristics of the studied groups in this study (amongst others age, gender, lipid levels) should be taken into account upon extrapolation of our thresholds. Finally, this study was not designed to associate ^{18}F-FDG uptake with additional structural or functional features of the artery, since we used a non–contrast-enhanced CT as part of the PET/CT. Future studies using magnetic resonance imaging (MRI) should improve such assessments, as well as correct for partial volume effects; a well-described limitation of PET imaging[31].

Clinical relevance. For interventional studies, ^{18}F-FDG PET can help to identify subgroups with inflammation above the physiological range and can provide reproducible measures of drug action. The majority of patients with known CVD have increased inflammatory activity in one or more arteries, despite standard-of-care treatments, including statin use in >80%. This residual inflammatory activity suggests the potential for further anti-inflammatory strategies in CVD

patients[49]. We await the results of large-scale studies of such interventions[50,51]. Nevertheless, because of the considerable overlap of ^{18}F-FDG values between healthy control subjects, those at increased CVD risk and patients with known CVD, it is uncertain whether ^{18}F-FDG PET imaging is capable of identifying individual patients most likely to benefit from new therapies.

Acknowledgments: We would like to thank M.F. Lam and M.E. Hemayat for their assistance with ^{18}F-FDG PET/CT, and P.F. Groot with the CAC scores.

Disclosures and funding: This work was supported by a European Framework Program 7 grant (ESS: FP7-Health 309820: Nano-Athero). Erik Stroes has received lecturing fees from Merck, Novartis, ISIS, Amgen - none of are related to the contents of this manuscript. All other authors declare that they have no conflict of interest and no relationships with industry relevant to this study. JHFR is part-supported by the NIHR Cambridge Biomedical Research Centre, the British Heart Foundation and the Wellcome Trust.

REFERENCES

1. Libby P et al. Progress and challenges in translating the biology of atherosclerosis. Nature 2011;473:317–25.
2. Bloom D. The Global Economic Burden of Noncommunicable Diseases. Geneva World Econ. Forum 2011.
3. Wildgruber M et al. Molecular imaging of inflammation in atherosclerosis. Theranostics 2013;3:865–84.
4. Tarkin JM et al. PET imaging of inflammation in atherosclerosis. Nat. Rev. Cardiol. 2014;11:443–457.
5. Rudd J et al. Imaging Atherosclerotic Plaque Inflammation With [18F]-Fluorodeoxyglucose Positron Emission Tomography. Circulation 2002;105:2708–2711.
6. Tawakol A et al. In vivo 18F-fluorodeoxyglucose positron emission tomography imaging provides a noninvasive measure of carotid plaque inflammation in patients. J. Am. Coll. Cardiol. 2006;48:1818–24.
7. Masteling MG et al. High-resolution imaging of human atherosclerotic carotid plaques with micro 18F-FDG PET scanning exploring plaque vulnerability. J. Nucl. Cardiol. 2011;18:1066–75.
8. Paulmier B et al. Arterial wall uptake of fluorodeoxyglucose on PET imaging in stable cancer disease patients indicates higher risk for cardiovascular events. J. Nucl. Cardiol. 2008;15:209–17.
9. Rominger A et al. 18F-FDG PET/CT identifies patients at risk for future vascular events in an otherwise asymptomatic cohort with neoplastic disease. J. Nucl. Med. 2009;50:1611–20.
10. Grandpierre S et al. Arterial foci of F-18 fluorodeoxyglucose are associated with an enhanced risk of subsequent ischemic stroke in cancer patients: a case-control pilot study. Clin. Nucl. Med. 2011;36:85–90.
11. Figueroa AL et al. Measurement of arterial activity on routine FDG PET/CT images improves prediction of risk of future CV events. JACC. Cardiovasc. Imaging 2013;6:1250–9.
12. Davies JR et al. Identification of culprit lesions after transient ischemic attack by combined 18F fluorodeoxyglucose positron-emission tomography and high-resolution magnetic resonance imaging. Stroke. 2005;36:2642–7.
13. Marnane M et al. Carotid plaque inflammation on 18F-fluorodeoxyglucose positron emission tomography predicts early stroke recurrence. Ann. Neurol. 2012;71:709–18.
14. Tahara N et al. Simvastatin attenuates plaque inflammation: evaluation by fluorodeoxyglucose positron emission tomography. J. Am. Coll. Cardiol. 2006;48:1825–31.
15. Lee SJ et al. Reversal of vascular 18F-FDG uptake with plasma high-density lipoprotein elevation by atherogenic risk reduction. J. Nucl. Med. 2008;49:1277–82.
16. Potter K et al. Effect of long-term homocysteine reduction with B vitamins on arterial wall inflammation assessed by fluorodeoxyglucose positron emission tomography: a randomised double-blind, placebo-controlled trial. Cerebrovasc. Dis. 2009;27:259–65.
17. Ishii H et al. Comparison of atorvastatin 5 and 20 mg/d for reducing F-18 fluorodeoxyglucose uptake in atherosclerotic plaques on positron emission tomography/computed tomography: a randomized, investigator-blinded, open-label, 6-month study in Japanese adults scheduled. Clin. Ther. 2010;32:2337–47.
18. Wu Y-W et al. The effects of 3-month atorvastatin therapy on arterial inflammation, calcification, abdominal adipose tissue and circulating biomarkers. Eur. J. Nucl. Med. Mol. Imaging 2011;39:399–407.
19. Fayad ZA et al. Safety and efficacy of dalcetrapib on atherosclerotic disease using novel non-invasive multimodality imaging (dal-PLAQUE): a randomised clinical trial. Lancet 2011;378:1547–59.
20. Elkhawad M et al. Effects of p38 mitogen-activated protein kinase inhibition on vascular and systemic inflammation in patients with atherosclerosis. JACC. Cardiovasc. Imaging 2012;5:911–22.
21. Tawakol A et al. Intensification of Statin Therapy Results in a Rapid Reduction in Atherosclerotic Inflammation: Results of A Multi-Center FDG-PET/CT Feasibility Study. J. Am. Coll. Cardiol. 2013;62:909–17.
22. van Wijk DF et al. Nonpharmacological Lipoprotein Apheresis Reduces Arterial Inflammation in Familial Hypercholesterolemia. J. Am. Coll. Cardiol. 2014;64:1418–26.

23. Tawakol A et al. Effect of treatment for 12 weeks with rilapladib, a lipoprotein-associated phospholipase A2 inhibitor, on arterial inflammation as assessed with 18F-fluorodeoxyglucose-positron emission tomography imaging. J. Am. Coll. Cardiol. 2014;63:86–8.
24. van der Valk FM et al. Prednisolone-containing liposomes accumulate in human atherosclerotic macrophages upon intravenous administration. Nanomedicine 2015;11:1039–1046.
25. Kootte RS et al. Effect of open-label infusion of an apoA-I-containing particle (CER-001) on RCT and artery wall thickness in patients with FHA. J. Lipid Res. 2015;56:703–12.
26. Emami H, Vucic E, Subramanian S, et al. The effect of BMS-582949, a P38 mitogen-activated protein kinase (P38 MAPK) inhibitor on arterial inflammation: A multicenter FDG-PET trial. Atherosclerosis 2015;240:490–6.
27. Gaztanaga J et al. A phase 2 randomized, double-blind, placebo-controlled study of the effect of VIA-2291, a 5-lipoxygenase inhibitor, on vascular inflammation in patients after an acute coronary syndrome. Atherosclerosis 2015;240:53–60.
28. Huet P et al. Variability and Uncertainty of 18F-FDG PET Imaging Protocols for Assessing Inflammation in Atherosclerosis: Suggestions for Improvement. J. Nucl. Med. 2015;56:552–559.
29. Chen W et al. PET Assessment of Vascular Inflammation and Atherosclerotic Plaques: SUV or TBR? J. Nucl. Med. 2015;56:503–4.
30. Saraste A et al. Optimizing FDG-PET/CT imaging of inflammation in atherosclerosis. J. Nucl. Cardiol. 2015:18–20.
31. Gholami S et al. Assessment of atherosclerosis in large vessel walls: A comprehensive review of FDG-PET/CT image acquisition protocols and methods for uptake quantification. J. Nucl. Cardiol. 2015;22:468–79.
32. Muntendam P et al. The BioImage Study: novel approaches to risk assessment in the primary prevention of atherosclerotic cardiovascular disease--study design and objectives. Am. Heart J. 2010;160:49–57.
33. Fernández-Ortiz A et al. The Progression and Early detection of Subclinical Atherosclerosis (PESA) study: rationale and design. Am. Heart J. 2013;166:990–8.
34. Rudd JHF et al. Atherosclerosis inflammation imaging with 18F-FDG PET: carotid, iliac, and femoral uptake reproducibility, quantification methods, and recommendations. J. Nucl. Med. 2008;49:871–8.
35. Dong X et al. Statistical considerations in setting product specifications. J. Biopharm. Stat. 2015;25:280–94.
36. Bucerius J et al. Position paper of the Cardiovascular Committee of the European Association of Nuclear Medicine (EANM) on PET imaging of atherosclerosis. Eur. J. Nucl. Med. Mol. Imaging 2015;43:780–92.
37. Pedersen SF et al. Gene expression and 18FDG uptake in atherosclerotic carotid plaques. Nucl. Med. Commun. 2010;31:423–9.
38. Graebe M et al. Molecular pathology in vulnerable carotid plaques: correlation with [18]-fluorodeoxyglucose positron emission tomography (FDG-PET). Eur. J. Vasc. Endovasc. Surg. 2009;37:714–21.
39. Worthley SG et al. In vivo non-invasive serial monitoring of FDG-PET progression and regression in a rabbit model of atherosclerosis. Int. J. Cardiovasc. Imaging 2009;25:251–7.
40. Lederman RJ et al. Detection of atherosclerosis using a novel positron-sensitive probe and 18-fluorodeoxyglucose (FDG). Nucl. Med. Commun. 2001;22:747–753.
41. Schumacher H et al. Immunophenotypic characterisation of carotid plaque: increased amount of inflammatory cells as an independent predictor for ischaemic symptoms. Eur. J. Vasc. Endovasc. Surg. 2001;21:494–501.
42. Jander S et al. Inflammation in High-Grade Carotid Stenosis : A Possible Role for Macrophages and T Cells in Plaque Destabilization. Stroke 1998;29:1625–1630.
43. Crisby M et al. Pravastatin Treatment Increases Collagen Content and Decreases Lipid Content, Inflammation, Metalloproteinases, and Cell Death in Human Carotid Plaques : Implications for Plaque Stabilization. Circulation 2001;103:926–933.
44. Emami H et al. Splenic Metabolic Activity Predicts Risk of Future Cardiovascular Events: Demonstration of a Cardiosplenic Axis in Humans. JACC. Cardiovasc. Imaging 2014;8:121–130.

45. Kim EJ et al. Metabolic activity of the spleen and bone marrow in patients with acute myocardial infarction evaluated by 18f-fluorodeoxyglucose positron emission tomograpic imaging. Circ. Cardiovasc. Imaging 2014;7:454–60.
46. Moon SH et al. Carotid FDG Uptake Improves Prediction of Future Cardiovascular Events in Asymptomatic Individuals. JACC. Cardiovasc. Imaging 2015;8:949–956.
47. Carr SC et al. Activated inflammatory cells are associated with plaque rupture in carotid artery stenosis. Surgery 1997;122:757–764.
48. Rudd JHF et al. (18)Fluorodeoxyglucose positron emission tomography imaging of atherosclerotic plaque inflammation is highly reproducible: implications for atherosclerosis therapy trials. J. Am. Coll. Cardiol. 2007;50:892–6.
49. van der Valk FM et al. Novel anti-inflammatory strategies in atherosclerosis. Curr. Opin. Lipidol. 2012;23:532–9.
50. Ridker PM et al. Interleukin-1β inhibition and the prevention of recurrent cardiovascular events: rationale and design of the Canakinumab Anti-inflammatory Thrombosis Outcomes Study (CANTOS). Am. Heart J. 2011;162:597–605.
51. Ridker PM. Testing the inflammatory hypothesis of atherothrombosis: scientific rationale for the cardiovascular inflammation reduction trial (CIRT). J. Thromb. Haemost. 2009;7:332–9.

SUPPLEMENT

Detailed methods: Coronary artery calcium score. The CT scans were used to determine the Agatston score, the coronary artery calcium (CAC) score. In a manually set volume of interest, all pixels with intensity higher than 130 HU were selected. Connected areas of these threshold pixels were constructed. All areas smaller than 1 mm^2 were excluded. The score was determined by combining all selected connected areas with a weight. The weight was determined by the highest intensity value of a pixel in the connected areas: 1 for 130–199 HU, 2 for 200–299 HU, 3 for 300–399 HU, and 4 for 400 HU and greater. Because of the difference in slice thickness of the images in his study (5 mm) compared to default Agatston score images (3mm), the sum CAC score was multiplied with 5/3.

TABLE S1. Intervention studies using ^{18}F-FDG PET/CT as surrogate endpoint

First author and reference	Study population	Arterial segments analyzed	PET as selection criterion	Intervention	Primary endpoint	Observed %change
Tahara et al. 2006	43 subjects with incidental arterial ^{18}F-FDG uptake	Carotid and aorta combined	na	Diet alone or with simvastatin (max 20 mg/day) for 3 months	SUV_{max}	-10% in diet+statin group
Lee et al. 2008	60 subjects with atherogenic risk factors	Carotid, subclavian, aorta and iliac arteries combined	na	Life style modifications for 17 months	% positive lesions (SUV/ blood pool >1)	-64.8%
Potter et al. 2009	30 post-stroke patients	Carotid, aorta and femoral arteries combined	na	B-vitamin or placebo for 2 years	SUV_{max}	None
Ishii et al. 2010	30 patients with stable angina pectoris	Aorta, femoral	na	Atorvastatin 5 or 20 mg/day for 6 months	TBR_{mean}	-7.9% in aortic, and -9.9% in femoral TBR_{mean} in 20mg group
Wu et al. 2011	43 patients with atherosclerosis	Aorta and iliofemoral combined	na	Atorvastatin 40 mg/day for 12 weeks	TBR_{max}	-19%
Fayad et al. 2011	130 patients with (risk factors for) coronary heart disease	Carotid, aorta	$TBR_{mds} \geq 1.60$	Dalcetrapib 600mg/day or placebo for 24 months	TBR_{mds} index vessel	None in TBR_{mds} index, whereas -7% in carotid TBR_{mds}
Elkhawad et al. 2012	99 patients with atherosclerosis	Carotid, aorta	na	Losmapimod (p38MAPK inhibitor) 7.5 or 15 mg/day or placebo for 84 days	TBR_{max} index vessel	None in TBR_{max} index, whereas -5% in $TBR_{active\ segment}$ index in low and high dose group
Tawakol et al. 2013	67 patients with (risk factors for) atherosclerosis	Carotid, aorta	$TBR_{mds} \geq 1.60$	Atorvastatin 10 or 80 mg/day for 3 months	TBR_{mds} index vessel	-14.42% in 80mg group
Van Wijk et al. 2014	24 patients with familial hypercholesterolemia	Carotid, aorta	na	Lipid apheresis for 8 weeks	TBR_{mds} index vessel	-11.8%

TABLE S1. Continued

First author and reference	Study population	Arterial segments analyzed	PET as selection criterion	Intervention	Primary endpoint	Observed %change
Tawakol et al. 2014	71 patients with stable atherosclerosis	Carotid, aorta	na	Rilapladib 250 mg/day or placebo for 3 months	TBR_{max} index vessel	None
Van der Valk et al. 2015	30 patients with atherosclerosis	Carotid	TBR_{max} ≥2.20	2 infusions with liposomal prednisolone or placebo, readout after 12 days	Carotid TBR_{max}	+7%
Kootte et al. 2015	7 patients with genetically determined low HDL	Carotid	na	Infusions with apoA-I-containing HDL-mimetic for 6 months	TBR_{max} index vessel	-8.9%
Emami et al. 2015	72 patients with atherosclerosis	Carotid, aorta	TBR_{max} ≥1.60	BMS-582949 (p38MAPK inhibitor) 100 mg/day, atorvastatin 80 mg/day or placebo for 12 weeks	TBR_{max} index vessel	None for BMS-582949, whereas -6% for atorvastatin group
Gaztanaga et al. 2016	52 patients with ACS 1-3 months, 45 completed	Carotid, aorta	na	VIA-2291 (5-LO inhibitor) 100mg/day or placebo for 24 weeks	TBR_{max} index vessel	None

HDL-c indicates high-density lipoprotein cholesterol; na, not applicable; SUV, standardized uptake values; TBR, target to background ratio.

TABLE S2. Additional arterial wall ^{18}F-FDG uptake metrics

	Healthy control subjects	Patients at increased CVD risk	Patients with known CVD	P-value*
Remote arterial background SUV_{mean}				
Brachiocephalic arteries	1.04 ± 0.11	1.00 ± 0.14	1.01 ± 0.17	ns
Descending aorta	0.96 ± 0.13	0.96 ± 0.16	1.02 ± 0.21	ns
Arterial wall SUV – Remote arterial background SUV				
Carotid arteries	0.45 ± 0.21	0.78 ± 0.24	0.88 ± 0.29	<0.001
Aorta	1.01 ± 0.20	1.34 ± 0.25	1.61 ± 0.44	<0.001
TBR_{mean} §				
Carotid arteries	1.37 ± 0.18	1.55 ± 0.20	1.69 ± 0.29	<0.001
Aorta	1.82 ± 0.28	2.08 ± 0.30	2.20 ± 0.36	<0.001
$TBR_{most\ diseased\ segment}$ §				
Carotid arteries	1.63 ± 0.25	2.00 ± 0.36	2.18 ± 0.35	<0.001
Aorta	2.44 ± 0.28	2.93 ± 0.44	3.07 ± 0.61	<0.001

Multivariate analysis adjusted for age, gender, hypertension, smoking, body mass index, statin use, lipid profile and glucose. § TBR = arterial wall SUV_{max} / Venous background SUV_{mean}. *MDS indicates most diseased segment; TBR, target to background ratio; CVD, cardiovascular disease.*

TABLE S3. Active segment analysis in study groups

		Healthy control subjects	Patients at increased CVD risk	Patients with known CVD	P-value*
Carotid arteries	**Active defined as**				
	Active defined as ≥1.80	26% of subjects	86% of patients	93% of patients	
	$\%_{active\ slices}$	14 ± 26%	64 ± 32%	78 ± 66%	0.005
	$TBR_{active\ slices}$	1.96 ± 0.09	2.10 ± 0.27	2.19 ± 0.27	ns
	Active defined as ≥2.20	14% of subjects	63% of patients	79% of patients	
	$\%_{active\ slices}$	5 ± 14%	42 ± 41%	51 ± 40%	0.044
	$TBR_{active\ slices}$	2.09 ± 0.07	2.27 ± 0.20	2.28 ± 0.22	ns
Ascending aorta	**Active defined as**				
	Active defined as ≥2.60	76% of subjects	95% of patients	96% of patients	
	$\%_{active\ slices}$	75 ± 22%	80 ± 29%	83 ± 24%	ns
	$TBR_{active\ slices}$	2.85 ± 0.11	3.10 ± 0.31	3.10 ± 0.49	ns
	Active defined as ≥2.80	63% of subjects	74% of patients	80% of patients	
	$\%_{active\ slices}$	25 ± 33%	47 ± 48%	52 ± 46%	ns
	$TBR_{active\ slices}$	2.92 ± 0.08	3.17 ± 0.26	3.34 ± 0.37	0.015

* Multivariate analysis adjusted for age, gender, hypertension, smoking, body mass index, statin use, lipid profile and glucose. *TBR indicates target to background ratio; CVD, cardiovascular disease.*

TABLE S4. ^{18}F-FDG uptake criterion values for a 95% tolerance interval

Artery	Metric	Threshold*	Percentage above threshold	
			Patients at increased CVD risk	Patients with known CVD
Carotid	SUV_{max}	> 1.95	22%	43%
	TBR_{max}	> 1.93	43%	43%
Aorta	SUV_{max}	> 2.49	35%	51%
	TBR_{max}	> 2.77	50%	62%

* Thresholds were determined using the 95th percentile value observed in the healthy control subjects. *TBR indicates target to background ratio; CVD, cardiovascular disease.*

TABLE S5. Intra- and inter-observer agreement for TBR_{max}

	Carotid arteries	Aorta
Intra-observer		
Paired diff between read 1A and 1B	0.01 ± 0.05	0.02 ± 0.05
COV	2.7%	1.8%
Intra ICC [CI]	0.99 [0.98 – 1.00]	0.99 [0.99 – 1.00]
Inter-observer		
Paired diff between read 1A and 2	0.03 ± 0.11	0.07 ± 0.14
COV	6.0%	5.2%
Inter ICC [CI]	0.96 [0.93 – 0.97]	0.97 [0.96 – 0.99]

CI indicates confidence interval; COV, coefficient of variation; diff, difference; ICC, intraclass correlation coefficient; TBR, target to background ratio.

TABLE S6. Interscan agreement for ^{18}F-FDG uptake metrics

	Paired difference	COV	Interscan ICC [CI]
Arterial wall SUV	0.01 ± 0.08	3.0%	0.93 [0.73-0.98]
Venous background SUV	0.05 ± 0.05	5.5%	0.96 [0.81-0.99]
Remote arterial background SUV	0.06 ± 0.05	4.9%	0.93 [0.73-0.98]
Arterial wall SUV – Venous background SUV	0.03 ± 0.06	3.5%	0.93 [0.80-0.98]
Arterial wall SUV – Remote arterial background SUV	0.03 ± 0.07	4.3%	0.95 [0.78-0.94]
TBR§	0.02 ± 0.06	2.9%	0.98 [0.92-1.00]

§ TBR = arterial wall SUV_{max} / Venous background SUV_{mean}. *CI indicates confidence interval; COV, coefficient of variation; diff, difference; ICC, intraclass correlation coefficient; TBR, target to background ratio.*

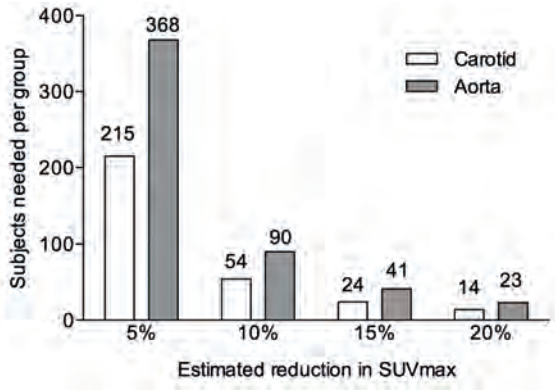

FIGURE S1. Estimated sample sizes for vascular intervention studies using SUV_{max}

Sample sizes, dependent on estimated drug effect (5-20%) and target vessel (carotid or aorta), required for studies using SUV_{max} as the primary endpoint are approximately 20-45% higher compared with TBR_{max} as an endpoint (see Figure 3 in main manuscript). *SUV indicates standardized uptake values; TBR, target to background ratio.*

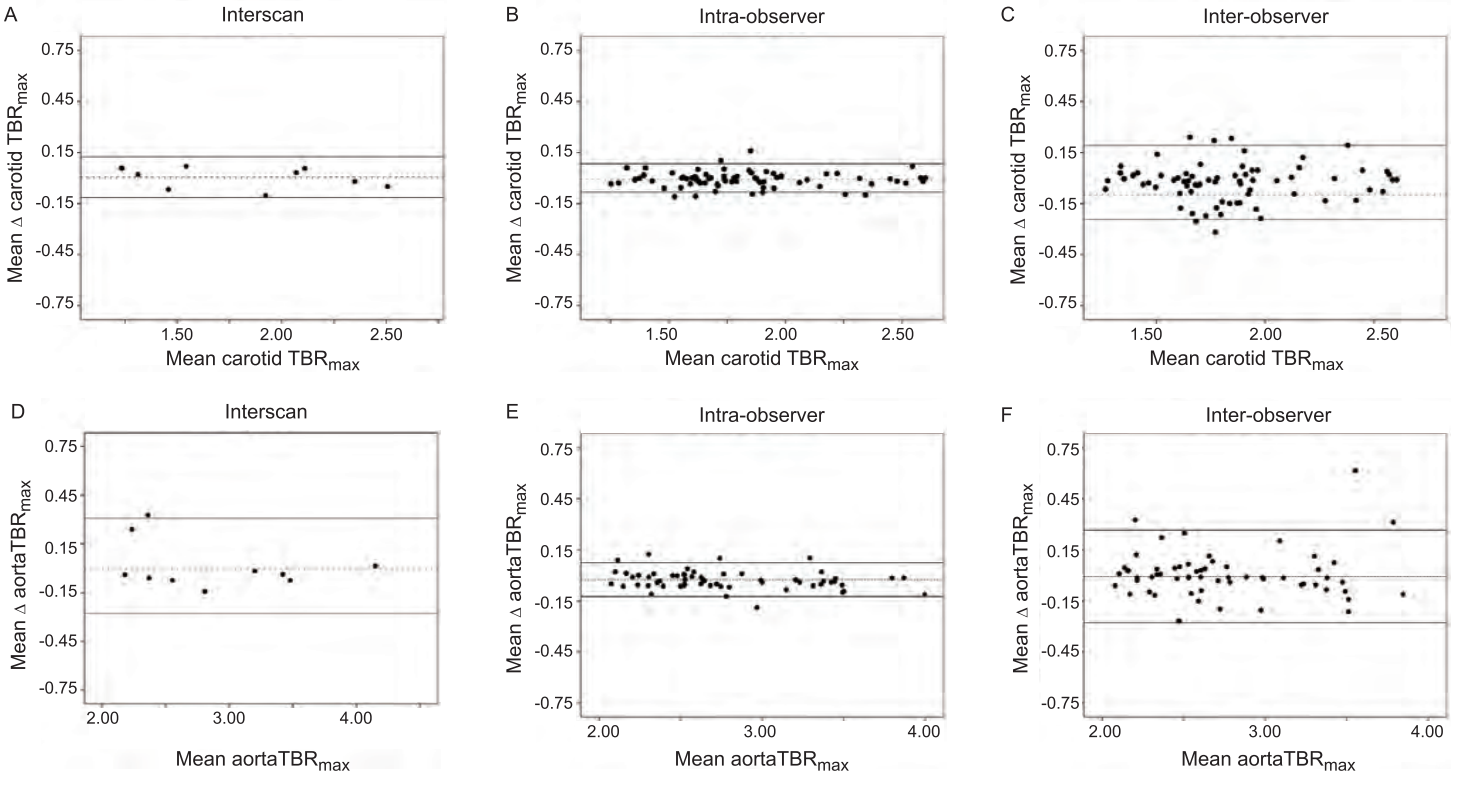

FIGURE S2. Bland-Altman plots for scan and observer agreement

Bland-Altman plots display no fixed or proportional bias for TBR_{max} in interscan, intra- and inter-observer agreement as shown for the carotids (**A-C**) and aorta (**D-F**). *TBR indicates target to background ratio.*

CHAPTER 3

IN VIVO IMAGING OF ENHANCED LEUKOCYTE ACCUMULATION IN ATHEROSCLEROTIC LESIONS IN HUMANS

Van der Valk FM, Kroon J, Potters WV, Thurlings RM, Bennink RJ, Verberne HJ, Nederveen AJ, Nieuwdorp M, Mulder WJ, Fayad ZA, van Buul JD, Stroes ESG

J Am Coll Cardiol. 2014;64:1019-29

ABSTRACT

Rationale: Understanding how leukocytes contribute to atherogenesis is crucial for our conception of atherosclerosis development and the identification of potential therapeutic targets. This study evaluates an in vivo imaging approach to visualize peripheral blood mononuclear cell (PBMCs) accumulation in atherosclerotic lesions in cardiovascular patients using single-photon emission computed tomography (SPECT/CT).

Methods and Results: At baseline, cardiovascular patients and healthy controls underwent ^{18}fluorodeoxyglucose positron emission tomography-computed tomography (^{18}F-FDG PET/CT) and magnetic resonance imaging (MRI) to assess arterial wall inflammation and dimensions, respectively. For *in vivo* trafficking, autologous PBMCs were isolated, labeled with technetium-99m and visualized 3, 4.5 and 6 hours post-infusion (pi) with SPECT/CT.

Ten cardiovascular patients and 5 healthy controls were included. Patients had an increased arterial wall inflammation (target-to-background-ratio (TBR) right carotid 2.00±0.26 in patients versus 1.51±0.12 in controls, p=0.022) and atherosclerotic burden (normalized wall index (NWI) 0.52±0.09 in patients versus 0.33±0.02 in controls, p=0.026). Elevated PBMCs accumulation in the arterial wall was observed in patients; for the right carotid the arterial-wall-to-blood-ratio (ABR) 4.5 hours pi was 2.13±0.35 in patients versus 1.49±0.40 in controls (p=0.038). In patients, the ABR correlated with the TBR of the corresponding vessel (for the right carotid: r=0.88, p<0.001).

Conclusion: PBMCs accumulation is markedly enhanced in patients with advanced atherosclerotic lesions and correlates with disease severity. This study provides a noninvasive imaging tool to validate the development and implementation of interventions targeting leukocytes in atherosclerosis.

INTRODUCTION

Atherosclerosis is a chronic low-grade inflammatory disease, which remains subclinical over decades prior to the acute onset of major cardiovascular (CV) events such as myocardial infarction and stroke[1]. Leukocytes are key cellular effectors in atherosclerosis, mediating pro-inflammatory processes throughout all stages of atherogenesis[2]. Following the increased expression of adhesion molecules by activated endothelial cells[3], monocytes -among other leukocytes- are recruited to these early atherosclerotic lesions[4], leading to initiation or accelerated progression of atherogenesis[5]. In support of a causal role of increased monocyte influx in experimental atherogenesis, attenuation of monocyte recruitment pathways by a variety of pharmacologic interventions has been shown to markedly attenuate atherosclerosis[6-9]. Although fewer in number, T cells also reside in the atherosclerotic lesions and contribute to the inflammatory response[10]. Absence of T cells in an atherosclerotic mouse model results in reduced atherosclerosis, indicating that T cells constitute a proatherogenic cell population[11]. In humans, a high white blood cell count correlates with the risk of a CV event both after a recent acute event[12] as well as in stable disease[13], suggesting that elevated levels of circulating leukocytes represent an expanded pool of inflammatory cells available to promote disease progression. In line, several risk factors for atherosclerosis have been associated with an increased activation state of circulating monocytes[14-16]. Nonetheless, data on the *in vivo* dynamics of leukocytes in human atherogenesis, as well as experience with strategies targeting leukocytes in CV prevention and treatment, are scarce.

Several imaging methods have emerged to quantify the inflammatory activity within atherosclerotic lesions, including ^{18}fluorodeoxyglucose positron emission tomography-computed tomography (^{18}F-FDG PET/CT) to assess arterial wall metabolic activity as an index of macrophage content[17] and iron oxide-enhanced magnetic resonance imaging (MRI) to quantify plaque macrophages[18]. These techniques, however, lack the ability to address the *in vivo* dynamics of leukocytes.

Understanding how leukocytes participate in the course of atherogenesis is pivotal for our understanding of the development of atherosclerotic lesions, and could aid in identifying potential therapeutic targets. In the present proof-of-concept study, we used single photon emission computed tomography (SPECT/CT) as a non-invasive imaging technique capable of visualizing the migratory behavior of technetium-99m (^{99m}Tc) labeled immune cells in humans[19]. In patients with advanced atherosclerosis, we evaluated SPECT/CT imaging to assess the accumulation of circulating peripheral blood mononuclear cells (PBMCs) into atherosclerotic plaques *in vivo*.

METHODS

Study participants and procedures

This was a single-center imaging study in patients with atherosclerotic cardiovascular disease and healthy controls. CV patients, aged ≥ 18 years of either gender, were recruited at our outpatient clinic and had to fulfill the following inclusion criteria: (i) documented history of myocardial infarction, transient ischemic attack or stroke, and (ii) stable medication for at least 6 weeks prior to study participation. Exclusion criteria included ongoing inflammatory diseases, use of systemic anti-inflammatory drugs and major renal (serum creatinine >2.0 mg/dL) or hepatic (ALT/AST >2 upper limit of normal (ULN)) dysfunction. Healthy controls were matched to the patients for age, gender and BMI, and were not eligible in case of a medical history of CVD, ongoing inflammatory diseases or the use of systemic medication. Each subject provided written informed consent. The study was approved by the local institutional review board and conducted according to the principles of the International Conference on Harmonization–Good Clinical Practice guidelines. In all subjects, we performed baseline laboratory tests including lipid and inflammatory profile, and vascular imaging, consisting of ^{18}F-FDG PET/CT, MRI and SPECT/CT for visualizing peripheral blood mononuclear cell (PBMCs) accumulation.

PBMCs isolation and labelling

In each subject, peripheral venous blood (120 ml) was drawn via an 18G intravenous (iv) line into 4 syringes (30 ml per syringe) containing 5 ml acid citrate dextrose (ACD; disodiumcitrate 3%/glucose 2.5%) and 5 ml EloHAES 6% (Fresenius Kabi, The Netherlands). On average $20{\cdot}10^6$ PBMCs were isolated using Ficoll-Paque Premium (d=1.077g/ml) density gradient centrifugation (GE Healtcare, UK). The radiolabel technetium 99m-hexamethylpropylene amine oxime (^{99m}Tc-HMPAO) was freshly prepared using a ready-for-labelling kit (Ceretec, GE Healthcare, the Netherlands). Directly after preparation, PBMCs were incubated with ^{99m}Tc-HMPAO (1100MBq/2ml) at room temperature for 10 min. Under these conditions, uptake of ^{99m}Tc-HMPAO intracellular is reached before the onset of its decomposition into the constituents, exametazime and pertechnetate, which both are unable to cross the cellular membrane, resulting in the cellular trapping of the radiotracer[20]. Excess of extracellular ^{99m}Tc-HMPAO was diluted and removed after centrifugation. Finally, radiolabelled autologous PBMCs (200 MBq) were resuspended in 3 ml EloHAES 6 prior to re-infusion into the patient.

Effects of PBMCs isolation and labelling

PBMCs migration and accumulation is a multistep process mediated by among other adhesion molecules. To assure plausible in vivo behavior of autologous labelled PBMCs, we set out to assess PBMCs behavior in terms of migratory and adhesive capacity via flow cytometry and an in vitro transendothelial migration assay[21] after isolation and labelling procedures. For flow cytometry, PBMCs were incubated with antibodies (PECy7-CD14, APC-Cy7-CD16, PerCpCy5.5-HLA-DR, APC-CD11c, APC-CD18 1:50, all BD Biosciences, CA) for 15 min and washed with PBS. Red blood cells were lysed with BD FACSTM-lysis solution (BD Biosciences, CA). Samples were analyzed by flow cytometry using a FACS Calibur (Becton Dickinson, NJ). For analysis, monocytes and their subsets were identified by CD14, CD16 and HLA-DR expression[21], and the integrins CD11c and CD18 were used as markers of adhesive capacity[23]. For the transendothelial migration assay, primary human arterial endothelial cells (HAEC, purchased from Lonza (Baltimore, MD)) were cultured on a FN-coated glass cover to confluency and stimulated overnight with TNF-α (10 ng/ml). PBMCs at a concentration of $1{\cdot}10^6$ cells/ml were added to the HAEC monolayer for 30 min at 37 °C, 5% CO2 and then fixed with 3.7% formaldehyde (Sigma-Aldrich, Zwijndrecht, the Netherlands). After fixation, multiple images were recorder with a Zeiss Axiovert 200 microscope (Plan-apochromat 10x/0.45 M27 Zeiss-objective; Carl Zeiss Inc., Jena, Germany) and analyzed using Image-J software (http://rsb.info.nih.gov/nih-image/).

Vascular imaging

^{18}F-FDG PET/CT scans were performed on a Gemini time-of-flight multi-detector helical PET/CT scanner (Philips, Best, the Netherlands) as previously described[24]. In brief, subjects fasted for at least 6 hours prior to infusion of 200 MBq of ^{18}F-FDG (5.5 mCi). After 90 min, subjects underwent PET/CT imaging initiated with a low-dose non-contrast enhanced CT for attenuation correction and anatomic co-registration. PET/CT images stripped of metadata were analyzed at the core laboratory by one blinded experienced reader (F.M.) using OsiriX (Geneva, Switzerland; http://www.osirix-viewer.com/). ^{18}F-FDG uptake was assessed in the arterial wall of the ascending aorta, left and right carotid artery, as follows. In each artery 5 ROIs were drawn, delineating the arterial wall. Maximum standardized uptake values (SUV) were averaged for each artery. The target-to-background-ratio (TBR) was calculated from the ratio of maximal arterial SUV and mean venous background activity (within the superior caval vein (correction for aorta) and the jugular vein (correction for carotids)), according to previously described methods[24,25].

MR images were obtained with a 3.0 T whole-body scanner (Ingenia, Philips Medical Systems, Best, The Netherlands), using an 8 channel dedicated bilateral carotid artery coil (Shanghai Chenguang Medical Technologies, Shanghai, China). Quantitative image analysis was performed by one blinded experienced reader at the core laboratory using semi-automated

measurement software (VesselMass, Leiden, the Netherlands). Mean wall thickness (MWT), mean wall area (MWA) and the normalized wall index (NWI= mean wall area/outer wall area) were calculated[26].

PBMCs trafficking by SPECT/CT

All subjects underwent SPECT imaging (Symbia T16, Siemens, Erlangen, Germany) with a low-dose non-contrast enhanced CT for attenuation correction and anatomic co-registration, at 3, 4.5 and 6 hours post infusion of 200 MBq ^{99m}Tc-HMPAO labelled autologous PBMCs. SPECT/CT images were analyzed using OsiriX (Geneva, Switzerland; http://www.osirix-viewer.com/) and MeVisLab (Bremen, Germany). Two experienced readers, who were offered data sets stripped of metadata on subject history and time post-infusion, analyzed the SPECT images twice at the core laboratory. Accumulation of labelled PBMCs in the arterial wall was quantified in the ascending aorta, left and right carotid artery, as follows. Anatomical landmarks were used to ensure that the same arterial segments were analyzed over time; i.e. for the carotids, one slice caudal to the bifurcation; for the ascending aorta, one slice cranial to the joining of the pulmonary arteries. In each artery 5 ROIs were drawn, delineating the arterial wall. The maximum counts in the 5 arterial wall ROIs were averaged over each artery, to derive an averaged maximum counts of the artery. To correct for the ^{99m}Tc activity in the blood, 5 venous ROIs were drawn within the superior caval vein (correction for aorta) and the jugular vein (correction for carotids), to obtain the averaged mean counts of the blood. The values provided in the present paper represent the ratio of the averaged maximum counts of the artery divided by the averaged mean counts in the blood. These values are reported as the arterial-wall-to-blood-ratio (ABR).

Statistical analysis

Baseline values and distributional characteristics are shown as mean (SD), number (frequency) or median (min-max). Independent samples t-tests, Mann-Whitney U tests and Chi-square tests were used to assess differences between patients and controls. To assess the differences over time in PBMCs accumulation a paired t-test or Wilcoxon signed-ranks test was applied. The following correlations were assessed using Pearson's or Spearman's correlation coefficient; (i) ABR at 4.5 and 6 hours for every artery, with the TBR of the corresponding artery, (ii) carotid ABR at 4.5 and 6 hours with carotid NWI, MWT, MWA, and (iii) ABR of the index vessel (highest ABR of either the left/right carotid or aorta) at 4.5 and 6 hours to non-imaging parameters. To assess interobserver variability, two readers analyzed the SPECT/CT images and intraclass correlation coefficients (ICC) with 95% confidence intervals were calculated. A two-sided *P*-value below 0.05 was considered statistically significant. All data were analyzed using Prism version 5.0 (GraphPad software, La Jolla, California) and SPSS version 19.0 (SPSS Inc., Chicago, Illinois).

RESULTS

Clinical characteristics

In total, 10 CV patients and 5 healthy control subjects were included (Table 1). The groups were balanced for age and gender. CV patients had a history of myocardial infarction (n=5), transient ischemic attack (n=2) or ischemic stroke (n=3). At baseline, traditional CV risk factors, including blood pressure, smoking and diabetes, did not significantly differ between groups (Table 1). Almost all CV patients (90%) were on stable statin therapy. Baseline laboratory analysis revealed no differences in lipid profiles between CV patients and controls (Table 1). Moreover, as a marker of systemic inflammation, there were no significant differences in white blood cell count or C-reactive protein (CRP), although CV patients did exhibit a higher level of circulating monocytes compared to control subjects (0.52 ± 0.16·10^9/L in patients versus 0.35 ± 0.06 10^9/L in controls, p= 0.013).

TABLE 1. Clinical characteristics of subjects

Characteristic	CV patients (n=10)	Control subjects (n=5)	P value
Age, y	56 ± 7	50 ± 3	ns
Gender, m (%)	7 (70)	4 (80)	ns
BMI, kg/m2	28 ± 5	28 ± 6	ns
SBP, mmHg	132 ± 12	133 ± 10	ns
DBP, mmHg	82 ± 8	82 ± 2	ns
Active smoking, yes (%)	3 (30)	0 (0)	ns
Statin use, yes (%)	9 (90%)	0 (0)	0.03
Tchol, mmol/L	5.26 ± 2.26	5.04 ± 0.19	ns
LDL-c, mmol/L	3.30 ± 2.24	3.08 ± 0.21	ns
HDL-c, mmol/L	1.37 ± 0.47	1.47 ± 0.41	ns
WBC, 10E9/L	6.93 ± 2.00	5.42 ± 0.95	ns
Monocytes, 10E9/L	0.52 ± 0.16	0.35 ± 0.06	0.01
CRP, mg/L	0.65 (0.30-10.70)	1.90 (0.30-3.60)	ns

Continuous data are shown as mean ± SD, or median [min-max], and categorical data as number (percentage). *BMI indicates body mass index; CRP, C-reactive protein; CV, cardiovascular; DBP, diastolic blood pressure; HDL-c, high density lipoprotein cholesterol; LDL-c, low density lipoprotein cholesterol; ns, not significant; SBP, systolic blood pressure; Tchol, total cholesterol; WBC, white blood cell count.*

Baseline vascular imaging confirmed that the CV patients included in the study were characterized by advanced atherosclerotic lesions (Table 2). First, MR imaging showed an increased atherosclerotic burden in the CV patients compared to healthy controls; (i) mean wall thickness (MWT) was increased (1.54 ± 0.54 in patients versus 0.64 ± 0.03, p=0.046), (ii) mean wall area (MWA) was enlarged (40.38 ± 18.15 in patients versus 14.32 ± 1.62 in controls, p=0.029) and in line, (iii) normalized wall index (NWI) was higher in patients compared with

controls (0.52 ± 0.09 versus 0.33 ± 0.02; p=0.026). Second, PET/CT imaging corroborated an enhanced target-to-background ratio (TBR) of the right carotid artery in CV patients (TBR_{max} 2.00 ± 0.26) versus controls (TBR_{max} 1.51 ± 0.12, p=0.022). Comparable differences in TBR in patients versus controls were observed in the left carotid and aorta (Table 2). Figure 1 shows representative cross-sectional MRI and PET/CT images of the right carotid artery, illustrating the atherosclerotic burden in a CV patient.

TABLE 2. Baseline vascular imaging parameters

Imaging parameter	CV patients (n=10)	Control subjects (n=5)	P value
NWI	0.52 ± 0.09	0.33 ± 0.02	0.026
MWT, mm	1.54 ± 0.54	0.64 ± 0.03	0.046
MWA, mm2	40.38 ± 18.15	14.32 ± 1.62	0.029
TBR left carotid	1.77± 0.27	1.34 ± 0.16	0.050
TBR right carotid	2.00 ± 0.26	1.51 ± 0.12	0.022
TBR aorta	2.84 ± 0.69	1.90 ± 0.14	0.003

Data shown as mean ± SD. *CV indicates cardiovascular; MWA, mean wall area; MWT, mean wall thickness; NWI, normalized wall index; TBR, target to background ratio.*

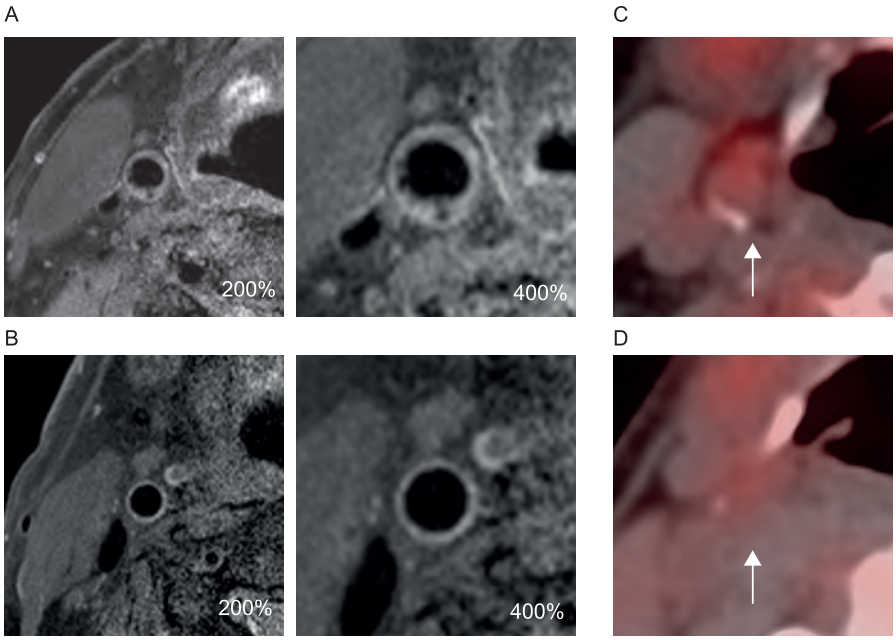

FIGURE 1. MRI and PET/CT images of the carotid artery at baseline

Representative cross-sectional MRI images of the right common carotid artery of (**A**) a CV patient and (**B**) a healthy control are shown, zoomed in 200 and 400%. Corresponding cross-sectional fused PET/CT images of the right common carotid (white arrow) are shown of (**C**) a CV patient and (**D**) healthy control. *CT indicates computed tomography; CV, cardiovascular disease; MRI, magnetic resonance imaging; PET, positron emission tomography.*

Effect of isolation and labelling

Prior to evaluating the *in vivo* behavior of PBMCs, we first assessed the effects of our isolation and labelling procedures in terms of migratory and adhesive capacity via flow cytometry and an *in vitro* transendothelial migration assay. First, the differentiation of monocytes in their pro-inflammatory, intermediate and anti-inflammatory subsets[13], respectively mon 1, mon 2 and mon 3, was not significantly affected by the isolation and labelling procedures (for mon 1: 90.67 % prior and 90.63 % after labelling procedures, p=ns; Figure 2A). Second, the expression of adhesion markers also did not change significantly. Delta MFI of CD11c was 316 ± 2 prior to labelling versus 304 ± 8 after labelling (p=ns) and ΔMFI of CD18 was 618 ± 18 prior to labelling versus 586 ± 14 after labelling (p=ns) (Figure 2B). Third, the transendothelial migration (TEM) assay corroborated that the labelling procedure did not affect the capacity of monocytes to cross the endothelial monolayer (prior to labelling 36 ± 12 versus 25 ± 3 cells/mm^2 after labelling, p=ns; Figure 2C).

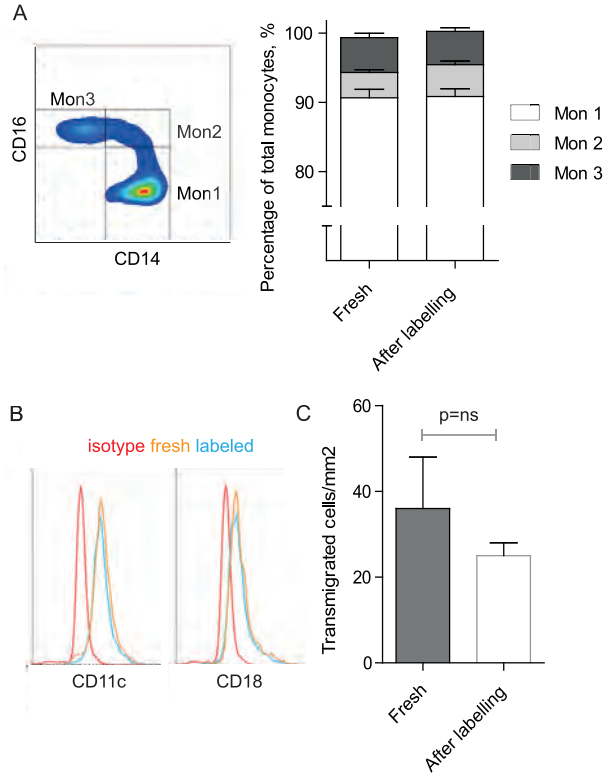

FIGURE 2. PBMCs behavior after isolation and labelling

Flow cytometry analysis showed that labelling procedures (**A**) did not significantly alter monocyte subset division and (**B**) did not significantly change the expression of adhesion markers CD11c and CD18. Transendothelial migration assays corroborated that the labelling procedure did not significantly change their migratory capability (**C**). Ns = non significant. *Mon indicates monocyte subset; PBMCs, peripheral blood mononuclear cells.*

Imaging PBMCs accumulation in atherosclerotic lesions with SPECT/CT

In all subjects, we performed SPECT/CT imaging 3, 4.5 and 6 hours post-infusion (pi) of radiolabeled autologous PBMCs. Prior to assessing the differences between groups, interobserver agreement for the SPECT/CT images reading demonstrated proper ICC of 0.87 with a narrow 95% confidence interval (0.75-0.96).

At the first time point - 3 hours pi - the arterial-wall-to-blood-ratio (ABR), representing PBMCs accumulation, although higher in patients, was not significantly different between CV patients and controls (ABR for aorta 3.68 ± 1.23 in patients versus 2.93 ± 1.37 in controls, p = ns; Figure 3A). In contrast, 4.5 and 6 hours pi, there was a significantly higher ABR in the arterial wall in patients compared to controls. For the ascending aorta, the ABR 4.5 hours pi was 5.41 ± 2.29 in patients versus 2.59 ± 0.90 in controls (p= 0.013), and 6 hours pi 8.19 ± 4.49 in patients versus 2.80 ± 1.19 in controls (p= 0.012; Figure 3A). Figure 4 depicts illustrative cross-sectional SPECT/CT images of the ascending aorta at three anatomic levels at 4.5 hours pi, showing an enhanced PBMCs accumulation in a CV patient versus a control subject. Corresponding results were found when analyzing the left and right carotid artery (Figure 3B). See Table 3 for an overview of the PBMCs accumulation at the three time points for every artery in patients versus controls.

TABLE 3. ABR and delta ABR in patients and controls

	Time pi (h)		CV patients (n = 10)	Controls (n = 5)	P value
Left carotid	3		1.44 ± 0.65	1.44 ± 0.24	0.981
	4.5		2.18 ± 1.01	1.47 ± 0.23	0.050
	6		2.57 ± 1.21	1.50 ± 0.45	0.044
		ΔABR	1.13 ± 0.72	0.07 ± 0.27	0.004
Right carotid	3		1.70 ± 0.41	1.45 ± 0.41	0.359
	4.5		2.13 ± 0.35	1.49 ± 0.40	0.038
	6		2.69 ± 0.61	1.45 ± 0.43	0.003
		ΔABR	1.00 ± 0.53	0.00 ± 0.05	0.001
Aorta	3		3.68 ± 1.23	2.93 ± 1.37	0.390
	4.5		5.41 ± 2.29	2.59 ± 0.90	0.013
	6		8.19 ± 4.49	2.80 ± 1.19	0.012
		ΔABR	4.50 ± 3.63	-0.13 ± 0.25	0.009

Data shown as mean ± SD. *Δ indicates delta; ABR, arterial wall to blood pool ratio; CV, cardiovascular; pi, post infusion.*

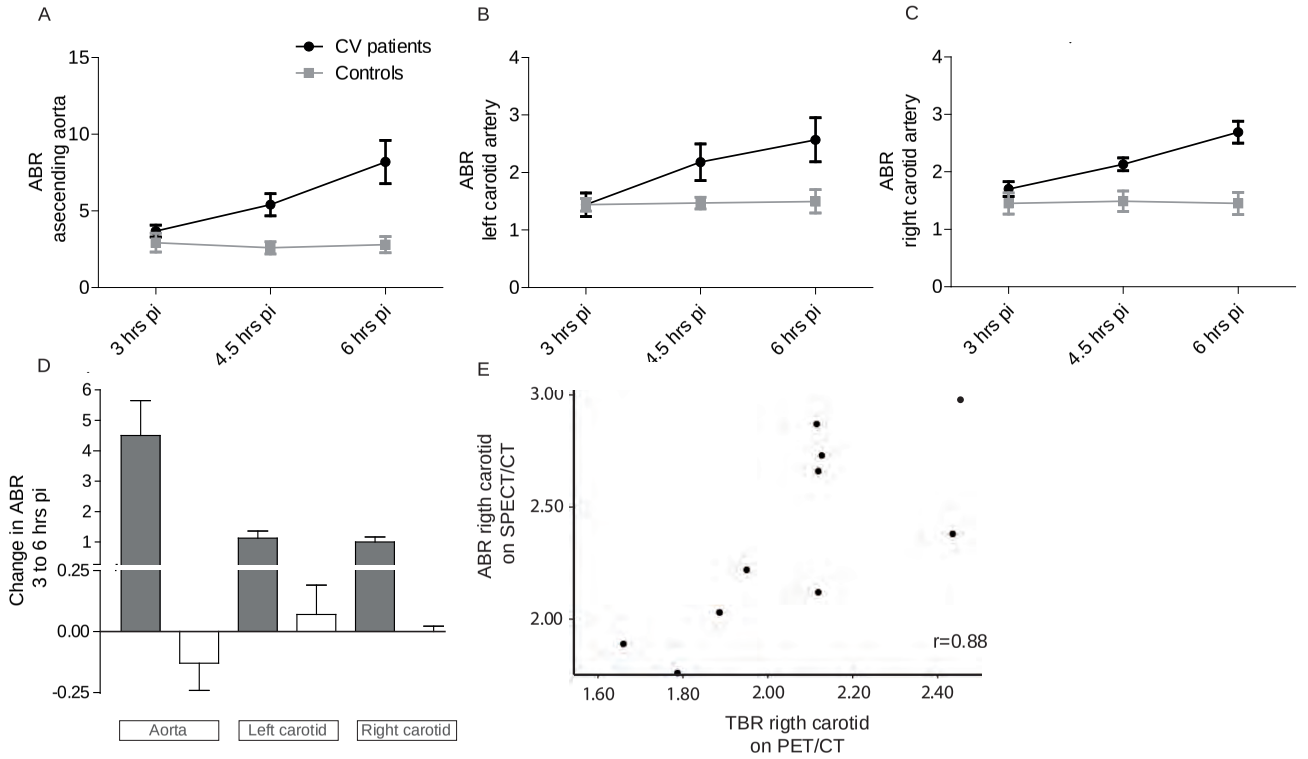

FIGURE 3. ABR of PBMCs accumulation on SPECT/CT

Line graphs showing increased signal intensities in CV patients versus control subjects in three time points at three different anatomical locations, i.e. ascending aorta (**A**), left carotid artery (**B**) and right carotid artery (**C**). The bar graphs indicate the change in signal intensity from 3 to 6 hours post-injection, showing a marked increase over time in patients versus no significant changes in control subjects (**D**). Shown here for the right carotid artery, the ABR at 4.5 hours pi correlated with the TBR assessed via PET/CT (**E**). *ABR indicates arterial wall to blood pool ratio; CT, computed tomography; CV, cardiovascular; PET, positron emission tomography; SPECT, single photon emission computed tomography; TBR, target to background ratio.*

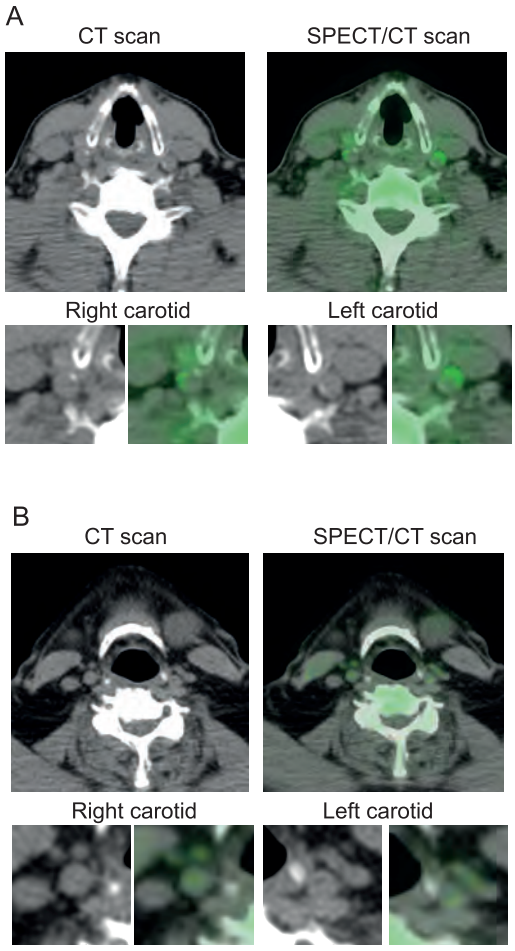

FIGURE 4. SPECT/CT of the carotids in a CV patient and control

Representative cross-sectional SPECT/CT images at 4.5 hours pi of the neck region, and zoomed in for the left and right carotid artery of (**A**) a CV patient and (**B**) a healthy control. *CT indicates computed tomography; CV, cardiovascular patient; SPECT, single photon emission computed tomography.*

Whereas from 3 to 6 hours pi the PBMCs accumulation increased significantly in patients, there was no change in ABR over time in control subjects (change in ABR from 3 to 6 hours 4.50 ± 3.63 in patients versus -0.13 ± 0.25 in controls, p=0.009; figure 3D). Figure 5 depicts representative SPECT/CT images in which the ascending aorta was segmented out and PBMCs accumulation was visualized over time, showing the increase in ABR from 3 to 4.5 pi in a typical CV patient versus no change in a control subject.

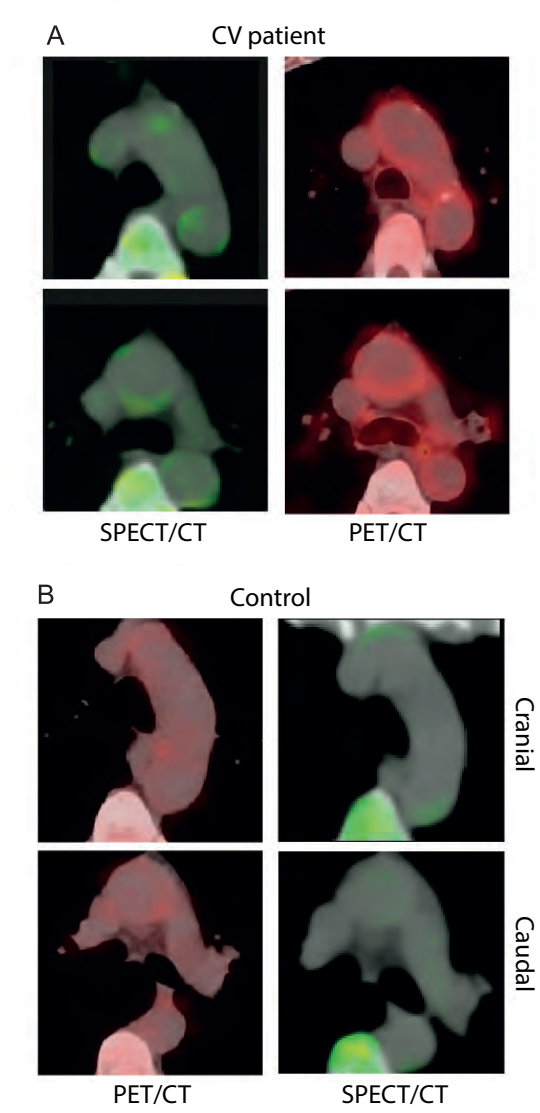

FIGURE 5. SPECT/CT and PET/CT images of the ascending aorta

Representative cross-sectional SPECT/CT at 4.5 hours pi and PET/CT images of the ascending aorta at two levels of (**A**) a CV patient and (**B**) a healthy control are shown, indicating the significant differences in both PBMCs accumulation (ABR) as arterial wall inflammation (TBR) between the CV patient and the control subject, and the correlation between ABR and TBR. *ABR indicates arterial wall to blood pool ratio; CT, computed tomography; CV, cardiovascular; PBMCs, peripheral blood mononuclear cells; PET, positron emission tomography; SPECT, single photon emission computed tomography; TBR, target to background ratio.*

Correlation between PBMCs accumulation and disease severity

In patients, the ABR (PBMCs accumulation) as measured with SPECT/CT correlated with the TBR (arterial wall inflammation) of the corresponding vessel assessed via PET/CT. For the right carotid, both the ABR at 4.5 and at 6 hours pi correlated with the right carotid artery TBR (r=0.76, p=0.007 and r=0.88, p=0.014, respectively). Figure 3E shows the correlation of ABR at 4.5 hours pi with the TBR of the right carotid. Moreover, the change in ABR from 3 to 6 hours pi in the right carotid artery also correlated with TBR (r=0.79, p=0.011). In line, in the left carotid artery and ascending aorta the ABR also correlated with TBR, as shown in Table 4. Figure 4 shows cross-sectional SPECT/CT images at 4.5 hours pi with corresponding PET/CT images of the ascending aorta at three anatomic levels, indicating (i) the significant differences between a CV patient and a control subject, and (ii) the correlation between ABR and TBR. No significant correlations were found between ABR and arterial wall dimensions as assessed with MRI (Table 4). Besides, no correlation between circulating immune cells and PBMCs accumulation was observed (for circulating monocytes r=0.15, p=ns), whereas, the level of CRP did correlate with PBMCs accumulation in the arterial wall (r=0.76, p=0.030). For the classical CV risk factors, total cholesterol and LDL-c also correlated to the change in ABR over time (r=0.72, p=0.044 and r=0.77, p=0.027, respectively).

TABLE 4. Correlation between PBMCs accumulation and arterial wall dimensions (MRI) or inflammation (PET/CT)

		ABR 4.5h pi	p-value	ABR 6h pi	p-value	ΔABR 3-6h pi	p-value
PET/CT							
	TBR left carotid	0.67	0.049	0.69	0.042	0.78	0.012
	TBR right carotid	0.76	0.007	0.881	<0.001	0.79	0.011
	TBR aorta	0.72	0.028	0.52	0.150	0.53	0.142
MRI							
	NWI	0.70	0.125	0.74	0.09	0.52	0.292
	MWT	0.67	0.145	0.72	0.107	0.51	0.303
	MWA	0.68	0.140	0.72	0.106	0.51	0.299

Data show correlation coefficients. *Δ indicates delta; ABR, arterial wall to blood pool ratio; MWA, mean wall area; MWT, mean wall thickness; MRI, magnetic resonance imaging; NWI, normalized wall index; PET/CT, positron emission tomography with computed tomography; pi, post infusion; TBR, target to background ratio.*

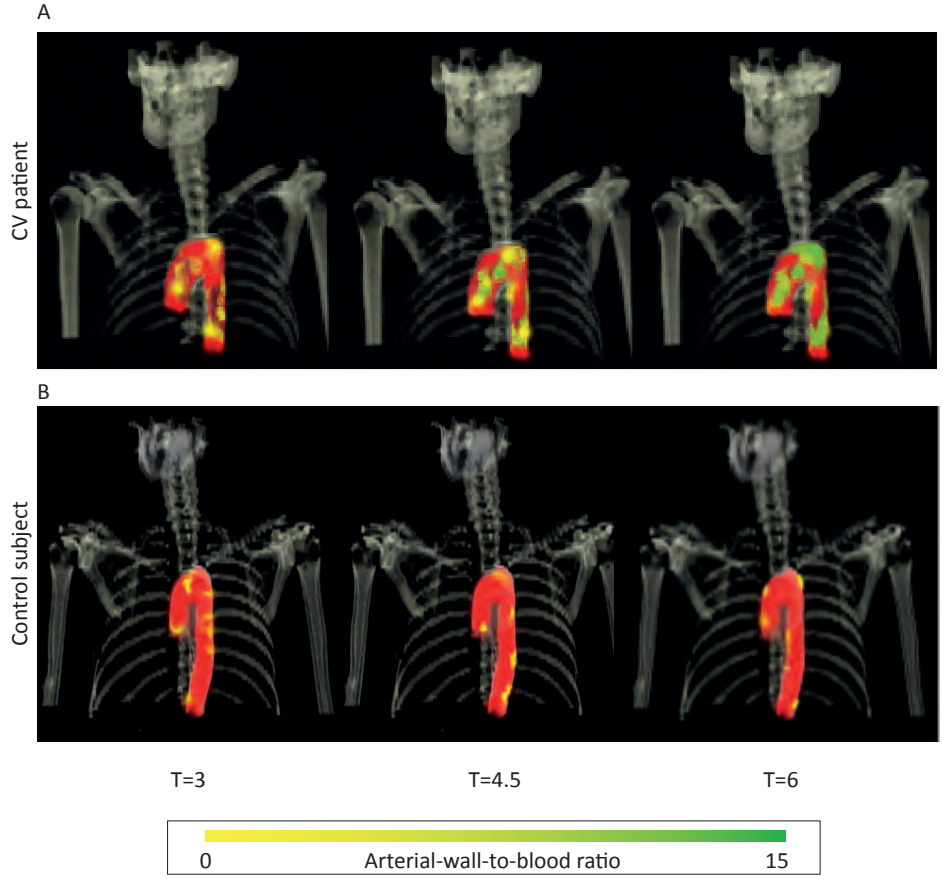

FIGURE 6. PBMCs accumulation over time portrayed with SPECT/CT

SPECT/CT images to guide the eye, in which the ascending aorta was segmented out (shown in red) to visualize the significant increase in PBMCs accumulation from 3 to 4.5 and 6 hours post-infusion in (**A**) the CV patient versus (**B**) no increase in the control subject. *CT indicates computed tomography; CV, cardiovascular; PBMCs, peripheral blood mononuclear cells; SPECT, single photon emission computed tomography.*

DISCUSSION

In the present proof-of-concept study we demonstrate that *in vivo* SPECT/CT imaging is able to detect PBMCs accumulation in the arterial wall, showing a marked increase in PBMCs accumulation over time in patients with overt atherosclerotic disease in absence of such a signal in control subjects. The degree of PBMCs accumulation in the arterial wall correlated to the degree of arterial wall inflammation as assessed with PET/CT. Moreover, PBMCs accumulation was correlated with established CV risk factors comprising LDL-c and CRP. These preliminary data lend further support to strategies aimed at attenuating leukocyte recruitment as a therapeutic target in CV patients.

Dissecting how leukocytes participate in atherogenesis is challenging due to their dynamics and functional heterogeneity[4]. In the present study, we observed marked and rapid PBMCs accumulation in atherosclerotic lesions in humans. In support, several experimental models corroborated active monocyte accumulation in the course of atherogenesis[27,28], which was proportional to the atherosclerotic burden[29]. Notwithstanding the presence of active leukocyte recruitment in atherogenesis[30], the biological fate of extravasated leukocytes remains less defined[31]. In early lesions, leukocytes are recruited via activated endothelium and infiltrate the arterial wall, giving rise to the initial pool of tissue descendants including macrophages and T cells[32]. However in advanced lesions, the contribution of freshly infiltrated monocytes to the macrophage content has been suggested to be less significant[33], following the observation that local proliferation may in fact be the major source of lesional macrophages in experimental atherosclerosis[34]. The latter, however, does not indemnify the importance of leukocyte recruitment in advanced atherosclerosis[35]. Integrating the data suggests that in early lesions freshly recruited cells contribute to the subintimal inflammatory cell burden, whereas in more advanced lesions continuous leukocyte influx propagates inflammation, eventually promoting plaque vulnerability[5,36] and the risk of a (recurrent) CV event[38]. In fact, circulating leukocytes of CV patients already exhibit a distinct functional phenotype, which is proportional to the CV event rate[12,13] and potentially mediated via alterations of the epigenome[14-16].

In the present study, we observed several correlations between CV risk factors and PBMCs accumulation. First, PBMCs accumulation correlated with ^{18}F-FDG uptake in the corresponding vessel as assessed with PET/CT. In turn, arterial wall ^{18}F-FDG uptake has been correlated to plaque macrophage content[24,37] and the risk of a recurrent CV event[38]. Second, PBMCs accumulation also correlated to the level of plasma CRP, a marker of systemic inflammation which is also correlated to CV risk[39]. Another correlation was observed between PBMCs accumulation and LDL-c, which may have several explanations. First, patients with higher LDL-c may have a higher atherosclerotic disease burden and hence higher PBMCs influx. However, we did not observe a correlation between PBMCs accumulation and arterial wall dimensions (i.e. NWI, MWA, MWT) as assessed with MRI. Alternatively, higher levels of circulating LDL-c

may lead to the activation of leukocytes and increased arterial wall PBMCs influx. In support, monocytes in hyperlipidemic conditions have an increased expression of adhesion makers[40] and are more avidly recruited to the atherosclerotic lesion[29,30]. Overall, these data imply that increased PBMCs recruitment is involved in disease progression in patients with advanced atherosclerotic lesions.

The present approach of PBMCs imaging with SPECT/CT merits some considerations. A confounding variable in our findings is the potential in vitro PBMCs activation by the labelling procedures. However, in vitro flow cytometry and transendothelial migration assays did not show marked PBMCs activation regarding adhesive capacity by the labelling procedures. In support, the infusion of labelled PBMCs was not associated with an increased ABR in healthy controls. Second, the current technique could be refined by applying more sophisticated isolation procedures allowing to specifically study subpopulations of leukocytes. Extensive ex vivo procedures, however, could change the in vivo behaviour of the leukocytes prior to re-infusion. Third, our current approach is not capable of quantifying leukokinetics in terms of continuous recruitment, influx, differentiation and efflux or apoptosis. If recruited cells rapidly undergo apoptosis, this may lead to loss of radiotracer and an underestimation of the SPECT signal. Fourth, since we performed three SPECT scans in series we chose a low-dose non-contrast CT for attenuation correction and co-registration. Increasing the CT dose or infusing a contrast agent prior to scanning could provide greater anatomic and radiotracer signal detail. However, this will invariably increase the radiation burden. Moreover, we used ^{99m}Tc as a radiotracer, which has a half-life for gamma emission of 6 hours, thereby allowing rapid data collection and limiting radiation exposure. Applying a radiotracer with a longer half-life, such as ^{111}Indium (half-life 2.8 days) for SPECT or a positron emitter like ^{89}Zirconium (half-life 3.3 days) for PET, would enable to study the trafficking of leukocytes for longer periods of time. However, both a higher radiation exposure for the patient, as extension of the time of scanning would compromise the utility of the current imaging approach for future clinical studies.

In an attempt to silence the inflammatory activity of the plaque, therapeutic interventions targeting leukocytes could act at multiple levels, i.e. modulation of circulating leukocytes, reduction of recruitment and adhesion, and changes in differentiation, survival or emigration of leukocytes. Regarding recruitment and adhesion, alteration in the expression of the adhesion molecule VCAM-1[41] and chemotactic factors amongst which CCR2[6,7] and its ligand MCP-1[8,9], or combined inhibition of MCP-1, CX3CR1, and CCR5[42] favorably affects plaque size and progression in experimental models. To date, however, interventions in these pathways in patients have not been shown to contribute to a clinical benefit[43,33]. Notwithstanding, our current observation of active and rapid PBMCs accumulation in patients with advanced atherosclerotic disease lends further support to the targeting of leukocytes as a promising strategy against atherogenesis[45]. Our presented approach of in vivo leukocyte trafficking with SPECT/CT imaging could be applied to study mechanistic hypotheses in humans, as well as

provide early insights in the efficacy of interventions targeting leukocytes in CV patients.

In conclusion, we present an imaging approach to visualize leukocyte migration to atherosclerosis in humans and demonstrate an increased PBMCs accumulation in patients with advanced atherosclerosis. Current proof-of-concept data supports efforts to develop and implement intervention strategies targeting leukocytes to modulate the inflammatory processes in atherosclerosis.

Acknowledgments: We would like to thank G.M. Dallinga-Thie for lab advice and W.M. de Jong for assistance with SPECT/CT.

Disclosures and funding: This study was supported by a Dutch Heart Foundation grant (CVON-2011/B-019: GENIUS), a Dutch Technology Foundation grant (STW CARISMA 11629) and an educational grant of BMS (New York, US; study ID: CV197-006).

REFERENCES

1. Nahrendorf M and Swirski FK. Monocyte and macrophage heterogeneity in the heart. Circ Res 2013;112:1624-1633.
2. Weber C et al. The multifaceted contributions of leukocyte subsets to atherosclerosis: lessons from mouse models. Nat Rev Immunol 2008;8:802-815.
3. Galkina E and Ley K. Vascular adhesion molecules in atherosclerosis. Arterioscler Thromb Vasc Biol 2007;27:2292-2301.
4. Ley K et al. Monocyte and macrophage dynamics during atherogenesis. Arterioscler Thromb Vasc Biol 2011;31:1506-1516.
5. Dutta P et al. Myocardial infarction accelerates atherosclerosis. Nature 2012;487:325-329.
6. Leuschner F et al. Therapeutic siRNA silencing in inflammatory monocytes in mice. Nat Biotechnol 2011;29:1005-1010.
7. Okamoto M et al. A novel C-C chemokine receptor 2 antagonist prevents progression of albuminuria and atherosclerosis in mouse models. Biol Pharm Bull 2012;35:2069-2074.
8. Peters W and Charo IF. Involvement of chemokine receptor 2 and its ligand, monocyte chemoattractant protein-1, in the development of atherosclerosis: lessons from knockout mice. Curr Opin Lipidol 2001;12:175-180.
9. Potteaux S et al. Suppressed monocyte recruitment drives macrophage removal from atherosclerotic plaques of Apoe-/- mice during disease regression. J Clin Invest 2011;121:2025-2036.
10. Hansson GK and Hermansson A. The immune system in atherosclerosis. Nat Immunol 2011;12:204-212.
11. Zhou X et al. Lesion development and response to immunization reveal a complex role for CD4 in atherosclerosis. Circ Res 2005;96:427-434.
12. Sabatine MS et al. Relationship between baseline white blood cell count and degree of coronary artery disease and mortality in patients with acute coronary syndromes: a TACTICS-TIMI 18 substudy. J Am Coll Cardiol 2002;40:1761-1768.
13. Rogacev KS et al. CD14++CD16+ monocytes independently predict cardiovascular events: a cohort study of 951 patients referred for elective coronary angiography. J Am Coll Cardiol 2012;60:1512-1520.
14. Bekkering S et al. Trained innate immunity and atherosclerosis. Curr Opin Lipidol 2013;24:487-492.
15. Stenvinkel P et al. Impact of inflammation on epigenetic DNA methylation - a novel risk factor for cardiovascular disease? J Intern Med 2007;261:488-499.
16. Wierda RJ et al. Epigenetics in atherosclerosis and inflammation. J Cell Mol Med 2010;14:1225-1240.
17. Wu C et al. PET imaging of inflammation biomarkers. Theranostics 2013;3:448-466.
18. Trivedi RA et al. Identifying inflamed carotid plaques using in vivo USPIO-enhanced MR imaging to label plaque macrophages. Arterioscler Thromb Vasc Biol 2006;26:1601-1606.
19. Herenius MM et al. Monocyte migration to the synovium in rheumatoid arthritis patients treated with adalimumab. Ann Rheum Dis 2011;70:1160-1162.
20. Van Hemert FJ et al. Labeling of autologous monocytes with 99mTc-HMPAO at very high specific radioactivity. Nucl Med Biol 2007;34:933-938.
21. Van Rijsel RJ et al. The Rho-guanine nucleotide exchange factor Trio controls leukocyte transendothelial migration by promoting docking structure formation. Mol Biol Cell 2012;23:2831-2844.
22. Abeles RD et al. CD14, CD16 and HLA-DR reliably identifies human monocytes and their subsets. Cytometry A 2012;81:823-834.
23. Gower RM et al. CD11c/CD18 expression is upregulated on blood monocytes during hypertriglyceridemia and enhances adhesion to vascular cell adhesion molecule-1. Arterioscler Thromb Vasc Biol 2011;31:160-166.
24. Rudd JH et al. (18)Fluorodeoxyglucose positron emission tomography imaging of atherosclerotic plaque inflammation is highly reproducible: implications for atherosclerosis therapy trials. J Am Coll Cardiol 2007;50:892-896.
25. Rudd JH et al. Relationships among regional arterial inflammation, calcification, risk factors, and biomarkers: a prospective fluorodeoxyglucose positron-emission tomography/computed tomography imaging study. Circ Cardiovasc Imaging 2009;2:107-115.
26. Duivenvoorden R et al. In vivo quantification of carotid artery wall dimensions: 3.0-Tesla MRI versus B-mode ultrasound imaging. Circ Cardiovasc Imaging 2009;2:235-242.

27. Ye YX et al. Monitoring of monocyte recruitment in reperfused myocardial infarction with intramyocardial hemorrhage and microvascular obstruction by combined fluorine 19 and proton cardiac magnetic resonance imaging. Circulation 2013;128:1878-1888.
28. Kircher MF et al. Noninvasive in vivo imaging of monocyte trafficking to atherosclerotic lesions. Circulation 2008;117:388-395.
29. Swirski FK et al. Monocyte accumulation in mouse atherogenesis is progressive and proportional to extent of disease. Proc Natl Acad Sci U S A 2006;103:10340-10345.
30. Galkina E and Ley K. Leukocyte influx in atherosclerosis. Curr Drug Targets 2007;8:1239-1248.
31. Yona S et al. Fate mapping reveals origins and dynamics of monocytes and tissue macrophages under homeostasis. Immunity 2013;38:79-91.
32. Libby P et al. Progress and challenges in translating the biology of atherosclerosis. Nature 2011;473:317-325.
33. Stoneman V et al. Monocyte/macrophage suppression in CD11b diphtheria toxin receptor transgenic mice differentially affects atherogenesis and established plaques. Circ Res 2007;100:884-893.
34. Robbins CS et al. Local proliferation dominates lesional macrophage accumulation in atherosclerosis. Nat Med 2013;19:1166-1172.
35. Yla-Herttuala S et al. Stabilization of atherosclerotic plaques: an update. Eur Heart J 2013;34:3251-3258.
36. Kataoka Y et al. Myeloperoxidase levels predict accelerated progression of coronary atherosclerosis in diabetic patients: Insights from intravascular ultrasound. Atherosclerosis 2014;232:377-383.
37. Menezes LJ et al. Investigating vulnerable atheroma using combined (18)F-FDG PET/CT angiography of carotid plaque with immunohistochemical validation. J Nucl Med 2011;52:1698-1703.
38. Marnane M et al. Carotid plaque inflammation on 18F-fluorodeoxyglucose positron emission tomography predicts early stroke recurrence. Ann Neurol 2012;71:709-718.
39. Ridker PM et al. Relation of baseline high-sensitivity C-reactive protein level to cardiovascular outcomes with rosuvastatin in JUPITER. Am J Cardiol 2010;106:204-209.
40. Mosig S et al. Different functions of monocyte subsets in familial hypercholesterolemia: potential function of CD14+ CD16+ monocytes in detoxification of oxidized LDL. FASEB J 2009;23:866-874.
41. Cybulsky MI et al. A major role for VCAM-1, but not ICAM-1, in early atherosclerosis. J Clin Invest 2001;107:1255-1262.
42. Combadiere C et al. Combined inhibition of CCL2, CX3CR1, and CCR5 abrogates Ly6C(hi) and Ly6C(lo) monocytosis and almost abolishes atherosclerosis in hypercholesterolemic mice. Circulation 2008;117:1649-1657.
43. Tardif JC et al. Effects of succinobucol (AGI-1067) after an acute coronary syndrome: a randomised, double-blind, placebo-controlled trial. Lancet 2008;371:1761-1768.
44. Kalinowska A and Losy J. Investigational C-C chemokine receptor 2 antagonists for the treatment of autoimmune diseases. Expert Opin Investig Drugs 2008;17:1267-1279.
45. Weber C and Noels H. Atherosclerosis: current pathogenesis and therapeutic options. Nat Med 2011;17:1410-1422.

CHAPTER 4

INCREASED HEMATOPOIETIC ACTIVITY IN PATIENTS WITH ATHEROSCLEROSIS

Van der Valk FM, Kuijk C, Verweij SL, Stiekema LCA, Kaiser Y, Zeerleder S, Nahrendorf M, Voermans C and Stroes ESG

Accepted in European Heart Journal, 2016

ABSTRACT

Rationale: Experimental work posits that acute ischemic events trigger hematopoietic activity, driving monocytosis and atherogenesis. Considering the chronic low-grade inflammatory state in atherosclerosis, we hypothesized that hematopoietic hyperactivity is a persistent feature in cardiovascular disease (CVD). Therefore, we aimed to assess the activity of hematopoietic organs and hematopoietic stem and progenitor cells (HSPCs) in humans.

Methods and Results: First, we performed ^{18}fluorodeoxyglucose positron emission tomographic (^{18}F-FDG PET) imaging in 26 patients with stable atherosclerotic CVD (ischemic event >12 months ago), and 25 matched controls. In splenic tissue, ^{18}F-FDG uptake was 2.68±0.65 in CVD patients versus 1.75±0.54 in controls (1.6-fold higher; p<0.001), and in bone marrow 3.20±0.76 versus 2.72±0.46 (1.2-fold higher; p=0.003), closely related to low-density-lipoprotein cholesterol levels (LDL-c, r=0.72). Subsequently, we determined progenitor potential of HSPCs harvested from 18 patients with known atherosclerotic CVD, and 30 matched controls; both groups were selected from a cohort of cancer patients undergoing autologous stem cell transplantation. In CVD patients, the normalized progenitor potential, expressed as the number of colony forming units-granulocyte/monocyte (CFU-GM) colonies/ CD34$^+$ cell, was 1.6-fold higher compared with matched controls (p<0.001). Finally, we assessed the effects of native and oxidized lipoproteins on HSPCs harvested from healthy donors *in vitro*. HSPCs displayed a 1.5-fold increased CFU-GM capacity in co-culture with oxidized LDL *in vitro* (p=0.002), which was inhibited by blocking oxidized phospholipids via E06 (p=0.001).

Conclusion: Collectively, these findings strengthen the case for a chronically affected hematopoietic system, potentially driving the low-grade inflammatory state in patients with atherosclerosis.

INTRODUCTION

Atherosclerosis is a chronic disease of the arterial wall, in which lipoproteins and inflammation are closely intertwined[1]. Early lesions arise when, amongst other atherogenic risk factors, elevated low-density-lipoprotein (LDL) particles induce endothelial dysfunction at susceptible arterial sites. The latter allows for LDL accumulation in the intimal space followed by modification into its oxidized forms (oxLDL). In parallel, inflammatory cells, of which monocytes/macrophages are the most abundant, are recruited to the intima and form foam cells after taking up oxLDL[1]. Ultimately, these fatty streaks advance into atherosclerotic plaques, predominantly driven by low-grade inflammatory responses[1].

A unifying view posits the bone marrow as the primary site of monocyte production, however, in an inflammatory disorder, other lymphoid tissues, such as the spleen, can also produce monocytes[2,3]. In the context of atherosclerosis, murine studies showed that an acute ischemic event, such as myocardial infarction (MI) or stroke, induced the release of hematopoietic stem and progenitor cells (HSPCs) from bone marrow niches via sympathetic nervous signaling[4]. A large number of HSPCs seeded the spleen, to subsequently serve as an extramedullary production site of monocytes[5,6]. Moreover, the systemic oversupply of inflammatory monocytes aggravated pre-existing atherosclerotic lesions[4].

Recent clinical studies validated the enhanced hematopoietic activity in MI patients, proposing the acute ischemic event as its trigger[7–9]. However, while signs and symptoms of an ischemic event fade within hours to days, the low-grade inflammatory state might be chronically present in cardiovascular disease (CVD) patients, as suggested by both experimental studies showing the high turn-over of inflammatory lesional cells[6,10], and clinical imaging corroborating continuous influx of immune cells into advanced lesions[11]. Therefore, we hypothesized that hematopoietic activity is chronically enhanced in patients with atherosclerosis.

To this end, we first performed ^{18}fluorodeoxyglucose positron emission tomographic with computed tomography (^{18}F-FDG PET/CT) imaging in patients with stable atherosclerotic CVD and matched control subjects to assess the metabolic activity of both the arterial wall and hematopoietic tissues. Next, we evaluated the progenitor potential of HSPCs that had been harvested from atherosclerotic CVD patients and matched control patients, both identified from a cohort of cancer patients. Finally, we co-incubated healthy donor derived HSPCs with native and oxidized lipoproteins *in vitro* and assessed changes in progenitor potential and phenotype.

METHODS

Study subjects

All subjects provided informed consent, and studies were conducted according to the principles of the International Conference on Harmonization–Good Clinical Practice guidelines. Patients in the PET study were characterized by stable atherosclerotic CVD, which was defined as a positive history of an ischemic event >1 year ago (myocardial or cerebral infarction due to significant coronary or carotid artery stenosis, respectively) and stable medication use for >3 months prior to inclusion. In addition, patients had been diagnosed with elevated LDL cholesterol levels due to familial hypercholesterolemia (FH). For comparison, subjects matched for age, gender and BMI though without a history for CVD underwent PET imaging. In a cohort of hemato-oncological patients (n=953), we identified patients with documented atherosclerotic CVD >1 year prior to (i) the diagnosis of a malignancy and (ii) to the harvesting of HSPCs in the context of an autologous stem cell transplantation (autoSCT), and selected control patients without known CVD, matched for age, gender, BMI, and indication for autoSCT. In general, subjects with (pre)diabetes were excluded.

^{18}F-FDG PET/CT imaging

PET/CT scans were performed on a dedicated scanner (Philips, Best, the Netherlands). Subjects fasted for at least 6 hours prior to infusion of 200 MBq of ^{18}F-FDG (5.5 mCi). 90 min after ^{18}F-FDG infusion, PET imaging was initiated with a low-dose, non-contrast enhanced CT for attenuation correction and anatomic co-registration (slice thickness 3 mm). PET/CT images were analysed with dedicated analysis software (OsiriX, Geneva, Switzerland; http://www.osirix-viewer.com/). Two readers (FM, YK) analysed all images to assess inter-observer variability. One reader (FM) analysed all images twice to assess intra-observer variability. Readers were blinded for patient data.

The maximal target-to-background-ratios (TBR_{max}) in the carotids were determined as described previously[12]. The carotid TBR_{max} represents the average of the left and right carotid arteries. The mean and maximal standard uptake values (SUV_{max} and SUV_{mean}) in the BM and spleen was determined as previously described[9]. In brief, SUV_{max} for each vertebra (T1 to L5) was assessed, and BM activity was calculated as the mean of SUV_{max} of all vertebrae. For the spleen, SUV_{max} was assessed in axial, sagittal, and coronal planes, and splenic activity was calculated as the mean of SUV_{max} values of the 3 planes. A similar approach was used for the SUV_{mean}.

Coronary artery calcium score. CT scans were used to determine the Agatston score, the coronary artery calcium (CAC) score. In a manually set volume of interest, all pixels with intensity higher than 130 HU were selected. Connected areas of these threshold pixels were constructed. All areas smaller than 1 mm^2 were excluded. The score was determined by

combining all selected connected areas with a weight. The weight was determined by the highest intensity value of a pixel in the connected areas: 1 for 130–199 HU, 2 for 200–299 HU, 3 for 300–399 HU, and 4 for 400 HU and greater. Because of the difference in slice thickness of the images in his study (5 mm) compared to default Agatston score images (3mm), the sum CAC score was multiplied with 5/3.

CFU-GM assay of patient derived HSPCs

HPSC from patients were mobilized by chemotherapy and G-CSF. Cells were plated in duplicate in 35 mm tissue culture plates at concentrations of 1.0, 0.5 and 0.25*10 5 cells/ml, respectively, in MethoCult GF 4534 (StemCell Technologies, Vancouver, BC, Canada). Cultures were incubated for 12-14 days at 37°C at 5% CO2. CFU-GM colonies, defined as containing at least 40 translucent myelocytic cells, were scored in triplo by microscopy (Leica, Solms, Germany).

In vitro model using healthy HSPCs

Leukapheresis material of healthy donors treated with G-CSF (5-10 mg/kg/day) was used to obtain CD34+ cells. These cells were enriched by magnetic cell sorting according to the manufacturer instructions (MACS; Miltenyi Biotec, Bergisch Gladbach, Germany), resulting in a purity of more than 90 %, as determined by flow cytometry. CD34+ cells were plated in 96 well plates (Thermo Scientific, Waltham, MA, USA) at 30.000 cells/well and kept in maintenance cocktail of 100 µl StemSpan (Stemcell Technologies, Vancouver, British Columbia, Canada) per well, supplemented with 100 U/ml pencillin, 100 µg/ml streptomycin, 50 ng/ml n-plate, 100 ng/ml SCF and 100 ng/ml Flt3. At day 0, CD34+ cells were stimulated with control medium, native LDL (nLDL) or oxLDL (Alfa Aesar, for both 10 µg/ml). In inhibition experiments using E06 (1 nM), the above 3 stimuli were co-incubated with the inhibitor. LAL assay showed negligible endotoxin levels (<0.05 EU/mL) in the stimuli. All cells were cultured at 37°C at 5% CO2. At day 7, cells were counted and flow cytometric and CFU-GM assays were performed.

The cultured cells were counted at day 7 by flow cytometric assays with Cyto-Cal fluorescent beads (Thermo scientific, Fremont, CA, USA), using a CANTO II + HTS flow cytometer (BD) and were characterized for surface expression of various receptors by flow cytometry. Cells were washed and resuspended in PBS containing 0.2% BSA prior to incubation (20 minutes at RT) with the following monoclonal antibodies. Antibodies purchases from BD, San Jose CA: CD13-PE (clone WM15), CD14-PerCP-Cy5.5 (clone M5E2), CD33-PE (clone WM53), CD34-PECy7 (clone 8G12), CD38-APC (clone HB7), CD45-PB (clone H130) and CD192 (CCR2)-Alexa-Fluor 647 (clone 48607). Purchased from Sanquin, Amsterdam, The Netherlands: CD16-FITC (clone CLB-Fc-gran/1, 5D2) and CD36-FITC (clone M1613). Purchased from Dako, Cambridgeshire, UK: CD41-FITC (clone 5B12). A minimum of 10.000 cells was recorded, using a CANTO II + HTS flow cytometer (BD).

For CFU-GM assays, cultured cells were plated in duplicate 0.5 ml in 24 well plates (Corning, NY, USA) at a concentration of 150 cells/well, respectively, in MethoCult H4434 (StemCell Technologies, Vancouver, BC, Canada). Cultures were incubated for 12-14 days at 37°C at 5% CO2. CFU-GM, colonies were scored in triplo by microscopy (Olympus CK2, Shinjuku, Tokyo, Japan).

Statistical analysis

Continuous variables are expressed as mean ± standard deviation (SD) or median and range (either interquartile range [IQR] or 25th to 75th percentile), and categorical variables as percentage and number (n). Differences in PET imaging parameters between groups were assessed with a multivariable model to account for cardiovascular risk factors. Correlations were assessed using Spearman's tests. The agreement between ^{18}F-FDG PET/CT analyses was assessed using intraclass correlation coefficients (ICC, r). Differences in G-SCF harvested cells between patients were assessed using nonparametric Mann-Whitney U tests. *In vitro* stimulation assays were repeated at least 5 times, and the differences between control, nLDL and oxLDL stimulations were assessed using a Kruskal Wallis analysis. P values were tested two-sided, and <0.05 was defined as statistically significant. All data were analysed using SPSS version 21.0 (SPSS Inc., Chicago, Illinois).

RESULTS

Enhanced hematopoietic activity in CVD patients

PET imaging was performed in 26 patients (aged 54 ± 7) with atherosclerosis disease, as evidenced by increased CAC scores 688 [IQR 356]. The median time post event was 18 months (IQR 3 months), comprising 70% MI and 30% ischemic stroke. In addition, 25 control subjects (aged 52 ± 5) without known atherosclerosis (confirmed by the CAC scores 0 [0]) matched for age, gender and BMI were included. The clinical characteristics are listed in Table 1. In line with secondary prevention, patients were on lipid lowering therapy, ACE-inhibition, acetylsalicylic acid and B-blockage, and C-reactive protein (CRP) levels were higher in patients. Other characteristics were comparable between groups (Table 1).

TABLE 1. Clinical characteristics of subjects in imaging study

Characteristic	Controls (n=25)	CVD patients (n=26)	P-value
Age, y	52 ± 5	54 ± 7	0.115
Gender, %male	72 (18)	80 (20)	0.493
BMI, kg/m^2	25 ± 3	26 ± 3	0.168
SBP, mmHg	131 ± 14	132 ± 6	0.752
DBP, mmHg	80 ± 9	80 ± 6	0.748
Smoking, %active	0 (0)	8 (2)	0.092
MI, %yes	-	70 (18)	
Ischemic stroke, %yes	-	30 (8)	
Time post-event, *months*	-	18 [3]	
Lipid lowering drugs, %yes	-	100 (26)	
Statin use (%)[§]	-	81 (21)	
Ezetimibe use (%)[§]	-	19 (5)	
ACE-inhibitor use (%)[§]	-	100 (26)	
Acetylsalicylic acid use (%)[§]	-	100 (26)	
B-blocker use, %yes[§]	-	100 (26)	
CT-CAC-score*	0 (0)	688 (356)	<0.001
TChol, mmol/L	5.29 ± 0.94	5.92 ± 2.74	0.302
LDL-c, mmol/L	3.14 ± 1.01	3.91 ± 2.67	0.233
Glucose, mmol/L	5.03 ± 0.31	5.29 ± 0.83	0.168
Creatinin, µmol/L	78 [23]	85 [16]	0.075
CRP, mg/L	1.30 [1.35]	2.45 [3.60]	0.029
Leukocytes, 10^9/L	6.09 ± 1.44	6.05 ± 1.39	0.911
Lymphocytes, 10^9/L	1.90 ± 0.49	1.82 ± 0.40	0.568
Monocytes, 10^9/L	0.46 ± 0.14	0.54 ± 0.19	0.054
Neutrophils, 10^9/L	3.58 ± 1.44	3.50 ± 1.13	0.835

Continuous data are shown as mean ± SD, or median [IQR], and categorical data as percentage and (n). * Agatston score. [§] Drug name and dosages for statin (simvastatin 40mg/day), ezetimibe (10mg/day), ace-inhibitor (lisinopril or perindopril 5-10mg), ASA (ascal 100mg/day) and B-blocker (metoprolol retard 100-150mg/day). *BMI indicates body mass index; CAC, coronary calcium score, CVD, cardiovascular disease; CRP, C-reactive protein; DBP, diastolic blood pressure; LDL-c, low density lipoprotein cholesterol; MI, myocardial infarction; SBP, systolic blood pressure; Tchol, total cholesterol.*

Figure 1A-C illustrates the multiple levels at which ^{18}F-FDG uptake was assessed in both patients and matched controls. Carotid ^{18}F-FDG uptake was increased in patients compared with controls (1.95 ± 0.33 versus 1.58 ± 0.20, p<0.001, Figure 1D). In addition, ^{18}F-FDG uptake in the spleen and bone marrow was also higher in patients compared with controls (Figure 1E-F, Table 2); the mean difference in splenic SUV_{max} was 0.93 ± 0.17 (p<0.001) between patients and controls, and 0.48 ± 0.18 (p=0.003) for the bone marrow. SUV_{mean} values for spleen and bone marrow showed a similar increase in patients (Table 2).

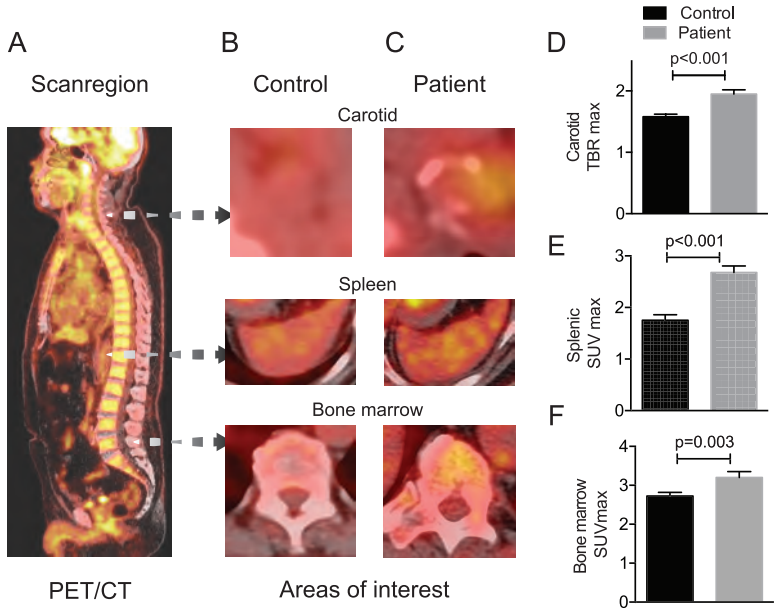

FIGURE 1. Persistent increased hematopoietic activity in CVD patients

Representative ^{18}F-FDG PET/CT images showing (**A**) an exemplary PET/CT scan region with (**B-C**) an enlarged inlay of the 3 areas of interest (carotids, spleen and bone marrow) for a (B) control subject and (C) patient, (**D-F**) with the corresponding ^{18}F-FDG uptake values depicted in bar graphs for (**D**) carotid TBR_{max} (p<0.001), (**E**) splenic (p<0.001) and (**F**) bone marrow SUV_{max} (p=0.003), for both controls (n=25, black bars) and patients (n=26, grey bars). *^{18}F-FDG indicates ^{18}Fluorodeoxyglucose; PET/CT, positron emission tomographic with computed tomography; SUV, standardized uptake values; TBR, target to background ratio.*

TABLE 2. ^{18}F-FDG uptake in arterial wall and hematopoietic tissues

Characteristic	Controls (n=25)	CVD patients (n=26)	P-value
Carotid, TBR_{max}	1.58 ± 0.20	1.95 ± 0.33	<0.001
Spleen, SUV_{mean}	1.13 ± 0.40	1.85 ± 0.44	<0.001
Spleen, SUV_{max}	1.75 ± 0.54	2.68 ± 0.65	<0.001
Bone marrow, SUV_{mean}	1.80 ± 0.21	2.15 ± 0.52	0.004
Bone marrow, SUV_{max}	2.72 ± 0.46	3.20 ± 0.76	0.003

Data are shown as mean ± SD. *^{18}F-FDG indicates ^{18}Fluorodeoxyglucose; CVD, cardiovascular disease; SUV, standardized uptake values; TBR, target to background ratio.*

In patients, splenic and bone marrow ^{18}F-FDG uptake strongly correlated with each other (r=0.76, p<0.001). Additional correlations for hematopoietic organ activity were determined (Table S1) in patients, revealing significant correlations with LDL-c and CRP levels, and monocyte count. No correlation between ^{18}F-FDG uptake and inflammatory biomarkers (MCP-1, TNFα, IL-6) or traditional cardiovascular risk factors was observed. Lastly, the intra- and inter-observer agreement was excellent for SUV values in bone marrow or spleen, as indicated by the ICCs of >0.94 with narrow 95% confidence intervals (Table S2).

Increased progenitor potential of HSPCs in CVD patients

Provoked by the enhanced bone marrow ^{18}F-FDG uptake in CVD patients *in vivo*, we screened a cohort of 953 cancer patients in whom HSPCs had been harvested via G-CSF. We identified 18 subjects with documented atherosclerosis, consisting of MI with significant coronary artery stenosis or ischemic stroke with significant carotid artery stenosis, having occurred 17 months (IQR 5 months) prior to HSPCs harvesting. The latter was performed in the context of an autoSCT due to the diagnosis of a multiple myeloma (61%) or relapse of non-Hodgkin lymphoma (39%) in disease stage I-III. For comparison, we selected 30 control patients without known CVD, matched for age, gender, BMI and indication for autoSCT (53% multiple myeloma and 47% relapse of non-Hodgkin lymphoma, in matched disease stages, p=0.886). Clinical characteristics at the time of HSPCs harvesting are listed in Table 3. Conform secondary prevention management all CVD patients used lipid lowering, ACE-inhibition, acetylsalicylic acid and B-blockage, whereas control subjects did not. Glucose, kidney and liver function were comparable between groups. Lipid profiles were not available. In addition, Table S3 shows the agreement between both CVD patient cohorts.

TABLE 3. Clinical characteristics of autoSCT patients

Characteristic*	Control patients (n=30)	CVD patients (n=18)	P-value
Age, years	54 ± 5	56 ± 10	0.403
Gender, m%	70 (21)	72 (12)	0.870
BMI, kg/m^2	25 ± 3	26 ± 4	0.382
Indication autoSCT			
- Multiple myeloma	53 (16)	61 (11)	0.148
- Relapse NHL	47 (14)	39 (7)	
Disease stage I-II-III, %	31-19-50%	38-15-46%	0.886
Smoking, *%active*	7 (2)	17 (3)	0.272
Ischemic event			
- MI, *%yes*		50 (9)	
- Ischemic stroke, *%yes*		50 (9)	
Time post-event#, *months*		17 [5]	
Statin use (%)§		100 (18)	
ACE-inhibitor use (%)§		100 (18)	
Acetylsalicylic acid use (%)§		100 (18)	
B-blocker use (%)§		100 (18)	
Glucose, *mmol/L*	5.0 ± 0.4	5.3 ± 0.7	0.333
Creatinin, µmol/L	72 [51]	75 [191]	0.451
ALT, *U/L*	21 ± 9	24 ± 9	0.183

Continuous data are shown as mean ± SD, or median [IQR], and categorical data as percentage and (n). *Characteristics of the subject prior to G-CSF harvesting of HSPCs. # time between ischemic event and G-CSF harvesting of HSPCs. § Drug name and dosages for statin (simvastatin 40mg/day), ace-inhibitor (lisinopril or perindopril 5-10mg), ASA (ascal 100mg/day) and B-blocker (metoprolol retard 100-150mg/day). *ALT indicates alanine aminotransferase; autoSCT, autologous stem cell transplantation; BMI, body mass index; CVD, cardiovascular disease; MI, myocardial infarction; NHL, non-Hodgkin lymphoma.*

Whereas the percentage of CD34+ cells was comparable between groups (Figure 2A; p=0.744), the CFU-GM capacity of the G-CSF HSPCs harvested from CVD patients was 1.6-fold higher compared with control patients (0.31 ± 0.18 versus 0.19 ± 0.07, p<0.001; Figure 2B).

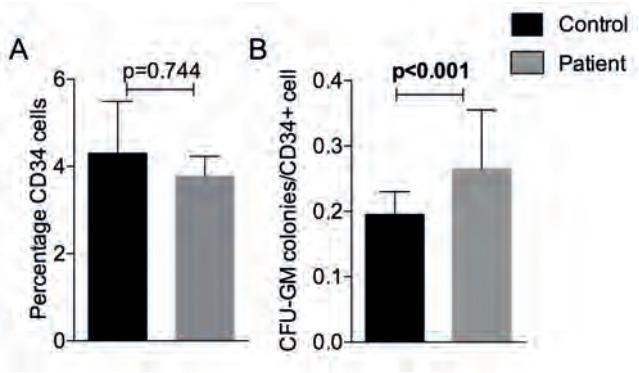

FIGURE 2. Increased progenitor potential in CVD patients

Bar graphs showing (**A**) no change in the percentage of CD34+ cells of the mononuclear cells mobilized by G-CSF (p=0.744), whereas (**B**) an increased progenitor capacity (expressed as the CFU-GM/CD34+ cell) in patients (n=18, grey bars) compared with controls (n=30, black bars, p<0.001). *CFU-GM indicates colony forming units-granulocyte/monocyte; CVD, cardiovascular disease.*

Lipid risk factors change function and phenotype of HSPCs in vitro

Considering the correlation between bone marrow ^{18}F-FDG uptake and LDL-c, we cultured unrelated healthy donor G-CSF harvested HSPCs (CD34+ cells) with either native LDL (nLDL) or oxidized LDL (oxLDL). After 7 days of co-incubation, the normalized cell count was not different between stimuli (p=0.444; Figure 3A). However, the normalized progenitor capacity, assessed with CFU-GM (Figure 3B), was 1.5-fold higher after co-incubation with oxLDL compared with control (p=0.002; Figure 3C). In addition, we applied the monoclonal antibody E06, which blocks the phosphocholine (PC) headgroup of oxidized phospholipids, and not native phospholipids[13–15]. Blockage of the oxidized phospholipid load on oxLDL via E06 robustly inhibited the effect of oxLDL on normalized progenitor potential (p=0.001; Figure 3D).

Next to CFU-GM capacity, flow cytometric assays were performed to determine the phenotypic changes after nLDL or oxLDL co-incubation. No changes in the expression of CD41, CD13/33 or CD36 were observed (Figure S1), whereas the cells showed a myeloid bias after 7 days of oxLDL co-incubation as indicated by the significant increased expression of CD14/CD16 (p=0.002) and borderline significant increased C-C chemokine receptor type 2 (CCR2; p=0.051) (Figure 3E-G).

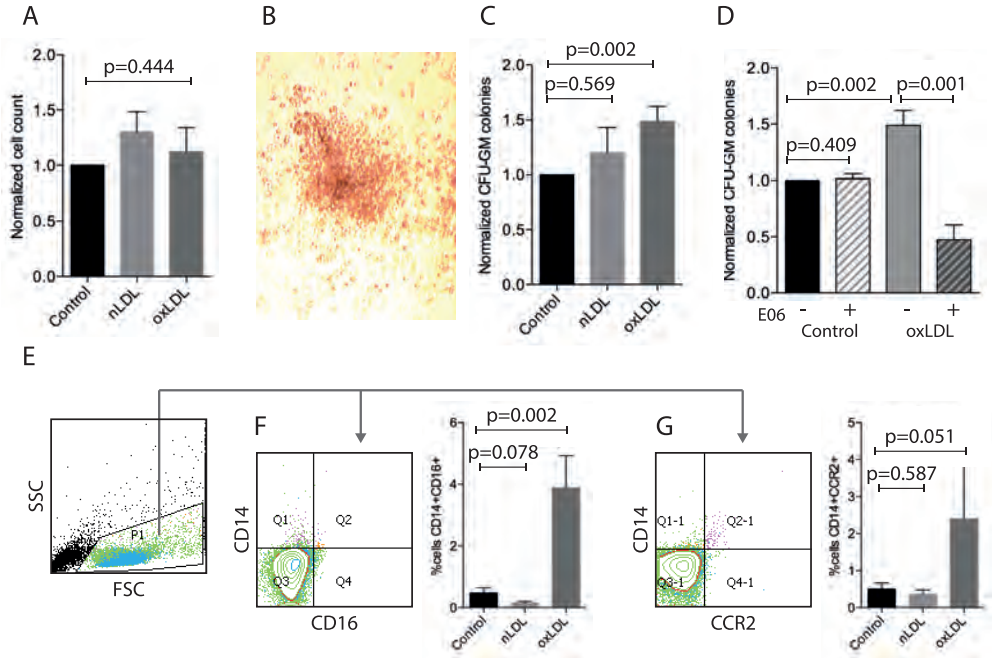

FIGURE 3. Increased progenitor potential and myeloid differentiation bias induced by oxLDL

Bar graphs showing (**A**) no differences (p=0.444) in the cell counts after healthy HSPCs were co-incubated for 7 days with either control medium (black bars), nLDL (10 ug/mL, light grey bars) or oxLDL (10 ug/mL, dark grey bars), whereas (**B-D**) the CFU-GM capacity, as illustrated by the microscopy image (**B**), increased upon co-incubation with oxLDL (p=0.002) (**C**), which is inhibited by the antibody E06 (p=0.001) (**D**), and (**E-G**) gating strategy with accompanying results showing that the expression of CD14, CD16 and CCR2 was increased after 7 days of HSPCs co-incubation with oxLDL (p=0.002 and p=0.051, respectively). Assays were performed at least 8 times. *CFU-GM indicates colony forming units-granulocyte/monocyte; CCR2, C-C chemokine receptor type 2; HSPCs, hematopoietic stem and progenitor cells; nLDL, native low-density-lipoprotein; oxLDL, oxidized LDL.*

DISCUSSION

Here, we report that patients with stable atherosclerotic CVD have a high metabolic activity of the carotid arterial wall, as well as hematopoietic tissues *in vivo*. In addition, we show that HSPCs have a higher proliferative capacity *ex vivo* when obtained from patients with atherosclerotic CVD, compared with those without known CVD. *In vitro*, this enhanced proliferative potential and myeloid differentiation bias was substantiated in healthy HSPCs by co-incubation with oxLDL; the oxidized phospholipid antibody E06 could inhibit this adverse effect. Collectively, these findings support the hypothesis that hematopoietic activity is chronically enhanced in patients with table atherosclerotic CVD.

Previously, PET imaging studies demonstrated an increased bone marrow and splenic activity in patients with CVD[7–9]. Whereas these studies all focused on the (semi)-acute phase following a MI[7–9], we now show that more than 12 months after the CVD event patients still exhibit higher activity of hematopoietic tissues despite CVD guideline-based management.

What does the chronically increased ^{18}F-FDG uptake in hematopoietic tissues imply for the patient? In general, cellular accumulation of ^{18}F-FDG is increased in proinflammatory, hypoxic as well as rapidly proliferating cells[16]. In the present stable condition, we can speculate that the ^{18}F-FDG in hematopoietic tissues reflects an increased proliferative rate, since HSPCs harvested from patients with CVD also showed an increased proliferative capacity of the GM-precursor cells. A prospective study combining PET imaging with HSPC harvesting is warranted, however, to corroborate this concept.

Besides the increased metabolic activity, we also show an enhanced functional capacity of HSPCs harvested from CVD patients compared with controls. During the last decade, differences in both number and function of circulating CD34+ cells have been reported. Thus, in patients following an acute myocardial infarction, the number of endogenous circulating progenitors was significantly increased compared with controls[17]. This phasic increase in number fell significantly within 60 days after the acute event[17]. Such a transient response of hematopoietic cells following an acute ischemic event has subsequently been corroborated in patients following either a myocardial[18–20] or a cerebral[21,22] infarction. Interestingly, despite normalization of cell number, we observe functional changes of CD34+ cells persisting more than 12 months after the acute event. Whereas the clinical relevance of a tonic hematopoietic activity warrants further validation, animal studies have indicated that the increased activity of HSPCs can promote features characteristic of vulnerable atherosclerotic lesions [23]. In addition, whether repeating acute events or long-lasting chronic stimulation could also exhaust the bone marrow[24] warrants further studies.

Murine ligation studies evidenced that in the acute phase following a MI, anxiety, pain and impaired left ventricular function promote sympathetic nervous signalling, proposing an

important role for the β3-adrenoceptor[4] in mediating the increased HSPC response. In view of the chronic, stable phase of the CVD, the absence of left ventricular failure and the use of beta-blockers in the patients included in the present study, these acute stimuli are less likely to be major contributors in our patients. Alternative causal pathways comprise persistent effects of an ischemic event on senescent stem cells[25], or a potential role of atherosclerotic risk factors on HSPCs[26]. In this respect, we observed a significant correlation between plasma LDL-c concentration and metabolic activity in hematopoietic tissues lending further support to a direct role of elevated LDL-c in mediating bone marrow hyperresponsiveness.

Several studies detailed an interaction between lipoproteins and the myeloid lineage, both of upstream as well as downstream, differentiated cells[26]. Regarding the differentiated cells, mice with high-fat diet induced hypercholesterolemia display a marked expansion of proinflammatory monocytes[27]. In parallel, patients with significantly elevated LDL levels are also characterized by an increased number of proatherogenic monocytes[28] as well as arterial wall inflammation[29] compared with subjects with normal cholesterol levels.

With respect to the myeloid progenitors, murine studies have showed that elevated cholesterol levels increased the number of HSPCs in the blood[30,31] as well as the bone marrow[32]. In a large community-based study the number of circulating CD34+ cells in humans correlated also positively with total cholesterol levels[33]. Conversely, a reduction in cholesterol levels via statin therapy was followed by a reduction in circulating HSPCs in patients[34].

Besides the relation between lipids and HSPC number, we also addressed the potential impact on HSPC functionality. First, oxLDL was found to increase the CFU-GM capacity of the HSPCs, whereas nLDL had no effect. The monoclonal antibody E06, which blocks the phosphocholine (PC) headgroup of oxidized phospholipids[13–15], abolished this effect of oxLDL. Oxidized phospholipids represent danger-associated molecular patterns (DAMPs) which can be recognized by multiple innate pattern recognition receptors (PRRs)[35], igniting a variety of pro-inflammatory and plaque destabilizing processes[35–37]. Secondly, oxLDL also promoted the myeloid differentiation bias of HSPCs of healthy donors, evidenced by the increased expression of the monocytic cell markers CD14 and CD16. This is of specific interest, since HSPC-derived monocytes and macrophages are key cellular effectors in atherosclerosis[38]. In addition, we also observed an increased expression of CCR2 on progenitor cells, which is elementary on upstream hematopoietic precursors contributing to myelopoiesis following ischemic organ injury[39]. Interestingly, a CCR2 positive subset was also present in patients with CVD, whereas this subset had a profound higher proliferative rate and displayed a myeloid differentiation bias[39]. Whereas the latter study examined $CCR2^{+}$ progenitors in the setting of an acute ischemic event[39], our findings underscore the need to evaluate these pathways also in the setting of chronic atherosclerosis.

Several limitations need to be acknowledged. First, due to ethical constraints for clinical research, PET imaging and HSPCs studies were not performed in the same patients. The clinical characteristics, including age, gender, BMI, time post event and medication use,

however, were comparable between the CVD patients in both studies (Table S3). Nevertheless, extrapolation and generalizability of our findings are limited. In addition, the relative small sample sizes restrain correlation analysis, with amongst others inflammatory biomarkers. Secondly, regarding the HSPCs *ex vivo* assays, we acknowledge that the manner of harvesting (G-CSF), the retrospective nature as well as the type, stage and (pre)treatment of the cancer and statin treatment in the CVD group are confounding variables. Also, a potential causal or accelerating effect of the presence of cancer on ischemic events cannot be excluded. In order to minimize the impact of these effects, however, we carefully matched patients and controls for disease and therapy specifications and only included patients with significant atherosclerotic disease (elevated CAC scores and/or significant carotid artery stenosis). Thirdly, the design of the studies, i.e. harvested HSPCs, precludes repetitive assessments of hematopoietic activity within patients over time. Finally, although we observed a significant interaction between oxidized lipoproteins and HSPC function and phenotype, the present study cannot address causality or consequence of this mechanism in vivo.

Whereas during the past decade downstream myeloid cells, mostly monocytes and macrophages, have been studied intensively in atherogenesis, the interest in the more upstream HSPCs and their involvement in atherogenesis is expanding[40]. The present experimental work describes that (i) hematopoietic tissues are more active in patients with atherosclerotic disease, (ii) HSPCs are functionally different in these patients, and (iii) potentially affected by oxidized lipoproteins. Further translational research is needed to dissect the interactions between up- and downstream cells and the drivers of chronic low-grade inflammation in human atherogenesis.

Acknowledgements: We would like to thank Bernadet Odijk for her assistance with the autoSCT patient cohort.

Disclosures and funding: This work was supported by the Netherlands CardioVascular Research Initiative: the Dutch Heart Foundation, Dutch Federation of University Medical Centers, the Netherlands Organization for Health Research and Development, and the Royal Netherlands Academy of Sciences (CVON 2011/ B019 GENIUS). All authors declare that they have no relationships relevant to the contents of this paper to disclose.

REFERENCES

1. Libby P et al. Progress and challenges in translating the biology of atherosclerosis. Nature 2011;473:317–25.
2. Baldridge MT et al. Quiescent haematopoietic stem cells are activated by IFN-gamma in response to chronic infection. Nature 2010;465:793–7.
3. Takizawa H et al. Dynamic variation in cycling of hematopoietic stem cells in steady state and inflammation. JEM 2011;208:273–84.
4. Dutta P et al. Myocardial infarction accelerates atherosclerosis. Nature 2012;487:325–9.
5. Swirski FK et al. Identification of splenic reservoir monocytes and their deployment to inflammatory sites. Science 2009;325:612–6.
6. Leuschner F et al. Rapid monocyte kinetics in acute myocardial infarction are sustained by extramedullary monocytopoiesis. J. Exp. Med. 2012;209:123–37.
7. Assmus B et al. Acute myocardial infarction activates progenitor cells and increases Wnt signalling in the bone marrow. Eur Heart J 2012;33:1911–1919.
8. Kim EJ et al. Metabolic activity of the spleen and bone marrow in patients with acute myocardial infarction evaluated by 18f-fluorodeoxyglucose positron emission tomograpic imaging. Circ Cardiovasc Imaging 2014;7:454–60.
9. Emami H et al. Splenic Metabolic Activity Predicts Risk of Future Cardiovascular Events. JACC Cardiovasc Imaging 2015;8:121–130.
10. Robbins CS et al. Local proliferation dominates lesional macrophage accumulation in atherosclerosis. Nat Med 2013;19:1166–72.
11. Van der Valk FM et al. In vivo imaging of enhanced leukocyte accumulation in atherosclerotic lesions in humans. J Am Coll Cardiol 2014;64:1019–29.
12. Rudd JHF et al. (18)Fluorodeoxyglucose positron emission tomography imaging of atherosclerotic plaque inflammation is highly reproducible: implications for atherosclerosis therapy trials. J Am Coll Cardiol 2007;50:892–6.
13. Boullier A et al. Phosphocholine as a pattern recognition ligand for CD36. J Lipid Res. 2005;46:969–76.
14. Friedman P et al. Correlation of antiphospholipid antibody recognition with the structure of synthetic oxidized phospholipids. Importance of Schiff base formation and aldol condensation. J Biol Chem. 2002;277:7010–20.
15. Chang MK et al. Apoptotic cells with oxidation-specific epitopes are immunogenic and proinflammatory. J Exp Med. 2004;200:1359–70.
16. Tarkin JM et al. PET imaging of inflammation in atherosclerosis. Nat Rev Cardiol. 2014;11:443–457.
17. Massa M et al. Increased circulating hematopoietic and endothelial progenitor cells in the early phase of acute myocardial infarction. Blood. 2005;105:199–206.
18. Brehm M et al. Enhanced mobilization of CD34(+) progenitor cells expressing cell adhesion molecules in patients with STEMI. Clin Res Cardiol. 2009;98:477–86.
19. Leone AM et al. Endogenous G-CSF and CD34+ cell mobilization after acute myocardial infarction. Int J Cardiol. 2006;111:202–8.
20. Spevack DM et al. Increase in circulating bone marrow progenitor cells after myocardial infarction. Coron Artery Dis. 2006;17:345–349.
21. Paczkowska E et al. Human hematopoietic stem/progenitor-enriched CD34(+) cells are mobilized into peripheral blood during stress related to ischemic stroke or acute myocardial infarction. Eur J Haematol. 2005;75:461–7.
22. Hennemann B et al. Mobilization of CD34+ hematopoietic cells, colony-forming cells and long-term culture-initiating cells into the peripheral blood of patients with an acute cerebral ischemic insult. Cytotherapy. 2008;10:303–11.
23. Heidt T et al. Chronic variable stress activates hematopoietic stem cells. Nat Med. 2014;20:754–8.
24. Kissel CK et al. Selective functional exhaustion of hematopoietic progenitor cells in the bone marrow of patients with postinfarction heart failure. J Am Coll Cardiol. 2007;49:2341–9.
25. Álvarez-Errico D et al. Epigenetic control of myeloid cell differentiation, identity and function. Nat Rev Immunol. 2015;15:7–17.
26. Lang JK et al. Cholesterol and hematopoietic stem cells: inflammatory mediators of atherosclerosis. Stem Cells Transl Med. 2014;3:549–52.
27. Swirski FK et al. Ly-6C hi monocytes dominate hypercholesterolemia-associated monocytosis and give rise to macrophages in atheromata. J Clin Invest. 2007;117:195–205.

28. Mosig S et al. Different functions of monocyte subsets in familial hypercholesterolemia: potential function of CD14+ CD16+ monocytes in detoxification of oxidized LDL. FASEB J. 2009;23:866–74.
29. van Wijk DF et al. Nonpharmacological Lipoprotein Apheresis Reduces Arterial Inflammation in Familial Hypercholesterolemia. J Am Coll Cardiol. 2014;64:1418–26.
30. Gomes AL et al. Hypercholesterolemia promotes bone marrow cell mobilization by perturbing the SDF-1:CXCR4 axis. Blood. 2010;115:3886–94.
31. Feng Y et al. Hematopoietic Stem/Progenitor Cell Proliferation and Differentiation Is Differentially Regulated by High-Density and Low-Density Lipoproteins in Mice. PLoS One. 2012;7.
32. Yvan-Charvet L et al. Combined deficiency of ABCA1 and ABCG1 promotes foam cell accumulation and accelerates atherosclerosis in mice. J Clin Invest. 2007;117:3900–3908.
33. Cohen KS et al. Circulating CD34(+) progenitor cell frequency is associated with clinical and genetic factors. Blood. 2013;121:e50–6.
34. Cimato TR et al. LDL Cholesterol Modulates Human CD34+ HSPCs through Effects on Proliferation and the IL-17 G-CSF Axis. PLoS One. 2013;8:1–11.
35. Miller YI et al. Oxidation-specific epitopes are danger-associated molecular patterns recognized by pattern recognition receptors of innate immunity. Circ Res. 2011;108:235–48.
36. Lee S et al. Role of phospholipid oxidation products in atherosclerosis. Circ Res. 2012;111:778–99.
37. Leibundgut G et al. Oxidation-specific epitopes and immunological responses: Translational biotheranostic implications for atherosclerosis. Curr Opin Pharmacol. 2013;13:168–79.
38. Moore KJ et al. Macrophages in atherosclerosis: a dynamic balance. Nat Rev Immunol. 2013;13:709–721.
39. Dutta P et al. Myocardial Infarction Activates CCR2+ Hematopoietic Stem and Progenitor Cells. Cell Stem Cell. 2015;16:477–487.
40. Nahrendorf M et al. Lifestyle Effects on Hematopoiesis and Atherosclerosis. Circ Res. 2015;116:884–894.

SUPPLEMENT

TABLE S1. Correlations with hematopoietic activity

Characteristic	Bone marrow ^{18}F-FDG uptake	Splenic ^{18}F-FDG uptake
Age	0.25	0.16
Gender	0.10	0.11
BMI	0.11	0.03
MAP	0.37	0.25
Smoking	0.36	0.28
Lipid lowering drugs	0.14	0.13
ACE-inhibitor	0.09	0.14
Acetylsalicylic acid	0.03	0.08
B-blocker	0.11	0.04
Carotid TBR	0.21*	0.34*
TChol	0.12	0.15
LDL-c	0.72***	0.55***
HDL-c	0.19	0.18
CRP	0.72***	0.49***
MCP-1	0.20	0.22
TNFα	0.21	0.19
IL-6	0.17	0.16
Leukocytes	0.10	0.01
Monocytes	0.18*	0.25*

Data show Spearman correlation coefficients, flagged if significant as *=p<0.05, **=p<0.01, ***=p<0.001. *^{18}F-FDG indicates ^{18}fluorodeoxyglucose; BMI, body mass index; CACscores, coronary artery calcium score; HDL-c, high-density lipoprotein cholesterol; LDL-c, low-density lipoprotein cholesterol; IL-6, interleukin 6; MAP, mean arterial pressure; MCP-1, monocyte chemoattractant protein-1; TBR, target to background ratio; TChol, total cholesterol, TNFα, tumor necrosis factor α.*

TABLE S2. Excellent agreement of image analysis

	Bone Marrow SUV_{max}	Spleen SUV_{max}
Intra-observer		
Paired difference	0.01 ± 0.02	0.00 ± 0.15
Intra ICC [CI]	0.98 [0.93 – 0.99]	0.99 [0.96 – 0.99]
Inter-observer		
Paired difference	0.03 ± 0.13	0.02 ± 0.19
Inter ICC [CI]	0.98 [0.94 – 0.99]	0.94 [0.85 – 0.97]

Intra-observer reflects the variability within one reader (FM) and inter-observer reflects the variability between two readers (FM and YK). *ICC indicates intraclass correlation coefficient; CI, 95% confidence interval; SUV, standardized uptake values.*

TABLE S3. Additional patient characteristics

	PET study		HSPC study		
Characteristic	**Controls**	**CVD patients**	**Control patients**	**CVD patients**	**Pvalue**
Number	*25*	*26*	*30*	*18*	
Age, y	52 ± 5	54 ± 7	54 ± 5	56 ± 10	0.361
Gender, %male	72 (18)	80 (20)	70 (21)	72 (12)	0.568
BMI, kg/m^2	25 ± 3	26 ± 3	25 ± 3	26 ± 4	0.784
Smoking, %active	0 (0)	8 (2)	7 (2)	17 (3)	0.732
Time post-event, *months*	-	18 [3]	-	17 [5]	-
Lipid lowering use (%)	-	100 (26)	-	100 (18)	-
ACE-inhibitor use (%)	-	100 (26)	-	100 (18)	-
Acetylsalicylic acid use (%)	-	100 (26)	-	100 (18)	-
B-blocker use, %yes	-	100 (26)	-	100 (18)	-
Glucose, mmol/L	5.03±0.31	5.29 ± 0.83	5.0 ± 0.4	5.3 ± 0.7	0.383
Creatinin, µmol/L	78 [23]	85 [16]	72 [51]	75 [191]	0.462

Continuous data are shown as mean ± SD, or median [IQR], and categorical data as percentage and (n). *ACE-inhibitor indicates angiotensin-converting-enzyme inhibitor; CVD, cardiovascular disease; BMI, body mass index; HSPC, hematopoietic stem-/progenitor cell; ns, non-significant; PET, positron emission tomography.*

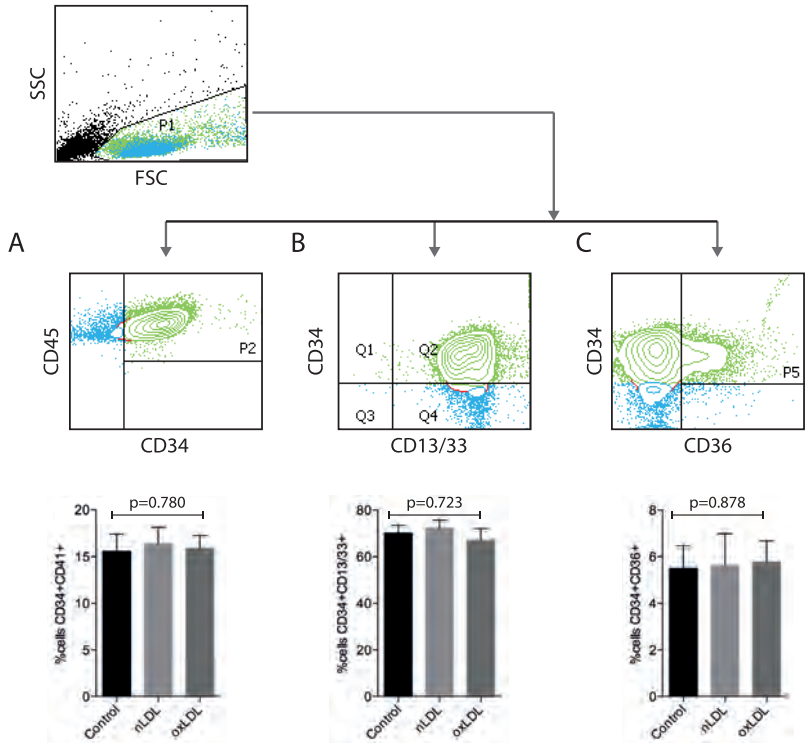

Figure S1. Additional expression markers after oxLDL

Representative gating strategy and bar graphs (**A-C**) showing no differences in the expression of CD34, CD41, CD13/33 or CD36 after 7 days of HSPCs co-incubation with oxLDL. Assays were performed at least 5 times. HSPCs, hematopoietic stem and progenitor cells; nLDL, native low-density-lipoprotein; oxLDL, oxidized LDL.

PART II

THE IMPACT OF LIPIDS ON ATHEROSCLEROTIC INFLAMMATION

CHAPTER 5

NONPHARMACOLOGICAL LIPOPROTEIN APHERESIS REDUCES ARTERIAL INFLAMMATION IN FAMILIAL HYPERCHOLESTEROLEMIA

van Wijk DF*, Sjouke B*, Figueroa A, Emami H, **van der Valk FM**, MacNabb HA, Hemphill LC, Schulte DM, Koopman MG, Lobatto ME, Verberne HJ, Fayad ZA, Kastelein JJP, Mulder WJM, Hovingh GK, Tawakol A, Stroes ESG

*Authors contributed equally

J Am Coll Cardiol. 2014;64:1418–26

ABSTRACT

Rationale: Patients with familial hypercholesterolemia (FH) are characterized by elevated atherogenic lipoprotein particles, predominantly low-density lipoprotein cholesterol (LDL-c) which is associated with accelerated atherogenesis and increased cardiovascular risk. Here, we used ^{18}fluorodeoxyglucose-positron emission tomography with computed tomography (^{18}F-FDG PET/CT) to investigate whether arterial inflammation is higher in patients with FH and, moreover, whether lipoprotein-apheresis attenuates arterial wall inflammation in FH patients.

Methods and Results: In total, 38 subjects were recruited: 24 FH patients and 14 normolipidemic controls. All subjects underwent ^{18}F-FDG PET/CT imaging at baseline. Twelve FH patients who met the criteria for lipoprotein apheresis underwent apheresis procedures followed by a second ^{18}F-FDG PET/CT imaging 3 days (range 1 to 4 days) after apheresis. Subsequently, the target to background ratio (TBR) of ^{18}F-FDG uptake within the arterial wall was assessed. In FH patients, the arterial TBR_{max} was higher compared with healthy controls (2.12±0.27 versus 1.92±0.19; p=0.03). A significant correlation was observed between baseline arterial TBR_{max} and LDL-c (r=0.37; p=0.03) that remained significant after adjusting for statin use (β=0.001; p=0.02) and atherosclerosis risk factors (β=0.001; p=0.03). LDL-c levels were significantly reduced after lipoprotein apheresis (284±118 mg/dl vs. 127±50 mg/dl;p<0.001). There was a significant reduction of arterial inflammation after lipoprotein apheresis (TBR_{max} 2.05±0.31 vs. 1.91±0.33; p<0.02).

Conclusion: The arterial wall of FH patients is characterized by increased inflammation, which is markedly reduced following lipoprotein-apheresis. This lends further support to a causal role of apolipoprotein B-containing lipoproteins in arterial wall inflammation and supports the concept that lipoprotein lowering therapies may impart anti-inflammatory effects by reducing atherogenic lipoproteins.

INTRODUCTION

Atherosclerosis is a chronic, lipid-driven inflammatory disease of the arterial wall[1]. Lipid accumulation in the subintimal compartment ignites an inflammatory response, perpetuated by oxidized lipoproteins and activated macrophages[2]. Findings of prior studies in patients with cardiovascular disease (CVD) exemplify the relevance of this process by demonstrating that both a large lipid-rich necrotic core[3] and increased arterial inflammation[4] strongly predict plaque vulnerability and subsequent rupture.

The detrimental interaction between lipids and inflammation is a hallmark in patients suffering from familial hypercholesterolemia (FH). These patients are predominantly characterized by extremely elevated low-density lipoprotein cholesterol (LDL-c) levels, increased levels of inflammatory markers (e.g. C-reactive protein (CRP)) and premature cardiovascular disease[5,6]. Prior studies have demonstrated some beneficial effects of statin therapy in FH patients[7], however, a substantial residual cardiovascular (CV) risk remains[8] possibly due to the fact that many FH patients do not reach the target LDL-c level by statins.

The direct link between lipid accumulation and induction of local inflammation has been widely acknowledged. Potent lipid lowering interventions have been shown to attenuate the degree of arterial wall and atherosclerotic plaque inflammation in experimental animal models[9]. In humans, high-dose statin therapy has been shown to reduce serum levels of inflammatory biomarkers[5,10], which was independent from its LDL-c lowering effect[11]. During the last decade, assessment of the local inflammatory activity of the arterial wall or the atherosclerotic plaque has been introduced using novel imaging strategies including ^{18}F-fluorodeoxy-glucose positron emission tomography (^{18}F-FDG PET)[12]. The ^{18}F-FDG signal has been shown to correlate with arterial macrophage content[13], and is predictive of subsequent risk of atherothrombotic events[14]. Recently, rapid reduction of local arterial wall inflammation via intensification of statin therapy was observed using PET imaging, though again independent of changes in lipid profile[15].

Taking the widely acknowledged pleiotropic effects of statins into account, we can therefore not dissect whether this statin-induced reduction in arterial wall inflammation is merely LDL-c dependent or also due to pleiotropic, anti-inflammatory effects. In the present study we assessed whether patients with FH are characterized by increased arterial wall inflammation as determined by ^{18}F-FDG PET/CT imaging. Subsequently, we explored whether a potent nonpharmacologic lipid lowering strategy can attenuate local arterial wall inflammation.

METHODS

Study population

This pilot study comprised a cross-sectional analysis, investigating arterial ^{18}F-FDG uptake in FH patients versus healthy controls, as well as a prospective interventional analysis, investigating the effects of lipoprotein-apheresis on arterial ^{18}F-FDG uptake. This study was conducted at two centers; the Academic Medical Center (AMC), Amsterdam, the Netherlands and Massachusetts General Hospital (MGH), Boston, United States. For the cross-sectional analysis at the AMC, 18 patients with established diagnosis of FH were recruited from the outpatient clinic. Healthy and normolipidemic controls without known cardiovascular disease (CVD) were recruited via local advertisements. For the prospective analysis, 12 FH patients (6 of whom were also included in the cross sectional analysis of the study) meeting the eligibility criteria for lipoprotein-apheresis according to the Apheresis Guidelines[16] were included (6 from each centre). Six FH patients (50%) were previously apheresis naïve and 6 patients had previously undergone lipoprotein-apheresis. Written informed consent was obtained from all participants and the local institutional review boards approved the protocol.

^{18}F-FDG PET/CT imaging

^{18}F-FDG PET/CT imaging was performed in all FH patients and healthy controls at baseline. In the apheresis-naive FH patients (n=6) treated with weekly lipoprotein-apheresis sessions, a second ^{18}F-FDG PET/CT scan was performed after 8 weeks, 3 days after the last apheresis session (median interval [IQR] = 3 [1-4] days). FH patients who were on chronic apheresis therapy (n=6), a 2 week wash-out period was introduced, after which the baseline ^{18}F-FDG PET/CT scan was performed. The second ^{18}F-FDG PET/CT scan in these patients was performed after a single apheresis episode (median interval [IQR] = 3 [1-5] days). PET/CT imaging of the aorta and carotid arteries was performed using a PET/CT scanner (Philips Gemini, Philips, Best, the Netherlands or similar). In brief, patients were placed in a supine position for intravenous administration of ^{18}F-FDG. Approximately ninety minutes after ^{18}F-FDG injection (~180 MBq), a PET/CT scan was performed in two separate positions. The first position covered the carotid arteries extending inferiorly from the internal auditory meatus (15.5 cm) and acquired in 3-dimensional mode for 15 min. The second position covered the ascending aorta, aortic arch and upper thoracic part of descending aorta. Attenuation-corrected PET images were used for analysis.

Image analysis

All scans were analysed by one investigator (MM) who was blinded to patient characteristics and temporal sequence of images. Arterial ^{18}F-FDG uptake was quantified by drawing a region of interest (ROI) around each artery on every slice of the co-registered transaxial CT image. Subsequently, the maximal arterial standardized uptake value (SUV_{max}) was recorded as the maximal pixel activity within the ROI of every slice of the artery. The SUV is the decay-corrected tissue concentration of ^{18}F-FDG in kilo becquerel per milliliter, adjusted for the injected ^{18}F-FDG dose and body weight of the patient. Mean SUV_{max} for each artery was derived as the average of SUV_{max} of individual slices of that artery. Arterial target-to-background ratio (TBR_{max}) was calculated by correcting the mean SUV_{max} for average background blood activity as detailed in prior studies[15,17]. Additionally, the artery with the highest ^{18}F-FDG uptake (TBR_{max}) at baseline was identified as the index vessel, as previously described[18]. Thereafter, the average of the maximum TBR activity within the most diseased segment (mds) of the index vessel (TBR_{mds}) was recorded. The most diseased segment was defined as the 1.5 cm arterial segment that demonstrated the highest ^{18}F-FDG uptake at baseline, and was calculated as the average of the TBR_{max} derived from three contiguous axial segments as detailed in prior studies[15].

Lipoprotein apheresis

Twelve FH patients underwent lipoprotein-apheresis procedures performed either with the Direct Adsorption of Lipoprotein (DALI) system (Fresenius Medical Care, Bad Homburg, Germany) or the Liposorber system (Kaneka Corporation, Japan). The apheresis procedures' treated time/blood volume was individually calculated according to standard operating procedures. Blood samples were obtained on the day of the PET/CT imaging (n=10) or within 4 days of imaging (n=2). Blood was centrifuged for 10 minutes at 3,000 rates per minute at 20ºC. Total cholesterol (TC), high density lipoprotein cholesterol (HDL-c) and triglycerides (TG) were measured by a commercially available enzymatic colorimetric assay (Roche, Basel, Switzerland). LDL-c levels were calculated by the Friedewald formula[19]. Lipoprotein(a) [Lp(a)] levels were measured by a commercially available immunoturbidometric assay (Abbott Laboratories, Abbott Park, Illinois, USA). CRP was measured by a commercially available immunoturbidometric assay (Roche, Basel, Switzerland).

Statistical analysis

Continuous variables were tested for normality of distribution using the Shapiro-Wilk test and are expressed as mean ± SD or median [IQR] for normally and non-normally distributed variables, respectively. Independent samples t tests and Mann-Whitney U tests were used where appropriate to assess baseline differences between FH patients and healthy controls. Categorical variables are expressed as absolute numbers and percentages throughout this paper, and the

chi-square test is employed for between-group analyses. To evaluate the relationship between continuous variables [e.g., LDL-c, Lp(a), and TBR] at baseline, Pearson's correlation coefficient or Spearman's ρ is reported according to the distribution of variables. Furthermore, a linear regression model was fitted when adjustment for potential confounding variables was required, and the unstandardized regression coefficient (β) is reported. For longitudinal analysis in the 12 patients undergoing lipoprotein apheresis, the Wilcoxon signed rank test and paired-samples t test were used where appropriate. To assess the relationship between lipoproteins and TBR in these patients, Spearman's ρ was assessed in addition to a linear mixed-model analysis to provide an estimate of fixed effect of different lipoproteins on TBR. In order to limit the confounding effect of different imaging instruments, all between-group comparisons of imaging endpoints (between FH and controls) were confined to subjects imaged on a single PET/CT camera. By contrast, for longitudinal analyses (before and after apheresis of FH patients), where the impact of the imaging instrument is largely controlled for, analysis included subjects from both institutions. A 2-sided p value <0.05 was considered statistically significant. All data were analyzed using IBM SPSS software (version 21, Armonk, New York).

RESULTS

Arterial wall inflammation and blood biomarkers at baseline

Baseline demographics of 24 FH patients and 14 control subjects are outlined in Table 1. Apart from clear differences in the lipid profile, the control subjects were older and had a lower body mass index (BMI) compared with FH patients. Approximately 46% of FH patients were using statins; most commonly, those who did not were statin intolerant. Although the baseline LDL-c levels in FH patients was significantly higher compared with the control group, some patients had modestly elevated LDL-c levels. The latter finding might be due to intensive lipid-lowering therapies in these patients.

Baseline arterial TBR_{max} was significantly higher in FH patients compared to control subjects (2.12±0.27 vs. 1.92±0.19, p=0.03) (Figure 1A-B). This difference remained significant after excluding FH patients with prior CVD (p=0.04). Moreover, arterial TBR_{max} remained higher in FH patients after adjusting for statin use (β=0.25, p=0.01), and risk factors of atherosclerosis (age, male gender, blood pressure, smoking) (β=0.19, p=0.03). A significant correlation was observed between baseline arterial TBR_{max} and LDL-c (R=0.37, p=0.03), as well as CRP level (R=0.48, p=0.006). The relationship between baseline arterial TBR_{max} and LDL-c remained significant after adjustment for statin use (β=0.001, p=0.02), and previously stated atherosclerosis risk factors (β=0.001, p=0.03). Moreover, the relationship between LDL-c and arterial inflammation remained significant (β=0.001, p=0.043) after adjusting for the baseline factors that were significantly different between patient groups (FH diagnosis, age, BMI).

TABLE 1. Baseline demographic and clinical characteristics of subjects

	Familial hypercholesterolemia (n=24)	Healthy controls (n = 14)	p-value
Age	56.79 ± 5.64	63.21 ± 7.4	0.005
Male gender	16 (66.7%)	11 (78.6%)	0.16
Body Mass Index (kg/m^2)	28.57 ± 4.1	24.35 ± 1.3	0.001
Current smoker	2 (8.3%)	2 (14.3%)	0.56
CVD (% (n))	7 (29%)	0	0.027
Blood pressure			
Systolic (mmHg)	132.67 ± 9 .58	141.21 ± 10.78	0.016
Diastolic (mmHg)	79.21 ± 8.94	83.57 ± 5.64	0.11
Total cholesterol (mg/dL)	320.9 ± 112.36	228.7 ± 32.93	0.005
LDL cholesterol (mg/dL)	236.4 ± 108.3	147.02 ± 31.14	0.005
HDL cholesterol (mg/dL)	54.83 ± 15.11	62.26 ± 11.6	0.12
Triglycerides (mg/dL)	140.27 ± 75.5	109.4 ± 79.7	0.24
Lipoprotein(a) (nmol/L)	73 [43-401]**	197 [40-480]	0.464
CRP (mg/L)	1.1 [0.6-2.0]**	0.7 [0.4-1.0]	0.115
Statin use	11 (45.83%)	0	na
Non-statin lipid-lowering therapy*	11 (45.83%)	0	na

Continuous data are shown as mean ± SD or median [min-max], categorical data as number (%). * 8 subjects were receiving both statin and a non-statin lipid lowering agent. ** Data available for apheresis naïve patients only (n=6). *CRP indicates C-reactive protein; CVD, cardiovascular disease; HDL, high density lipoprotein; LDL, low density lipoprotein; na, not assessed.*

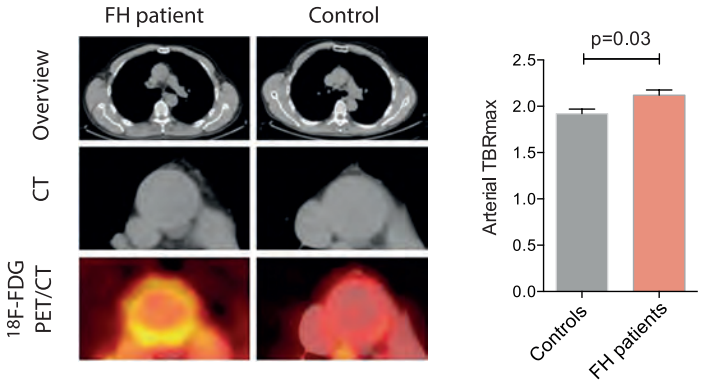

FIGURE 1. Patients with FH have higher arterial inflammation than control subjects

Representative images of CT and ^{18}F-FDG PET/CT of the aorta in a patient with FH (left) and an age-matched healthy control (right), showing that the arterial TBR_{max} (average of aorta and carotids) is significantly higher in patients with FH compared to healthy control subjects. This difference remained significant after adjustment for statin use (β=0.25, p=0.01), and risk factors of atherosclerosis (age, male gender, blood pressure, smoking) (β=0.19, p=0.03). Error bars represent standard error of mean. *FH indicates familial hypercholesterolemia; TBR_{max}, maximal target to background ratio.*

Impact of lipoprotein-apheresis on arterial Inflammation

The characteristics of the 12 FH patients treated with lipoprotein-apheresis are summarized in Table 2. Of note, 75% of patients undergoing apheresis were intolerant of statins. Following lipoprotein-apheresis, LDL-c levels were significantly reduced compared to baseline (284±118 vs. 127±50, p<0.001) which corresponded to a mean acute LDL-c reduction of 51±23%. Figure S1 displays the LDL-c levels during the apheresis treatment period of the apheresis naïve patients. We observed a significant reduction of arterial wall inflammation (TBR) following LDL-apheresis in arterial TBR_{max} (aorta and carotids) (2.05±0.31 versus 1.91±0.33, p=0.02, Figure 2A) and in TBR_{mds} of the index vessel (2.31±0.44 versus 2.03±0.48, p=0.03, Figure 2B). Corresponding reductions in arterial TBR_{max} and index TBR_{mds} were 6.47±8.08% and 11.8±14.2%, respectively. Notably, in the 6 non-apheresis-naïve patients, follow-up PET/CT imaging was performed after a single cycle of lipoprotein-apheresis (median interval [IQR]: 3 days [range 1 to 5 days]). In that sub-group, the index TBR_{mds} was significantly reduced after a single-cycle of apheresis (TBR_{mds}: 2.05±0.29 vs. 1.73±0.13 pre vs. post apheresis, respectively, p=0.03).

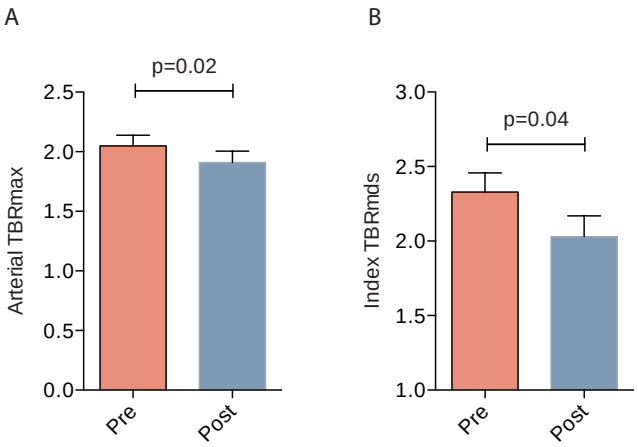

FIGURE 2. Reduction of arterial inflammation following lipoprotein-apheresis

Arterial ^{18}F-FDG uptake is significantly reduced after LDL-apheresis of 12 FH patients compared to baseline as assessed by average arterial TBR_{max} (2.05±0.31 vs. 1.91±0.33, p=0.02) (**A**) and index TBR_{mds} (2.31±0.44 vs. 2.03±0.48, p=0.037) (**B**). Corresponding reductions in arterial TBR_{max} and index TBR_{mds} were 6.47±8.08% and 11.8±14.2%, respectively. Error bars represent standard error of mean. *^{18}F-FDG indicates ^{18}F-fluorodeoxyglucose; FH, familial hypercholesterolemia; LDL, low density lipoprotein; TBR, target to background ratio; max, maximal; mds, most diseased segment.*

TABLE 2. Baseline and post-apheresis characteristics of patients treated with lipoprotein-apheresis

	Patients treated with lipoprotein-apheresis (n = 12)			
Age	57 ± 5.8			
Male gender	7 (58.3%)			
Body Mass Index (kg/m^2)	29.5 ± 2.3			
Current smoker	1 (8.3%)			
CVD (n, (%))	7 (58.3%)			
Blood pressure				
Systolic	130.3 ± 9.4			
Diastolic	79.1 ± 10.6			
Statin use	3 (25%)			
Non-statin lipid-lowering therapy	2 (16.7%)			
	Pre-apheresis	**Post-apheresis**	**Change (%)**	**p-value**
Mean arterial TBR_{max}	2.05 ± 0.31	1.91 ± 0.33	-6.5	0.020
Index TBR_{mds}	2.33 ± 0.44	2.03 ± 0.48	-11.8	0.037
Total cholesterol (mg/dL)	364.7 ± 117.9	189.2 ± 54.6	-45.1	<0.001
LDL cholesterol (mg/dL)	284.3 ± 118.0	127.3 ± 49.8	-51.2	<0.001
HDL cholesterol (mg/dL)	52.1 ± 16.8	55.1 ± 20.1	+5.4	0.224
Triglycerides (mg/dL)	114.0 [97.5-237.1]	103.1 [75.2-137.5]	-16.6	0.180
Lipoprotein(a) (mg/L)*	73.0 [43.3-400.5]	29.5 [19.3-174.5]	-56.4	0.043
CRP (mg/L)*	1.5 [0.6-5.5]	4.5 [1.1-9.3]	+77.7	0.120

Continuous data are shown as mean ± SD or median [min-max], categorical data as number (%). * post-apheresis values of Lp(a) and CRP were available from apheresis naïve patients only (n=6). *CVD indicates cardiovascular disease; CRP, C-reactive protein; mds, most diseased segment, LDL, low density lipoprotein, HDL, high density lipoprotein, IQR, interquartile range, TBR, target to background ratio.*

Table S1 summarizes TBR values of individual arteries before and after lipoprotein-apheresis. While reduction of LDL-c post-apheresis was greater in apheresis-naive subjects (-222±76 versus -91±69, p=0.01), there was no significant difference in changes of arterial TBR between apheresis-naive subjects and the patients who previously had undergone lipoprotein apheresis (p=0.39). Mean arterial TBR_{max} and TBR_{mds} of the index vessel strongly correlated with baseline LDL-c (R=0.71, p=0.01 and R=0.59, p=0.04 respectively, Figure 3), but not after lipoprotein apheresis (r=0.42, p=0.17 and r=0.44, p=0.18, respectively). We did not observe a significant change in HDL-c, triglycerides or CRP after lipoprotein-apheresis, whereas we did observe a reduction in Lp(a) levels (Table 2). However, changes in arterial TBR_{max} did not correlate with changes in CRP (p=0.21), triglycerides (p=0.16), HDL-c (p=0.20), or Lp(a) (p=0.78).

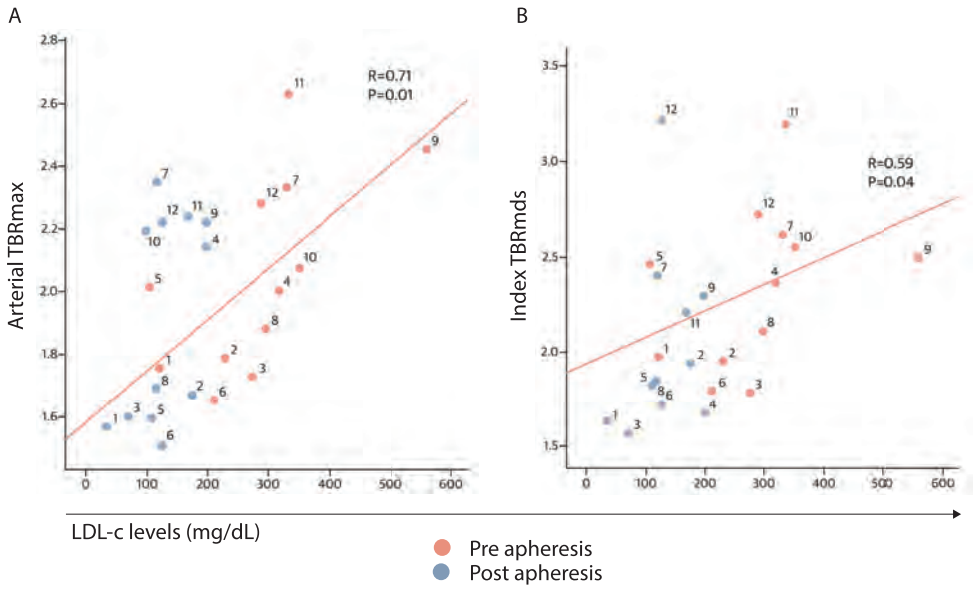

FIGURE 3. Arterial inflammation correlates with LDL-c level in the course of lipoprotein-apheresis

Arterial ^{18}F-FDG uptake (average TBR_{max} of aorta and carotids) (**A**) and TBR_{mds} of the index vessel (**B**) significantly correlated with LDL-c levels at baseline before, but not after, lipoprotein apheresis (r=0.42; p=0.17 and R=0.44; p=0.18, for arterial TBR_{max} and TBR_{mds}, respectively). The regression lines and correlation coefficients represent the baseline data only (salmon dots), and individual subjects are numerically labelled. *^{18}F-FDG indicates ^{18}F-fluorodeoxyglucose; LDL-c, low density lipoprotein cholesterol; TBR, target to background ratio; max, maximal; mds, most diseased segment.*

DISCUSSION

In the present study, we demonstrate that patients with FH, characterized by severely elevated plasma LDL-c levels, have markedly increased arterial wall inflammation compared with healthy control subjects without a history of CVD or hyperlipidemia as deter- mined by ^{18}F-FDG PET/CT scan. The degree of arterial wall inflammation correlated with LDL-c levels after adjusting for statin use and atherosclerotic risk factors. After lipoprotein apheresis in 12 FH patients who met the apheresis-treatment criteria, a significant reduction in arterial wall inflammation was observed.

Previous studies that addressed inflammation in FH patients have consistently reported a systemic, proinflammatory state, usually expressed as in- creased levels of plasma inflammatory biomarkers such as CRP[20]. Children afflicted by FH were characterized by higher levels of CRP compared with healthy control subjects[21,22]. Later in life, a low-grade inflammatory state was corroborated in adult FH patients with increased CRP levels as well as other inflammatory markers[23,24]. We observed a significant correlation between baseline CRP and arterial ^{18}F-FDG uptake in the study subjects. This finding aligns with prior observations concluding that both arterial ^{18}F-FDG uptake and CRP are surrogate markers of arterial inflammation. Moreover,

arterial TBR was reduced significantly after lipoprotein apheresis. In line with previous studies, we did not find a correlation between change in CRP and arterial TBR[18].

Although numerous studies with B-mode carotid ultrasound and magnetic resonance imaging have confirmed an increased atherosclerotic burden in FH[25], local arterial inflammation and the magnitude of its sensitivity to lipoprotein apheresis remained to be investigated. The beneficial effect of lipoprotein apheresis at the vascular function level has previously been demonstrated[26], reporting improved endothelial function after lipoprotein apheresis. Recently, PET/CT studies have been introduced as an imaging modality to quantitatively assess inflammation within the vessel wall[27]. Subsequent studies showed that an increased TBR correlated with macrophage content[13] as well as with gene expression markers for plaque vulnerability in atherosclerotic lesions[28]. Further, increased ^{18}F-FDG uptake has been associated with the presence of high-risk plaque morphology[29] and with atherosclerosis progression[30]. Moreover, the arterial ^{18}F-FDG PET/CT signal is linked to an increased risk of CV events[31,32] and recurrent cerebral infarction[4], and has been shown to be a potent predictor of future CVD after multivariate adjustment[14]. Here, we demonstrated that increased local arterial wall inflammation in patients with FH, irrespective of statin use and other potential confounding factors, was modifiable by lipoprotein-apheresis treatment. This observation underlines the close correlation between elevated lipoprotein levels and inflammatory activation within the arterial wall.

Most studies addressing anti-inflammatory effects of medications in CVD patients have used statins as an LDL-c–lowering agent, because statins exert numerous pleiotropic effects, including anti- inflammatory properties[15,33]. To address the impact of atherogenic lipoprotein-lowering therapy independent from pleiotropic effects, we applied lipoprotein apheresis in eligible FH patients. Here, we observed that the magnitude of reduction in arterial TBR seen with apheresis appears to be similar to that seen with high-dose statins[15]. However, it also is apparent that statins are associated with a somewhat greater reduction in arterial inflammation per mg/dl reduction in LDL-c. For example, in a prior study evaluating the effects of atorvastatin on arterial inflammation, each 10% reduction in LDL-c was associated with a 2.9% and 3.2% reduction in TBR_{mds} in the 10-mg and 80-mg atorvastatin groups, respectively[15]. With apheresis, the absolute change in arterial TBR was relatively smaller in magnitude compared with changes in LDL-c; each 10% reduction in LDL-c induced a 2.1% reduction in TBR_{mds}. Thus, on one hand, the significant reduction in arterial PET signal observed after apheresis demonstrates that nonpharmacological LDL-c lowering per se results in reduced atherosclerotic inflammation independently of the pleiotropic effects of pharmacotherapy. On the other hand, the fact that statins are associated with a modestly higher reduction in arterial inflammation per unit reduction in LDL-c supports the concept that a portion - albeit a limited one - of statins' anti-inflammatory actions may also relate to pleiotropic effects.

We also observed a numerically higher reduction in TBR of carotids compared with the aorta by apheresis; a prior study evaluating the effect of high-dose atorvastatin on arterial

inflammation made a similar observation[15]. The potential superiority of carotids to aorta as an imaging endpoint has been previously suggested[18]. Although it is not fully understood why, after lipid lowering, reductions in arterial inflammation (by ^{18}F-FDG PET/CT) may be more evident in the carotids over the aorta, which may be potentially due to biological differences in vessel walls or technical issues relating to the PET/CT imaging approach[18].

It is worth noting that reductions in arterial ^{18}F-FDG uptake occurred very rapidly in this study. In the subset of non–apheresis-naive subjects who under- went a single session of apheresis, the arterial PET signal was substantially reduced within a median of 3 days after apheresis. Prior studies in humans have noted that lipid lowering with statins produces reductions in arterial FDG uptake within 4 weeks (the earliest time point previously assessed). The current study shows that functional changes in the human artery wall occur even earlier, comparable to that demonstrated in animal studies[34].

Finally, it is notable that the magnitude of reduction in arterial TBR in our study is comparable to the impact potent anti-inflammatory agents, such as anti- tumor necrosis factor (TNF)-a therapy, exert on vessel wall inflammation. Recently, it was reported that after 8 weeks of treatment with a TNF-a antagonist in patients with rheumatoid arthritis, the TBR across the aorta was reduced by 6%[35]. Collectively, these data support a direct, strong role of atherogenic lipoprotein particles including LDL-c in driving atherogenic vascular inflammation, which implies that all potent atherogenic lipoprotein-lowering therapies might contain the potential to attenuate vessel wall inflammation in hyperlipidemic, atherosclerotic patients.

When interpreting the results of this study, several limitations need to be considered. First, matching between FH patients and controls was not optimal. For example, BMI was higher in FH patients compared with controls. Because higher BMI has been associated with increased ^{18}F-FDG uptake, this may have contributed to the higher signal in FH in our study[36]. However, this effect is partly counterbalanced by the more advanced age of controls, which can be expected to result in an increased ^{18}F-FDG uptake[36]. Overall, the matching is unlikely to have been of major influence, because the relation between LDL-c and TBR was retained after adjustment for confounding factors, including both BMI and age. Second, lipoprotein apheresis affects other plasma factors beyond apoprotein B–containing lipoproteins[37], including inflammatory proteins and oxidized phospholipids[38]. Part of these factors are bound to LDL-c and/or Lp(a), making it impossible to separate the impact of pure atherogenic lipoprotein lowering from the impact of lowering of their associated proinflammatory molecules. TBR change was significantly correlated with LDL-c change, whereas no correlation could be demonstrated for Lp(a), suggesting that most of the TBR change appears to be LDL-c driven. However, we cannot exclude the possibility that changes in other plasma factors may have contributed to the TBR decrease. Additionally, this study had a small sample size, especially in the treatment group, and we did not incorporate a control treatment arm in this study.

In conclusion, the present data indicate that prolonged and severe elevation of atherogenic apoprotein B–containing lipoproteins comprising LDL-c are important drivers of arterial

wall inflammation. The latter remains, however, amenable to improvement as attested by a significant decrease of arterial wall ^{18}F-FDG uptake after short-term lipoprotein apheresis. The fact that TBR in FH patients was higher at baseline, independent from statin use, combined with a TBR decrease after lipoprotein apheresis, lends further support to therapeutic efforts aimed at aggressive lowering of atherogenic lipoprotein particles, particularly in patients with severe LDL-c elevations and an increased CVD risk. Our findings emphasize the relevance of incorporating vessel wall inflammation imaging into future studies aimed at lowering atherogenic lipoprotein particles, particularly in high-risk patients with persistent LDL-c elevation. Moreover, the findings support the contention that nonpharmacological lipoprotein removal directly reduces arterial inflammation.

Acknowledgements: We wish to thank W.M. de Jong and P.F.C. Groot for their assistance in data acquisition.

Disclosures and funding: This work was partly supported by a grant from the Dutch Heart Foundation (CVON 2012: Genius, no. 2011B019). JJK is supported by a life-time achievement award of the Dutch Heart Foundation. GK Hovingh received funding by the Veni grant (project number 91612122) from the Netherlands Organization for Scientific Research (NWO).

REFERENCES

1. Ross R. Atherosclerosis: an inflammatory disease. N Engl J Med 1999;340:115–26.
2. Libby P et al. Progress and challenges in translating the biology of atherosclerosis. Nature 2011;473:317–25.
3. Underhill HR et al. Predictors of surface disruption with MR imaging in asymptomatic carotid artery stenosis. AJNR Am J Neuroradiol 2010;31:487–93.
4. Marnane M et al. Carotid plaque inflammation on (18)fluorodeoxyglucose positron emission tomography predicts early stroke recurrence. Ann Neurol 2012;71:709–18.
5. Van Wissen S et al. Differential hs-CRP reduction in patients with familial hypercholesterolemia treated with aggressive or conventional statin therapy. Atherosclerosis 2002;165:361–6.
6. Sjouke B et al. Familial hypercholesterolemia: present and future management. Curr Cardiol Rep 2011;13:527–36.
7. Smilde TJ et al. Effect of aggressive versus conventional lipid lowering on atherosclerosis progression in familial hypercholesterolaemia (ASAP). Lancet 2001;357:577–81.
8. Mohrschladt MF et al. Cardiovascular disease and mortality in statin-treated patients with familial hypercholesterolemia. Atherosclerosis 2004;172: 329–35.
9. Feig JE et al. Reversal of hyperlipidemia with a genetic switch favorably affects the content and inflammatory state of macrophages in atherosclerotic plaques. Circulation 2011;123:989–98.
10. Antonopoulos AS et al. Statins as anti- inflammatory agents in atherogenesis: molecular mechanisms and lessons from the recent clinical trials. Curr Pharm Des 2012;18:1519–30.
11. Ridker PM et al. Relation of baseline high-sensitivity C-reactive protein level to cardiovascular outcomes with rosuvastatin in JUPITER. Am J Cardiol 2010;106: 204–9.
12. Rudd JH et al. Imaging atherosclerotic plaque inflammation with (18)fluorodeoxyglucose positron emission tomography. Circulation 2002;105:2708–11.
13. Tawakol A et al. In vivo 18fluorodeoxyglucose positron emission tomography imaging provides a noninvasive measure of carotid plaque inflammation in patients. J Am Coll Cardiol 2006;48:1818–24.
14. Figueroa AL et al. Measurement of arterial activity on routine FDG PET/CT images improves prediction of risk of future cardiovascular events. J Am Coll Cardiol Img 2013;6:1250–9.
15. Tawakol A et al. Intensification of statin therapy results in a rapid reduction in atherosclerotic inflammation: results of a multi-center FDG-PET/CT feasibility study. J Am Coll Cardiol 2013;62:909–17.
16. Szczepiorkowski ZM et al. Guidelines on the use of therapeutic apheresis in clinical practice. J Clin Apher 2010; 25:83–177.
17. Rogers IS et al. Feasibility of FDG imaging of the coronary arteries: comparison between acute coronary syndrome and stable angina. J Am Coll Cardiol Img 2010;3: 388–97.
18. Fayad ZA et al. Safety and efficacy of dalcetrapib on atherosclerotic disease using novel non-invasive multimodality imaging (dal-PLAQUE). Lancet 2011;378:1547–59.
19. Friedewald WT et al. Estimation of the concentration of low-density lipoprotein cholesterol in plasma, without use of the preparative ultracentrifuge. Clin Chem 1972;18: 499–502.
20. Gokalp D et al. Levels of proinflammatory cytokines and hs-CRP in patients with homozygous familial hypercholesterolaemia. Acta Cardiol 2009;64:603–9.
21. Holven KB et al. Chemokines in children with heterozygous familiar hypercholesterolemia: selective upregulation of RANTES. Arterioscler Thromb Vasc Biol 2006;26: 200–5.
22. Narverud I et al. Children with familial hypercholesterolemia are characterized by an inflammatory imbalance between the tumor necrosis factor alpha system and interleukin-10. Atherosclerosis 2011;214:163–8.
23. Cheng HM et al. Vascular stiffness in familial hypercholesterolaemia is associated with C-reactive protein and cholesterol burden. Eur J Clin Invest 2007;37:197–206.

24. Real JT et al. Circulating mononuclear cells nuclear factor-kappa B activity, plasma xanthine oxidase, and low grade inflammatory markers in adult patients with familial hypercholesterolaemia. Eur J Clin Invest 2010;40:89–94.
25. Caballero P et al. Detection of subclinical atherosclerosis in familial hypercholesterolemia using non-invasive imaging modalities. Atherosclerosis 2012;222:468–72.
26. Igarashi K et al. Improvement of endothelium-dependent coronary vasodilation after a single LDL apheresis in patients with hypercholesterolemia. J Clin Apher 2004;19:11–6.
27. Rudd JH et al. Inflammation imaging in atherosclerosis. Arterioscler Thromb Vasc Biol 2009;29:1009–16.
28. Pedersen SF et al. Gene expression and 18FDG uptake in atherosclerotic carotid plaques. Nucl Med Commun 2010;31:423–9.
29. Figueroa AL et al. Distribution of inflammation within carotid atherosclerotic plaques with high-risk morphological features: a comparison between positron emission tomography activity, plaque morphology, and histopathology. Circ Cardiovasc Imaging 2012; 5:69–77.
30. Abdelbaky A et al. Focal arterial inflammation precedes subsequent calcification in the same location: a longitudinal FDG-PET/CT study. Circ Cardiovasc Imaging 2013; 6:747–54.
31. Paulmier B et al. Arterial wall uptake of fluorodeoxyglucose on PET imaging in stable cancer disease patients indicates higher risk for cardiovascular events. J Nucl Cardiol 2008;15:209–17.
32. Rominger A et al. 18F-FDG PET/CT identifies patients at risk for future vascular events in an otherwise asymptomatic cohort with neoplastic disease. J Nucl Med 2009; 50:1611–20.
33. Davignon J. Beneficial cardiovascular pleiotropic effects of statins. Circulation 2004;109: III39–43.
34. Lobatto ME et al. Multimodal clinical imaging to longitudinally assess a nanomedical anti-inflammatory treatment in experimental atherosclerosis. Mol Pharm 2010;7: 2020–9.
35. Maki-Petaja KM et al. Anti-tumor necrosis factor-alpha therapy reduces aortic inflammation and stiffness in patients with rheumatoid arthritis. Circulation 2012; 126:2473–80.
36. Bucerius J et al. Prevalence and risk factors of carotid vessel wall inflammation in coronary artery disease patients: FDG-PET and CT imaging study. J Am Coll Cardiol Img 2011;4:1195–205.
37. Hovland A et al. LDL apheresis and inflammation—implications for atherosclerosis. Scand J Immunol 2012;76:229–36.
38. Arai K et al. Acute impact of apheresis on oxidized phospholipids in patients with familial hypercholesterolemia. J Lipid Res 2012;53:1670–8.

SUPPLEMENT

TABLE S1. Differences in target-to-background ratios pre and post apheresis

	Pre-apheresis	Post-apheresis	p-value
Aorta TBR_{max}	2.12 ± 0.50	2.03 ± 0.59	0.42
Carotid TBR_{max}	1.94 ± 0.25	1.78 ± 0.19	0.01
Mean arterial TBR_{max}	2.05 ± 0.31	1.91 ± 0.33	0.02
Index TBR_{max}	2.19 ± 0.47	2.13 ± 0.50	0.57
Aorta TBR_{mds}	2.19 ± 0.54	2.05 ± 0.48	0.20
Carotid TBR_{mds}	2.06 ± 0.28	1.81 ± 0.21	0.004
Mean arterial TBR_{mds}	2.15 ± 0.32	1.94 ± 0.28	<0.001
Index TBR_{mds}	2.31 ± 0.44	2.03 ± 0.48	0.04

Data are shown in mean ± SD. *Mds indicates most diseased segment; TBR, target target-to-background ratio.*

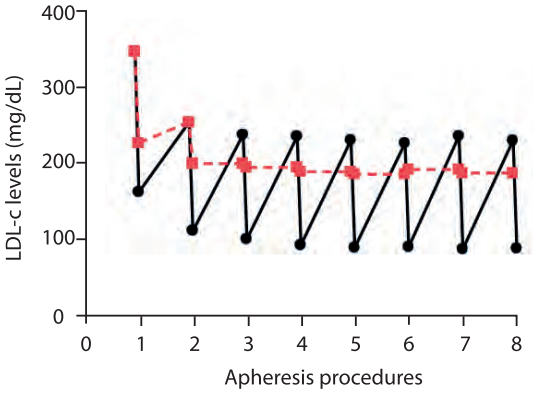

Figure S1. Mean LDL-c levels pre and post apheresis procedures in six apheresis naïve patients

Black line represents mean LDL-c levels prior and post apheresis procedures. Red dotted line represents time-averaged mean LDL-c levels between separate Lipoprotein apheresis procedures calculated according to the Kroon Formula (Thompson GR. Lipoprotein apheresis. Curr Opin Lipidol 2010). *LDL-c indicates low density lipoprotein cholesterol.*

CHAPTER 6

ANTI-INFLAMMATORY EFFECTS OF LIPID LOWERING IN PATIENTS WITH FAMILIAL HYPERCHOLESTEROLEMIA: BEYOND STATINS AND C-REACTIVE PROTEIN

Bernelot Moens SJ*, Neele AE*, Kroon J, **van der Valk FM**, van den Bossche J, Hoeksema MA, Schnitzler JG, Baccara-Dinet MT, Manvelian G, de Winther MPJ, Stroes ESG.

* Authors contributed equally

Submitted

ABSTRACT

Rationale: Monocytes are important contributors to atherosclerosis**.** Recent studies revealed direct effects of lipids on monocytes' migratory capacity, suggesting that lipid lowering may reverse this effect. Here, we assessed monocyte phenotype in function in patients with familial hypercholesterolemia (FH) compared with controls. In a subset of FH patients we subsequently evaluated the effect on monocytes of proprotein convertase subtilisin/kexin type 9 (PCSK9) monoclonal antibodies, which selectively reduce low density lipoprotein cholesterol (LDL-c).

Methods and Results: We assessed monocyte phenotype and function using flow cytometry and a trans-endothelial migration (TEM) assay in FH patients (n=15, mean LDL-c 6.2±1.7 mmol/L) and healthy controls (n=11, mean LDL-c 2.4±0.7 mmol/L). Monocyte chemokine receptor (CCR) 2 expression was approximately 3-fold higher in FH patients compared with controls, and correlated significantly with plasma LDL–c levels (r=0.621). Moreover, monocytes from FH patients showed enhanced migratory capacity *ex vivo* and CCR2 expression positively associated with intracellular lipid accumulation. In a subset of FH patients (n=10), we assessed the effect of 24 weeks of PCSK9 inhibition (alirocumab) on monocyte phenotype. LDL-c was reduced, with concomitant reductions in monocyte CCR2 expression and intracellular lipid content, without affecting CRP levels. Treatment with PCSK9 inhibition (alirocumab) on monocyte phenotype. LDL-c was reduced, with concomitant reductions also reduced monocyte inflammatory responsiveness, with lower tumor necrosis factor production following lipopolysaccharide challenge.

Conclusion: Monocytes of FH patients have a pro-inflammatory phenotype, which is dampened by LDL-c lowering via PCSK9 inhibition (alirocumab), independent of CRP lowering. LDL-c lowering was paralleled by reduced monocyte intracellular lipid content, suggesting that LDL-c lowering itself is associated with anti-inflammatory effects on circulating monocytes.

INTRODUCTION

A unifying view of atherosclerotic cardiovascular (CV) disease posits that inflammation has a key role in its pathogenesis and transduces the effects of many known CV risk factors, including low-density-lipoprotein cholesterol (LDL-c). The study of systemic inflammatory biomarkers, such as C-reactive protein (CRP), has supported this concept, yet not without controversy.[1] For instance, the CV benefit conveyed by statin therapy is independently associated with both LDL-c and C-reactive protein (CRP) lowering.[2-4] However, Mendelian randomization studies have not supported a causal role of CRP in atherogenesis[5].

To further dissect the lipid-inflammation interaction, past years focus has shited towards more cell-specific studies[6,7], with a predominant role for monocytes[8-14]. The advent of proprotein convertase subtilisin/kexin type 9 (PCSK9) monoclonal antibodies (mAb) enables the study of specific LDL-c lowering on monocytes in patients. Via antibody-mediated scavenging of the free PCSK9 protein, PCSK9 inhibition results in increased hepatic LDL-receptor (LDLR) expression.[15] Consequently, PCSK9 antibodies can provide a mean LDL-c reduction of up to 60%,[16–18] without affecting CRP levels.[19]

In this proof-of-concept study, we first assessed the impact of elevated LDL-c levels on monocyte phenotype and function in patients with familial hypercholesterolemia (FH) not using statins versus normolipidemic control subjects. Subsequently, we assessed the impact of PCSK9 inhibition (via alirocumab) in FH patients on monocytes, compared to a reference group of FH patients on stable statin dose for at least 6 months. Overall, these studies demonstrate that selective lowering of LDL-c with PCSK9 inhibition reduces the pro-inflammatory profile of circulating monocytes.

METHODS

Patient selection

This single-center study comprised four groups:

1. Age- and gender-matched healthy controls (n=11).
2. Patients with definite or probable FH[20] (n=15) not receiving statin therapy.
3. A subset of the FH patients (n=10), in whom we assessed the effect of 24-weeks of treatment with PCSK9 mAb alirocumab in a single-center substudy of the ODYSSEY CHOICE II (NCT02023879). In this trial patients with hypercholesterolemia not receiving a statin were randomized to alirocumab (150 mg every 4 weeks [Q4W] or 75 mg every 2 weeks [Q2W]), or placebo. After study completion, patients were offered the opportunity to enter an open-label extension (OLE) receiving alirocumab 150 mg Q4W. Considering the planned randomization rate (Supplemental methods), for this

proof-of-concept study placebo samples (n=3) were not analyzed. All analyses were performed after 24 weeks of active treatment (either during the double blind period or in OLE). All measurements were performed at the AMC, except for lipids, which were determined in the ODYSSEY CHOICE II study.

4. Age- and gender-matched FH patients (n=11) on stable (at least 24 weeks) statin therapy, for comparison of treatment effects.

Exclusion criteria were a history CVD in the past 12 months, infection or diabetes. The study protocol was approved by the institutional review board of the Academic Medical Center in Amsterdam, The Netherlands, and written informed consent was obtained from each participant.

Baseline data collection

Subjects visited the hospital after an overnight fast for physical examination, medical history recording and blood withdrawal. Lipid levels, CRP, creatitin, leukocyte count and differentiation were determined using standard laboratory procedures.

Flow cytometry

After removing red blood cells, white blood cells were stained with antibodies for various surface markers (Table S1). Fluorescence was measured with BD Canto II and analyzed with FlowJo software version 7.6.5. (FlowJo, LLC, Ashland, OR). Monocytes were gated based on CD14, CD16, and HLA-DR expression.[21] Monocyte area was gated by forward/side scatter, CD14+ and/or CD16+ cells were gated, and HLA-DR positive cells were considered monocytes, which were divided into classical (CD14++/CD16-), intermediate (CD14++/CD16+), or non-classical ($CD14^{dim}$/CD16+).The expression of surface markers was calculated as delta (Δ) median fluorescence imaging (MFI) (ΔMFI= MFI surface staining – MFI isotype control).

Monocyte characterization

Mononuclear cells were isolated through density centrifugation using Lymphoprep™ (Axis-Shield, Dundee, Scotland) and isolated using human CD14 magnetic beads and MACS® cell separation columns (Miltenyi, Bergisch Gladbach, Germany). *Migration assays:* To functionally assess adhesive and migratory capacity, a trans-endothelial migration (TEM) assay was performed[8], outlined in the supplement. To investigate whether migration was mediated by MCP-1, we performed representative chemotaxis assays, detailed in the Supplemental material. *Lipid accumulation:* Monocytes were added to fibronectin (FN; 30 µg/mL) coated glass slides ($0.5*10^6$/mL), incubated for 1 hour (37°C, 5% CO_2), fixed with 4% formaldehyde , permeabilized with 0.1% Triton-X100 and incubated with the lipid dye Nile Red (1 µg/mL; N3013-100MG, Sigma Aldrich, Zwijndrecht, The Netherlands), after which cells were mounted

(Dako, Heverlee, Belgium). Quantification of lipid droplets was performed on a Leica TCS SP8 Confocal laser scanning microscope, assessing total number of monocytes with lipid droplets, and number of lipid droplets per monocyte, in 6–10 field of views (FOVs). To study interdependency of CCR2 expression and lipid accumulation, $CCR2^{high}$ monocytes were sorted by flow cytometry (Supplemental methods), plated and stained with Nile Red. For representative images, co-immunohistochemistry with Nile Red and CCR2 was performed (Supplemental material).

RNA isolation and quantitative PCR analysis

RNA was isolated with High Pure RNA Isolation kits (Roche, Basel, Switzerland) from 500,000 cells. 400 ng of RNA was used for cDNA synthesis with iScript (BioRad, Veenendaal, The Netherlands). qPCR was performed with 4 ng cDNA using Sybr Green Fast on a ViiA7 PCR machine (Applied Biosystems, Bleiswijk, The Netherlands). Gene expression was normalized to the mean of two housekeeping genes (*B2M* , *GAPDH)* (all primer sequences outlined in Table S2).

Ex vivo lipopolysaccharide (LPS) challenge for cytokine production

Cells were untreated or stimulated with 10 ng/mL LPS in triplo (Supplemental material). After 24 h, the medium was stored at –80°C. Production of cytokines was measured in a panel consisting of TNF and interleukin (IL)-10 using luminex (Bioplex, BioRad, Veenendaal, The Netherlands).

Statistical analysis

Data are mean (standard deviation), median (inter-quartile range) or number (percentage), unless stated otherwise. Differences in clinical characteristics and monocyte phenotype and function between FH patients and controls were assessed with student T-tests or Mann-Whitney U tests. Correlations were assessed using univariate linear regression. Data pre- and post-alirocumab combined with stable statin users were assessed with a one-way ANOVA using a dunnett post-hoc test. A two-way ANOVA with bonferroni post-hoc analysis was performed for all flow cytometry analysis. A 2-sided *P*-value<0.05 was considered statistically significant. Data were analyzed using Prism version 5.0 (GraphPad software, La Jolla, California) or SPSS version 22.0 (SPSS Inc., Chicago, Illinois).

RESULTS

Study population

Characteristics of 15 FH patients not using statins and 11 control subjects are listed in Table 1. FH patients had higher cholesterol levels and body mass index (BMI), and more frequent history of CVD. CRP levels were comparable between control subjects and FH patients (0.85 [0.58–1.4] versus 0.96 [0.4–1.5] mg/dl respectively, *P*=0.504). Disease specifications and medication use are outlined in Table S3.

Table 1. Characteristics of control subjects and FH patients

	Control n= 11	FH (no statin) n= 15	*P*-value
Age, years	48 ± 11	52 ± 14	0.452
Gender, n, male (%)	6 (55)	9 (64)	0.781
BMI, kg/m^2	23 ± 2	27 ± 4	0.003
Smoking, (% active)	0 (0)	1 (7)	0.366
CVD history, (%)	0 (0)	7 (50)	0.006
SBP, mmHg	124 ± 14	136 ± 13	0.118
DBP, mmHg	79 ± 5	81 ± 11	0.692
CRP, mg/L	0.85 [0.58–1.4]	0.96 [0.4–1.5]	1.000
Total cholesterol, mmol/L	4.8 ± 0.9	9.2 ± 1.9	<0.001
LDL-c, mmol/L	2.6 ± 0.8	7.1 ± 1.6	<0.001
HDL-c, mmol/L	1.9 ± 0.4	1.6 ± 0.8	0.159
Triglycerides, mmol/L	0.68 [0.57–0.96]	1.6 [1.0–2.3]	0.036
Lp(a), mg/dL	6 [5–44]	17 [5–108]	0.299
Leukocytes, 10^9/L	5.1 ± 1.0	5.5 ± 1.1	0.339
Neutrofils, 10^9/L	2.8 ± 0.8	3.4 ± 0.9	0.094
Lymphocytes, 10^9/L	1.6 ± 0.4	1.6 ± 0.3	0.830
Monocytes, 10^9/L	0.4 ± 0.1	0.4 ± 0.1	0.652

Values are n (%), mean±SD or median [IQR,] for skewed data. *BMI indicates body mass index; CRP, c-reactive protein; CVD, cardiovascular disease; DBP, diastolic blood pressure; FH, familial hypercholesterolemia; HDL-c, high density lipoprotein cholesterol; IQR, inter-quartile range; LDL-c, low density lipoprotein cholesterol; Lp(a), lipoprotein (a); SBP, systolic blood pressure, SD, standard deviation.*

Increased CCR2 expression and migratory capacity of monocytes

Monocytes were gated based on their CD14 and CD16 expression (Figure 1A). Subset distribution was comparable between FH patients and control subjects (Figure 1B). Monocyte CCR2 expression was induced on classical monocytes in FH patients (ΔMFI 558±209 versus 189±97, *P*<0.001) (Figure 1C-D), with concurrent increases in the chemokine receptor CX3CR1, and integrins CD11b, CD18 and CD29 (Figure S1). LDL-c levels correlated with monocyte CCR2

expression in FH patients (r=0.621, *P*=0.042) (Figure 1E). As CCR2 is involved in monocyte recruitment,[10] we assessed trans-endothelial migration (TEM) rate of monocytes in an additional group of FH patients and control subjects (n=7 for each group, Table S4). We found a 1.5-fold increase in monocyte migration in FH patients compared with control subjects (number of transmigrated cells/mm^2: FH 91±25, control 57±13; *P*=0.008) (Figure 1F). In chemotaxis assays (n=3) monocytes of an FH subject showed strong directional movement towards MCP-1, the ligand for CCR2, whereas monocytes of a control subject showed non-directional, random migration (Supplemental Video, Figure S4).

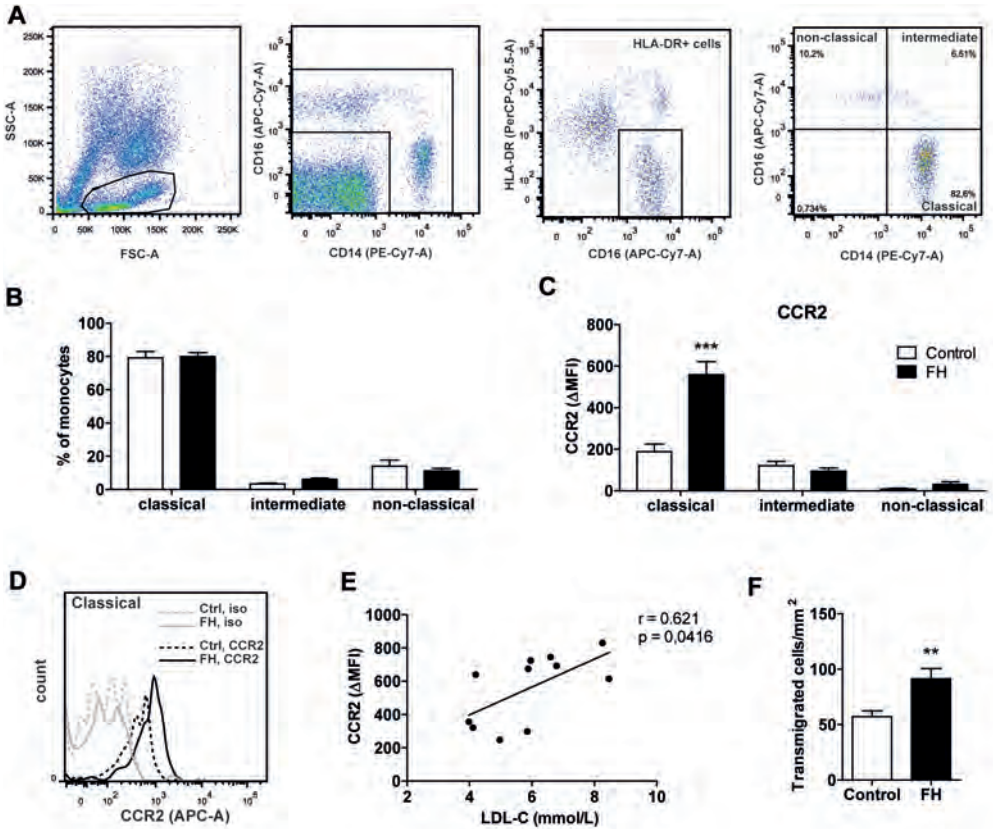

FIGURE 1. Monocytes of FH patients show enhanced CCR2 expression and migratory capacity

Flow cytometry on whole blood was performed to study monocyte surface expression. (**A**) CD14+ and/or CD16+ cells were gated, and only HLA-DR positive cells were considered to be monocytes. (**B**) Percentage of monocyte subsets (classical (CD14++/CD16-), intermediate (CD14++/CD16+), or non-classical (CD14^{dim}/CD16+)) in FH patients (n=15) versus controls (n=11). (**C**) Surface expression of monocyte CCR2 represented as delta median fluorescence intensity. (**D**) Histogram of CCR2 expression in classical monocytes of an FH patient (solid, black) or controls (dashed, black) with isotype controls (gray). (**E**) Correlation between plasma LDL-c levels and CCR2 surface expression of FH patients (**F**) Trans-endothelial migratory capacity presented as the transmigrated cells/mm^2. For each subject, transmigrated cells are calculated of independent counts of five frames of view. Data represent mean ± SEM **P*<0.05; ***P*<0.01; ***P<0.001. *APC indicates allophycocyanin; CCR, chemokine receptor; FH, familial hypercholesterolemia; LDL-c, low-density lipoprotein cholesterol; SEM, standard error of the mean.*

Enhanced lipid accumulation in monocytes

We assessed monocyte intracellular lipid content with Nile red dye, and genes involved in lipid handling in FH patients and controls (in the TEM subset, n=7 for both groups, Table S4). FH patients with elevated LDL-c levels (7.8±1.9 mmol/L) had a higher fraction of lipid positive monocytes (FH: 76±12% versus controls: 59±13%, *P*=0.03; Figure 2), with increased numbers of lipid droplets per cell (8±1 in FH versus 5±2 in controls, *P*=0.02) (Figure 2A–D). Higher lipid content coincided with higher surface expression of CD36 on classical monocytes, and SRA on intermediate monocytes (Figure 2E–F). *ABCA1* and *ABCG1* were also upregulated (Figure 2G), most likely due to induction by lipids. Next, we assessed the interdependency of increased lipid content and CCR2 expression. FACS sorting revealed that $CCR2^{high}$ cells (MFI cutoff 3500) had a higher number of lipid droplets ($CCR2^{high}$ 33±3 versus $CCR2^{intermediate/low}$ 10±1, *P*<0.001) (Figure S2A–B). Visually, using immunocytochemistry, cells without lipid droplets had low levels of CCR2, whereas monocytes with high numbers of lipid droplets had higher CCR2 expression (Figure S2C).

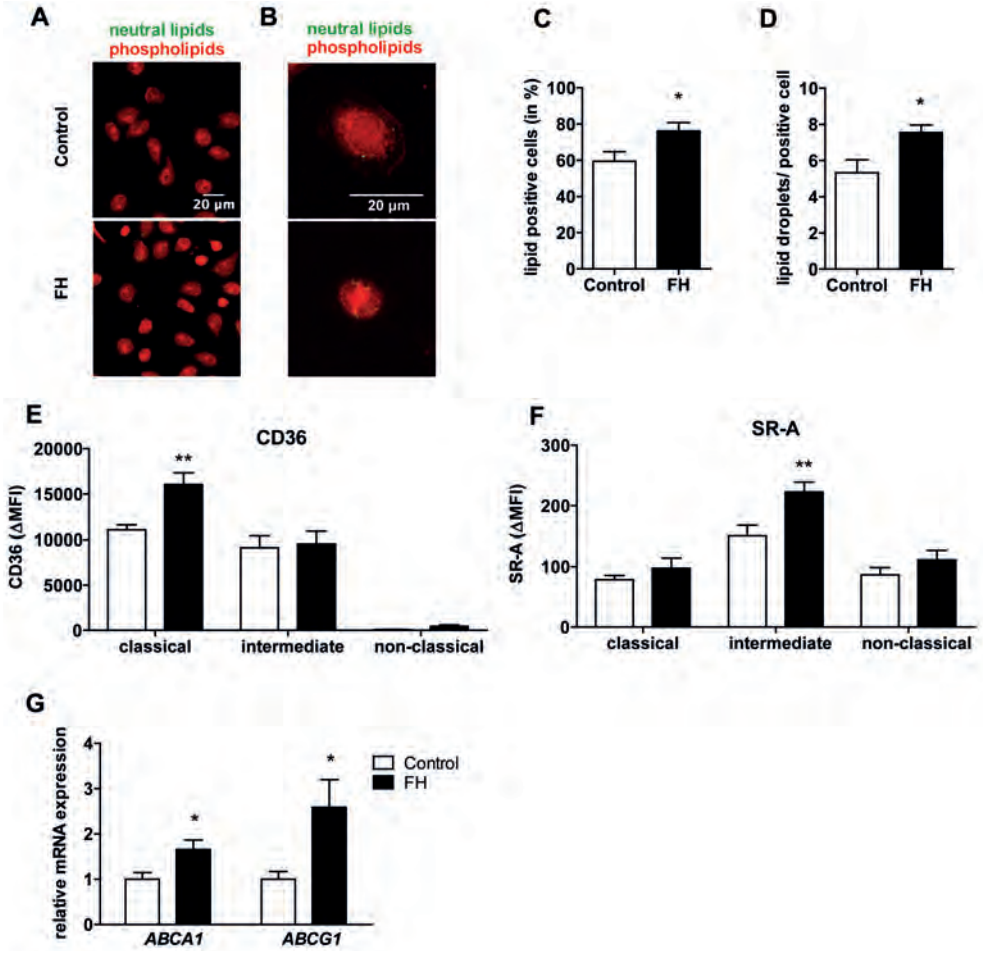

FIGURE 2. Lipids accumulate in monocytes of FH patients

Lipid accumulation in FH patients (n=7) and control subjects (n=7) was assessed. (**A,B**) Neutral lipid droplets in green of isolated monocytes. (**C**) Quantification of lipid accumulation presented as the percentage of lipid positive cells (represented in A). (**D**) Number of lipid droplets per lipid positive monocytes (represented in **B**). (**E,F**) Surface expression of the scavenger receptors CD36 and SR-A assessed by flow cytometry. Quantified as delta median fluorescence intensity. (**G**) mRNA expression, of cholesterol efflux genes *ABCA1* and *ABCG1*, normalized to housekeeping genes (*B2M, GAPDH)*. Data represent mean ± SEM **P*<0.05; ***P*<0.01; ****P*<0.001. *ABCA indicates ATP binding cassette transporter; B2M, beta-2-microglubilin; FH, familial hypercholesterolemia; GAPDH, glyceraldehyde 3-phosphate dehydrogenase; NR, Nile Red; SEM, standard error of the mean; SR, scavenger receptor.*

PCSK9 mAb lowers LDL-c levels in FH patients

Ten FH patients not using statins participated in the substudy of the ODYSSEY CHOICE II (treatment allocation and dosing outlined in Table S5). For comparison, we simultaneously evaluated 11 FH patients using statins (Table 2 and Table S6). FH subjects receiving PSCK9 mAb (alirocumab) had an adverse cardiovascular risk profile compared with statin-treated subjects, with higher BMI, SBP and triglycerides. Following alirocumab, LDL-c dropped 49% (±14%), from 5.8±1.3 mmol/L to 2.9±1.2 mmol/L (p=<0.001). Post-alirocumab levels were comparable with statin treated FH-patients (2.6±0.5; *P*=0.437 versus alirocumab). CRP was unaffected by alirocumab (pre-alirocumab: 1.2 [0.7–2.4] mg/ld., post-alirocumab: 1.2 [0.6–1.7] mg/ld., *P*=0.6). CRP levels in statin treated FH patients were 0.7 [0.2–1.2] mg/L, *(P*=0.134 versus post-alirocumab and 0.370 versus pre-alirocumab). Other pre- and post-treatment lipid levels are summarized in Table 2.

TABLE 2. Characteristics of FH patients

	FH, pre PCSK9 mAb	**FH, post PCSK9 mAb**	***P*-value**	**FH stable statin use**	***P*-value** *(vs. untreated)*
	n=10	n=10		n=11	
Age, years	54 ± 12	54 ± 12	na	53 ± 12	0.800
Gender, n, male (%)	6 (60)	6 (60)	na	6 (55)	0.801
BMI, kg/m^2	28 ± 5	29 ± 5	0.342	24 ± 3	0.020
Smoking (% active)	1 (10)	1 (10)	na	2 (18)	0.329
CVD history	6 (60)	6 (60)	na	2 (18)	0.028
SBP, mmHg	137 ± 11	134 ± 19	0.488	122 ± 14	0.015
DBP, mmHg	82 ± 10	80 ± 9	0.407	77 ± 8	0.241
CRP, mg/L	1.2 [0.7-2.4]	1.2 [0.6-1.7]	0.600	0.7 [0.2-1.2]	0.370
Total cholesterol, mmol/L	8.1 ± 1.2	5.1 ± 1.4	<0.001	4.8 ± 0.8	<0.001
LDL-c, mmol/L	5.8 ± 1.3	2.9 ± 1.2	<0.001	2.6 ± 0.5	<0.001
HDL-c, mmol/L	1.5 ± 0.6	1.4 ± 0.5	0.645	1.6 ± 0.6	0.581
Triglycerides, mmol/L	1.7 [1.3–2.7]	1.5 [0.9–2.4]	0.069	0.9 [0.6–1.2]	0.005
Lp(a), mg/dL	9 [5–113]	12 [5.7–87.7]	0.753	26 [10–93]	1.000
Leukocytes, 10^9/L	6.0±0.8	6.0 ± 0.5	0.864	5.6 ± 1.8	0.534
Neutrofils, 10^9/L	3.7 ± 0.6	3.7 ± 0.8	0.869	3.0 ± 1.3	0.120
Lymphocytes, 10^9/L	1.7 ± 0.3	1.7 ± 0.4	0.949	2.0 ± 0.7	0.158
Monocytes, 10^9/L	0.4 ± 0.1	0.5 ± 0.1	0.673	0.5 ± 0.2	0.224

Values are n (%), mean±SD or median [IQR,] for skewed data. *BMI indicates body mass index; CRP, c-reactive protein; CVD, cardiovascular disease; DBP, diastolic blood pressure; FH, familial hypercholesterolemia; HDL-c, high density lipoprotein cholesterol; IQR, inter-quartile range; LDL-c, low density lipoprotein cholesterol; Lp(a), lipoprotein (a); na, not applicable; SBP, systolic blood pressure; SD, standard deviation.*

Lipid lowering by PCSK9 mAb reduces CCR2 expression and lipid accumulation

Alirocumab did not affect monocyte subset distribution (Figure 3A), but resulted in a 60% reduction of monocyte CCR2 surface expression (ΔMFI: pre-alirocumab: 551±201, post-alirocumab: 229±205, *P*<0.001), to levels comparable to those observed in FH patients using statins (ΔMFI, 274±256, *P*=non-significant versus post-alirocumab; *P*<0.001 versus pre-alirocumab) (Figure 3B-C). We also found lower levels of intracellular lipid accumulation in alirocumab-treated FH patients (fraction of monocytes with lipid droplets post-treatment: 50±16, *P*=0.005 versus FH-no statin, number of lipid droplets/monocyte: 5±2, *P*=0.01 versus FH-no statin)(Figure 3D–E). Other chemokines and integrin's showed non-significant declines upon treatment and were comparable with those in FH patients using statins (Figure S3). Although surface expression of CD36 and SR-A was unaffected by lipid lowering (Figure 3F–G), in line with lower lipid content, expression of *ABCA1 and ABCG1* dropped to levels observed in control subjects (Figure 3H). Finally, in a representative experiment, alirocumab resulted in lower motility and migration distance of monocytes compared to an FH patient without statin or alirocumab (Supplemental Video and Figure S4).

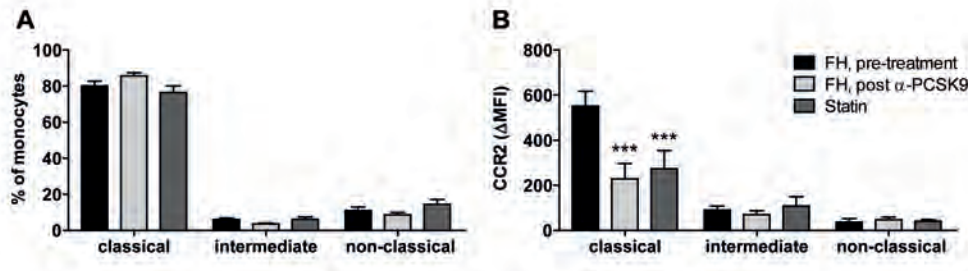

FIGURE 3. PCSK9 inhibition reduces CCR2, lipid accumulation, and inflammatory cytokine production To assess the effect of lipid lowering of PCSK9 antibody, 10 FH patients were treated with alirocumab for 6 months. A group of stable statin users (n=11) was added as a reference. (**A**) Percentage of monocyte subsets, divided into classical, (CD14++/CD16-), intermediate (CD14++/CD16+), or non-classical ($CD14^{dim}$/CD16+). (**B**) Surface expression of monocyte CCR2 represented as delta median fluorescence intensity. (**C**) Histogram of CCR2 expression in classical monocytes of an FH patient , pre-alirocumab(solid, black), FH patient, post-alirocumab (solid, light-gray) or stable statin (solid, dark –gray) with isotype controls (dashed lines). (**D**) Quantification of intracellular lipid accumulation using NR immunohistochemistry presented as the percentage of lipid positive cells. (**E**) Number of lipid droplets per lipid positive cell. (**F,G**) Expression of the scavenger receptors CD36 and SR-A assessed by flow cytometry, quantified as delta median fluorescence intensity. (**H**) mRNA expression of the cholesterol efflux genes *ABCA1* and *ABCG1*, normalized to housekeeping genes (*B2M, GAPDH).* (**I,J**) Cytokine secretion of TNF and IL-10 by monocytes after 24 h of LPS stimulation measured by luminex. Data represent mean ± SEM **P*<0.05; ***P*<0.01; ****P*<0.001. *ABCA indicates ATP binding cassette transporter; B2M, beta-2-microglubilin; CCR, chemokine receptor; FH, familial hypercholesterolemia; GAPDH, glyceraldehyde 3-phosphate dehydrogenase; IL-10, interleukin-10; LPS, lipopolysaccharide; NR, Nile Red; PCSK9, proprotein convertase subtilisin/kexin type 9; SEM, standard error of the mean; TNF, tumor necrosis factor.*

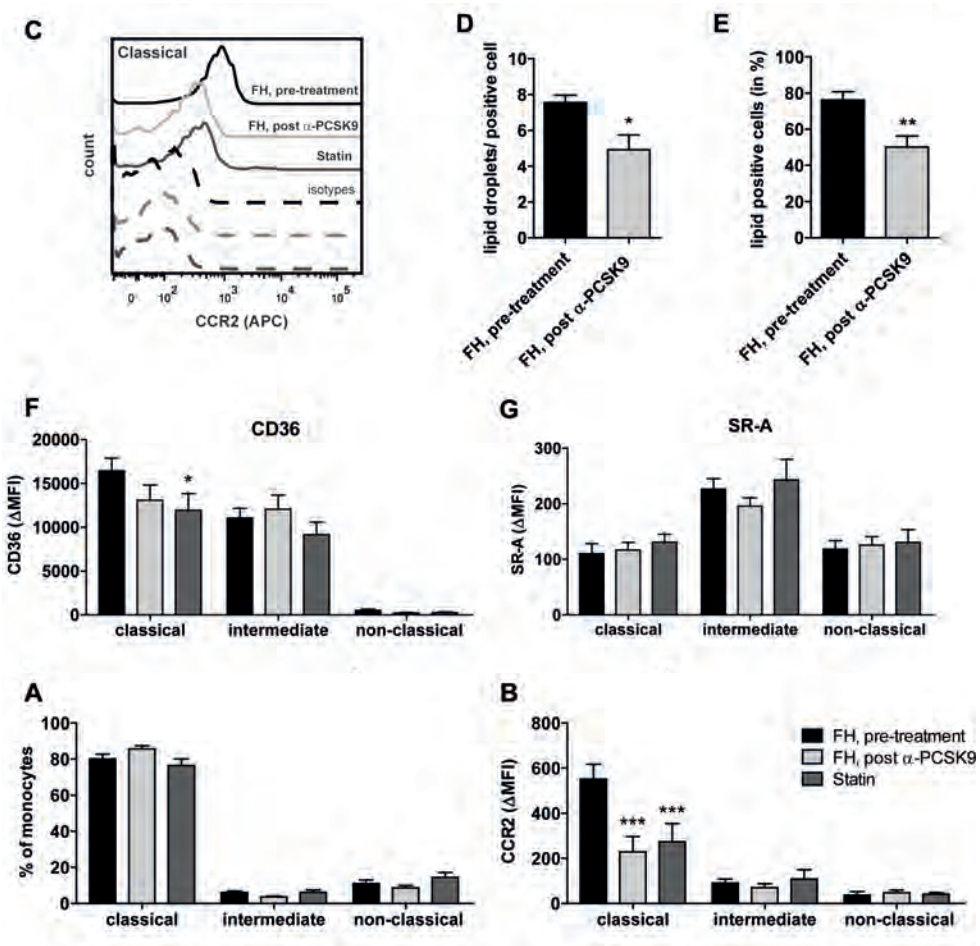

FIGURE 3. Continued

PCSK9 mAb affects monocyte cytokine production

Upon entry into the arterial wall, production of (pro-inflammatory) cytokines contributes to plaque destabilization. To assess whether alirocumab affected the inflammatory response of monocytes we measured cytokine production following LPS stimulation. Alirocumab reduced production of TNF (pre-alirocumab: 896±593 pg/mL, post-alirocumab: 471±272 pg/mL, $P<0.01$), whereas secretion of the anti-inflammatory IL-10 was enhanced (pre-alirocumab: 950±624 pg/mL, post-alirocumab: 2097±772 pg/mL, $P<0.001$). Cytokine levels of monocytes from alirocumab treated patients were comparable to those observed in stable statin users (Figure 3I-J).

DISCUSSION

We show that monocytes circulating in FH patients, not using statins, display pro-inflammatory and migratory changes, which coincide with an increase in cytoplasmic lipid droplets, implying a direct relation between intracellular lipid accumulation and inflammatory changes. Following 6 months of treatment with the PCSK9 mAb alirocumab, monocyte lipid content as well as pro-inflammatory phenotype decreased towards levels observed in FH patients using statins. These data imply an LDL-c mediated pro-inflammatory effect on circulating monocytes in patients with FH, which reverses upon LDL-c lowering by alirocumab.

Circulating monocytes of FH patients have marked accumulation of lipids, which coincided with elevated CCR2 expression in FH patients. Previous *in vitro* data support the uptake of native LDL in monocytes eliciting increased CCR2 expression and monocyte chemotaxis.[22] The strong correlation between lipid accumulation and CCR2 expression observed in monocytes of FH patients implies a causal relation between cytoplasmatic lipid increase and pro-inflammatory changes. The functional relevance of these changes is substantiated by the marked increase in the endothelial migration rate *ex vivo* of monocytes obtained from FH patients.

PCSK9 inhibition with alirocumab significantly reduced plasma LDL-c levels as well as lipid content in circulating monocytes. In conjunction, monocyte CCR2 expression reduced to levels comparable to those observed in FH patients using statins. In parallel, the response of circulating monocytes to an inflammatory challenge was also attenuated following alirocumab, illustrated by decreased TNF release with increased secretion of the anti-inflammatory cytokine IL-10. These data imply that decreased intracellular lipid accumulation leads to an attenuated inflammatory activity of the monocytes, which is independent of the mechanism by which LDL-c reduction is established. Interestingly, the anti-inflammatory changes in monocyte phenotype and responsiveness following alirocumab were not accompanied by a decrease in CRP levels. The reduction in CRP following statin therapy[3,23] reflects a direct effect of statins in hepatocytes,[24] which is not present following PCSK9 mAb administration.[19] Whereas the clinical relevance of the absence of a CRP change remains to be established, recent studies have revealed that CRP is not a mediator but a marker for CVD risk.[5,25] In parallel, the reduction in arterial inflammation following statin therapy is not correlated to statin-induced changes in CRP.[26,27] Whether the reduction in immune cell activity following PCSK9 mAb will translate into decreased inflammatory activity in atherosclerotic lesions is currently being addressed in the ANITSCHKOW study (NCT02729025).

Several limitations merit attention. First, this was a proof-of-concept study without placebo comparison. However, since potent and selective LDL-c reduction was achieved in all subjects, this study for the first time allows us to address the impact of LDL-c lowering on cellular inflammation in patients not receiving statins. Second, although murine data is consistent, the role of CCR2 expression on monocytes in predicting CVD risk has not been established

prospectively in patients.[10] Finally, it should be considered that besides potentially beneficial effects, lowering of inflammatory responses may also increase vulnerability towards infectious diseases. Since cardiovascular disease is widely recognized as a pro-inflammatory state, the use of anti-inflammatory strategies is considered to be justified, underscored by ongoing large outcome studies using anti-inflammatory agents (Cantos, NCT01327846, CIRT, NCT01594333).

In conclusion, we show that lipid lowering with the PCSK9 mAb alirocumab reduces the pro-inflammatory phenotype of monocytes without affecting CRP, implying that potent lowering of LDL-c has an anti-inflammatory impact in hypercholesterolemic patients. These data highlight that inflammation is not solely captured by CRP measurement and warrant future investigations to assess the role of attenuating cellular inflammation in patients at high cardiovascular risk.

Acknowledgements: The authors thank J.P. Kelder, S. Rameckers, and S. Krebbex for their assistance in patient recruitment and collection of baseline data. The main study (ODYSSEY CHOICE II) was funded by Sanofi and Regeneron Pharmaceuticals, Inc.

Disclosures and funding: E Stroes reports having received (non-significant) lecturing fees from Merck, Amgen, Sanofi-Regeneron and Chiesi. All other authors have nothing to disclose. This research is supported by The Netherlands Heart Foundation (CVON 2011/ B019: Generating the best evidence-based pharmaceutical targets for atherosclerosis [GENIUS]) and REPROGRAM grant (European commission Horizon2020-PHC-2015: 667837). J. van den Bossche received a Junior Postdoc grant from The Netherlands Heart Foundation (2013T003) and a VENI grant from ZonMW (91615052).

REFERENCES

1. Libby et al. Progress and challenges in translating the biology of atherosclerosis. Nature. 2011;473:317-25.
2. Mihaylova B et al. The effects of lowering LDL cholesterol with statin therapy in people at low risk of vascular disease: meta-analysis of individual data from 27 randomised trials. Lancet. 2012; 380:581–90.
3. Tawakol A et al. Intensification of statin therapy results in a rapid reduction in atherosclerotic inflammation: results of a multicenter fluorodeoxyglucose-positron emission tomography/computed tomography feasibility study. J. Am. Coll. Cardiol. 2013; 62:909–17.
4. Ridker PM et al. Rosuvastatin to prevent vascular events in men and women with elevated C-reactive protein. N. Engl. J. Med. 2008; 359:2195–207.
5. Wensley F et al. Association between C reactive protein and coronary heart disease: mendelian randomisation analysis based on individual participant data. BMJ. 2011; 342:d548.
6. Passacquale G et al. The role of inflammatory biomarkers in developing targeted cardiovascular therapies: lessons from the cardiovascular inflammation reduction trials. Cardiovasc. Res. 2015;227.
7. Ghattas A et al. Monocytes in coronary artery disease and atherosclerosis: where are we now? J. Am. Coll. Cardiol. 2013; 62:1541–51.
8. Van Der Valk FM et al. In vivo imaging of enhanced leukocyte accumulation in atherosclerotic lejas. J. Am. Coll. Cardiol. 2014; 64:1019–1029.
9. Tousoulis D et al. Inflammatory cytokines in atherosclerosis: current therapeutic approaches. Eur. Heart J. 2016;759.
10. Charo IF et al. Chemokines in the pathogenesis of vascular disease. Circ. Res. 2004; 95:858–866.
11. Han KH et al. Chemokine receptor CCR2 expression and monocyte chemoattractant protein-1-mediated chemotaxis in human monocytes. A regulatory role for plasma LDL. Arterioscler. Thromb. Vasc. Biol. 1998; 18:1983–1991.
12. Han KH et al. Expression of the monocyte chemoattractant protein-1 receptor CCR2 is increased in hypercholesterolemia. Differential effects of plasma lipoproteins on monocyte function. J. Lipid Res. 1999; 40:1053–63.
13. Hegele RA et al. Nonstatin Low-Density Lipoprotein–Lowering Therapy and Cardiovascular Risk Reduction—Statement From ATVB Council. Arterioscler. Thromb. Vasc. Biol. 2015;ATVBAHA.115.306442.
14. Kinlay S. Low-Density Lipoprotein-Dependent and -Independent Effects of Cholesterol-Lowering Therapies on C-Reactive Protein. A Meta-Analysis. J. Am. Coll. Cardiol. 2007; 49:2003–2009.
15. Zaid A et al. Proprotein convertase subtilisin/kexin type 9 (PCSK9): Hepatocyte-specific low-density lipoprotein receptor degradation and critical role in mouse liver regeneration. Hepatology. 2008; 48:646–654.
16. Raal F et al. Low-Density Lipoprotein Cholesterol-Lowering Effects of AMG 145, a Monoclonal Antibody to Proprotein Convertase Subtilisin/Kexin Type 9 Serine Protease in Patients With Heterozygous Familial Hypercholesterolemia. Circulation. 2012; 126:2408–2417.
17. Stein EA et al. Effect of a monoclonal antibody to PCSK9, REGN727/SAR236553, to reduce low-density lipoprotein cholesterol in patients with heterozygous familial hypercholesterolaemia on stable statin dose with or without ezetimibe therapy: a phase 2 randomised controlle. Lancet. 2012; 380:29–36.
18. Robinson JG et al. Efficacy and Safety of Alirocumab in Reducing Lipids and Cardiovascular Events. N. Engl. J. Med. 2015; 372:1489–1499.
19. Sahebkar A et al. Effect of Monoclonal Antibodies to PCSK9 on high-sensitivity C-reactive protein levels: A Meta-Analysis of 16 Randomized Controlled Treatment Arms. Br. J. Clin. Pharmacol. 2016;n/a–n/a.
20. Nordestgaard BG et al. Familial hypercholesterolaemia is underdiagnosed and undertreated in the general population: guidance for clinicians to prevent coronary heart disease: Consensus Statement of the European Atherosclerosis Society. Eur. Heart J. 2013; 34:3478–3490.
21. Abeles RD et al. CD14, CD16 and HLA-DR reliably identifies human monocytes and their subsets in the context of pathologically reduced HLA-DR expression by CD14hi/CD16neg monocytes. Cytom. Part A. 2012; 81:823–834.

22. Han KH et al. Chemokine Receptor CCR2 Expression and Monocyte Chemoattractant Protein-1 Mediated Chemotaxis in Human Monocytes : A Regulatory Role for Plasma LDL. Arterioscler. Thromb. Vasc. Biol. 1998; 18:1983–1991.
23. Balk EM et al. Effects of Statins on Nonlipid Serum Markers Associated with Cardiovascular Disease: A Systematic Review. Ann. Intern. Med. 2003; 139:670–682.
24. Arnaud C et al. Statins reduce interleukin-6-induced C-reactive protein in human hepatocytes: New evidence for direct antiinflammatory effects of statins. Arterioscler. Thromb. Vasc. Biol. 2005; 25:1231–1236.
25. Tennent GA et al. Transgenic human CRP is not pro-atherogenic, pro-atherothrombotic or pro-inflammatory in apoE-/- mice. Atherosclerosis. 2008; 196:248–255.
26. Duivenvoorden R et al. Relationship of Serum Inflammatory Biomarkers With Plaque Inflammation Assessed by FDG PET/CT. JACC Cardiovasc. Imaging. 2013; 6:1087–1094.
27. Van Wijk DF et al. Nonpharmacological Lipoprotein Apheresis Reduces Arterial Inflammation in Familial Hypercholesterolemia. J. Am. Coll. Cardiol. 2014; 64:1418–26.

SUPPLEMENT

The ODYSSEY CHOICE II study. The ODYSSEY CHOICE II was a randomized, double-blind, placebo-controlled, Phase 3 multinational study including 233 patients from 43 study sites. The CHOICE II study enrolled adult patients with hypercholesterolemia, (1) not receiving a statin due to statin associated muscle symptoms (SAMS) with moderate, high, or very-high cardiovascular risk, or (2) not receiving a statin but who did not fulfill the SAMS definition. CHOICE II comprised 24 weeks of double-blind treatment with alirocumab 150 mg every 4 weeks (Q4W), alirocumab 75 mg every 2 weeks (Q2W), or placebo Q2W, respectively. Patients were randomized as follows to one of the three arms, placebo for alirocumab, alirocumab 75 Q2W/up 150 Q2W, or alirocumab 150 Q4W/Up 150 Q2W in a planned 1:1:2 ratio, during the double-blind treatment period:

- Placebo for alirocumab subcutaneous (SC) Q2W starting at Week 0 (randomization) and continuing up to Week 22, i.e. 2 weeks before the end of the double-blind treatment period.
- Alirocumab SC 75 mg Q2W starting at Week 0 (randomization) up to Week 12. Based on the patients' Week 8 LDL-c level, patients either continued with alirocumab 75 mg Q2W or had their dose up-titrated to 150 mg Q2W up to Week 22, i.e. 2 weeks before the end of the double-period.
- Alirocumab SC 150 mg Q4W starting at Week 0 (randomization) up to Week 12. Based on the patients' Week 8 LDL-c level, patients either continued with alirocumab 150 mg Q4W or had their dose up-titrated to 150 mg Q2W up to Week 22, i.e. 2 weeks before the end of the double-period (the blind was maintained in patients receiving Alirocumab 150 Q4W by alternating with placebo SC Q4W).

After study completion, all patients were offered the opportunity to enter an open-label extension study during which all patients received alirocumab 150 mg Q4W.

Migratory capacity: Trans-endothelial migration (TEM) and chemotaxis. Primary human arterial endothelial cells (Lonza, Baltimore, MD) were cultured to confluence. After overnight stimulation with 10 ng/mL tumor necrosis factor- α (TNF-α, Peprotech, London, United Kingdom), CD14+ MACS-sorted (Milteny Biotec, Leiden, The Netherlands) monocytes were added at a concentration of 1*106 cells/mL for 30 min at 37°C, 5% CO2 and then fixed with 3.7% formaldehyde (Sigma-Aldrich, Zwijndrecht, The Netherlands). Images were recorded with a Zeiss Axiovert 200 microscope (Plan-apochromat 10x/0.45 M27 Zeiss-objective; Carl Zeiss Inc., Jena, Germany). Transmigrated monocytes were distinguished from adhered monocytes by their transitions from bright to dark morphology. Quantification was performed by using the cell counter plugin (http://rsbweb.nih.gov/ij/plugins/cell-counter.html) in the Image-J software (http://rsb.info.nih.gov/nih-image/). To investigate whether migration was mediated by MCP-1 a chemotaxis assay was performed.

The EZ-TAXIScan chamber (Effector Cell Institute, Tokyo, Japan) was assembled with a 260 µm wide and 4 µm thick silicon chip coated with Fibronectin (FN) (30 µg/ml) for 1 h at 37^{0}C and subsequently blocked with 2% Bovine Serum Albumin (BSA) phosphate buffered saline (PBS) for 30 min. The chamber was assembled on a 30 mm round FN-coated (30 µg/mL) glass coverslip and filled with monocyte migration medium (RPMI/0.1% BSA). Isolated monocytes (1*10^6 cells/mL) were added to the upper reservoir of each of the six channels and allowed to line up by removing 10 µL from the lower reservoir. Five µL monocyte chemoattractant protein-1 (100 ng/mL) was added to the lower reservoir and monocyte migration was captured every 120 s for 120 min using a 10x objective. Cell migration was quantified using ImageJ and the available manual tracking plugin (http://rsb.info.nih.gov/ij/plugins/manual-tracking.html). This plugin allowed us to manually track monocyte migration. Obtained datasets were further analyzed using the chemotaxis tool plugin (version 1.1) from Ibidi (Ibidi, Planegg, Germany). At least 30 cells per condition were tracked. Distance towards MCP-1 (either positive or negative) was averaged to calculate mean migration distance towards MCP-1.

FACS. Freshly isolated monocytes were stained for chemokine receptor (CCR) 2 (Novus Biologicals, Littleton, CO) expression and subsequently cells were sorted by fluorescent activated cell sorting (FACS). Cells with a median fluorescence intensity higher than 3500 were quantified as CCR2 high expressing cells, whereas cells with a median MFI lower than 3500 were quantified as CCR2 low and intermediate-expressing cells. Next, sorted cells were spread on a FN-coated microscopy slide and stained for Nile red as described.

Co-immuno staining. For the co-immuno staining of CCR2 and Nile Red, after fixation cells were blocked for 15 minutes with 2% BSA/PBS. Subsequently cells were stained with CCR2 Alexa 405 (Novus Biologicals, Littleton, CO) in 1% BSA/PBs for 45 minutes, washed with PBS and incubated with the lipid dye Nile red as described.

Ex vivo lipopolysaccharide (LPS) challenge for cytokine production. Cells (0.2*106) were plated in a 96-well tissue culture plate for 45 min allowing monocyte adherence in Iscove's Modified Dulbecco's Medium (IMDM, Sigma-Aldrich, Zwijndrecht, The Netherlands) supplemented with 2 mM l-glutamine, penicillin (100 U/mL), streptomycin (100 µg/ml) and 1% fetal calf serum (FCS; all Gibco, Walth). Hereafter, the medium was removed and replaced by IMDM with 10% FCS.

TABLE S1. Markers used for flow cytometry

Surface marker	Color	Dilution	Company
CD14	PE-Cy7	1/50	BD
CD16	APC-Cy7	1/50	BD
HLA-DR	PerCpCy5.5	1/50	BD
CCR2	APC	1/50	BD
CCR5	FITC	1/10	BD
CX3CR1	PE	1/50	Biolegend
CD18	APC	1/50	BD
CD29	APC	1/10	BD
CD11b	PE	1/25	BD
SR-A	PE	1/10	R&D
CD36	APC	1/25	BD
Mouse IgG1 κ isotype control	FITC	1/50	BD
Mouse IgG1 κ isotype control	PE	1/50	BD
Mouse IgG1 κ isotype control	APC	1/50	BD

APC indicates allophycocyanin; CD, cluster of differentiation; CR, chemokine receptor; Cy, CyChrome; FITC, Fluorescein isothiocyanate; HLA, human leucocyte antigen; PE, phycoerythrin ; PerCP, peridinin-chlorophyll-protein; SR, scavenger receptor.

TABLE S2. Primer sequences for qPCR

Gene	Forward primer (5'-3')	Reverse primer (5'-3')
ABCA1	CCTGTCATCTACTGGCTCTC	ACAACGTAATTGCACATATCCC
ABCG1	GAGATGGGAGTCTTTCTTCGG	CACTGGGAACATGATCTGAAAGG
B2M	AGCGTACTCCAAAGATTCAGGTT	ATGATGCTGCTTACATGTCTCGAT
GAPDH	GAAGGTGAAGGTCGGAGTCAAC	CAGAGTTAAAAGCAGCCCTGGT

ABCA indicates ATP binding cassette transporter; B2M, beta-2-microglubilin; GAPDH, glyceraldehyde 3-phosphate dehydrogenase.

TABLE S3. Disease specifications of the FH patients not receiving statin therapy

Characteristic	FH patients, no statin (n=15)
Diagnosis	
- FH, genetic mutation, n (%)	8 (57)
- FH, clinical diagnosis (DLN criteria), n (%)	7 (43)
Medication use	
- Ezetrol, n (%)	11 (73)
- Antihypertensive, n (%)	6 (43)

Data are n (%). *FH indicates familial hypercholesterolemia. DLN; Dutch Lipid Network.*

TABLE S4. Characteristics of subjects in migratory and immunohistochemical experiments

	Control n=7	FH no statin n=7	*P*-value
Age, years	56 ± 8	61 ± 11	0.338
Gender, n, male (%)	3 (43)	3 (43)	1.000
BMI, kg/m^2	24 ± 3	27 ± 5	0.200
Smoking, (% active)	0/7	0/7	1.000
CVD history	0/7	3/7	0.051
SBP, mmHg	125 ± 14	125 ± 15	0.953
DBP, mmHg	77 ± 10	82 ± 9	0.448
CRP, mg/L	0.6 [0.2–1.9]	2.9 [0.4–4.2]	0.181
Total cholesterol, mmol/L	5.3 ± 1.0	9.8 ± 1.9	<0.001
LDL-c, mmol/L	3.0 ± 0.5	7.8 ± 1.9	<0.001
HDL-c, mmol/L	1.8 ± 0.7	1.3 ± 0.5	0.143
Triglycerides, mmol/L	0.8 [0.2–1.9]	1.49 [1.1–1.7]	0.432
Leucocytes, 10^9/L	5.1 ± 0.9	6.3 ± 2.4	0.265
Neutrophils, 10^9/L	3.0 ± 0.7	3.7 ± 1.4	0.284
Lymphocytes, 10^9/L	1.5 ± 0.3	1.9 ± 1.0	0.278
Monocytes, 10^9/L	0.4 ± 0.1	0.5 ± 0.2	0.407

Values are n (%), mean ± SD or median [IQR,] for skewed data. *BMI indicates body mass index; CRP, c-reactive protein; CVD, cardiovascular disease; DBP, diastolic blood pressure; FH, familial hypercholesterolemia; HDL-c, high density lipoprotein cholesterol; IQR, inter-quartile range; LDL-c, low density lipoprotein cholesterol; Lp(a), lipoprotein (a); SBP, systolic blood pressure, SD, standard deviation.*

TABLE S5. Treatment allocation of PCSK9 inhibition (alirocumab) patients

Subject	Double-blind period	Uptitrated at Week 12 in the DB	OLE	Sample used
1	75 MG Q2W	Yes 150 mg Q2W	150 mg Q4W	Week 24 double-blind period With 150Q2W
2	75 MG Q2W	Yes 150 mg Q2W	150 mg Q4W	Week 24 double-blind period With 150Q2W
3	75 MG Q2W	Yes 150 mg Q2W	150 mg Q4W	Week 24 double-blind period With 150Q2W
4	150 MG Q4W	Yes 150 mg Q2W	150 mg Q4W	Week 24 double-blind period With 150Q2W
5	150 MG Q4W	No 150 mg Q4W	150 mg Q4W	Week 24 double-blind period With 150Q4W
6	Placebo	na	150 mg Q4W Up-titrated in the OLE	Week 24 OLE With 150Q2W
7	150 MG Q4W	Yes 150 mg Q2W	150 mg Q4W	Week 24 double-blind period With 150Q2W
8	Placebo	na	150 mg Q4W Up-titrated in the OLE	Week 24 OLE With 150Q2W
9	Placebo	na	150 mg Q4W Up-titrated in the OLE	Week 24 OLE With 150Q2W

150Q2W =150 mg every 2 weeks; 150Q4W, 150 mg every 4 weeks; 75Q2W, 75 mg every 2 weeks. *LMT indicates lipid-modifying treatment; na, not applicable; OLE, open label extension.*

TABLE S6. Disease specifications of the FH patients

Characteristic	FH, alirocumab (n=10)	FH, Stable statin (n=11)
Diagnosis		
- FH, genetic mutation	5 (50)	6 (55)
- FH, clinical diagnosis (DLN criteria)	5 (50)	5 (36)
Medication use		
- Ezetrol, n (%)	9 (90)	5 (46)
- Antihypertensive, n (%)	5 (50)	2 (18)
- statin	0	11

Data are n (%). *FH indicates familial hypercholesterolemia; DLN; Dutch Lipid Network; PCSK9, proprotein convertase subtilisin/kexin type 9.*

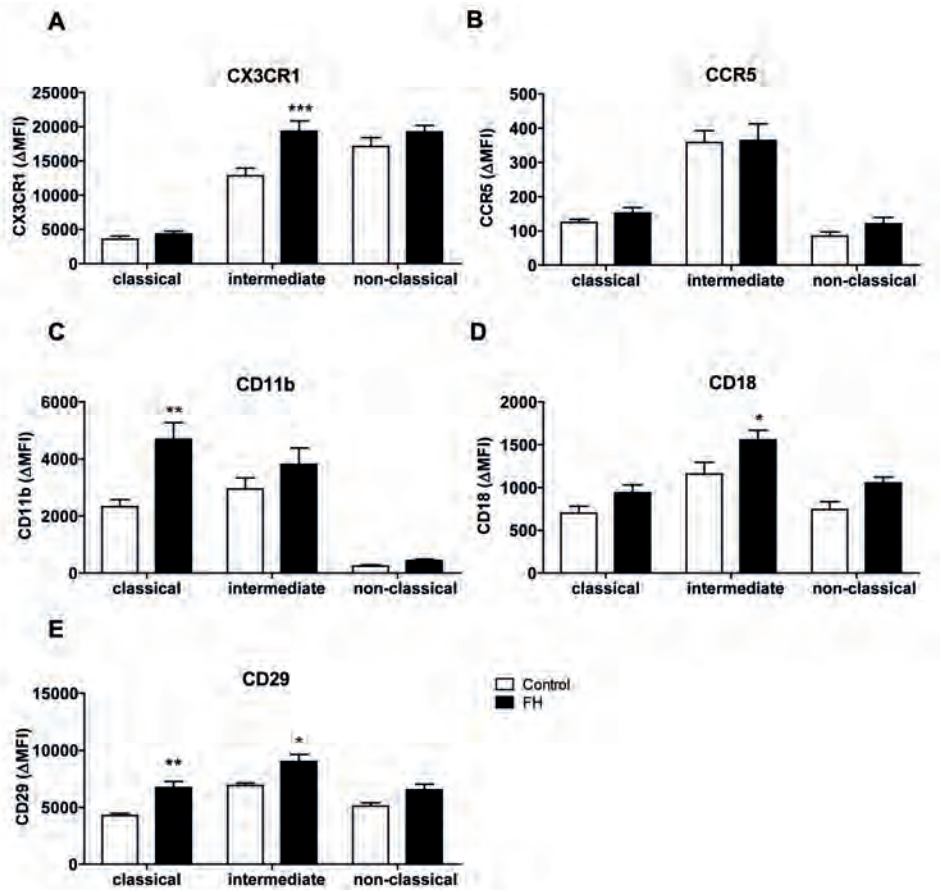

FIGURE S1. Expression of chemokine receptors and integrins in FH patients

Flow cytometry on whole blood was performed to study monocyte surface expression of chemokine receptors and integrins in FH-patients (n=14) versus controls (n=11). Surface expression of CX3CR1 (**A**), CCR5 (**B**), CD11b (**C**), CD18 (**D**), and CD29 (**E**) is represented as delta median fluorescence intensity. Data represent mean ± SEM **P*<0.05; ***P*<0.01; ****P*<0.001. *CD indicates cluster of differentiation; CCR, c-motif chemokine receptor; FH, familial hypercholesterolemia; SEM, standard error of the mean.*

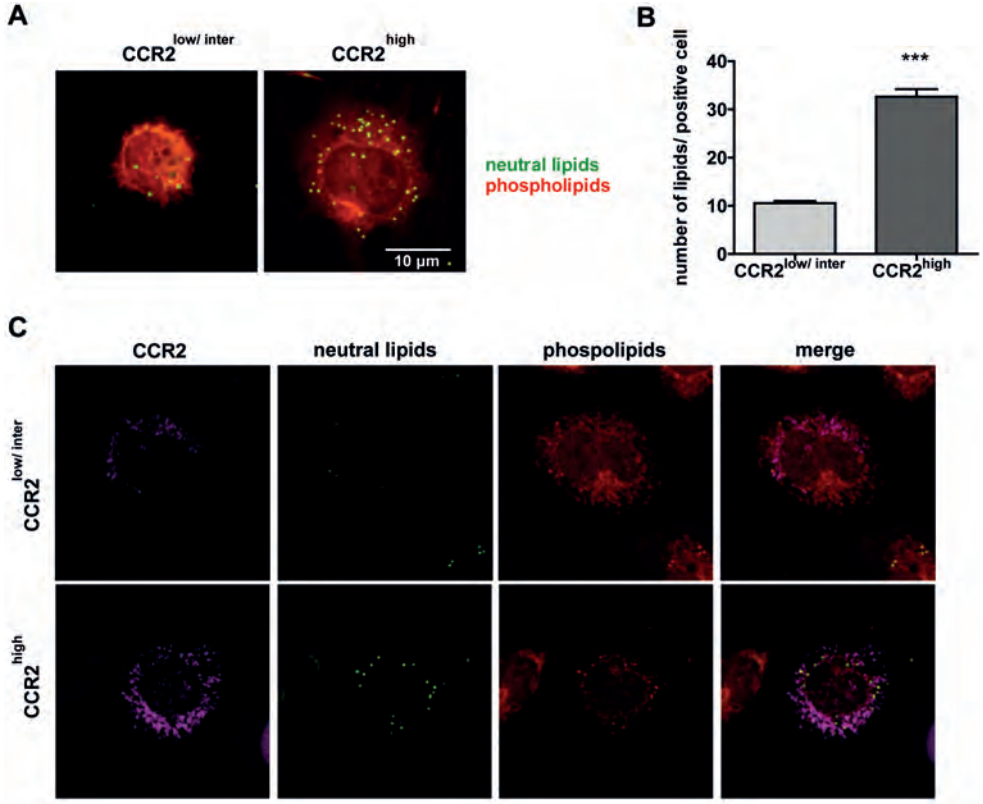

FIGURE S2. Co-occurrence of CCR2 expression and lipid accumulation in isolated monocytes

Monocytes were separated with FACS, distinguishing high (MFI xx) and intermediate or low CCR2 expression. (**A,B**) Lipid content of CCR2 low/intermediate and high subsets assessed by NR immunohistochemistry. (**C**) Co-immunohistochemistry of CCR2 (purple) and neutral lipids (green). Data represent mean ± SEM. ***P<0.001. *CCR indicates c-motif chemokine receptor; FACS, fluorescence activated cell sorting; MFI, median fluorescence intensity; NR, Nile Red.*

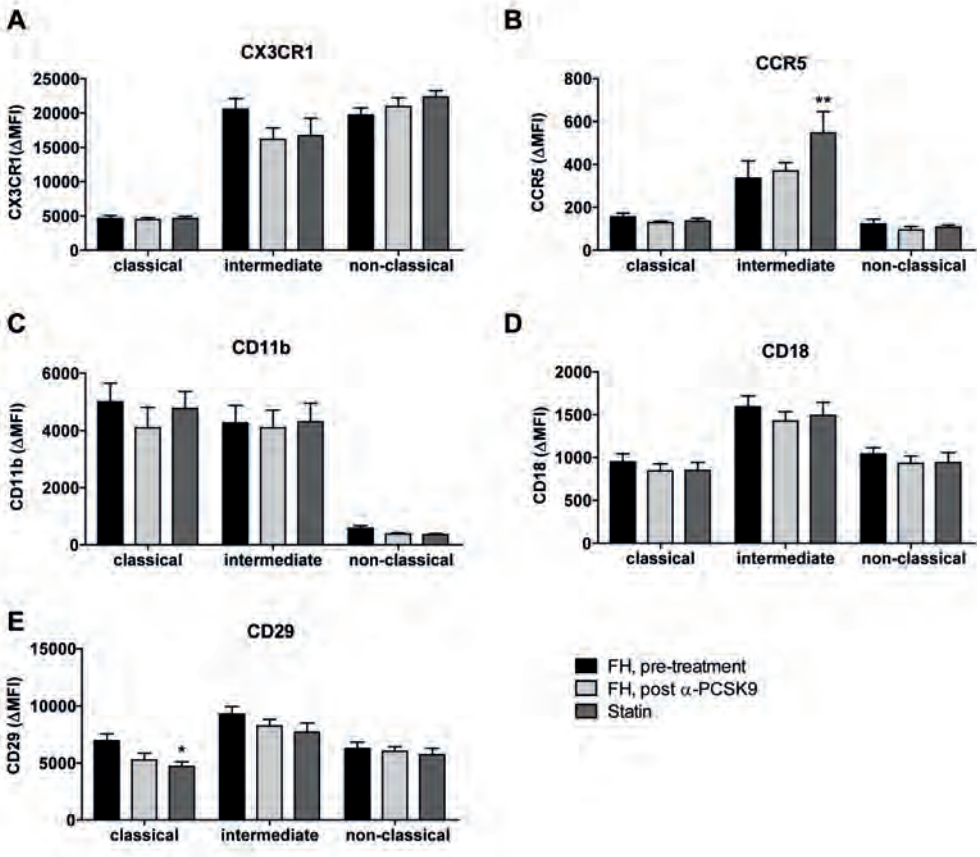

FIGURE S3. Expression of chemokine receptors and integrins after treatment

Flow cytometry on whole blood was performed to study monocyte surface expression of chemokine receptors and integrins after lipid lowering. FH, pre-alirocumab (n=10), FH, post-alirocumab (n=10), FH, stable statin (n=11). Surface expression of CX3CR1 (**A**), CCR5 (**B**), CD11b (**C**), CD18 (**D**), and CD29 (**E**) is represented as delta median fluorescence intensity. Data represent mean ± SEM *P<0.05; **P<0.01; ***P<0.001. *CD indicates cluster of differentiation; CCR, c-motif chemokine receptor; FH, familial hypercholesterolemia; PCSK9, proprotein convertase subtilisin/kexin type 9; SEM, standard error of the mean.*

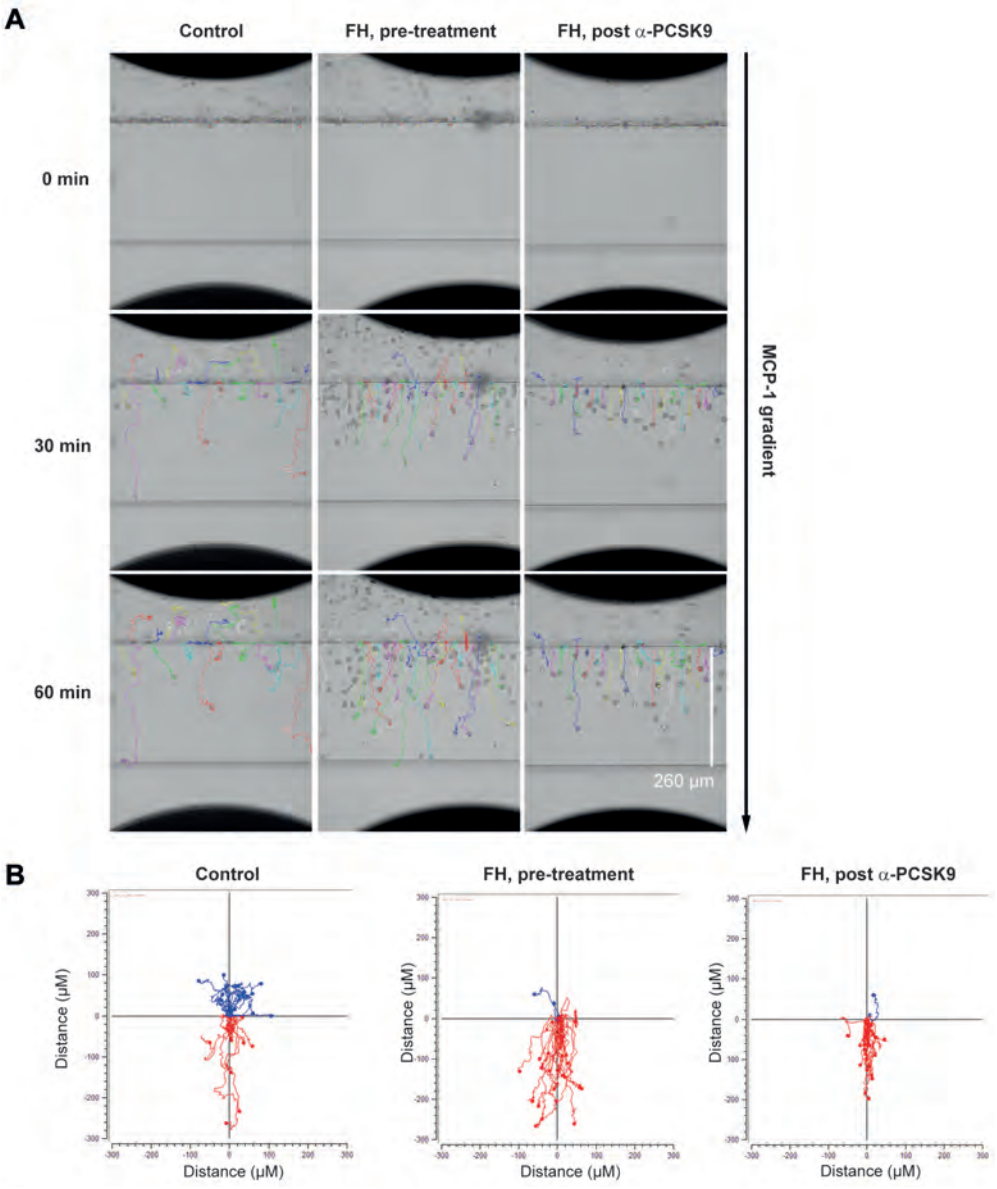

FIGURE S4. Monocytes of FH patients show increased migration towards MCP-1

Representative image (**A**) and plots (**B**) of migration towards a MCP-1 gradient, observed in a control subject (left), FH (no statin) (middle), and FH alirocumab-treated (right). Migration is quantified in 30 cells per subject as migrated distance in µm, distance in red (towards MCP-1) is considered positive, distance in blue (away from MPC-1) is considered negative, all values are used to calculate average migration towards MCP-1 (**C**). *FH indicates familial hypercholesterolemia; MCP-1, monocyte chemoattractant protein-1; PCSK9, proprotein convertase subtilisin/kexin type 9.*

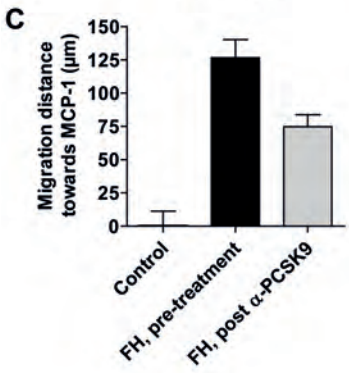

FIGURE S4. Continued

VIDEO S1. Monocytes of FH patients show increased migration towards MCP-1

Video of representative experiment performing a MCP-1 chemotaxis assay (Link: https://youtu.be/KTHLqaaWdmQ). Over a 2 h period, monocytes of an FH patient (middle, LDL-c 7.62 mmol/L) move rapidly towards an MCP-1 gradient, whereas monocytes of a control subject (left: LDL-c 2.53 mmol/L) do not show significant directional movement. After alirocumab treatment (right: LDL-c 3.03 mmol/L) monocyte movement is slower compared to the FH patient (no statin). *FH indicates familial hypercholesterolemia; LDL-c, low-density lipoprotein cholesterol; MCP-1, monocyte chemoattractant protein-1; PCSK9, proprotein convertase subtilisin/kexin type 9.*

CHAPTER 7

OXIDIZED PHOSPHOLIPIDS ON LIPOPROTEIN(A) ELICIT ARTERIAL WALL INFLAMMATION AND AN INFLAMMATORY MONOCYTE RESPONSE IN HUMANS

Van der Valk FM, Bekkering S, Kroon J, Yeang C, van den Bossche J, van Buul JD, Ravandi A, Nederveen AJ, Verberne HJ, Scipione C, Nieuwdorp M, Joosten LAB, Netea MG, Koschinksy ML, Witztum JL, Tsimikas S, Riksen NP, Stroes ESG

Accepted in Circulation, 2016

ABSTRACT

Rationale: Elevated lipoprotein(a) [Lp(a)] is a prevalent, independent cardiovascular risk factor but the underlying mechanisms responsible for its pathogenicity are poorly defined. Since Lp(a) is the prominent carrier of pro-inflammatory oxidized phospholipids (OxPL), part of its atherothrombosis might be mediated through this pathway.

Methods and Results: Using *in vivo* imaging techniques, we show that subjects with elevated Lp(a) (108 [50-195] mg/dL; n=30) have increased arterial inflammation and enhanced PBMCs trafficking to the arterial wall, compared with subjects with normal Lp(a) (7 [2-28] mg/dL; n=30). In addition, monocytes isolated from subjects with elevated Lp(a) remain in a long-lasting primed state, as evidenced by an increased capacity to transmigrate and produce pro-inflammatory cytokines upon stimulation. *In vitro* studies show that Lp(a) contains OxPL and augments the pro-inflammatory response in monocytes derived from healthy controls. This effect was markedly attenuated by inactivating OxPL on Lp(a) or removing OxPL on apo(a).

Conclusion: These findings demonstrate that Lp(a) induces monocyte trafficking to the arterial wall and mediates pro-inflammatory responses through its OxPL content. These findings provide a novel mechanism by which Lp(a) mediates cardiovascular disease.

INTRODUCTION

Lipoprotein(a) [Lp(a)] is a plasma lipoprotein composed of apolipoprotein(a) [apo(a)] covalently bound to apolipoprotein B-100 (apoB) of a low density lipoproteins (LDL)-like particle (Figure S1). A role for Lp(a) in atherogenesis has now been established by both meta-analyses of epidemiological studies, as well as by genome-wide association and Mendelian randomization studies showing a strong, independent and likely causal relationship between Lp(a) and myocardial infarction, stroke, peripheral artery disease and calcific aortic valve stenosis.[1,2]

Despite evidence of causality and the fact that one-fifth of the general community has elevated Lp(a) levels of >50 mg/dl[3], Lp(a) is not routinely measured in clinical risk assessment. This reluctance appears to be due to a lack of understanding of the pathophysiological mechanisms by which Lp(a) mediates cardiovascular disease (CVD), as well as the lack of specific therapeutic interventions to potently lower Lp(a) levels[4]. Consistent with known mechanisms of atherogenicity of LDL, Lp(a)'s atherogenic capacity could in part reflect the *response-to-retention* phenomenon of an apoB-containing particle[5]. The disproportionately large impact of Lp(a) on CVD risk compared with LDL, however, implies that additional pathogenic pathways need to be considered[6].

Over the last decade, a large body of experimental and clinical evidence has documented that Lp(a) is the main lipoprotein carrier of phosphocholine (PC) containing oxidized phospholipids (OxPL) in plasma[7–9], which has led to the hypothesis that a major component of the risk mediated by Lp(a) is through its content of OxPL[10]. OxPL is recognized as a danger associated molecular pattern (DAMP) by pattern recognition receptors (PRRs) on innate immune cells, leading to a wide range of pro-inflammatory and plaque destabilizing processes[11–13]. In epidemiological studies, the level of OxPL on apoB-containing lipoproteins (OxPL-apoB), which predominantly reflects Lp(a) associated OxPL, was found to be highly predictive of future CVD risk[14,15]. Most recently, a further link between Lp(a), OxPL and inflammation was discovered, showing that the risk of Lp(a) and OxPL-apoB in mediating coronary atherogenesis and cardiovascular events was conditional on an inflammatory IL-1 haplotype[16].

Here, we report that subjects with elevated plasma Lp(a) levels are characterized by increased inflammatory activity of the arterial wall as well as an enhanced inflammatory response of circulating monocytes, for which OxPL carried by Lp(a) were identified as obligatory intermediates. These findings indicate a novel link between Lp(a), its associated OxPL and accelerated atherogenesis in humans.

METHODS

Study subjects

This was a single-center study in subjects with elevated Lp(a) and subjects with normal Lp(a), matched for age, gender and BMI. Exclusion criteria consisted of active smoking, history of clinically-manifest cardiovascular disease or diabetes, and lipid lowering therapies including statins. Each subject provided written informed consent. The study and radiation exposure (<10mSv in total) was approved by the local institutional review board and conducted according to the principles of the International Conference on Harmonization–Good Clinical Practice guidelines.

Biochemical Measurements

EDTA plasma obtained through venous blood samples were taken after overnight fasting and stored using standardized protocols. Plasma Lp(a), total cholesterol (TChol), high density lipoprotein cholesterol (HDL-c) and triglyceride (TG) levels were analyzed using commercially available enzymatic methods. Low density lipoprotein cholesterol (LDL-c) levels were calculated using the Friedewald equation and subsequently corrected for Lp(a)-cholesterol (LDL-c – [Lp(a) in mmol/L*0.3])[17]. Oxidized phospholipids on apolipoprotein B-100 (OxPL-apoB) and on apolipoprotein(a) (OxPL-apo(a)), were measured as follows: apoB-100 and apo(a) were captured on microtiter wells using appropriate antibodies and the content of OxPL quantified by monoclonal antibody E06 and reported as nM, as previously described[10].

MR imaging

MR images were obtained with a 3.0 T whole-body scanner (Ingenia, Philips Medical Systems, Best, The Netherlands), using an 8 channel dedicated bilateral carotid artery coil (Shanghai Chenguang Medical Technologies, Shanghai, China). The normalized wall index (NWI= mean wall area/outer wall area) was calculated[18] by one blinded experienced reader at the core laboratory using semi-automated measurement software (VesselMass, Leiden, the Netherlands).

PET/CT imaging

PET/CT scans were performed on a dedicated scanner (Philips, Best, the Netherlands)[19]. All subjects fasted for at least 6 hours prior to infusion of ^{18}F-FDG (200 MBq). After 90 min, subjects underwent PET imaging initiated with a low-dose non-contrast enhanced CT for attenuation correction and anatomic co-registration. PET/CT images were analyzed by blinded readers using OsiriX (Geneva, Switzerland; http://www.osirix-viewer.com/). The target-to-background-ratio (TBR) was calculated from the ratio of arterial SUV and venous background activity, as described previously[19].

SPECT/CT imaging

SPECT/CT scans were performed at 3, 4.5 and 6 hours post infusion of ^{99m}Tc-labeled autologous peripheral blood mononuclear cells (PBMCs) (200 MBq) on a dedicated scanner (Symbia T16, Siemens, Erlangen, Germany)[20]. In each subject, around $20{\cdot}10^6$ PBMCs were isolated and labeled with ^{99m}Tc-(1100 megabecquerel/2mililiter). SPECT/CT images were analyzed by blinded readers using OsiriX[20]. Accumulation of labeled PBMCs in the arterial wall was quantified by the ratio of the averaged maximum counts in the artery divided by the averaged mean counts in the blood, reported as the arterial-wall-to-blood-ratio (ABR)[20].

Flow cytometry

Blood samples were collected into K3EDTA BD Vacutainer1 (BD Biosciences, San Jose, CA) tubes, after which 50 µL of whole blood was added to each flow cytometry tube plus the appropriate amounts of each antigen specific mAb were added, defined after titration of the dose recommended by the manufactures. See supplementary for detailed information.

Cells

Human PBMCs were isolated from blood using Ficoll-Paque Premium (d=1.077g/ml) density gradient centrifugation (GE Healthcare, UK). For *in vitro* experiments, human PBMCs were isolated from blood of healthy volunteers (Sanquin Bloodbank, Nijmegen, The Netherlands). $CD14^{pos}$ monocytes were isolated using a Ficoll-Paque plus (Pharmacia Biotech, Uppsala, Sweden) density gradient, followed by magnetic activated cell sorting (MACS) using CD14-coated MicroBeads according to manufacturer's instructions (MACS, Miltenyi Biotec, Leiden, The Netherlands). Primary Human Arterial Endothelial Cells (HAECs) were purchased from Lonza (Baltimore, MD) and routinely cultured on fibronectin (FN; 10 µg/ml) coated culture flasks (TPP, Switzerland) or glass-slides for imaging in EGM2 medium containing SingleQuots (Lonza). Endothelial cells were cultured up to 6 passages.

Antibodies and reagents

Actin (clone AC-40) mAb was purchased from Sigma-Aldrich (Zwijndrecht, Netherlands). Filamentous actin (F-actin) was stained with Phalloidin Texas-red (Invitrogen), and the nucleus with Hoechst 33258. β-glucan (b-1,3-(D)-glucan) was kindly provided by Professor David Williams (College of Medicine, Johnson City, USA), r-apo(a) (8K-IV), r-apo(a) 17K and 17KΔLBS10 were derived as previously described[9]. Stimuli and inhibitors used are oxPAPC (Invivogen), LPS (Sigma-Aldrich, St. Louis, MO; from *E. coli* serotype 055:B5, further purified as described)[21], Pam3Cys (EMC microcollections, Tübingen, Germany; L2000), anti-OxPL antibody Mouse monoclonal EO6 (Avanti Polar Lipids, Inc, Alabaster, Alabama, USA, 330001), purified mouse IgM Isotype control antibody (Biolegend, San Diego, California, USA, 401602).

In the monocyte assays, Lp(a), LDL and HDL were isolated from 3.5 mL plasma from subjects with either high or normal Lp(a) levels by KBr-density gradient ultracentrifugation; plasma density was adjusted to d=1.25 g/mL with solid KBr (0.385 g/mL plasma), a discontinuous gradient was formed by carefully layering 2 mL of d=1.225 g/mL KBr solution, followed by 4 mL of d=1.100 g/mL KBr solution, and a top layer of 3 mL of d=1.006 g/mL KBr solution was added. The samples were centrifuged for 20 hours at 10°C at 29,000 rpm in a SW 41 Ti rotor (Beckman Coulter Inc., CA). The LDL, Lp(a) and HDL fractions were sliced out and dialyzed against PBS. LAL assay showed negligible endotoxin levels (<0.05 EU/mL) in the isolated fractions. For the western immunoblots, Lp(a) was purified from the lipid apheresis eluate of a single donor undergoing LDL apheresis with high Lp(a) levels (140 mg/dL) and 16 KIV and 18 KIV repeats. The apheresis eluate was subjected to ultracentrifugation in NaBr and the 1.08 > d > 1.06 g/mL fraction was collected. This fraction was applied to a SW-400 gel filtration column, which was eluted in 0.5mL fractions. Each fraction was assayed for the presence of apo(a) and apoA-I by ELISA. The fractions containing apo(a) but not apoAI were pooled, buffer exchanged into PBS and concentrated using Amicon centrifugal filter units (Millipore). Apo(a) was dissociated from Lp(a) based on the methods described previously[22,23]. Briefly, the solution containing Lp(a) was adjusted to a final concentration of 100 mM ACA and 2 mM dithiothrietol and incubated at room temperature for 1 h. The reaction mixture was adjusted to a density of 1.3 g/ml with NaBr and the solution was centrifuged at 50,000 rpm to separate apo(a) from the LDL released by reduction and intact Lp(a).

Western immunoblot

Sodium dodecyl sulfate polyacrylamide gel electrophoresis (SDS-PAGE) of apo(a), Lp(a), and LDL (100 ng protein), in reducing (with beta-mercaptoethanol (BME)) and non-reducing conditions, was carried out using 3-8% gradient polyacrylamide gels in Tris-acetate SDS running buffer. Proteins were transferred to a PVDF membrane, which was blocked with 3% BSA in PBS-Tween. Membranes were then incubated with either biotinylated LPA4 (0.004 mg/ml), biotinylated E06 (0.004 mg/ml), or MB47 (0.006 mg/ml) probing for apo(a), OxPL, and human apoB-100 respectively. Protein detection was performed with streptavidin conjugated to horseradish peroxidase (HRP) from (R and D Systems) and visualized with ECL (Amersham).

Detection of OxPL by LC-MS/MS

To document the presence of PC-containing OxPL in Lp(a) purified by ultracentifugation, Lp(a) was isolated from 3 donors. Details of the LC-MS/MS procedures is described in the Supplement.

Transendothelial migration assay

Human aortic endothelial cells (HAECs) were cultured on a fibronectin (FN)-coated glass cover to confluency and stimulated overnight, i.e. 12 hours with TNFα (10 ng/ml)[24]. Monocytes ($1*10^6$ cells/ml) were added to the HAECs monolayer for 30 min in a humidified atmosphere of 5% CO2 at 37 °C and fixed with 3.7% formaldehyde (Sigma-Aldrich, Zwijndrecht, the Netherlands). After fixation, multiple images were recorded with a Zeiss Axiovert 200 microscope (Plan-apochromat 10x/0.45 M27 Zeiss-objective; Carl Zeiss Inc., Jena, Germany), and analyzed using Image-J software (http://rsb.info.nih.gov/nih-image/). After treatment and fixation in 3.7% formaldehylde in PBS (+1 mM $CaCl_2$, 0.5 mM $MgCl_2$), cells were permeabilized in PBS-T (PBS + 0.1% Triton-X100) for 10 min, stained for nuclei and filamentous actin for 45 min, washed and stored in PBS (+1 mM $CaCl_2$, 0.5 mM $MgCl_2$) until imaged using a confocal laser-scanning microscope (LSM510 META, Carl Zeiss MicroImaging, Jena, Germany) with a Zeiss Plan-Apochromat, 63x /1.40 oil objective. Monocyte motility was determined by plating freshly isolated monocytes into fibronectin (Sanquin Reagents, Netherlands) coated Lab-Tek Chambers (Thermo-Scientific, Rochester, NY) containing N-2-Hydroxyethylpiperazine-N'-2-Ethanesulfonic Acid (HEPES)-buffer + 1mM CaCl2 + 0.5% v/v human albumin and 0.1% w/v glucose. Videos were acquired using a wide-field microscope (Axio Observer Z1, Carl Zeiss MicroImaging, Jena, Germany) equipped with a humidified atmosphere climate chamber with 5 % CO_2 and 37 °C, and analyzed using the Tracking Tool (Gradientech, Uppsala Science Park, Uppsala, Sweden).

In vitro monocyte priming and challenge assay

Monocytes were isolated from PBMCs by adhering $5{\cdot}10^6$ PBMCs/ml to polystyrene for 1h at 37°C, 5% CO_2 in 96-, or 6-well culture plates (Corning, New York, USA). Non-adherent cells were removed by washing three times with warm PBS. Monocytes were cultured in RPMI 1640 Dutch-modified culture medium (Life Technologies/Invitrogen, Breda, The Netherlands) supplemented with 10 mM glutamine (Invitrogen), 10 µg/mL gentamicin (Centraform), 10 mM pyruvate (Invitrogen) and 10% pooled human plasma. The monocytes were primed for 24 hours with either RPMI, β-glucan (5 µg/ml), isolated Lp(a) (0.5-250 µg/ml), LDL (10 µg/ml), HDL (10 µg/ml), r-apo(a) constructs (8K-IV 0.001-0.5 µg/ml; 17K and 17KΔLBS10 0.1 µg/ml), OxPAPC (0.05-10 µg/ml) or 10% plasma from subjects with high or normal Lp(a) levels (before and after apoB precipitation of the apoB-containing lipoprotein fraction with polyethylene glycol 8000, Sigma P-2139[25]), after which the cells were washed and incubated in supplemented culture medium for 6 days. In inhibition experiments using E06 (1 nM) or IgM control (1 nM), stimuli were pre-incubated with the inhibitors 1h prior to adding the stimuli to the cells. After 6 days of rest in supplemented RPMI medium, cells were exposed to either medium alone, 10 µg/mL Pam3Cys or 10 ng/ml lipopolysaccharide. After 24h of incubation, supernatants were collected and stored at -20°C. Production of cytokines was measured in supernatants by ELISA

according to the manufacturer's instructions (TNFα (R&D Systems, Minneapolis, USA) and IL-6 (Sanquin, Amsterdam, The Netherlands), or the human inflammatory cytokine Cytometric Bead Array according to the manufacturer's instructions (BD Biosciences, 551811).

Statistical analysis

Data are presented as the mean (standard deviation) or the median (min-max) for continuous variables, and as a number (percentage) for categorical variables. To examine the difference in clinical characteristics, imaging parameters and monocyte phenotype and function between subjects with elevated or normal Lp(a) we performed student T-test or Mann-Whitney U test for normal and non-normal distributed variables, respectively. Normality was examined by means of inspection of histograms and the Shapiro-Wilk test. Variances in both groups were examined and tested for similarity using Levene's Test for Variance. To assess the differences in PBMCs accumulation as imaged with SPECT, a linear mixed model for repeated measurements was applied. *Ex vivo* and *in vitro* monocyte experiments were performed at least 6 times, and analyzed using the Wilcoxon signed-rank test. A two-sided *P*-value below 0.05 was considered statistically significant. All data were analyzed using Prism version 5.0 (GraphPad software, La Jolla, California) or SPSS version 21.0 (SPSS Inc., Chicago, Illinois).

RESULTS

Increased arterial wall inflammation in subjects with elevated Lp(a)

To determine if Lp(a) influences arterial wall inflammation, we included subjects with elevated Lp(a) levels (mean of 108 mg/dL [range 50-195]; n=30) or normal Lp(a) levels (mean of 7 mg/dL [range 2-28]; n=30) matched for age, gender and body mass index (Table 1). None of the subjects were currently smoking, had a history of clinically-manifest cardiovascular disease or diabetes, or used lipid-lowering therapies such as statins. Aside from Lp(a) levels, subjects did not differ in blood pressure, non-Lp(a) lipoprotein profile or circulating leukocytes (Table 1). As expected, subjects with elevated Lp(a) exhibited significantly higher levels of OxPL-apoB and specifically, OxPL on apo(a) lipoproteins (OxPL-apo(a)) (Table 1). The normalized wall index (NWI) of the carotids, as assessed with magnetic resonance imaging (MRI)[18], was not significantly different between groups (Table 1, Figure S2A).

TABLE 1. Clinical characteristics of included subjects

Characteristic	Subjects with normal Lp(a) (n=30)	Subjects with elevated Lp(a) (n=30)	P value
Age, y	53 ± 12	52 ± 11	0.858
Gender, %male (n)	45 (9)	43 (15)	0.820
BMI, kg/m2	24 ± 4	24 ± 3	0.914
DBP, mmHg	79 ± 7	81 ± 8	0.399
SBP, mmHg	131 ± 8	134 ± 12	0.144
Smoking, %active	0 (0)	0 (0)	-
NWI	0.42 ± 0.06	0.39 ± 0.04	0.161
Lp(a), mg/dL	7 [2-28]	108 [50-195]	*<0.001*
OxPL-apo(a), nM	3.0 [0.5-26.0]	69.1 [40.9-92.5]	*<0.001*
OxPL-apoB, nM	4.1 [2.3-6.3]	15.8 [5.9-31.1]	*<0.001*
TChol, mmol/L	5.21 ± 0.83	5.79 ± 1.44	0.127
LDL-c*, mmol/L	2.91 ± 0.80	2.80 ± 1.16	0.621
HDL-c, mmol/L	1.68 ± 0.42	1.60 ± 0.40	0.481
TG, mmol/L	0.80 [0.24-2.18]	0.82 [0.39-2.16]	0.684
CRP, mg/L	2.30 [0.40-4.40]	1.13 [0.30-1.90]	0.180
HbA1c, mmol/mol	36 [34-39]	35 [33-38]	0.100
Creatinine, umol/L	76 [66-80]	70 [55-87]	0.304
ALT, U/L	27 ± 10	27 ± 6	0.766
AST, U/L	25 ± 11	27 ± 8	0.427
WBC, 10^9/L	5.4 ± 1.3	5.7 ± 1.3	0.522
Monocytes, 10^9/L	0.43 ± 0.15	0.43 ± 0.12	0.996
Neutrophils, 10^9/L	3.1 ± 1.4	3.3 ± 1.09	0.710
Lymphocytes, 10^9/L	2.4 ± 2.6	2.2 ± 1.7	0.666
Eosinophils, 10^9/L	0.16 ± 0.13	0.15 ± 0.16	0.891
Basophils, 10^9/L	0.03 ± 0.01	0.03 ± 0.01	0.809

Data are presented as mean ± SD, n (%) or median [min-max]. *LDL-c corrected for Lp(a)-cholesterol.

ALT indicates alanine transaminase; apo(a), apolipoprotein(a); apoB, apolipoprotein B-100; AST, aspartate transaminase; BMI, body mass index; CRP, C-reactive protein, CVD, cardiovascular disease (including myocardial infarction, stroke or peripheral artery disease); HbA1c, hemoglobin A1c; HDL-c, high density lipoprotein cholesterol; DBP, diastolic blood pressure; LDL-c, low density lipoprotein cholesterol; Lp(a), lipoprotein(a); NWI, normalized wall index; OxPL, oxidized phospholipids; SBP, systolic blood pressure; Tchol, total cholesterol; TG, triglycerides; WBC, white blood cell count.

Positron emission tomography with computed tomography (PET/CT) imaging was performed to image arterial wall ^{18}F-fluorodeoxyglucose uptake (^{18}F-FDG), as a marker of arterial wall inflammation[26]. In subjects with elevated Lp(a), arterial wall ^{18}F-FDG uptake, quantified as the target to background ratio (TBR), was significantly higher compared with subjects with

normal Lp(a) (Figure 1A); both in the carotids (Figure 1B) as well as in the aorta (Figure 1C). Of note, the inflammatory activity in subjects with elevated Lp(a) did not correlate to arterial wall dimensions (NWI, normalized wall index) as assessed with MRI (Figure S2B).

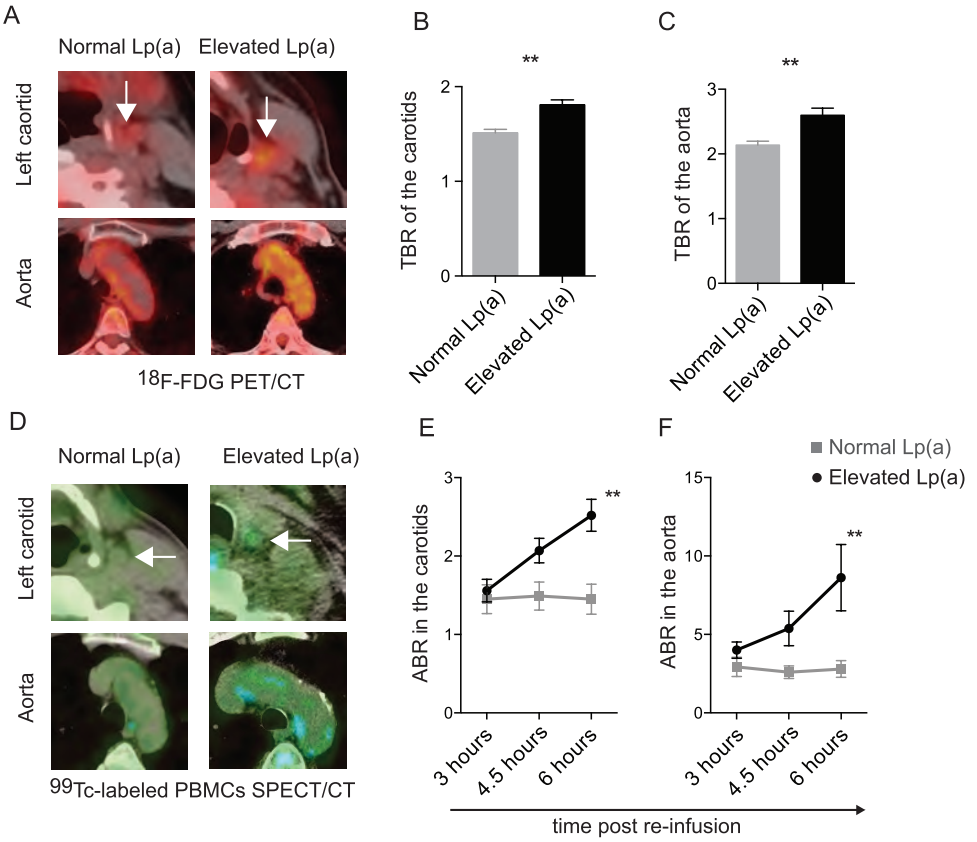

FIGURE 1. Increased arterial wall inflammation in subjects with elevated Lp(a)

(**A**) Cross-sectional ^{18}F-FDG PET/CT images demonstrating an increased ^{18}F-FDG uptake (yellow) in the left carotid (top, indicated by white arrow) and aorta (bottom) in a subject with normal Lp(a) (left) and a subject with elevated Lp(a) (right), quantified as the maximum TBR in the (**B**) carotid arteries, and (**C**) ascending aorta in subjects with elevated Lp(a) (n=30) and normal Lp(a) (n=30), (**D**) cross-sectional SPECT/CT images demonstrating increased autologous ^{99m}Tc-labeled PBMCs accumulation (blue; at T=6 hours post-infusion), depicted as the ABR at the level of (**E**) the carotids and (**F**) ascending aorta in subjects with elevated Lp(a) (n=15) and normal Lp(a) (n=15). **=p<0.01. *^{18}F-FDG indicates ^{18}fluorodeoxyglucose; ABR, arterial wall to bloodpool ratio; CT, computed tomography; Lp(a), lipoprotein (a); PBMCs, peripheral mononuclear blood cells; PET, positron emission tomography; SPECT, single photon emission computed tomography; TBR, target to background ratio.*

In view of the intricate relation between resident arterial wall macrophages and circulating monocytes[27], we subsequently investigated the impact of elevated Lp(a) on circulating immune cells *in vivo*. We used an imaging approach to monitor the trafficking of technetium-99m (^{99m}Tc)-labeled autologous PBMCs to the arterial wall, using single photon emission computed tomography with computed tomography (SPECT/CT)[20]. PBMCs were found to accumulate at a substantially higher rate in the arterial wall within 3-6 hours after re-infusion in subjects with elevated Lp(a) compared with those with normal Lp(a) (Figure 1D). The arterial wall-to-blood-pool ratio (ABR)[20] values were significantly higher in subjects with elevated Lp(a) in both the carotids (Figure 1E) and aorta (Figure 1F). Collectively, these *in vivo* imaging studies indicate that subjects with elevated Lp(a) levels have increased arterial inflammatory activity, which coincides with more autologous immune cell accumulation in their arterial wall. Further, there is a strong correlation between the TBR indices from PET/CT imaging and the ABR values from PMBCs imaging and respective Lp(a) plasma levels (Table 2).

TABLE 2. Correlations between inflammatory metrics and Lp(a) levels

Method	Parameter	Spearman correlation with Lp(a) level
PET imaging	TBR, carotid	0.31^
	TBR, aorta	0.45**
SPECT imaging	ABR, carotid	0.72*
	ABR, aorta	0.65*
Whole plasma level	CRP, mg/L	0.24
Flow cytometric assay	CD11b, ΔMFI	0.27
	CD11c, ΔMFI	0.42^
	CD29, ΔMFI	0.50*
	SRA, ΔMFI	0.42^
	CD36, ΔMFI	0.48*
Ex vivo monocyte cytokine production	TNFα, pg/mL	0.27
	IL-6, pg/mL	0.18

Correlation coefficients of the Spearman's rho test are shown, correlations are flagged with ^p<0.06, *p<0.05, **p<0.01, ***p<0.001. TBR and ABR are imaging metrics, CRP was measured in whole plasma, TNFα and IL-6 were measured as products of monocytes after TLR ligand challenge, and CD11b, CD11c, CD29 and CD36 expression on monocytes were measured by flow cytometry as described in Methods. *ABR indicates arterial wall to bloodpool ratio; CRP, C-reactive protein; IL-6, interleukin 6; PET, positron emission tomography; SPECT, single photon emission computed tomography; SRA, scavenger receptor A; TBR, target to background ratio, TNFα, tumor necrosis factor α.*

Monocytes increasingly migrate in subjects with elevated Lp(a)

We next questioned whether the increased arterial wall immune cell accumulation was preceded by an intrinsic cellular activation leading to enhanced migration. To this end, we analyzed adhesion and migration markers of blood monocytes in subjects with elevated versus normal Lp(a) using flow cytometry (gating strategy in Figure S3A)[28]. Monocytes from subjects with elevated Lp(a) expressed more C-C chemokine receptor type 7 (CCR7), L-selectin (also described as the cluster of differentiation 62 ligand; CD62L) and integrin alpha and beta chains; CD11b, CD11c and CD29[29] (Figure 2A), for which the latter two showed a (borderline) significant correlation with the Lp(a) plasma levels (Table 2).

To evaluate the functional relevance of increased expression of adhesion and migration markers, we performed transendothelial migration (TEM) experiments[24] with monocytes isolated from subjects with and without elevated Lp(a). Twelve hours prior to performing the migration assay, human arterial endothelial cells (HAECs) were stimulated with TNFα to mimic dysfunctional endothelium. Freshly isolated monocytes of subjects with elevated Lp(a) showed a 3-fold higher TEM rate compared with monocytes isolated from subjects with normal Lp(a) (Figure 2B). Staining of the nucleus and F-actin illustrated that monocytes derived from subjects with elevated Lp(a) have augmented spreading and adhesion compared with monocytes of subjects with normal Lp(a) (Figure 2C). In addition, monocytes of subjects with elevated Lp(a) also showed higher motility when plated on fibronectin-coated surfaces (movie S1), lending further support to an increased transmigratory tendency.

Thus, in subjects with elevated Lp(a), circulating monocytes exhibit an enhanced capacity to adhere and transmigrate the endothelium. Whereas generalized markers of inflammation, such as plasma levels of CRP, do not relate with Lp(a) levels, a number of inflammatory markers measured on the monocytes of the subjects are proportional to their Lp(a) levels (Table 2).

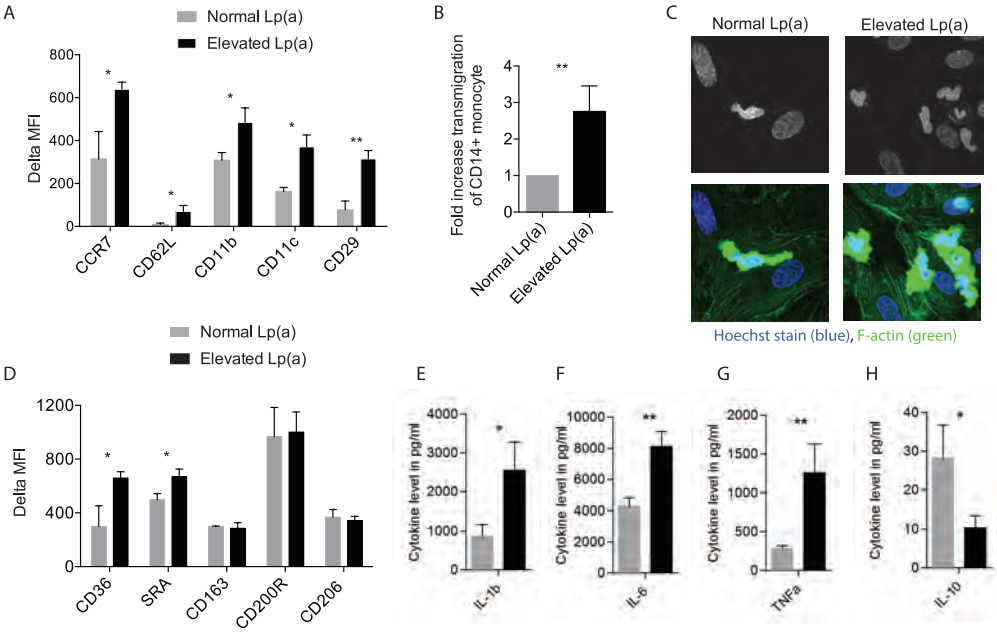

FIGURE 2. Monocytes have an activated and inflammatory phenotype in Lp(a) subjects

(**A**) Bar graphs display the expression (quantified as delta MFI) of chemokine, adhesion and transmigration markers on monocytes as assessed with flow cytometry in subjects with elevated Lp(a) (n=15, black bars) compared with normal Lp(a) (n=15, grey bars), (**B**) bar graph and (**C**) microscope images demonstrating increased endothelial transmigration of monocytes (calculated per at least 4 fields of view) isolated from subjects with elevated Lp(a) (n=15, black bar) compared with normal Lp(a) (n=15, grey bar), coinciding with augmented spreading and adhesion as illustrated nucleus (Hoechst, blue) and F-actin (green) stain, (**D**) bar graphs showing expression (quantified as delta MFI) of scavenger and other receptors on monocytes in subjects with elevated Lp(a) (n=15, black bars) compared with subjects with normal Lp(a) (n=15, grey bars), (**E-H**) in response to an overnight challenge to Pam3Cys (10 µg/ml), monocytes isolated from subjects with elevated Lp(a) (n=15, black bars) produced higher levels of IL-1β (**E**), IL-6 (**F**) and TNFα (**G**) and lower levels of IL-10 (H), compared with monocytes of subjects with normal Lp(a) (n=15, grey bars). ^=p<0.06, *=p<0.05, **=p<0.01, ***=p<0.001. *IL indicates interleukin; Lp(a), lipoprotein (a); MFI, mean fluorescence intensity; SRA, scvavenger receptor A; TNFα, tumor necrosis factor* α.

Atherogenic monocyte response in subjects with elevated Lp(a)

In addition to migration markers, monocytes of subjects with elevated Lp(a) expressed increased levels of the scavenger receptors CD36 and SRA (Figure 2D), also correlating to Lp(a) plasma levels (Table 2), whereas the expression of other receptors such as CD163, CD200R and CD206 was not different (Figure 2D). To assess whether this activated phenotype also translated to an enhanced inflammatory response, we performed a challenge assay using Toll-like receptor (TLR) ligands. After an overnight stimulation with a TLR2 ligand (Pam3Cys), monocytes isolated from subjects with elevated Lp(a) produced higher levels of tumor necrosis factor alpha (TNFα), interleukin 1 beta (IL-1β) and IL-6 (Figure 2E-G). Conversely, the production of IL-10 was lower (Figure 2H). Similar results were observed upon stimulation with the TLR4 ligand lipopolysaccharide (LPS) (Figure S4A-D). In aggregate, we observed an activated state of monocytes, potentially resulting from their priming by Lp(a), or some associated component found in the plasma of subject with elevated Lp(a).

Lp(a) and its associated OxPL induce prolonged responsiveness in monocytes

Lp(a) was isolated by ultracentrifugation, the lipid soluble material was extracted, and LC-MS/MS was performed on the extracted material an shown to have the following OxPLs: POVPC, PGPC, PONPC, PAzPC and KDdiA-PC, with PONPC being the most abundant (Figure S5A-B).

To address priming by Lp(a), or some associated component found in the plasma of subject with elevated Lp(a), we performed a series of in vitro studies, in which we analyzed the ability of various plasma components to activate monocytes. As a positive control for monocyte activation we used β-glucan, a cell wall component of *C. Albicans*, since we have extensively demonstrated that β-glucan induces a long-lasting pro-inflammatory phenotype in monocytes[31].

First, priming of healthy monocytes with plasma from subjects with high Lp(a) for 24 hours, with a subsequent washout and resting period, increased the production of TNFα and IL-6 after an overnight challenge with the TLR2 and TLR4 ligands Pam3Cys or LPS, respectively (Figure 3A,B and Figure S6A,B), whereas normal Lp(a) plasma did not activate monocytes. Lipid depletion of the above plasma profoundly decreased the cytokine production of the in-origin high Lp(a) plasma, indicating that a lipophilic particle might be responsible for the observed effect (Figure 3A,B and Figure S6A,B).

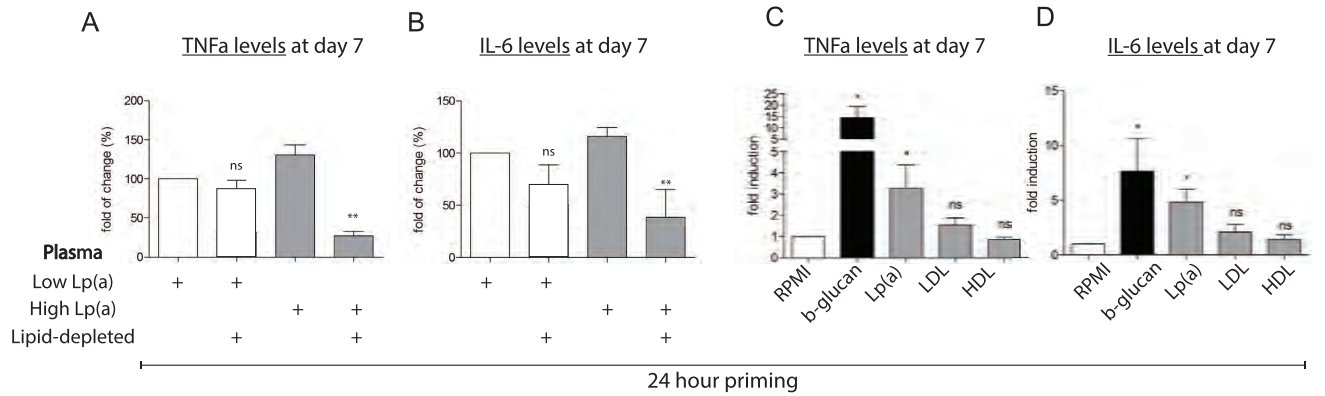

FIGURE 3. Isolated Lp(a) primes monocytes towards a responsive state

(**A,B**) priming of healthy monocytes with plasma containing high Lp(a) (grey bars) for 24h resulted in an increased production of TNFα and IL-6 upon re-stimulation with Pam3Cys (10 µg/mL) on day 6, compared with plasma of normal Lp(a) (white bars). In addition, after lipid-depletion this effect was profoundly reduced (n=6), (**C,D**) priming of healthy monocytes with β-glucan (5 µg/mL, positive control, black bar) or Lp(a) (grey bar, 250 µg/mL) for 24h, induced an increased cytokine production upon Pam3Cys (10 µg/mL) on day 6, compared with priming with RPMI (negative control, white bar), LDL (grey bar, 10 µg/mL) or HDL (grey bar, 10 µg/mL) (n=6).

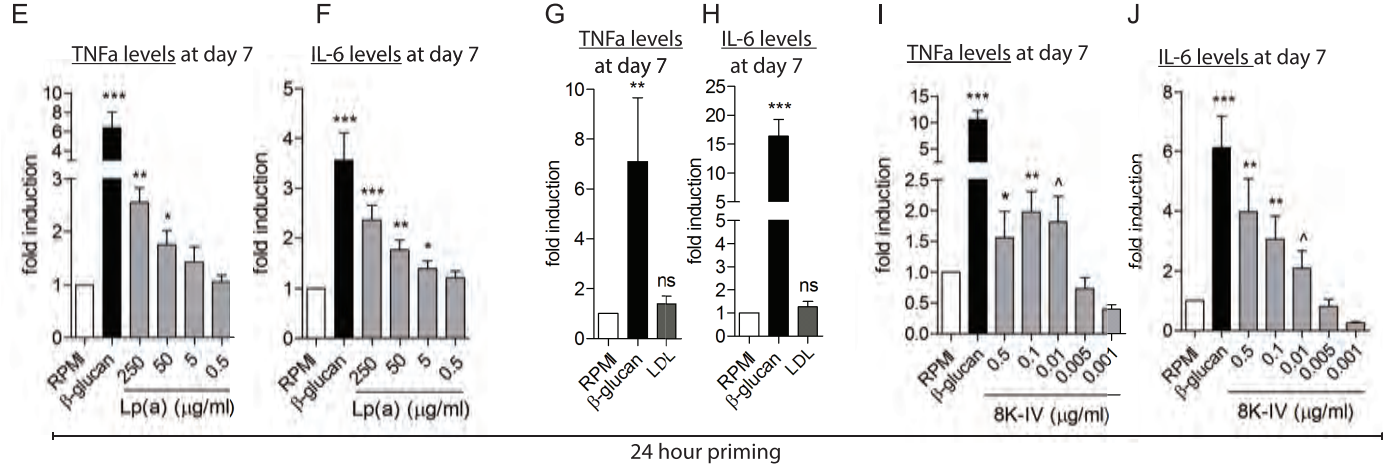

FIGURE 3. Continued

(**E,F**) in addition, various concentrations of Lp(a) (grey bars) for 24h, resulted in a dose-dependent increased cytokine production upon Pam3Cys (10 μg/mL) on day 6 (n=6), (**G,H**) priming of healthy monocytes with RPMI (negative control, white bar) or LDL (10 μg/mL) (grey bar) did not result in higher cytokine levels after Pam3Cys (10 μg/mL) compared with β-glucan (5 μg/mL, positive control, black bar) (n=6), whereas (**I,J**) priming of healthy monocytes with β-glucan (5 μg/mL, positive control, black bar) or the r-apo(a) construct 8K-IV (grey bars) induced increased cytokine levels after Pam3Cys (10 μg/mL) (n=6), compared with RPMI (negative control, white bar). *=p<0.05, **=p<0.01, ***=p<0.001. *HDL indicates high density lipoprotein; IL, interleukin; LDL, low density lipoprotein; Lp(a), lipoprotein (a); TNFα, tumor necrosis factor* α.

In line with the difference in Lp(a) levels between both plasma, priming of healthy monocytes with purified Lp(a) for 24 hours, induced an increased production of TNFα and IL-6 at day 7, after an overnight TLR challenge (Figure 3C-F and Figure S6C-F). Please note that priming with the isolated lipoprotein fractions LDL and HDL did not induce monocyte activation (Figure 3C,D and Figure S6C,D).

Next, we assessed the effects of Lp(a)'s main components separately; using isolated LDL, apo(a) separated from Lp(a), and recombinant apo(a) [r-apo(a)] constructs containing various numbers of kringles[9]. Whereas priming with LDL had no prolonged effects on monocytes (Figure 3G,H and Figure S6G,H), priming with an 8 kringle IV (8K-IV) r-apo(a) construct elicited an enhanced cytokine response in healthy donor monocytes at day 7 after overnight stimulation with TLR ligands (Figure 3I,J and Figure S6I,J).

In view of the role of Lp(a) as carrier of OxPL[7–9], we hypothesized an important role for OxPL in monocyte activation. In support of this concept, we show via immunoblotting that both Lp(a) and apo(a) contain OxPL, whereas LDL isolated from the same plasma as Lp(a) does not (Figure 4A). To further demonstrate the role of OxPL in mediating the activation of monocytes, we utilized monoclonal antibody E06, which binds to the PC moiety of OxPL and potently inhibits their pro-inflammatory properties, but does not bind to native, non-oxidized phospholipids[32–34]. Whereas the 8K-IV apo(a) construct, containing covalently bound OxPL[9], potently activated monocytes (Figure 3I,J and Figure S6I,J), pre-incubation of the 8K-IV construct with E06 inhibited its priming effects (Figure 4B,C and Figure S6K,L).

The role of OxPL was further validated using 2 additional constructs consisting of 17 kringles (17K) but varying in the functionality of the lysine binding site (LBS) on kringle IV type 10 (KIV_{10}), which in turn is related to the ability of the apo(a) constructs to have covalently bound OxPL [9,35]. Thus, 17K is a r-apo(a) construct with an intact LBS that has covalently bound OxPL, whereas 17KΔLBS10 has a mutated LBS and lacks immunologically detected OxPL[9,35]. Consistent with our previous findings with Lp(a), priming with 17K induced a state of increased responsiveness in monocytes, whereas such effects were absent with the mutant 17KΔLBS10 (Figure 4D,E and Figure S6M,N). Finally, we show that short-term priming with purified oxidized-1-palmitoyl-2-arachidonoyl-*sn*-3-glycero-phosphocholine (OxPAPC), a mixture of OxPL, also results in a dose-dependent enhanced cytokine production at day 7 in response to an overnight challenge with TLR ligands (Figure 4F,G and Figure S6O,P).

Collectively, these data show that subjects with elevated Lp(a) exhibit increased arterial wall inflammation coinciding with an increased responsiveness of monocytes, in which OxPL carried by Lp(a) are obligatory mediators.

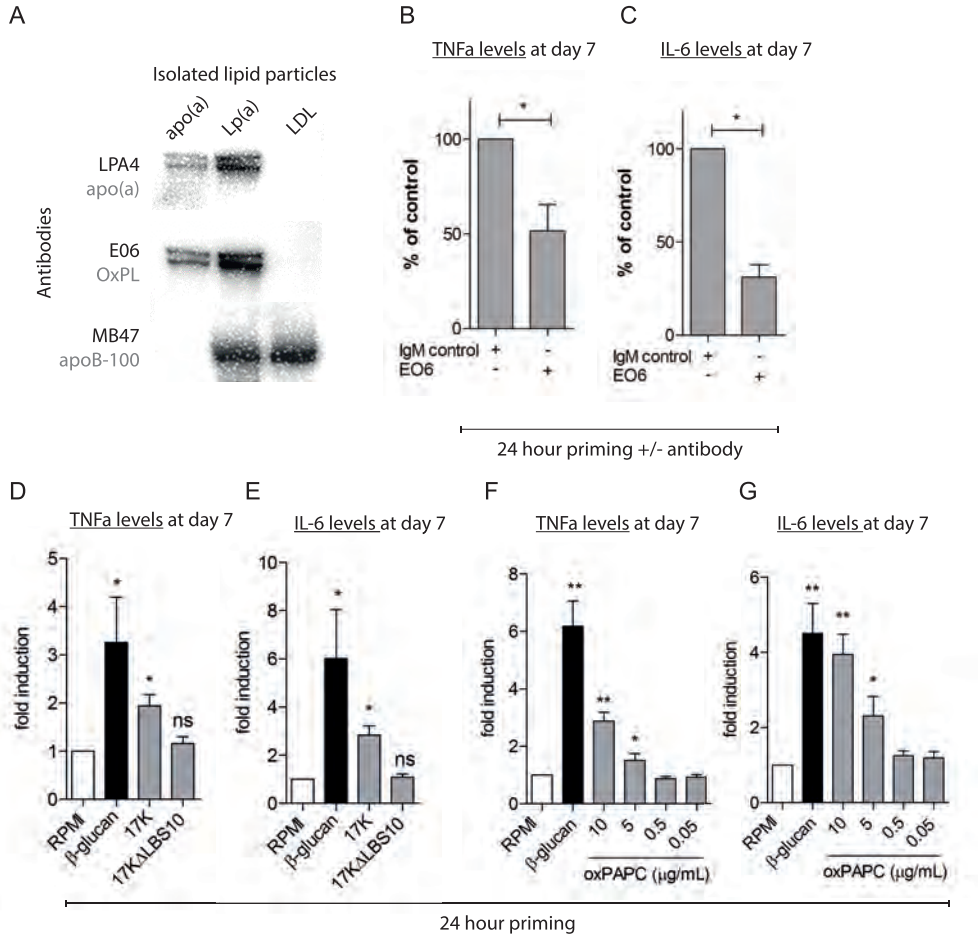

FIGURE 4. OxPL induce the enhanced monocyte response

(**A**) Immunoblotting of purified apo(a), Lp(a) and LDL; OxPL, apo(a), and apoB-100 resolved on SDS-PAGE in reducing and non-reducing conditions, were detected using the monoclonal antibodies E06, LPA4 and MB47 respectively. E06 immunostained apo(a) and Lp(a) but not LDL isolated from the same subject, (**B,C**) pre-treatment with the E06 antibody (1 nM) against OxPL inhibited the increased monocyte response after priming with 8K-IV (0.1 μg/mL, grey bars) and subsequent challenge with Pam3cys, shown as % of the initial priming with 8K-IV, corrected for IgM control antibody (n=6), (**D,E**) priming with β-glucan (5 μg/mL, positive control, black bar) and the r-apo(a) construct 17K (0.1 μg/mL, grey bar) induced increased cytokine production after Pam3Cys (10 μg/mL), whereas 17KΔLBS lacking OxPL (0.1 μg/mL, grey bar) did not (n=6), (**F,G**) priming with β-glucan (5 μg/mL positive control, black bar) and oxPAPC (grey bars) increased the monocyte responsiveness compared with RPMI (negative control, white bar) (n=6). ^=p<0.06, *=p<0.05, **=p<0.01, ***=p<0.001. *Apo(a) indicates apolipoprotein (a); IL, interleukin; LDL, low density lipoprotein; Lp(a), lipoprotein (a); oxPAPC, oxidized-1-palmitoyl-2-arachidonoyl-sn-3-glycero-phosphocholine; OxPL, oxidized phospholipids; TNFα, tumor necrosis factor α.*

DISCUSSION

In this translational work, we provide evidence in support of the concept that pro-inflammatory OxPL are major contributors to the atherogenicity of Lp(a) by showing that (i) subjects with elevated Lp(a) have increased arterial inflammation *in vivo*, (ii) monocytes isolated from subjects with elevated Lp(a) remain in a long-lasting activated state *ex vivo*, and (iii) Lp(a) elicits the pro-inflammatory response in healthy monocytes *in vitro*, an effect markedly attenuated by removing or inactivating OxPL present on Lp(a) and specifically on apo(a).

We demonstrate an increased inflammatory activity in the arterial wall in subjects with elevated Lp(a), who present with enhanced ^{18}F-FDG uptake in the arterial wall proportional to their Lp(a) levels. In analogy to the enhanced glucose consumption in inflamed tissue, arterial wall ^{18}F-FDG uptake has been proposed as a marker of atherogenic inflammation, supported by previous studies documenting ^{18}F-FDG uptake primarily in macrophage-rich areas in atherosclerotic plaques[26]. In addition, we report that this increased local inflammatory activity coincides with a higher accumulation rate of autologous PBMCs in the arterial wall as visualized by SPECT/CT imaging. Whereas we previously demonstrated augmented influx of PBMCs in advanced atherosclerotic plaques[20], the present finding emphasizes that in subjects at increased risk for atherosclerotic disease due to Lp(a) elevation, PBMC accumulation in the arterial wall is significantly enhanced also at sites without plaques. The increased arterial inflammatory signal in our subjects with elevated Lp(a) cannot be attributed to differences in atherosclerotic burden for two reasons: first, the normalized wall index of the carotids on MRI did not differ from controls, and second, inflammatory measures of the arterial wall did not correlate with structural arterial wall metrics. The absence of a consistent relation between Lp(a) elevation and established surrogate markers of atherosclerotic burden observed in this as well as in previous studies[36,37] implies that Lp(a) may increase CVD risk by enhancing plaque vulnerability rather than accelerating plaque burden.

To address whether intrinsic cellular activation precedes enhanced PBMC migration in Lp(a) subjects, we subsequently analyzed isolated circulating monocytes, which are key contributors to the technetium uptake by PBMCs[20]. Using *ex vivo* assays, we were able to recapitulate our *in vivo* findings. First, we found that monocytes isolated from subjects with elevated Lp(a) displayed an increased capacity to transmigrate the endothelium. Second, we observed that monocytes isolated from subjects with elevated Lp(a) have enhanced capacity to produce pro-inflammatory cytokines upon TLR stimulation. Previous experimental studies already showed that the apo(a) component of Lp(a) was able to also activate endothelial cells[38], whereas apo(a) also co-localized with the adhesion molecule Mac-1 in the arterial wall[39]. When integrating these data, subjects with elevated Lp(a) might be burdened by a double hit comprising activated monocytes as well as endothelial cells, both predisposing for increased arterial wall inflammation.

In support of a causal role for Lp(a) in driving monocyte activation, a series of *in vitro* experiments substantiate that (i) high Lp(a) plasma induce monocyte activation *in vitro*, which

is abolished after lipid-depletion, (ii) among the isolated lipoprotein fractions, only Lp(a) and apo(a) (particles both carrying OxPL) have the capacity to induce long-term monocyte activation.

In humans, more than 85% of plasma lipoprotein-associated OxPL are present on Lp(a). On Lp(a), OxPL is present in the lipid phase (i.e. removable from Lp(a) by delipidation with organic solvents) as well as covalently attached to apo(a)[8,9]. Here we found five oxPL species on Lp(a), comprising POVPC, PGPC, PONPC, PAzPC and KDdiA-PC, with PONPC being the most abundant. Previously, PONPC was shown to be the most abundant OxPL in the debris of distal protection devices from coronary bypass graft, carotid and renal interventions.[30]

Recombinant 17K apo(a) containing covalently bound OxPL but not 17KΔLBS r-apo(a), which lacks E06 detectable OxPL[9], reproduced Lp(a) priming of monocyte activation. The key epitope that E06 recognizes is the phosphocholine (PC) headgroup when presented in the proper conformation on OxPL. Sequencing the V_H and V_L chains of E06 revealed that these were identical to those regions of the T15 IgA natural antibody, which has been crystallized with its antigen, the PC moeity[40]. Further detailed lipidomic study of a large variety of lipids, oxidized lipids and oxidized-lipid adducts revealed that like T15, the IgM E06 only bound to oxidized phosphocholine containing phospholipids (e.g. PC - and only when the *sn2* side chain was oxidized and or adducted to a protein), but not to native PAPC suggesting that oxidation products of the *sn2* PUFA generated from oxidized PAPC appeared to generate the correct conformational epitope of the PC to allow recognition by E06[33,40].

Here, we demonstrate that the proinflammatory effects of apo(a) can be blocked by E06. Further we show that a recombinant apo(a) that contains bound OxPL is capable of activating monocytes, whereas the nearly identical, but mutated recombinant apo(a) that has lost the ability to bind OxPL does not have monocyte activation properties, indicating the necessity for OxPL to mediate monocyte activation. In aggregate, these data indicate that the OxPL carried by Lp(a) are obligatory danger signals in eliciting the prolonged potentiation of the monocyte response *in vitro*.

These findings are also complementary to prior reports demonstrating that OxPL are danger associated molecular patterns (DAMPs). The PC headgroup on OxPL is recognized by multiple innate PRRs[12]; for example, both CD36 and SR-B1 bind the PC on OxPL[32,41] and consequently, E06 blocked the uptake of OxLDL by these macrophage scavengers[42]. In addition, both acute and chronic lung injury in mice have been shown to lead to the generation of OxPL in the brochiolavage fluid, which in turn caused cytokine production by macrophages that was dependent on TLR4, and E06 was capable of blocking the pro-inflammatory properties of the OxPL[43]. Similarly, the OxPL content of apoptotic cells was shown to induce endothelial expression of IL-8, and more recently, the OxPL on apo(a) was shown to be necessary for apo(a) mediated upregulation of IL-8 by macrophages[34,35]. Hence, the mechanisms by which OxPL accelerates atherosclerosis have been attributed both to mediating uptake of OxLDL into macrophages to generate foam cells, as well as to a variety of pro-inflammatory and

plaque destabilizing processes[11–13]. In addition, recent studies suggest that such DAMP/PAMPs induce long-term potentiation of their inflammatory response *in vitro* via epigenetic alterations[31,44,45]. Future studies will need to focus on elucidating how and for how long OxPL-Lp(a) induce adaptive responses of monocytes.

Whereas the present study cannot substantiate that OxPL also is a prerequisite for monocyte activation in humans *in vivo*, it is interesting to note that our subjects with elevated Lp(a) exhibited 4-fold higher OxPL-apoB levels (OxPL associated with all apoB lipoproteins) and even 20-fold higher OxPL-apo(a) levels (OxPL associated with Lp(a) lipoproteins) compared with subjects with normal Lp(a). This increased circulating OxPL content in subjects with elevated Lp(a) suggests that a comparable impact of OxPL may hold true *in vivo*. In support, we have previously shown that OxPL-apoB levels were potent predictors of progressive atherosclerosis as well as the risk of cardiovascular disease and death in patients[14–16,46].

It remains to be established whether lowering of Lp(a) and OxPL will also lead to a reduction in arterial wall inflammation and eventually CVD risk. Recently, an antisense-based approach was reported that specifically lowered Lp(a) levels by ~80%, and to a similar degree their associated OxPL-apoB and OxPL-apo(a) levels[47,48]. With the development of such therapies to effectively lower Lp(a)[49], we should be able to design appropriate clinical trials to aid in dissecting the (causal) relation between Lp(a) and cellular as well as arterial wall inflammation. In addition to Lp(a)-lowering therapies, the present findings may also provide novel targets to modulate the atherogenic impact of Lp(a). Because the OxPL content of Lp(a) appears to mediate the pro-inflammatory effect on monocytes, oxidation-specific epitope targeted therapy using specific antibodies may also bear clinical potential[50]. At present these approaches are being evaluated in experimental settings only[51,52].

In summary, our findings strengthen the case for the inflammatory hypothesis of Lp(a) by addressing the increased inflammatory activity in the arterial wall, corresponding to an enhanced accumulation of activated immune cells, in which Lp(a)'s associated OxPL are obligatory intermediates.

Acknowledgments: We thank M.F. Lam and M.E. Hemayat for assistance in the nuclear imaging scans, and A. Edel for her help with the LC-MS/MS experiments.

Disclosures and funding: ESS has received lecturing fees from Merck, Novartis, Ionis, Amgen - none of which are related to the contents of this manuscript. NPR has served on a scientific advisory board of AstraZeneca, unrelated to the context of this study. ST and JLW are co-inventors of and receive royalties from patents or patent applications owned by the University of California San Diego on oxidation-specific and other antibodies and apoC-III-lipoprotein assays. ST has a dual appointment at UCSD and Ionis Pharmaceuticals, Inc. JLW has received honoraria for consulting for Ionis, CymaBay, Intercept and Prometheus Pharmaceuticals.

All other authors declare that they have no conflict of interest and no relationships with industry relevant to this study. This work was partly supported by a European Framework Program 7 grant (ESS: FP7-Health 309820: Nano-Athero), a European Horizon2020 grant (ESS, NPR: H2020-PHC-2015-667873-2), and by the Dutch CardioVascular Research Initiative (CVON 2011/ B019 GENIUS). NPR is financially supported by a grant from the Netherlands Heart Foundation (2012T051). Drs Tsimikas and Witztum are supported by NIH R01 grants HL119828, P01-HL088093, P01 HL055798, R01-HL106579, R01-HL078610, and R01-HL124174.

REFERENCES

1. Kronenberg F et al. Lipoprotein(a): resurrected by genetics. J Intern Med. 2013;273:6–30.
2. Thanassoulis G. Lipoprotein(a) in calcific aortic valve disease: from genomics to novel drug target for aortic stenosis. J Lipid Res. 2015
3. Nordestgaard BG et al. Lipoprotein(a) as a cardiovascular risk factor: current status. Eur Heart J. 2010;31:2844–53.
4. Tsimikas S et al. Lipoprotein(a) as a potential causal genetic risk factor of cardiovascular disease: a rationale for increased efforts to understand its pathophysiology and develop targeted therapies. J Am Coll Cardiol. 2012;60:716–21.
5. Tabas I et al. Subendothelial lipoprotein retention as the initiating process in atherosclerosis: update and therapeutic implications. Circulation. 2007;116:1832–44.
6. Dubé JB et al. Lipoprotein(a): more interesting than ever after 50 years. Curr Opin Lipidol. 2012;23:133–40.
7. Tsimikas S et al. Oxidized phospholipids, Lp(a) lipoprotein, and coronary artery disease. N Engl J Med. 2005;353:46–57.
8. Bergmark C et al. A novel function of lipoprotein [a] as a preferential carrier of oxidized phospholipids in human plasma. J Lipid Res. 2008;49:2230–9.
9. Leibundgut G et al. Determinants of binding of oxidized phospholipids on apolipoprotein (a) and lipoprotein (a). J Lipid Res. 2013;54:2815–30.
10. Tsimikas S et al. The role of oxidized phospholipids in mediating lipoprotein(a) atherogenicity. Curr Opin Lipidol. 2008;19:369–377.
11. Lee S et al. Role of phospholipid oxidation products in atherosclerosis. Circ Res. 2012;111:778–99.
12. Miller YI et al. Oxidation-specific epitopes are danger-associated molecular patterns recognized by pattern recognition receptors of innate immunity. Circ Res. 2011;108:235–48.
13. Leibundgut G et al. Oxidation-specific epitopes and immunological responses: Translational biotheranostic implications for atherosclerosis. Curr Opin Pharmacol. 2013;13:168–79.
14. Taleb A et al. Oxidized phospholipids on apoB-100-containing lipoproteins: a biomarker predicting cardiovascular disease and cardiovascular events. Biomark Med. 2011;5:673–694.
15. Tsimikas S et al. Oxidation-specific biomarkers, prospective 15-year cardiovascular and stroke outcomes, and net reclassification of cardiovascular events. J Am Coll Cardiol. 2012;60:2218–29.
16. Tsimikas S et al. Pro-inflammatory interleukin-1 genotypes potentiate the risk of coronary artery disease and cardiovascular events mediated by oxidized phospholipids and lipoprotein(a). J Am Coll Cardiol. 2014;63:1724–34.
17. Seman LJ et al. Quantification of Lipoprotein (a) Plasma Fraction in Plasma and Cholesterol in Lectin-Bound. Clin Chem. 1994;40:400–403.
18. Duivenvoorden R et al. In vivo quantification of carotid artery wall dimensions: 3.0-Tesla MRI versus B-mode ultrasound imaging. Circ Cardiovasc Imaging. 2009;2:235–42.
19. Rudd JHF et al. (18)Fluorodeoxyglucose positron emission tomography imaging of atherosclerotic plaque inflammation is highly reproducible: implications for atherosclerosis therapy trials. J Am Coll Cardiol. 2007;50:892–6.

20. van der Valk FM et al. In vivo imaging of enhanced leukocyte accumulation in atherosclerotic lesions in humans. J Am Coll Cardiol. 2014;64:1019–29.
21. Hirschfeld M et al. Cutting Edge: Repurification of Lipopolysaccharide Eliminates Signaling Through Both Human and Murine Toll-Like Receptor 2. J Immunol. 2000;165:618–622.
22. Cain WJ et al. Lipoprotein [a] is cleared from the plasma primarily by the liver in a process mediated by apolipoprotein [a]. J Lipid Res. 2005;46:2681–91.
23. Edelstein C et al. Determinants of Lipoprotein(a) Assembly: A Study of Wild-Type and Mutant Apolipoprotein(a) Phenotypes Isolated from Human and Rhesus Monkey Lipoprotein(a) under Mild Reductive Conditions. Biochemistry. 1995;34:16483–16492.
24. van Rijssel J et al. The Rho-guanine nucleotide exchange factor Trio controls leukocyte transendothelial migration by promoting docking structure formation. Mol Biol Cell. 2012;23:2831–44.
25. Franssen R et al. In Vivo Inflammation Does Not Impair ABCA1-Mediated Cholesterol Efflux Capacity of HDL. Cholesterol. 2012;2012:610741.
26. Tarkin JM et al. PET imaging of inflammation in atherosclerosis. Nat Rev Cardiol. 2014;11:443–457.
27. Moore KJ et al. Macrophages in the pathogenesis of atherosclerosis. Cell. 2011;145:341–55.
28. Abeles RD et al. CD14, CD16 and HLA-DR reliably identifies human monocytes and their subsets in the context of pathologically reduced HLA-DR expression by CD14(hi) /CD16(neg) monocytes. Cytometry. 2012;81:823–34.
29. Gordon S et al. Monocyte and macrophage heterogeneity. Nat Rev Immunol. 2005;5:953–64.
30. Ravandi A et al. Release and capture of bioactive oxidized phospholipids and oxidized cholesteryl esters during percutaneous coronary and peripheral arterial interventions in humans. J Am Coll Cardiol. 2014;63:1961–1971.
31. Cheng S-C et al. mTOR- and HIF-1 -mediated aerobic glycolysis as metabolic basis for trained immunity. Science. 2014;345:1250684–1250684.
32. Boullier A et al. Phosphocholine as a pattern recognition ligand for CD36. J Lipid Res. 2005;46:969–76.
33. Friedman P et al. Correlation of antiphospholipid antibody recognition with the structure of synthetic oxidized phospholipids. Importance of Schiff base formation and aldol condensation. J Biol Chem. 2002;277:7010–20.
34. Chang MK et al. Apoptotic cells with oxidation-specific epitopes are immunogenic and proinflammatory. J Exp Med. 2004;200:1359–70.
35. Scipione CA et al. Mechanistic insights into lipoprotein(a)-induced interleukin-8 expression: a role for oxidized phospholipid modification of apolipoprotein(a). J Lipid Res. 2015;56:2273-85.
36. Klein JH et al. Lipoprotein(a) is associated differentially with carotid stenosis, occlusion, and total plaque area. Arterioscler Thromb Vasc Biol. 2008;28:1851–6.
37. Guerra R et al. Lipoprotein(a) and apolipoprotein(a) isoforms: no association with coronary artery calcification in the Dallas Heart Study. Circulation. 2005;111:1471–9.
38. Pellegrino M et al. The apolipoprotein(a) component of lipoprotein(a) stimulates actin stress fiber formation and loss of cell-cell contact in cultured endothelial cells. J Biol Chem. 2004;279:6526–33.
39. Sotiriou SN et al. Lipoprotein(a) in atherosclerotic plaques recruits inflammatory cells through interaction with Mac-1 integrin. FASEB J. 2006;20:559–61.
40. Shaw PX et al. Natural antibodies with the T15 idiotype may act in atherosclerosis, apoptotic clearance, and protective immunity. J Clin Invest. 2000;105:1731–40.
41. Gillotte-Taylor K et al. Scavenger receptor class B type I as a receptor for oxidized low density lipoprotein. J Lipid Res. 2001;42:1474–82.
42. Bird DA et al. Receptors for oxidized low-density lipoprotein on elicited mouse peritoneal macrophages can recognize both the modified lipid moieties and the modified protein moieties: implications with respect to macrophage recognition of apoptotic cells. Proc Natl Acad Sci U S A. 1999;96:6347–52.
43. Imai Y et al. Identification of oxidative stress and Toll-like receptor 4 signaling as a key pathway of acute lung injury. Cell. 2008;133:235–249.
44. Saeed S et al. Epigenetic programming of monocyte-to-macrophage differentiation and trained innate immunity. Science. 2014;345:1251086–1251086.
45. Bekkering S et al. Oxidized Low-Density Lipoprotein Induces Long-Term Proinflammatory Cytokine Production and Foam Cell Formation via Epigenetic Reprogramming of Monocytes. Arterioscler Thromb Vasc Biol. 2014;34:1731–8.

46. Byun YS et al. Relationship of oxidized phospholipids on apolipoprotein B-100 to cardiovascular outcomes in patients treated with intensive versus moderate atorvastatin therapy: the TNT trial. J Am Coll Cardiol. 2015;65:1286–95.
47. Tsimikas S et al. Antisense Therapy Targeting Apolipoprotein (a) Reduces Plasma Lipoprotein(a) Levels. Lancet. 2015;386:1472-83.
48. Stroes ES et al. A sense of excitement for a specific Lp(a)-lowering therapy. Lancet. 2015;6736:23–24.
49. Kolski B et al. Emerging therapeutic agents to lower lipoprotein (a) levels. Curr Opin Lipidol. 2012;23:560–8.
50. Miller YI et al. Oxidation-specific epitopes as targets for biotheranostic applications in humans: biomarkers, molecular imaging and therapeutics. Curr Opin Lipidol. 2013;24:426–37.
51. Tsimikas S et al. Human oxidation-specific antibodies reduce foam cell formation and atherosclerosis progression. J Am Coll Cardiol. 2011;58:1715–27.
52. Gonen A et al. Atheroprotective immunization with malondialdehyde-modified LDL is hapten specific and dependent on advanced MDA adducts: implications for development of an atheroprotective vaccine. J Lipid Res. 2014;55:2137–55.

SUPPLEMENT

Additional Methods

Flow cytometry. The following fluorochrome labeled mAb were used: phycoerythrin-CyChrome7 (PE-CyTM7)-anti CD14, allophycocyanin (APC)-Cy7-anti CD16, peridinin-chlorophyll-protein (PerCP)-Cy5.5-anti HLA-DR, PE-anti CD11b, APC-anti CD11c, APC-anti CD18, APC-anti CD29, fluorescein isothiocyanate (FITC)-anti CD32, APC-anti CD36, PE-anti CD62L, APC-anti CD192 (CCR2), FITC-anti CD195 (CCR5) [all from BD Biosciences, San Jos, CA, USA]; PE-anti CD204 (SR-A) [R&D systems, Abingdon, UK] and PE-anti CD197 (CCR7) [Biolegend, SanDiego, CA, USA]. Samples were incubated for 20 min at RT in the dark. To lyse red blood cells, 700 µL of PharmLyse1 (BD Biosciences, San Jose, CA) was added for 12 min, after which the samples were centrifuged at 400g for 5 min, the supernatant discarded and the samples resuspended in 400 µL of staining buffer. All data were collected on a FACS Calibur (Becton Dickinson, NJ), compensation was performed using single color fluorochromes and BD FacsComp beads, and samples were analyzed using FlowJo software (version 5.4+); for gating strategy and representative histograms see Figure S3. Delta mean fluorescence intensity (MFI) was obtained by subtracting median MFI from the isotype from the median MFI of the marker in corresponding color. Please note that the delta MFI values of CD62L were scaled down by a factor 10.000 to fit the bar graph.

Lipid Extraction. The lipids were extracted by the method previously described by Folch *et al.* with modifications.[1, 2] The lipid extracts were stored in CM (2:1), flushed with nitrogen, capped and stored at -80^{0}C till analysis. The internal standard mixture spiked into each sample prior to extraction consisted of 1,2-dinonanoyl-*sn*-glycero-3-phosphocholine (DNPC), 1-heptadecanoyl-2-hydroxy-*sn*-glycero-3-phosphocholine (17:0 LPC)[3]. Synthetic 1-palmitoyl-2-(5-oxovaleroyl)-sn-glycero-3-phosphocholine (POVPC), 1-palmitoyl-2-glutaroyl- sn -glycero-3-phosphocholine (PGPC), 1-palmitoyl-2-azelaoyl-sn-glycero-3-phosphocholine (PAzPC), and 1-palmitoyl-2-(9'-oxo-nonanoyl)-sn-glycero-3-phosphocholine were purchased from Avanti Polar Lipids (Alabaster, AL). 1-palmitoyl-2-(4-keto-dodec-3-ene-dioyl) phosphatidylcholine (KDdiA-PC) were from Cayman Chemicals (Ann Arbor, MI)

HPLC. The detection of oxidized PCs were carried out in reverse-phase (RP) chromatography as reported previously[2, 4-7]. Briefly lipid extracts were reconstituted in an RP solvent system consisting of Acetonitrile-Isopropanol-Water (65:30:5 vol/vol/vol). Thirty microliters of the sample was injected on to Ascentis Express C18 HPLC column (15cmx2.1mm, 2.7µm; Supelco Analytical, Bellefonte, Pennsylvania, USA) and using a Prominence UFLC system from Shimadzu Corporation (Canby, Oregon, USA). Elution was performed by linear gradient of solvent A (Acetonitrile/Water, 60:40 vol/vol) and solvent B (Isopropanol/Acetonitrile, 90:10,

vol/vol) both the solvents containing 10 mM ammonium formate and 0.1% formic acid. The time program used was as follows: initial solvent B at 32% until 4.00 min; switched to 45% B; 5.00 min 52% B; 8.00 min 58% B; 11.00 min 66% B; 14.00 min 70% B; 18.00 min 75% B; 21.00 min 97% B; 25.00 min 97% B; 25.10 min 32% B until the elution was stopped at 30.10 min. A flow rate of 260 µl/min was used for analysis, and the column and sample tray were held at 45 and 4˚C, respectively.

Mass Spectrometry. The HPLC system was coupled to 4000 QTRAP® triple quadrupole mass spectrometer system with a Turbo V electrospray ion source from AB Sciex (Framingham, Massachusetts, USA). For phosphatidylcholine, the detection was carried out in positive ion mode by MRM of 6 transitions using PC-specific product ion (184.3 *m/z*, Da), which corresponds to the cleaved phosphatidylcholine. The MRM settings were as follows: declustering potential=125, entrance potential=10, collision energy=53, collision cell exit potential=9 and dwell time= 50 msec. [8,9]

For each synthetic OxPL, POVPC, PGPC, PONPC, PAzPC and KDdiA-PC external calibration (i.e., using plasma-free standard solutions) was carried out to estimate linear range and sensitivity for these analytes and relative ionization compared to DNPC at equimolar levels. Concentrations of analytes were determined from calibration curves (1/x weighted linear regression) plotted as ratio of analyte peak area/DNPC peak area versus the amount of analyte on a column. The instrument was tuned by direct infusion of poly(propylene glycol) (PPG) in both positive and negative modes and external mass calibration was performed at regular intervals. Retention time window in MRM was set to detect peaks of significance within 60 seconds of confirmed retention time and data was collected utilizing Analyst® Software 1.6 (AB Sciex). Multi-quant® Software 2.1 (AB Sciex) was used to compare peak areas of internal standards and unknown analytes to quantitate the results.

REFERENCES APPLIED TO SUPPLEMENT

1. Folch J et al. A simple method for the isolation and purification of total lipides from animal tissues. The Journal of biological chemistry. 1957;226:497-509.
2. White CW et al. A whole blood-based perfusate provides superior preservation of myocardial function during ex vivo heart perfusion. The Journal of heart and lung transplantation : the official publication of the International Society for Heart Transplantation. 2015;34:113-121.
3. Gruber F et al. A simplified procedure for semi-targeted lipidomic analysis of oxidized phosphatidylcholines induced by uva irradiation. Journal of lipid research. 2012;53:1232-1242.
4. Vo MN et al. Physiologic significance of coronary collaterals in chronic total occlusions. Canadian journal of physiology and pharmacology. 2015;93:867-71.
5. Zeglinski M et al. Congenital absence of nitric oxide synthase 3 potentiates cardiac dysfunction and reduces survival in doxorubicin- and trastuzumab-mediated cardiomyopathy. The Canadian journal of cardiology. 2014;30:359-367.
6. Hasanally D et al. Novel bioactive oxidized phospholipids are produced in myocardium during ischemia reperfusion and act as mediators of cell death within cardiac myocytes. European Heart Journal. 2014;35:306-306.
7. Ravandi A et al. Release and capture of bioactive oxidized phospholipids and oxidized cholesteryl esters during percutaneous coronary and peripheral arterial interventions in humans. Journal of the American College of Cardiology. 2014;63:1961-1971.
8. Bordun KA et al. The utility of cardiac biomarkers and echocardiography for the early detection of bevacizumab- and sunitinib-mediated cardiotoxicity. American journal of physiology. Heart and circulatory physiology. 2015;309:H692-701.
9. Yamaguchi T et al. Dietary flax oil rich in alpha-linolenic acid reduces renal disease and oxylipin abnormalities, including formation of docosahexaenoic acid derived oxylipins in the cd1-pcy/pcy mouse model of nephronophthisis. Prostaglandins, leukotrienes, and essential fatty acids. 2015;94:83-89.

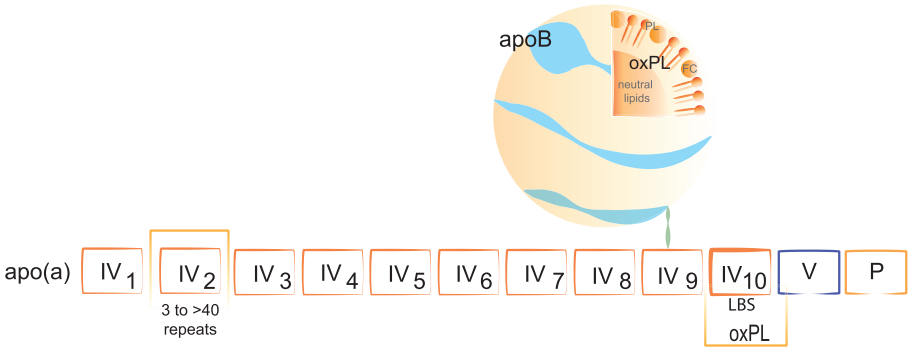

FIGURE S1. Schematic of lipoprotein(a)

Lp(a) is composed of apo(a) covalently linked to apoB of LDL. This LDL contains a central core of neutral lipids, surface phospholipids and free cholesterol. Apo(a) comprises an inactive protease domain and a series of loop structures termed kringle, including KIV type 2 which is present in 3 to >40 copies. Genes encoding an apo(a) allele with smaller numbers of KIV_2 repeats lead to higher levels of Lp(a) in plasma, presumably due to higher rates of hepatic synthesis. Phosphocholine containing OxPL are present in the lipid phase and covalently bound to apo(a) in the areas near KIV-10 and KV. *Apo(a) indicates apolipoprotein (a); apoB, apolipoprotein B-100; FC, free cholesterol; K, kringle; KIV_2, KIV type 2; LBS, lysine binding site; LDL, low density lipoprotein; Lp(a), lipoprotein (a); P, protease domain; PL, phospholipids; OxPL, oxidized phospholipids.*

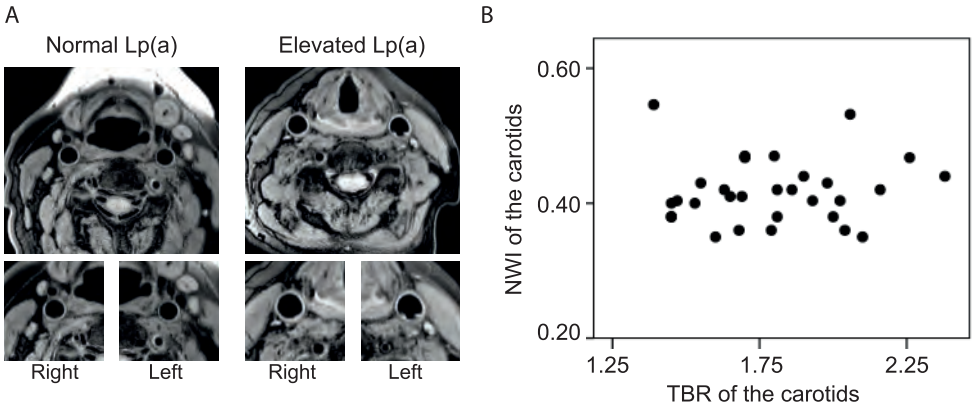

FIGURE S2. Arterial wall dimensions assessed with MR imaging

(**A**) Cross-sectional MR images used to quantify the arterial wall dimension, expressed as NWI, of the carotid arteries of normal Lp(a) and elevated Lp(a) subjects, (**B**) scatterplot illustrating no correlation between NWI and inflammation (TBR, assessed with PET) in subjects with elevated Lp(a). *Lp(a) indicates lipoprotein (a); MR, magnetic resonance; NWI, normalized wall index; PET, postiron emission tomography; TBR, target to background ratio.*

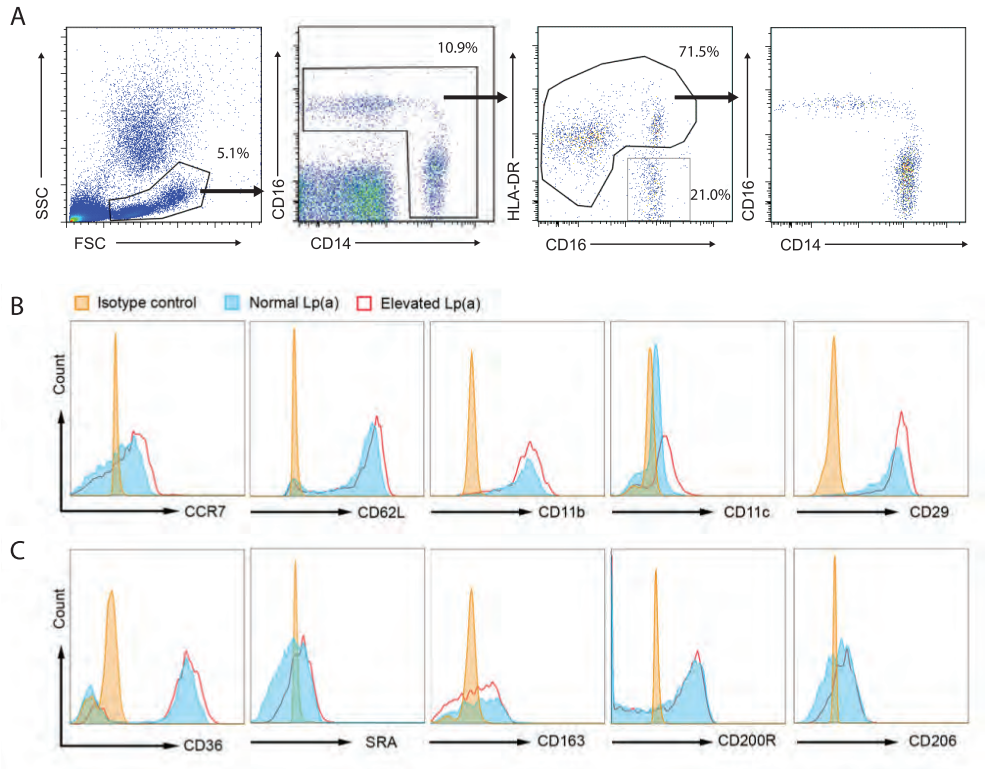

FIGURE S3. Gating strategy to define monocyte population and representative histograms

(**A**) The monocyte population was gated as follows; the leukocyte population was gated on a forward side scatter and subsequently viewed on a CD14/CD16 plot in which the $CD14^{pos}CD16^{pos}$ cell cloud was gated, after which these cells were then shown on the CD16/HLA-DR plot to exclude the $HLA\text{-}DR^{neg}CD16^{pos}$ cells. For gating graphs log scale was used, percentages of cells in gates are shown. Cells were analyzed using FlowJo software (version 5.4+). (**B**) Representative FACS histograms (of Figure 2A) show the expression of chemokine, adhesion and transmigration markers and (**C**) the expression of scavenger and other receptors (Figure 2D) on monocytes as assessed by flow cytometry of subjects with elevated Lp(a) (red line) compared with subjects with normal Lp(a) (blue line). The isotype control (orange line) was similar between the two groups and therefore only one isotype control is showed. *Lp(a) indicates lipoprotein (a).*

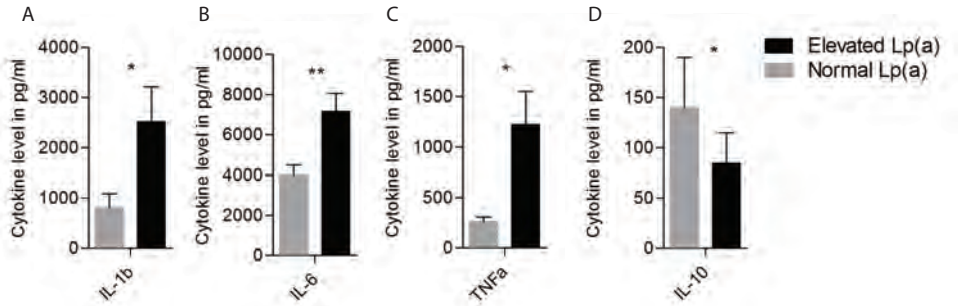

FIGURE S4. Monocytes of Lp(a) subjects have an increased response to LPS

In response to an overnight challenge to LPS (10 ng/ml) monocytes isolated from subjects with elevated Lp(a) (black bars, n=15) produced higher levels of IL-1β (**A**), IL-6 (**B**), TNFα (**C**) and lower levels of IL-10 (**D**), compared to monocytes of subjects with normal Lp(a) (grey bars, n=15). **=p<0.05, **=p<0.01. IL indicates interleukin; LPS, lipopolysacharide; TNFa, tumor necrosis factor a.*

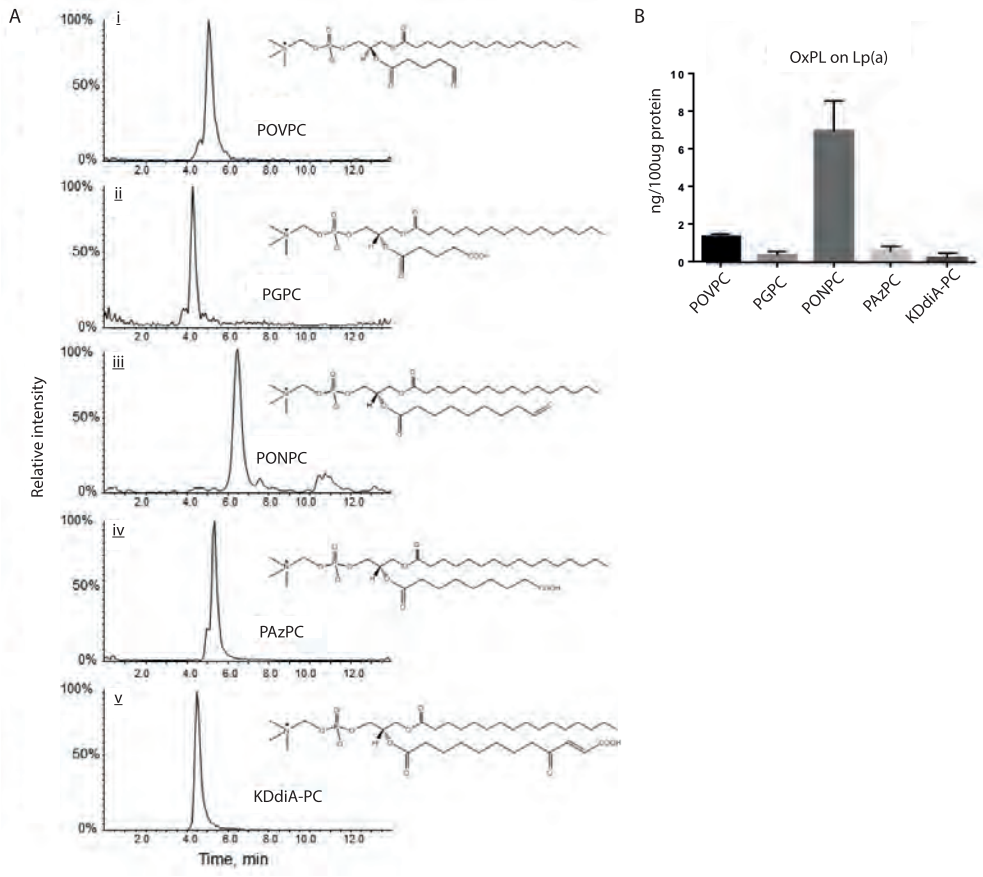

FIGURE S5. Levels of OxPC molecules identified in human Lp(a)

Quantitation was based on internal standard DNPC, details are given in methods. (**A**) Identification of oxPC molecules on human Lp(a). Single ion plots of MRM analysis of human Lp(a) lipid extract. Reversephase separation of the

most abundant fragmented OxPL products (**i**)POVPC, (**ii**) PGPC, (**iii**) PONPC, (**iv**) PAzPC, (**v**) KDdiA-PC (n=3), and (**B**) quantification of oxPC molecules on human Lp(a) (n=3). *Lp(a) indicates lipoprotein (a); OxPL, oxidized phospholipids.*

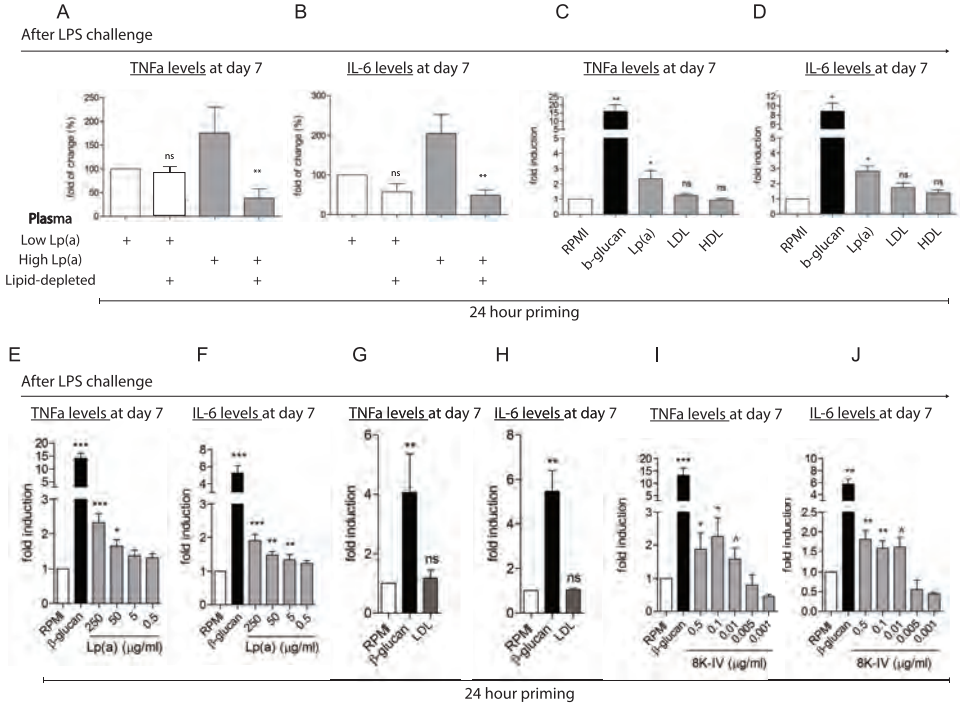

FIGURE S6. Lp(a) and its OxPL load induce an enhanced monocyte response to LPS

(**A,B**) priming healthy monocytes with high Lp(a) plasma (grey bars) for 24h resulted in an increased cytokine production upon re-stimulation with LPS (10 ng/mL) on day 6, compared control (white bars). After lipid-depletion this effect was profoundly reduced (n=3), (**C,D**) monocyte priming with β-glucan (5 µg/mL, positive control, black bar) or Lp(a) (grey bar, 250 µg/mL) for 24h, induced an increased cytokine production after LPS (10 ng/mL) on day 6, compared with priming with RPMI (negative control, white bar), LDL (grey bar, 10 µg/mL) or HDL (grey bar, 10 µg/mL) (n=6), (**E,F**) this Lp(a) is dose-dependent (n=6), (**G,H**) priming with LDL (10 µg/mL, grey bar) did not increase cytokine production after LPS (10 ng/mL) (n=6), (**I,J**) monocyte priming with β-glucan (5 µg/mL, positive control, black bar) or r-apo(a) construct, 8K-IV, (grey bars) increased cytokine production after LPS (10 ng/mL) (n=6), compared to RPMI (negative control, white bar),

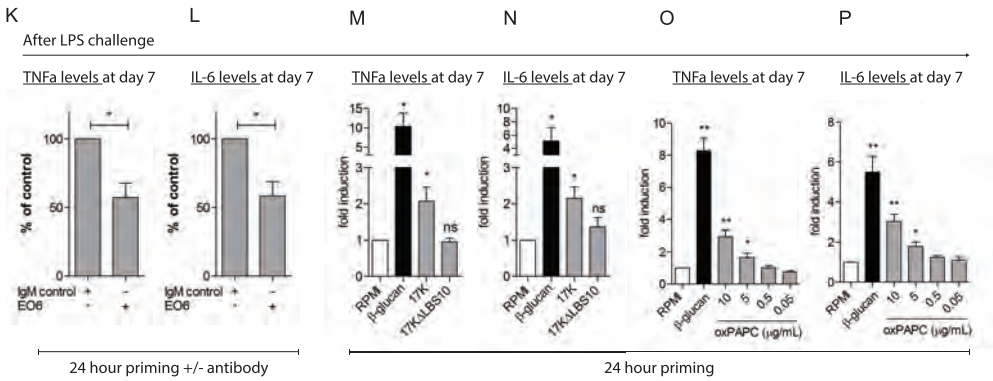

FIGURE S6. Continued

(**K,L**) pre-treatment with the E06 antibody (1 nM) against OxPL inhibited the priming effects of 8K-IV (0.1 μg/mL, grey bars), whereas IgM (1 nM) did not (n=6), (**M,N**) β-glucan (5 μg/mL, positive control, black bar) and the r-apo(a) construct 17K priming (0.1 μg/mL grey bar) increased cytokine production upon LPS (10 ng/mL), whereas 17KΔLBS lacking OxPL (0.1 μg/mL, grey bar) did not (n=6), (**O,P**) priming with β-glucan (5 μg/mL, positive control, black bar) and oxPAPC (grey bars) increased the monocyte response upon LPS (10 ng/mL) compared to RPMI (negative control, white bar) (n=6). *^=p<0.06, *=p<0.05, **=p<0.01, ***=p<0.001. Apo(a) indicates apolipoprotein (a); HDL, high density lipoproetin; IL, interleukin; LDL, low density lipoprotein; Lp(a), lipoprotein (a); LPS, lipopolysaccharide; oxPL, oxidized phospholipids; TNFα, tumor necrosis factor α.*

MOVIE S1. Migration of monocytes of subjects with elevated Lp(a) and normal Lp(a)

Freshly isolated monocytes of subjects with elevated Lp(a) (Link: https://youtu.be/X-hJwKVH17g) have increased monocyte motility compared to monocytes of subjects with normal Lp(a) (Link: https://youtu.be/uxFbvrmPWfI) when plated on a fibronectin matrix, whereas isolated monocytes of subjects with normal Lp(a) display less monocyte motility.

PART III

THERAPEUTIC TARGETING OF ATHEROSCLEROTIC INFLAMMATION

CHAPTER 8

NOVEL ANTI-INFLAMMATORY STRATEGIES IN ATHEROSCLEROSIS

Van der Valk FM, van Wijk DF, Stroes ESG

Curr Opin Lipidol. 2012;23:532-9

ABSTRACT

Rationale: Inflammation has been widely acknowledged to contribute throughout all stages of atherogenesis. However, inflammation's role in atherosclerosis has not been translated into clinical practice where the mainstay of treatment is still lipid-targeted therapy. This review provides an overview of anti-inflammatory therapies in atherosclerosis, and discusses potential drawbacks and clinical benefits.

Recent findings: We await the first immunosuppressive drugs to improve cardiovascular outcome in patients. In the meantime, several novel anti-inflammatory targets have reached clinical development stage, such as the cytokines targets IL-1 and IL-6, CCR2 antagonist, selective phospholipase and leukotriene inhibitors. Novel imaging modalities such as MRI and PET/CT provide valuable surrogate inflammatory endpoints for risk stratification and testing anti-inflammatory agents in cardiovascular randomized trials.

Conclusion: Anti-inflammatory therapies hold great promise in cardiovascular prevention regimens, however, atherosclerosis is a chronic disease and systemic long-term use of anti-inflammatory agents carries the risk of complications arising from immunosuppression. In order to successfully add anti-inflammatory strategies to our routine armament, we need to identify high-risk patients who benefit from anti-inflammatory treatment, increase our insight into the inflammatory pathogenesis of atherogenesis and find safe and effective compounds capable of directly suppressing plaque inflammation.

INTRODUCTION

The concept that atherosclerosis is a lipid-driven disease has dominated cardiovascular research for many years. The past two decades, however, our point of view of atherogenesis has changed; embracing atherosclerosis as a chronic inflammatory disease[1]. From its initiation to the progression of atherosclerosis, and eventually in the vulnerable stage of plaque rupture, inflammatory processes are critically involved[2].

Inflammation in atherosclerosis

Monocytes and macrophages comprise the central effectors of the initiation and progression of atherosclerosis. Upon activation of endothelium and subsequent adhesion of monocytes, proinflammatory chemokines provide stimuli to recruit circulating monocytes to the arterial wall[3]. Whilst crossing the endothelium, monocytes are exposed to various pro-inflammatory stimuli, including physical stress and oxidatively modified low-density lipoprotein (LDL) particles, together contributing to their differentiation into macrophages. In the intimal space, macrophages take up these modified lipid particles, advancing into foam cells. Over time, the local inflammation is continually reinforced, resulting in the progression of early lesions. Eventually, advanced plaques become prone to rupture, a phenomenon that strongly relates to the number of inflammatory cells within the plaque[4].

Inflammation: cause or consequence?

Several experimental studies showed that inhibition of inflammation can reduce atherogenesis. Inhibition of monocyte influx through reduced expression of endothelial adhesion molecules (VCAM) significantly reduced the formation of atherosclerotic lesions[5]. In addition, silencing of monocyte chemoattractant protein-1 (MCP-1) or its receptor (CCR2) in mice also resulted in a marked reduction of atherosclerotic burden[6-8]. Finally, inactivation of the macrophage colony stimulating factor (M-CSF) or macrophage migration inhibitory factor (MIF) has shown to substantially reduce atherogenesis[9,10]. These studies underscore the relevance of inflammatory processes in atherosclerosis[4].

In epidemiological studies inflammatory markers in the plasma, like C-reactive protein (CRP), independently predict the risk of cardiovascular disease[11]. In fact, by preselecting patients with increased CRP levels, the decrease in CRP following statin therapy independently related to the therapeutic benefit[12]. Yet, life-long exposure to increased CRP levels, due to single nucleotide polymorphisms (SNPs) in the CRP gene, was not associated with an increased cardiovascular risk[13]. Hence, the causality of this well described inflammatory marker is heavily debated[14]. In contrast, a causal role for interleukin-6 (IL-6), a cytokine upstream CRP[15,16], has been elegantly demonstrated by two independent research consortia[17,18]. SNPs associated with decreased IL-6 signaling correlated with lower acute-phase reactants, such as CRP and fibrinogen, with a concomitant proportional reduction in cardiovascular risk[17,18].

In support of these genetic studies, inflammatory diseases have shown to strongly associate with cardiovascular disease[19]. Even the short-term presence of community-acquired infections transiently increased the risk of vascular events[20]. Moreover, chronic inflammatory disorders (CID), such as rheumatoid arthritis (RA), are characterized by a marked increase in cardiovascular risk[21-24]. In addition, mutant mice with induced chronic inflammatory diseases showed a marked acceleration of atherogenesis[25]. This was further evidenced by several animal models revealing a profound acceleration of atherogenesis after repetitive infectious stimuli, such as intraperitoneal lipopolysaccharide administration, viral (e.g. herpes) or bacterial (e.g. porphyromonas gingivalis) infections[26-28]. More importantly, the reduction of the inflammatory burden in CID patients is paralleled by a marked reduction of this cardiovascular risk[29,30]. Taken together, experimental work, genetic studies and observational data in humans lend strong support to the concept that inflammation has a causal role in atherogenesis[31-33].

Inflammation: therapeutic target in cardiovascular diseases?

Prior to embarking on novel anti-inflammatory strategies, the effect of traditional therapies amending atherosclerotic inflammation need to be considered. First, statins have shown to attenuate inflammation, independent of its LDL lowering effect[34-36]. Also, the statin-induced anti-inflammatory impact is associated with a modest clinical benefit[37-39]. Moreover, high density lipoprotein (HDL) has been shown to exert potent anti-inflammatory effects[40,41]. However, clinical studies that therapeutically increased HDL levels showed no convincing effects on inflammatory parameters[42-44].

Next to lipid modulating drugs, several anti-inflammatory drugs prescribed in patients with CID might be beneficial in atherosclerosis, such as methotrexate (MTX), mycophenolate mofetil (MMF) or biologicals[45,49,50]. We recently showed that short-term pre-treatment with MMF in patients scheduled for a carotid endartectomy shifted the cellular composition and activation status of white blood cells in the plaque[46]. With respect to MTX, several observational trials in RA patients have shown that MTX not just attenuated systemic inflammation but also the cardiovascular event rate[29,47]. At present, the Cardiovascular Inflammation Reduction Trial (CIRT) is evaluating the direct effect of very low-dose MTX in patients with cardiovascular disease[48]. Thus, whereas several short-term anti-inflammatory strategies have shown to benefit atherogenesis, it will be a challenge to identify anti-inflammatory interventions that inhibit the inflammatory state of the atherosclerotic plaque, without posing individuals to the dangers of long-lasting immunosuppression[51].

Arterial wall inflammation: how to 'guestimate' in humans?

With the expected advent of novel anti-inflammatory strategies, it is imperative to be able to accurately quantify the drug response, preferably at the level of the target-organ: the arterial wall. Unfortunately, currently available biomarkers have not proven sensitive in estimating the

absence or presence of inflammatory plaques[52]. Novel imaging modalities, including magnetic resonance imaging (MRI), dynamic contrast-enhanced (DCE-) MRI and positron emission tomography (PET), hold promise for assessing plaque characteristics, including arterial wall inflammation[53,54]. MRI is a well suited technique to quantify human atherosclerosis because it is noninvasive, free from ionizing radiation and enables a reproducible assessment of vessel wall dimensions and composition[55-57]. In addition to various contrast-weighted imaging sequences, contrast agents in DCE-MRI can estimate the plaque's permeability, which is associated with plaque inflammation and rupture[58-60]. PET imaging gained its interest as a tool to quantify arterial wall inflammation since the inflamed plaque is metabolically very active[61]. Uptake of ^{18}fluorodeoxyglucose (^{18}F-FDG) is closely associated with both the degree of macrophage infiltration as well as levels of inflammatory gene expression in the atherosclerotic plaque[62,63]. In addition, ^{18}F-FDG uptake correlates with the risk of recurrent cardiovascular events[64]. Thus, MRI and PET can both image aspects of inflammation in atherosclerosis. Ultimately, these noninvasive imaging techniques will identify high risk patients and guide drug development studies in high-risk patients[65].

NOVEL ANTI-INFLAMMATORY STRATEGIES

Notwithstanding the significant reduction in cardiovascular risk achieved by statin therapy, the substantial residual risk presses the need for additional therapeutic moieties[66]. Table 1 lists several novel targets in atherosclerosis with corresponding compounds, comprising the cytokines targets IL-1 and IL-6, CCR2 antagonist, selective phospholipase and leukotriene inhibitors. The potential benefit of drugs targeting pathways illustrated in Figure 1 will be discussed below. In addition, the importance of local anti-inflammatory drug delivery is emphasized.

TABLE 1. Anti-inflammatory strategies in atherosclerosis

Target	Compound	Stage in human clinical development	Refs
Antiproliferative	Methotrexate	Phase III (CIRT)	47
IL-1 pathway	Canakinumab	Phase III (CANTOS)	66
	Anakinra	Phase III	67
IL-6 inhibitors	Tocilizumab	Not in atherosclerosis	68, 69
TNF-α inhibitors	E.g. Adalimumab, Infliximab	Not in atherosclerosis	48, 49
CCR2 antagonist	MLN1202	Phase II	70
Phospholipase inhibitors	sPLA2 inhibitors (varespladib)	Phase III	71, 72
	Lp-PLA2 inhibitors (darapladib)	Phase III	73-75
Leukotriene inhibitors	5-LO inhibitors (VIA-2291)	Phase II	76
	FLAP inhibitors (DG-031)	Phase II	77

CCR2 indicates C-C chemokine receptor 2; IL, interleukin; Lp-PLA2, lipoprotein-associated PLA2; PLA2, phospholipase A2; sPLA2, secretory PLA2; TNFα, tumor necrosis factor α.

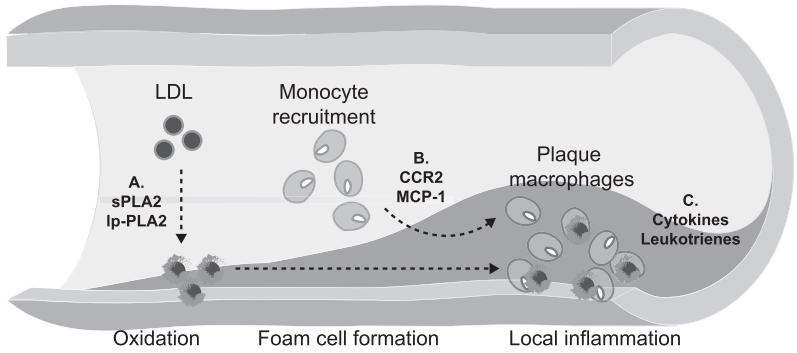

FIGURE 1. Schematic showing novel therapeutic inflammatory targets in atherosclerosis

Plasma LDL particles accumulate in the intimal space, (**A**) PLA2 family members, sPLA2 and LpPLA2, modify LDL and generate proatherogenic oxidized lipid particles. Monocytes are recruited by several chemokine signals, including CCR2 and MCP-1 (**B**). Following recruitment, monocytes differentiate into macrophages driven by multiple stimuli. Macrophages take up oxidized lipids moieties, yielding foam cells. Both foam cells and activated macrophages produce pro-inflammatory leukotrienes and cytokines, such as IL-1, IL-6 and TNFα (**C**). *CCR2 indicates C-C chemokine receptor 2; IL, interleukin; LDL, low density lipoprotein; Lp-PLA2, lipoprotein-associated PLA2; MCP-1, monocyte chemotactic protein-1; ox, oxidized; PLA2, phospholipase A2; PL, phospholipids; sPLA2, secretory PLA2; TNFα, tumor necrosis factor α.*

Cytokine and chemokine targets

Interleukin-1 inhibition

Interleukin-1 (IL-1) is one of the primary pro-inflammatory cytokines perpetuating the inflammatory response after injury[67]. Experimental studies emphasized the role of IL-1 in atherogenesis[50]. In humans, atherosclerotic arteries have elevated levels of IL-1, and the IL-1 receptor antagonist gene has been associated with a lower incidence of restenosis after coronary stenting[68,69]. Currently, IL-1β is evaluated as therapeutic target; a large secondary prevention trial (CANTOS) aims to assess the effects of canakinumab, a monoclonal antibody which neutralizes IL-1β, in patients after acute myocardial infarction[70]. In addition, the randomized controlled MRC-ILA-HEART study will address short-term use of anakinra, an IL-1 receptor antagonist, in patients presenting with myocardial infarction[71].

Interleukin-6 inhibitors

As discussed in the previous section, recent human genetic studies provided strong evidence for a causal role of IL-6 signaling in coronary heart disease. This suggests that targeting of the IL-6 receptor (IL-6R) might be a promising therapeutic approach to prevent coronary heart disease[17,18]. Tocilizumab is a monoclonal antibody blocking IL-6R and currently solely licensed for treatment of RA[72]. The potential adverse effects of tocilizumab on lipid profiles, however, need further attention prior to embarking on a full phase III trial with this compound in cardiovascular disease[73].

CCR2 antagonist

Monocyte recruitment via MCP-1 and CCR2 is an important step in early lesions, and as such considered a therapeutic target[7]. MLN1202 is a monoclonal antibody directed against CCR2. In a phase II trial, it was demonstrated that MLN1202 significantly reduced high-sensitivity CRP levels in patients at risk for atherosclerotic disease[74]. To date, however, no trials has been initiated to determine whether this approach will reduce cardiovascular event rates.

Selective phospholipase A2 inhibitors

Family members of phospholipase A2 (PLA2) can modify phospholipids and generate atherogenic pro-inflammatory lipid moieties. As such, PLA2 inhibition is considered a potential strategy in atherosclerosis[75]. Currently, two family members are in clinical drug development for atherosclerosis; secretory PLA2 (sPLA2) and lipoprotein-associated PLA2 (Lp-PLA2)[76,77]. With respect to the first, a phase II trial in patients in stable coronary heart disease suggested that sPLA2 inhibition was anti-inflammatory via an enhanced LDL clearance[78]. Unfortunately, the succeeding phase III trial with varespladib was discontinued in March this year; the sPLA2 inhibitor failed to show efficacy in patients following an acute event[79,80]. The alternative Lp-PLA2 inhibitor, darapladib, reduced levels of IL-6 and CRP in a phase II trial in patients with stable coronary heart disease[81]. At present, darapladib is being evaluated in two phase III trials on cardiovascular outcome; (i) the STABILITY trial in patients with chronic coronary heart disease in addition to existing standard care[82] and (ii) the SOLID-TIMI 52 study in patients after an acute coronary event[83].

Leukotrienes inhibition

Leukotrienes are (arachidonic acid-derived lipid) mediators of inflammation, promoting the accumulation and pro-inflammatory function of leucocytes at the site of inflammation[84]. 5-Lipoxygenase (5-LO) and 5-LO-activating protein (FLAP) are important factors in the formation of leukotrienes[84], and can be therapeutically targeted. The most prominent 5-LO inhibitor, VIA-2291, reduced leukotriene production in patients with coronary heart disease. Also, preliminary data from an imaging sub-study suggested that this effect also reduced atherosclerosis[85]. Meanwhile, an inhibitor of FLAP, DG-031, led to significant and dose-dependent reduction of inflammatory biomarkers in patients with specific at-risk variants of 2 genes in the leukotriene pathway[86]. Today, no phase III trial for these targets has been initiated.

Better targeting

Anti-inflammatory strategies hold promise for future therapeutics in atherosclerosis, however, systemic and long-term administration of immunosuppressive drugs may prove to be complicated by severe side effects, amongst which opportunistic infections[51]. More selective

and targeted approaches are warranted to overcome these potential side effects whilst maintaining efficacy. Whereas, until recently, interest in nanotechnology was precluded to oncology, it has now also gained attention in cardiovascular disease. Nanoparticles can be produced in various sizes and shapes, and fueled with specific contents or drugs,; all together making it an appealing novelty for both drug development as well as imaging[87].

Previous successful applications of nanotechnology comprise Ambisome and Doxil[88,89]. These nanodrugs have shown a retained or even augmented efficacy on infection and tumor, respectively, with a clear reduction of systemic side effects. A more recent example of a potential nanomedicine application in atherosclerosis is liposomal nanoparticles loaded with prednisolone phosphate (LN-PLP). In rabbits, LN-PLP was found to accumulate atherosclerotic lesions and rapidly reduce arterial wall inflammation[90,91]. At present, a phase II trial is ongoing to further explore the concept of local delivery and efficacy of LN-PLP in patients with advanced atherosclerotic lesions[92].

FUTURE PERSPECTIVE

Since atherosclerosis is an inflammatory disease, anti-inflammatory therapies bear potential in future cardiovascular management. Atherosclerosis is, however, a chronic disease and systemic long-term use of anti-inflammatory compounds carries the risk of complications arising from immunosuppression. In order to successfully manage this drawback, several issues need further delineation. First, we need to identify who is at risk and can be considered suitable for anti-inflammatory interventions, by refining our understanding of inflammatory cellular and imaging biomarkers. Second, we are in desperate need of a detailed understanding of essential inflammatory processes in atherosclerosis, to allow for the selection of the safest and most efficacious inflammatory targets. Third and last, we should strive for drug delivery to the target organ – the atherosclerotic plaque – or even the target cell such as plaque macrophages. Such advances will pave the way for selective and prolonged use of anti-inflammatory agents in cardiovascular disease management.

REFERENCES

1. Ross R. Atherosclerosis: an inflammatory disease. N Engl J Med 1999;340:115-126.
2. Libby P et al. Progress and challenges in translating the biology of atherosclerosis. Nature 2011;473:317-325.
3. Swirski FK et al. The ins and outs of inflammatory cells in atheromata. Cell Metab 2012;15:135-136.
4. Libby P. Vascular biology of atherosclerosis: overview and state of the art. Am J Cardiol 2003;91:3A-6A.
5. Cybulsky MI et al. A major role for VCAM-1, but not ICAM-1, in early atherosclerosis. J Clin Invest 2001;107:1255-1262.
6. Gu L et al. Absence of monocyte chemoattractant protein-1 reduces atherosclerosis in low density lipoprotein receptor-deficient mice. Mol Cell 1998;2:275-281.
7. Boring L et al. Decreased lesion formation in CCR2-/- mice reveals a role for chemokines in the initiation of atherosclerosis. Nature 1998;394:894-897.
8. Peters W and Charo IF. Involvement of chemokine receptor 2 and its ligand, monocyte chemoattractant protein-1, in the development of atherosclerosis: lessons from knockout mice. Curr Opin Lipidol 2001;12:175-180.
9. Qiao JH et al. Role of macrophage colony-stimulating factor in atherosclerosis: studies of osteopetrotic mice. Am J Pathol 1997;150:1687-1699.
10. Bernhagen J et al. MIF is a noncognate ligand of CXC chemokine receptors in inflammatory and atherogenic cell recruitment. Nat Med 2007;13:587-596.
11. Gilstrap LG and Wang TJ. Biomarkers and cardiovascular risk assessment for primary prevention: an update. Clin Chem 2012;58:72-82.
12. Ridker PM et al. Rosuvastatin to prevent vascular events in men and women with elevated C-reactive protein. N Engl J Med 2008;359:2195-2207.
13. Khera A et al. Relationship between C-reactive protein and subclinical atherosclerosis: the Dallas Heart Study. Circulation 2006;113:38-43.
14. Wensley F et al. Association between C reactive protein and coronary heart disease: mendelian randomisation analysis based on individual participant data. BMJ 2011;342:548.
15. Danesh J et al. Long-term interleukin-6 levels and subsequent risk of coronary heart disease: two new prospective studies and a systematic review. PLoS Med 2008;5:e78.
16. Ridker PM et al. Plasma concentration of interleukin-6 and the risk of future myocardial infarction among apparently healthy men. Circulation 2000;101:1767-1772.
17. Sarwar N et al. Interleukin-6 receptor pathways in coronary heart disease: a collaborative meta-analysis of 82 studies. Lancet 2012;379:1205-1213.
18. Hingorani AD and Casas JP. The interleukin-6 receptor as a target for prevention of coronary heart disease: a mendelian randomisation analysis. Lancet 2012;379:1214-1224.
19. Gurevich VS et al. Autoimmune nature of influenza atherogenicity. Ann N Y Acad Sci 2005;1050:410-416.
20. Smeeth L et al. Risk of myocardial infarction and stroke after acute infection or vaccination. N Engl J Med 2004;351:2611-2618.
21. van Leuven SI et al. Atherogenesis in rheumatology. Lupus 2006;15:117-121.
22. Sattar N et al. Explaining how "high-grade" systemic inflammation accelerates vascular risk in rheumatoid arthritis. Circulation 2003;108:2957-2963.
23. Wallberg-Jonsson S et al. Cardiovascular morbidity and mortality in patients with seropositive rheumatoid arthritis in Northern Sweden. J Rheumatol 1997;24:445-451.
24. Maradit-Kremers H et al. Increased unrecognized coronary heart disease and sudden deaths in rheumatoid arthritis: a population-based cohort study. Arthritis Rheum 2005;52:402-411.
25. van Leuven SI et al. Mycophenolate mofetil but not atorvastatin attenuates atherosclerosis in lupus-prone LDLr(-/-) mice. Ann Rheum Dis 2012;71:408-414.
26. Li L et al. Porphyromonas gingivalis infection accelerates the progression of atherosclerosis in a heterozygous apolipoprotein E-deficient murine model. Circulation 2002;105:861-867.
27. Westerterp M et al. Apolipoprotein C-I is crucially involved in lipopolysaccharide-induced atherosclerosis development in apolipoprotein E-knockout mice. Circulation 2007;116:2173-2181.

28. Alber DG et al. Herpesvirus infection accelerates atherosclerosis in the apolipoprotein E-deficient mouse. Circulation 2000;102:779-785.
29. van Halm VP et al. Disease-modifying antirheumatic drugs are associated with a reduced risk for cardiovascular disease in patients with rheumatoid arthritis: a case control study. Arthritis Res Ther 2006;8:R151.
30. Micha R et al. Systematic review and meta-analysis of methotrexate use and risk of cardiovascular disease. Am J Cardiol 2011;108:1362-1370.
31. Kleemann R et al. Cytokines and atherosclerosis: a comprehensive review of studies in mice. Cardiovasc Res 2008;79:360-376.
32. Ley K et al. Monocyte and macrophage dynamics during atherogenesis. Arterioscler Thromb Vasc Biol 2011;31:1506-1516.
33. Hansson GK and Libby P. The immune response in atherosclerosis: a double-edged sword. Nat Rev Immunol 2006;6:508-519.
34. Davignon J. Beneficial cardiovascular pleiotropic effects of statins. Circulation 2004;109:III39-III43.
35. Aikawa M et al. An HMG-CoA reductase inhibitor, cerivastatin, suppresses growth of macrophages expressing matrix metalloproteinases and tissue factor in vivo and in vitro. Circulation 2001;103:276-283.
36. Zapolska-Downar D et al. Simvastatin modulates TNFalpha-induced adhesion molecules expression in human endothelial cells. Life Sci 2004;75:1287-1302.
37. Ridker PM et al. Relation of baseline high-sensitivity C-reactive protein level to cardiovascular outcomes with rosuvastatin in JUPITER. Am J Cardiol 2010;106:204-209.
38. McCarey DW et al. Trial of Atorvastatin in Rheumatoid Arthritis (TARA). Lancet 2004;363:2015-2021.
39. Robinson JG et al. Pleiotropic effects of statins: benefit beyond cholesterol reduction? J Am Coll Cardiol 2005;46:1855-1862.
40. Barter PJ and Rye KA. Cholesteryl ester transfer protein (CETP) inhibition as a strategy to reduce cardiovascular risk. J Lipid Res 2012;53:1755–1766.
41. Birjmohun RS al. High-density lipoprotein attenuates inflammation and coagulation response on endotoxin challenge in humans. Arterioscler Thromb Vasc Biol 2007;27:1153-1158.
42. Fayad ZA et al. Safety and efficacy of dalcetrapib on atherosclerotic disease using novel non-invasive multimodality imaging (dal-PLAQUE). Lancet):1547-1559.
43. Barter PJ et al. Effects of torcetrapib in patients at high risk for coronary events. N Engl J Med 2007;357:2109-2122.
44. Tardif JC et al. Effects of reconstituted high-density lipoprotein infusions on coronary atherosclerosis: a randomized controlled trial. JAMA 2007;297:1675-1682.
45. Furst DE et al. Updated consensus statement on biological agents for the treatment of rheumatic diseases, 2011. Ann Rheum Dis 2012;71:i2-45.
46. van Leuven SI et al. Mycophenolate mofetil attenuates plaque inflammation in patients with symptomatic carotid artery stenosis. Atherosclerosis 2010;211:231-236.
47. Choi HK et al. Methotrexate and mortality in patients with rheumatoid arthritis: a prospective study. Lancet 2002;359:1173-1177.
48. Ridker PM. Testing the inflammatory hypothesis of atherothrombosis: scientific rationale for the CIRT. J Thromb Haemost 2009:332-339.
49. Karampetsou MP et al. TNF-alpha antagonists beyond approved indications: stories of success and prospects for the future. QJM 2010;103:917-928.
50. Chung ES et al. Randomized, double-blind, placebo-controlled, pilot trial of infliximab, a chimeric monoclonal antibody to tumor necrosis factor-alpha, in patients with moderate-to-severe heart failure. Circulation 2003;107:3133-3140.
51. Riminton DS et al. Managing the risks of immunosuppression. Curr Opin Neurol 2011;24:217-223.
52. Tardif JC et al. Vascular biomarkers and surrogates in cardiovascular disease. Circulation 2006;113:2936-2942.
53. Owen DR et al. Imaging of atherosclerosis. Annu Rev Med 2011;62:25-40.
54. Camici PG et al. Non-invasive anatomic and functional imaging of vascular inflammation and unstable plaque. Eur Heart J 2012;33:1309-1317.
55. Duivenvoorden R et al. Comparison of in vivo carotid 3.0-T magnetic resonance to B-mode ultrasound imaging and histology in a porcine model. JACC Cardiovasc Imaging 2009;2:744-750.
56. Duivenvoorden R et al. In vivo quantification of carotid artery wall dimensions: 3.0-Tesla MRI versus B-mode ultrasound imaging. Circ Cardiovasc Imaging 2009;2:235-242.

57. Li F et al. Scan-rescan reproducibility of carotid atherosclerotic plaque morphology and tissue composition measurements using multicontrast MRI at 3T. J Magn Reson Imaging 2010;31:168-176.
58. Calcagno C et al. Dynamic contrast enhanced (DCE) magnetic resonance imaging (MRI) of atherosclerotic plaque angiogenesis. Angiogenesis 2010;13:87-99.
59. Takaya N et al. Intra- and interreader reproducibility of magnetic resonance imaging for quantifying the lipid-rich necrotic core is improved with gadolinium contrast enhancement. J Magn Reson Imaging 2006;24:203-210.
60. Kumamoto M et al. Intimal neovascularization in human coronary atherosclerosis: its origin and pathophysiological significance. Hum Pathol 1995;26:450-456.
61. Rudd JH et al. Atherosclerosis inflammation imaging with 18F-FDG PET: carotid, iliac, and femoral uptake reproducibility, quantification methods, and recommendations. J Nucl Med 2008;49:871-878.
62. Tawakol A et al. In vivo 18fluorodeoxyglucose positron emission tomography imaging provides a noninvasive measure of carotid plaque inflammation in patients. J Am Coll Cardiol 2006;48:1818-1824.
63. Pedersen SF et al. Gene expression and 18FDG uptake in atherosclerotic carotid plaques. Nucl Med Commun 2010;31:423-429.
64. Marnane M et al. Carotid plaque inflammation on (18)fluorodeoxyglucose positron emission tomography predicts early stroke recurrence. Ann Neurol 2012;71:709-718.
65. Lindsay AC and Choudhury RP. Form to function: current and future roles for atherosclerosis imaging in drug development. Nat Rev Drug Discov 2008;7:517-529.
66. Cannon CP et al. Intensive versus moderate lipid lowering with statins after acute coronary syndromes. N Engl J Med 2004;350:1495-1504.
67. Abbate A et al. Blocking Interleukin-1 as a Novel Therapeutic Strategy for Secondary Prevention of Cardiovascular Events. BioDrugs 2012;26:217–233.
68. Galea J et al. Interleukin-1 beta in coronary arteries of patients with ischemic heart disease. Arterioscler Thromb Vasc Biol 1996;16:1000-1006.
69. Kastrati A et al. Protective role against restenosis from an interleukin-1 receptor antagonist gene polymorphism in patients treated with coronary stenting. J Am Coll Cardiol 2000;36:2168-2173.
70. Ridker PM et al. Interleukin-1beta inhibition and the prevention of recurrent cardiovascular events: rationale and design of CANTOS. Am Heart J 2011;162:597-605.
71. Crossman DC et al. Investigation of the effect of Interleukin-1 receptor antagonist (IL-1ra) on markers of inflammation in non-ST elevation acute coronary syndromes. Trials 2008;9:8.
72. Yabe Y et al. A review of tocilizumab treatment in 122 rheumatoid arthritis patients included in the Tsurumai Biologics Communication Registry Study. Mod Rheumatol 2012;379:1176–1178.
73. Boekholdt SM and Stroes ES. The interleukin-6 pathway and atherosclerosis. Lancet 2012;379:1176-1178.
74. Gilbert J et al. Effect of CC chemokine receptor 2 CCR2 blockade on serum C-reactive protein in individuals at atherosclerotic risk and with a single nucleotide polymorphism of the monocyte chemoattractant protein-1 promoter region. Am J Cardiol 2011;107:906-911.
75. Corson MA. Phospholipase A2 inhibitors in atherosclerosis: the race is on. Lancet 2009;373:608-610.
76. Thompson A et al. Lipoprotein-associated phospholipase A(2) and risk of coronary disease, stroke, and mortality: collaborative analysis of 32 prospective studies. Lancet 2010;375:1536-1544.
77. Mallat Z et al. Circulating secretory phospholipase A2 activity predicts recurrent events in patients with severe acute coronary syndromes. J Am Coll Cardiol 2005;46:1249-1257.
78. Rosenson RS et al. Effects of 1-H-indole-3-glyoxamide (A-002) on concentration of secretory phospholipase A2. Lancet 2009;373:649-658.
79. Nicholls SJ et al. Inhibition of secretory phospholipase A(2) in patients with acute coronary syndromes: rationale and design of the vascular inflammation suppression to treat acute coronary syndrome for 16 weeks trial. Cardiovasc Drugs Ther 2012;26:71-75.
80. Website Anthera Pharmaceuticals; http://investor.anthera.com/releases.cfm. 2012.
81. Mohler ER et al. The effect of darapladib on plasma lipoprotein-associated phospholipase A2 activity and cardiovascular biomarkers in patients with stable coronary heart disease or coronary heart disease risk equivalent. J Am Coll Cardiol 2008;51:1632-1641.

82. Vedin O et al. Secondary prevention and risk factor target achievement in a global, high-risk population with established coronary heart disease: baseline results from the STABILITY study. Eur J Prev Cardiol Eur 2013;20:678-85
83. O'Donoghue ML et al. Study design and rationale for the Stabilization of pLaques usIng Darapladib-Thrombolysis in Myocardial Infarction trial in patients after an acute coronary syndrome. Am Heart J 2011;162:613-619.
84. Funk CD. Leukotriene inflammatory mediators meet their match. Sci Transl Med 2011;3:66ps3.
85. Tardif JC et al. Treatment with 5-lipoxygenase inhibitor VIA-2291 (Atreleuton) in patients with recent acute coronary syndrome. Circ Cardiovasc Imaging 2010;3:298-307.
86. Hakonarson H et al. Effects of a 5-lipoxygenase-activating protein inhibitor on biomarkers associated with risk of myocardial infarction: a randomized trial. JAMA 2005;293:2245-2256.
87. Lobatto ME et al. Perspectives and opportunities for nanomedicine in the management of atherosclerosis. Nat Rev Drug Discov 2011;10:835-852.
88. Jung SH et al. Amphotericin B-entrapping lipid nanoparticles and their in vitro and in vivo characteristics. Eur J Pharm Sci 2009;37:313-320.
89. Barenholz YC. Doxil - The first FDA-approved nano-drug: Lessons learned. J Control Release 2012;160:117-134.
90. Metselaar JM et al. Complete remission of experimental arthritis by joint targeting of glucocorticoids with long-circulating liposomes. Arthritis Rheum 2003;48:2059-2066.
91. Dams ET et al. Scintigraphic evaluation of experimental chronic osteomyelitis. J Nucl Med 2000;41:896-902.
92. Clinicaltrials.gov; silencing Inflammatory Activity by Injecting Nanocort in Patients at Risk for Atherosclerotic Disease (SILENCE) 2012; NCT01601106 2012.

CHAPTER 9

PREDNISOLONE-CONTAINING LIPOSOMES ACCUMULATE IN HUMAN ATHEROSCLEROTIC MACROPHAGES UPON INTRAVENOUS ADMINISTRATION

Van der Valk FM*, van Wijk DF*, Lobatto M, Verberne HJ, Storm G, Willems MCM, Legemate DA, Nederveen AJ, Calcagno C, Venkatesh M, Ramachandran S, Paridaans MPM, Otten MJ, Dallinga GM, Fayad ZA, Nieuwdorp M, Schulte DM, Metselaar JM, Mulder WJM, Stroes ESG.

* Authors contributed equally

Nanomedicine. 2015;11:1039-46

ABSTRACT

Rationale: Drug delivery to atherosclerotic plaques via liposomal nanoparticles may improve therapeutic agents' risk-benefit ratios. Our paper details the first clinical studies of a liposomal nanoparticle encapsulating prednisolone (LN-PLP) in atherosclerosis.

Methods and Results: First, PLP's liposomal encapsulation improved its pharmacokinetic profile in humans (n=13) as attested by an increased plasma half-life of 63 hours (LN-PLP 1.5 mg/kg). Second, intravenously infused LN-PLP appeared in 75% of the macrophages isolated from iliofemoral plaques of patients (n=14) referred for vascular surgery in a randomized, placebo-controlled trial. LN-PLP treatment did however not reduce arterial wall permeability or inflammation in patients with atherosclerotic disease (n=30), as assessed by multimodal imaging in a subsequent randomized, placebo-controlled study.

Conclusion: In conclusion, we successfully delivered a long-circulating nanoparticle to atherosclerotic plaque macrophages in patients, whereas prednisolone accumulation in atherosclerotic lesions had no anti-inflammatory effect. Nonetheless, the present study provides guidance for development and imaging-assisted evaluation of future nanomedicine in atherosclerosis.

INTRODUCTION

Because inflammation plays a pivotal role in atherosclerotic plaque development[1], novel anti-inflammatory strategies[2] are expected to complement and improve existing therapeutic regimens. Delivering drugs via nanocarriers may reduce atherosclerotic plaque inflammation by enhancing drug accumulation at target sites, without compromising immunity[3]. Though several liposomally formulated anticancer drugs have already been approved for clinical use[4], nanomedicine remains unexplored in patients with cardiovascular disease. Theoretically, an inflamed atherosclerotic plaque, characterized by endothelial dysfunction and a highly permeable microvasculature, could be an excellent target for nanomedicinal delivery[5].

Of the numerous clinically-applied anti-inflammatory compounds, glucocorticoids (GC) are the most widely used and have potent anti-inflammatory effects[6]. However, systemic GC treatment has not been used in patients with cardiovascular disease because long-term GC use has pro-atherogenic effects, including dyslipidemia, glucose intolerance and hypertension[7]. In contrast, locally administering GC via drug-eluting stents has been shown to reduce neo-intimal formation and arterial wall inflammation in an experimental model[8]. These results suggest a liposomal GC formulation may minimize systemic adverse effects while improving local anti-inflammatory efficacy. In support of this idea, we previously reported markedly reduced arterial wall inflammation following intravenous administration of liposomal prednisolone in an atherosclerotic rabbit model[9].

Here we evaluate the clinical applicability of a long-circulating liposomal nanoparticle encapsulating prednisolone phosphate (LN-PLP) in patients with atherosclerosis. First, we determined liposomal prednisolone's pharmacokinetic profile in humans and assessed delivery to plaque macrophages isolated from iliofemoral plaques of patients referred for vascular surgery. Subsequently, we used noninvasive multimodal imaging to measure the anti-inflammatory efficacy of LN-PLP in patients with atherosclerosis.

METHODS

Study participants

All participants provided written informed consent. The clinical trials were approved by the local institutional review board and conducted according to the principles of the International Conference on Harmonisation–Good Clinical Practice guidelines (Clinicaltrials.gov registration NCT01039103, NCT01647685, NCT01601106).

Liposomal prednisolone

The liposomal nanoparticles (LN) were composed of a hydrophilic core encapsulating prednisolone phosphate (PLP), surrounded by a lipid bilayer of phospholipids and cholesterol, which was coated with polyethylene glycol (PEG). See supplementary methods for LN-PLP formulation.

Pharmacokinetic profile of LN-PLP in humans

We conducted a single-dose escalation study, using 13 subjects, to determine the pharmacokinetic performance of LN-PLP after a single intravenous (i.v.) dose of 0.375 mg/kg (n=3), 0.75 mg/kg (n=3) or 1.5 mg/kg (n=7) LN-PLP in a 2.5 hour time frame. Serum concentrations of PL and its pro-drug PLP were measured on days 1, 3, 7 and weekly up to 12 weeks using high-performance liquid chromatography. Safety evaluation after LN-PLP administration included documenting adverse events, checking vital signs and conducing safety laboratory tests.

LN-PLP delivery in patients with iliofemoral atherosclerosis

To study LN-PLP's delivery, we performed a randomized, placebo-controlled, double-blind trial in 14 patients with iliofemoral atherosclerotic plaques who were scheduled for endarterectomy. After 1:1 randomization, patients received either 1.5 mg/kg LN-PLP (n=7) or saline (n=7) via an antecubital vein on days 0 and 7, followed by vascular surgery on day 10. The dosing regimen for LN-PLP was based on a preclinical study in rabbits[9] and adjusted according to the drug-dose conversion from rabbit to human[10]. Plaque tissue macrophages were isolated to evaluate the presence of LN-PLP (see Supplementary methods). Cells were spotted on a glass slide using a cytospin centrifuge, fixed with 0.4% paraformaldehyde (30min), permeabilized with 0.1% Triton X-100 (10min) and stained overnight. Primary antibodies were mouse anti-human CD68 (Abcam, Cambridge, UK; 1:100) and rabbit anti-human PEG (Epitomics, Burlingame, CA, U.S.A.; 1:100), and secondary antibodies were CyTM3-conjugated donkey anti-mouse and FITC-conjugated donkey anti-rabbit (both Jackson, West Grove, PA, 1:200). Cells were examined with fluorescence microscopy (Leica, DMRA HC Upright). Per patient, at least 4 cell spin slides were used to examine the percentage of DAPI cells positive for CD68 (macrophages) and, DAPI/CD68 cells positive for PEG (LN-PLP). A reader who was blinded for treatment allocation performed these analyses.

Local efficacy in patients with atherosclerosis

Subsequently, we evaluated LN-PLP therapeutic efficacy in a randomized, placebo-controlled, double-blind trial of 30 patients with documented history of atherosclerotic cardiovascular disease (i.e. angina pectoris, myocardial infarction, TIA or stroke). Prospective participants

underwent ^{18}fluorodeoxyglucose positron emission tomography with computed tomography (^{18}F-FDG PET/CT) to identify patients with marked arterial wall inflammation (TBR_{max} > 2.2, measured in either the ascending aorta or carotid arteries). Based on this criterion, five (14%) of the 36 subjects screened were not included in the study. After enrolment, patients had dynamic contrast enhanced-magnetic resonance imaging (DCE-MRI) scans of their carotid arteries prior to treatment allocation. One of the remaining 31 patients dropped out due to claustrophobia during baseline MRI acquisition. After 2:1 randomization, patients received either LN-PLP 1.5 mg/kg (n=20) or saline (n=10) i.v. on days 0 and 7. On day 10, we assessed therapeutic efficacy by DCE-MRI and ^{18}F-FDG PET/CT imaging of both carotid arteries. A blinded, experienced reader analyzed the images at the core laboratory (TMII, Department of Radiology, Mount Sinai). Prior to analysis, the image set was assessed for quality, and standard operating procedures ensured that the same arterial segments, based on specified anatomical locations, would be analyzed by both PET/CT and (DCE)-MRI (see Supplementary methods).

Statistical analysis

Baseline values and distributional characteristics are shown as mean (SD), number (frequency) or median (min-max). Independent samples t-test, Mann-Whitney U test and Chi-square test were used to assess baseline differences between patients and controls. For efficacy analysis, Wilcoxon signed-rank test was used. A two-sided *P*-value below 0.05 was considered statistically significant. All data were analyzed using Prism version 5.0 (GraphPad software, La Jolla, CA, USA) and SPSS version 19.0 (SPSS Inc., Chicago, IL, USA).

RESULTS

Pharmacokinetic performance of LN-PLP in humans

Prior to investigating delivery and efficacy of LN-PLP in humans, we studied its PK profile in 13 subjects, 8 male and 5 female, with a mean age of 51 ± 10 years (Table 1). LN-PLP had a prolonged circulation half-life ($t_{½}$) ranging from 45 to 63 hours. The area-under-the-curve for LN-PLP indicated a dose-dependent relationship (from 856 ± 171, 1355 ± 352, to 4135 ± 1489 μg·h/mL for 0.375, 0.75 and 1.5 mg/kg LN-PLP, respectively). The peak plasma concentration of free PL was, on average, 0.5% of the total liposomal PLP plasma concentration and remained constant throughout the 28-day experimental period (Figure S1). This constancy indicates negligible encapsulated drug leakage from the liposome into circulation, since direct leakage would accelerate PLP plasma decay and increase the percentage of free PL. Table 1 provides an overview of PK data in humans. LN-PLP was well tolerated, and no serious adverse events occurred. Further, LN-PLP did not adversely affect cardiometabolic parameters, nor did it significantly change liver and/or kidney parameters (Table S1).

TABLE 1. Pharmacokinetic properties of LN-PLP in humans

Clinical characteristics	0.375 mg/kg (n = 3)	0.75 mg/kg (n = 3)	1.5 mg/kg (n = 7)
Age (years)	53 ± 12	44 ± 5	57 ± 12
Gender (male %)	2 (67)	2 (67)	4 (57)
PK parameters			
AUC (0-168h) (μg.ml.h^{-1})	856 ± 171	1355 ± 352	4135 ± 1489
t½ (hr)	45.0 ± 26.0	42.7 ± 12.8	62.5 ± 11.9
CL (L/hr)	0.041 ± 0.011	0.054 ± 0.016	0.031 ± 0.010
PL/PLP ratio	0.55	0.65	0.41

Data are shown as mean ± SD or number (%). *AUC indicates area under the concentration curve; t½, half-life; CL, plasma clearance; LN-PLP, liposomal prednisolone; PL/PLP ratio, proportion free prednisolone of total liposomal prednisolone phosphate; Vss, volume of distribution at steady state.*

Delivery of LN-PLP to plaque macrophages in patients

LN-PLP plaque delivery was evaluated in 14 patients, with a mean age of 70 ± 7 years, who were scheduled for endarterectomy due to symptomatic iliofemoral atherosclerosis. Patients were divided into two groups, one to receive LN-PLP and the other a placebo, with comparable clinical characteristics (Table 2). After surgery on day 10 post-treatment, macrophages were isolated from excised plaques and stained with DAPI (cell nuclei), CD68 (macrophages) and PEG (LN-PLP coating). In patients treated with LN-PLP, we observed a high degree of co-localization between PEG and macrophages (Figure 1A). We observed that 88% of DAPI positive cells isolated from plaques stained positive for the macrophage marker CD68, of which 77% was also positive for liposomal PEG. As expected, CD68 positive macrophages isolated from patients treated with saline did not stain positive for PEG (Figure 1B). This finding supports the feasibility of drug delivery to plaque macrophages in patients with atherosclerotic disease.

TABLE 2. Clinical characteristics of patients in the nanomedicine delivery study

Clinical characteristic	LN-PLP (n = 7)	Placebo (n = 7)
Age	67 ± 5.9	73 ± 7.8
Gender, male n (%)	7 (100%)	6 (86%)
BMI, kg/m2	27.3 ± 5.0	26.0 ± 5.2
SBP, mmHg	130 ± 8.0	136 ± 10.0
Lipid profile:		
TChol, mmol/L	4.4 ± 1.1	4.0 ± 1.0
LDL-c, mmol/L	2.3 ± 0.6	2.1 ± 0.5
HDL-c, mmol/L	1.1 ± 0.4	1.2 ± 0.4
TG, mmol/L	2.0 ± 1.1	2.1 ± 1.0

Data are shown as mean ± SD or number (%). *BMI indicates body mass index; HDL-c, high density lipid cholesterol; LDL-c, low density lipid cholesterol; LN-PLP, liposomal prednisolone; SBP, systolic blood pressure; TChol, total cholesterol; TG, triglycerides.*

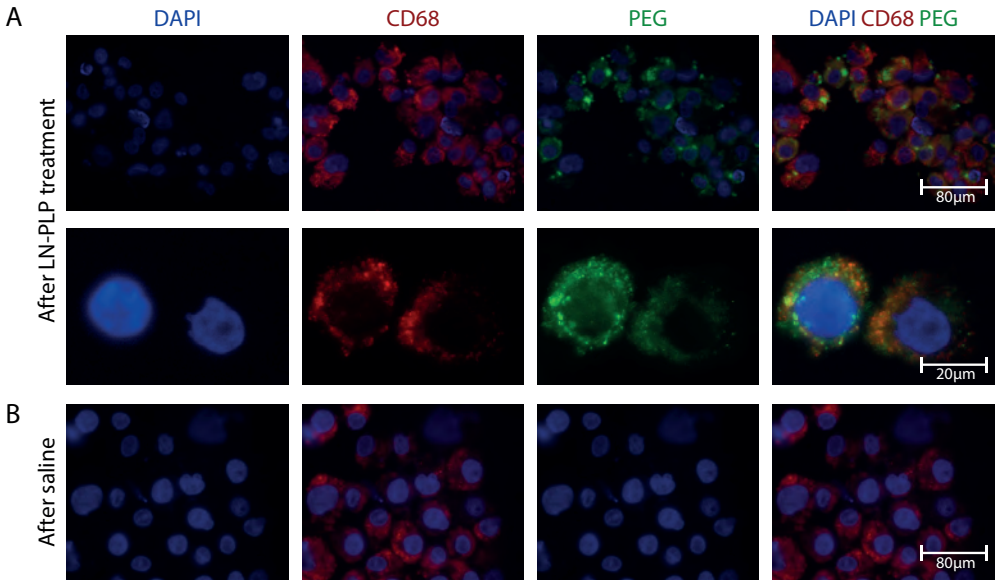

FIGURE 1. Local accumulation of LN-PLP in macrophages of iliofemoral plaques

(**A**) Microscopic images of cells isolated from a plaque of a patient treated with LN-PLP stained for cell nuclei (DAPI) and macrophages (CD68) and the liposome-coating PEG. Below, the enlargement of two cells corroborates the co-localization of CD68 cells and PEG. (**B**) Microscopic images illustrating that CD68 positive cells isolated from a plaque of a patient treated with saline do not show positivity for PEG. *LN-PLP indicates liposomal prednisolone, PEG, polyethylene glycol.*

LN-PLP efficacy in patients with atherosclerosis

Having established feasibility, our next step was to evaluate LN-PLP's therapeutic efficacy in patients with atherosclerotic disease. At baseline, the LN-PLP and saline treatment groups had similar clinical characteristics with the exception of higher systolic blood pressure in the saline group (Table 3). After two infusions of either LN-PLP (1.5 mg/kg) or saline, local efficacy was assessed with DCE-MRI and ^{18}F-FDG PET/CT. In contrast to the preclinical efficacy data[9], we did not observe a reduction in arterial wall permeability after LN-PLP treatment (Table 4). Illustrative pre- and post-treatment DCE-MRI overlay images are shown in Figure 2A and 2B. The non-model-based AUC remained unaltered after two LN-PLP infusions (for the left carotid artery, 0.1143 ± 0.0619 at baseline and 0.1294 ± 0.0686 after treatment, p=0.45). Accordingly, the kinetic parameter K^{trans} was not reduced by LN-PLP (for the left carotid artery, 0.1062 ± 0.0659 at baseline and 0.1259 ± 0.0651 after treatment, p=0.23). The lack of change in AUC and K^{trans} was also observed in the right carotid artery (Table 4). Figures 2 C-F illustrate the DCE-MRI parameters for the left and right carotid arteries in both the LN-PLP and saline groups.

TABLE 3. Clinical characteristics in the efficacy study

	LN-PLP (n = 20)	Placebo (n = 10)
Inclusion parameters		
TBR_{max} AA	2.80 ± 0.42	2.81 ± 0.42
TBR_{max} LCA	1.78 ± 0.31	1.83 ± 0.24
TBR_{max} RCA	1.87 ± 0.28	1.97 ± 0.22
Baseline characteristics		
Age	61 ± 7	59 ± 7
Gender, m (m %)	16 (80%)	8 (80%)
BMI, kg/m2	29.0 ± 4.5	28.4 ± 3.5
SBP, mmHg	130 ± 13 *	150 ± 13 *
Lipid profile		
Total cholesterol, mmol/L	5.86 ± 2.30	5.63 ± 1.71
LDL-c, mmol/L	3.96 ± 2.31	3.92 ± 1.53
HDL-c, mmol/L	1.33 ± 0.50	1.09 ± 0.45
TG, mmol/L	1.51 ± 1.10	1.56 ± 0.81

Data are shown as mean ± SD or number (%). * p<0.05. *AA indicates ascending aorta; BMI, body mass index; HDL-c, high density lipid cholesterol; LCA, left carotid artery; LDL-c, low density lipid cholesterol; LN-PLP, liposomal prednisolone; RCA, right carotid artery; SBP, systolic blood pressure; TG, triglycerides.*

In addition, we saw no reduction in arterial wall inflammation after LN-PLP treatment (Table 4). Figure 3A and 3B provide representative pre- and post-treatment CT and PET/CT images of a patient treated with LN-PLP. Treatment with LN-PLP resulted in a marginal 7% TBR_{max} increase in the left carotid artery (from 1.78 ± 0.31 at baseline to 1.90 ± 0.38 after treatment, p=0.03) versus no change in patients treated with placebo (from 1.82 ± 0.16 at baseline to 1.82 ± 0.24 after treatment, p=0.16; Figure 3C). Similarly, the TBR_{mean} increased 5% after LN-PLP infusions, whereas no change was observed in the saline treatment group (Figure 3E). The right carotid artery demonstrated corresponding measurements, as illustrated in Figures 3D and F. Patients tolerated LN-PLP well, with no observed changes in vital signs or lipid, inflammatory or safety markers (Table S2).

TABLE 4. DCE-MRI and PET/CT imaging at baseline and after treatment

		LN-PLP (n=20)			Placebo (n=10)		
		Pre	Post	P-value	Pre	Post	P-value
DCE-MRI							
Left carotid	AUC	0.1143±0.0619	0.1294 ± 0.0686	0.45	0.1103 ± 0.0472	0.1095 ± 0.0633	0.48
	K^{trans}	0.1062 ± 0.0659	0.1259 ± 0.0651	0.23	0.0904 ± 0.0323	0.1005 ± 0.0475	0.25
Right carotid	AUC	0.1061 ± 0.0712	0.1195 ± 0.0732	0.48	0.0821 ± 0.0455	0.0760 ± 0.0360	0.89
	K^{trans}	0.0929 ± 0.0673	0.1058 ± 0.0542	0.09	0.0798 ± 0.0613	0.0646 ± 0.0255	0.55
PET/CT							
Left carotid	TBR_{max}	1.78 ± 0.31	1.90± 0.38	*0.03*	1.82 ± 0.16	1.82 ± 0.24	0.16
	TBR_{mean}	1.43 ± 0.23	1.54± 0.29	*0.01*	1.42 ± 0.16	1.38 ± 0.14	0.39
Right carotid	TBR_{max}	1.87 ± 0.28	1.96± 0.38	*0.05*	1.86 ± 0.22	1.85 ± 0.20	0.07
	TBR_{mean}	1.51 ± 0.20	1.58± 0.26	*0.04*	1.57 ± 0.15	1.56 ± 0.17	0.86

Data are shown as mean ± SD. *AUC, indicates area under the curve; DCE-MRI, dynamic contrast enhanced-magnetic resonance imaging; LCA, left carotid artery; LN-PLP, liposomal prednisolone; PET/CT, positron emission tomography with computer tomography; RCA, right carotid artery; TBR, target to background ratio.*

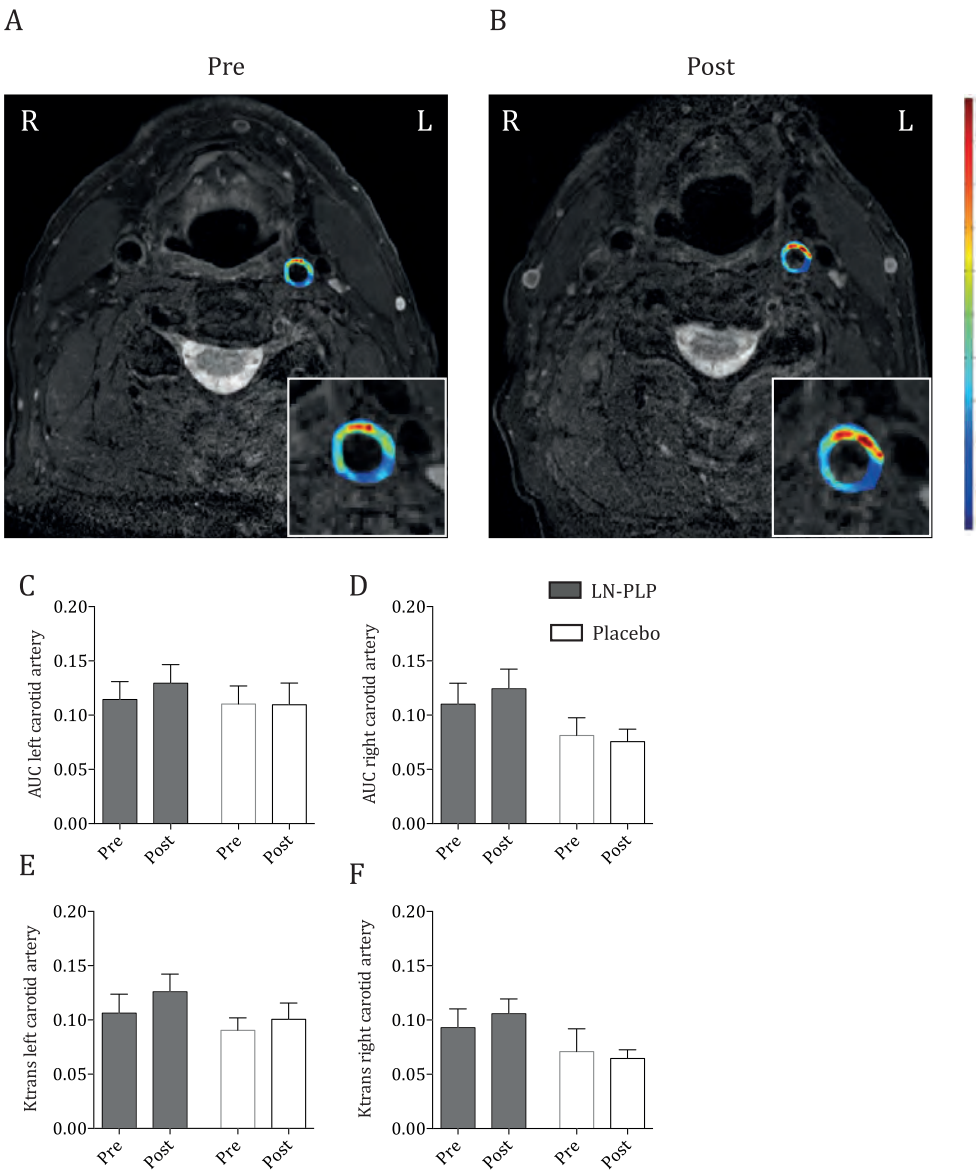

FIGURE 2. Arterial wall permeability after LN-PLP infusion in patients

(**A,B**) Representative axial T1-weighted MR images of the carotid arteries, the inset shows a magnification of the left carotid artery with a superimposed AUC map before and after LN-PLP treatment. (**C-F**) Bar graphs demonstrating the lack of reduction in AUC and K^{trans} for the left carotid artery (**C,D**) and right carotid artery (**E,F**) after LN-PLP (grey bars), compared with placebo (white bars). *AUC, indicates area under the curve; LN-PLP, liposomal prednisolone; MRI, magnetic resonance imaging.*

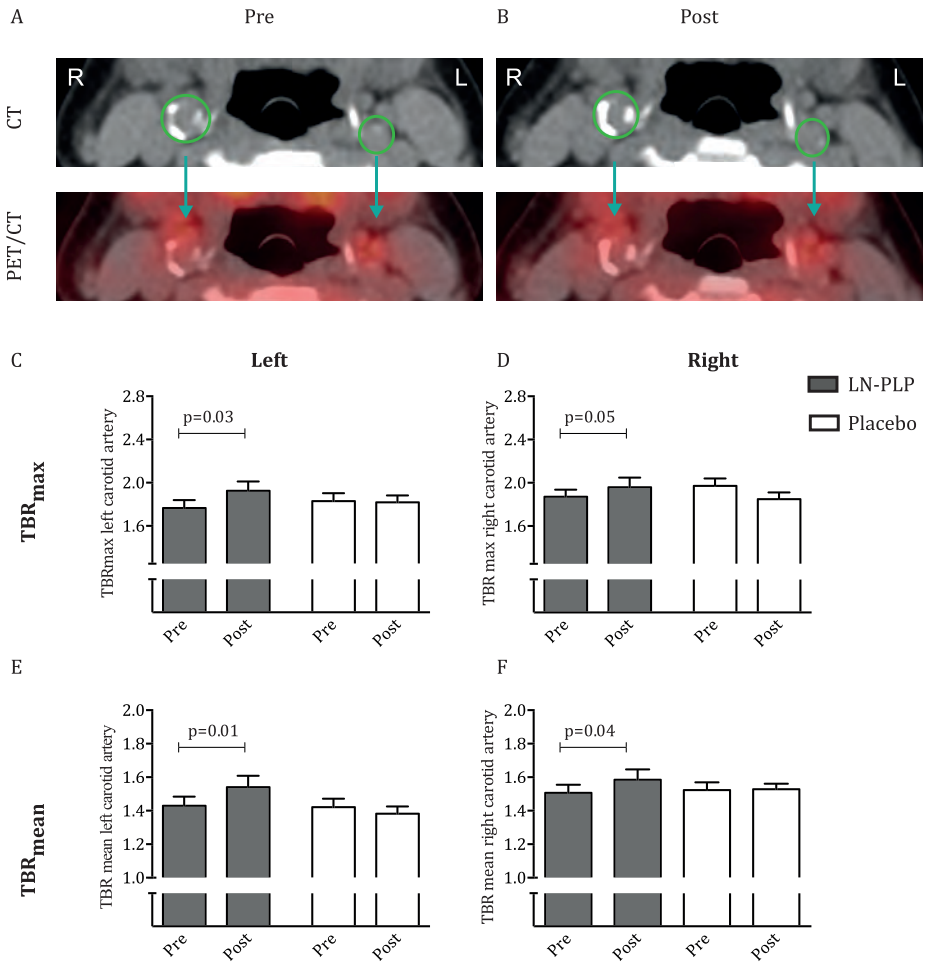

FIGURE 3. Arterial wall inflammation after LN-PLP infusion in patients

(**A,B**) Representative axial CT and PET/CT images of the carotid arteries before and after LN-PLP treatment, with region of interest shown in green. (**C-F**) Bar graphs showing the change in TBR_{max} and TBR_{mean} in the left carotid artery (**C,D**) and right carotid artery (**E,F**) after LN-PLP treatment (grey bars) or placebo (white bars). *CT indicates computed tomography; LN-PLP, liposomal prednisolone; PET, positron emission tomography; TBR, target to background ratio.*

DISCUSSION

Our present study aimed at exploring a liposomal nanoparticle loaded with prednisolone phosphate in the clinical frontier of atherosclerotic disease. First, we show the prolonged circulation half-life of prednisolone administered as a liposomal nanoparticle in humans, making this delivery approach potentially suitable for local delivery to atherosclerotic lesions. Indeed, we observed intravenously administered liposomal prednisolone to successfully

accumulate in macrophages isolated from atherosclerotic plaques of patients with symptomatic iliofemoral atherosclerosis. However, in atherosclerotic patients short-term LN-PLP treatment did not reduce arterial wall permeability or arterial wall inflammation, as assessed with multi-modal imaging. Despite the lack of anti-inflammatory efficacy, these data show, for the first time, that nanomedicinal delivery of drugs to atherosclerotic lesions is feasible in humans.

Although its applications have been explored primarily in oncology, nanomedicine is a promising therapeutic approach to cardiovascular disease[5]. Efficient delivery to atherosclerotic lesions requires preventing rapid nanoparticle removal from plasma, predominantly by the MPS. To block nanoparticle removal and allow nanoparticles to arrive at and accumulate in plaque, hydrophilic polymers, including PEG, are usually added to nanoparticle surfaces[3]. In the present study, packaging prednisolone phosphate in PEG-ylated liposomes markedly prolonged the drug's half-life to 45-63 hours in humans, which is 7 to 15-fold longer than for intravenously-administrated free prednisolone phosphate[6]. These PK features will theoretically facilitate LN-PLP delivery to atherosclerotic plaques.

Intravenously infusing LN-PLP into the antecubital vein 10 and 3 days prior to iliofemoral endarterectomy led to LN-PLP accumulation in plaque macrophages taken from patients with symptomatic iliofemoral atherosclerosis. LN accumulate in plaque macrophages through two possible routes. First, nanoparticles can potentially be taken up by splenic or circulating monocytes that subsequently migrate to the plaque. However, the PEG coating is designed to serve as a steric barrier that minimizes nanoparticle opsonization and uptake by phagocytic cells[12], thus suggesting little monocyte LN uptake. Nonetheless, if circulating LN may associate with circulating or splenic monocytes, they eventually migrate to areas of inflammation through a natural conduit[13], as has been demonstrated in mouse models of myocardial infarction and stroke[14]. Second, LN may extravasate due to atherosclerotic plaques' enhanced permeability, since the endothelial lining covering the atherosclerotic lesion is largely dysfunctional[15]. In addition, plaque's hypoxia-induced expansion of the vaso vasorum results in leaky neovessels with poor endothelial cell junctions[16,17]. This type of increased microvessel permeability has been shown to enhance local extravasation of long-circulating nanoparticles in cancer[18]. Thus, the increased permeability at the luminal and/or adventitial side allows for long-circulating nanoparticles to extravasate, resulting in accumulation of the LN within the subendothelial space and eventually phagocytosis by plaque macrophages. A limitation of the trial design is that we show accumulation in the iliofemoral segment but not in other atherosclerotic areas, such as the carotid arteries. This was dictated by the availability of and access to human material of patients that were allowed to enroll by the IRB. Future human studies using non-invasively traceable LN could provide more quantitative insight in LN accumulation in different anatomical locations.

Whereas previously LN-PLP showed to reduce inflammation in atherosclerotic lesions in rabbits[9], LN-PLP treatment did not induce measurable anti-inflammatory effects in the atherosclerotic artery wall in patients The discrepancy in therapeutic efficacy between the preclinical rabbit

study and human trial may have several explanations.

First, it may have resulted from an insufficient dose of prednisolone reaching the plaque. Unfortunately, the present study does not allow for quantitative assessment of the concentration of prednisolone delivered to the plaque. In contrast to the previously reported 4-10% accumulation rate of intravenously infused liposomal agents in tumors[19], accumulation in widely-spread plaques may not have been sufficient to exert a potent anti-inflammatory effect. While increasing the LN-PLP dose will likely resolve this issue, upping the dosage may introduce the risk of adverse effects caused by high intracellular GC concentrations. For instance, GC have been shown to polarize macrophages towards a phenotype with a higher propensity towards lipid accumulation[20,21], which may increase ER-stress and eventually lead to macrophage apoptosis in the plaque[22]. Moreover, GC-induced upregulation of 11β-hydroxysteroid dehydrogenase type 1 (11β-HSD1) in plaque macrophages can increase intracellular accumulation of pro-inflammatory GC[23,24]. These inadvertent negative consequences of GC imply that, prior to increasing LN-PLP doses in patients, we should clarify intracellular GC's impact on macrophages in the lipid-rich plaque environment.

A second reason for the lack of reduced inflammation in humans may relate to a timing issue: the trial may have been too short to detect anti-inflammatory effects. Most studies evaluating the impact of anti-inflammatory agents in human cardiovascular disease showed therapeutic efficacy only after 12 weeks of treatment, whereas our study evaluated results after only 10 days, based on the rapid reduction in arterial wall inflammation following LN-PLP treatment in atherosclerotic rabbits. The fact that we observed an increase in arterial wall ^{18}F-FDG uptake in patients, however, favors other factors than time contributing to the discrepant findings between rabbits and patients. In this respect, the pathobiology of rabbit and human atherosclerosis has marked differences. Atherosclerotic lesions in rabbits are induced in weeks following an acute injury response, whereas patients develop atherosclerotic plaques over the course of many decades. As a consequence, human atherosclerosis is characterized by complex plaques with a high lipid burden and a chronic low-grade inflammatory response. The observed differential therapeutic result between experimental and clinical atherosclerosis in the present study implies that the responsiveness of an acute injury reaction in the atherosclerotic rabbit model may not translate to anti-inflammatory compounds' efficacy in patients with advanced atherosclerosis.

Finally, the liposomal carrier may have had an adverse effect independent of the compound present inside the carrier, thereby masking a potential beneficial result. This scenario seems less likely, since the LN used in our study are composed of saturated phospholipids that are inherently resistant to oxidation or pro-inflammatory effects[25-28]. In accordance with our outcomes, other phase II/III studies using PEG-ylated compounds in humans have not reported pro-inflammatory effects[27-29]. Indeed, it has been suggested that empty liposomes can regress atherosclerosis, since such particles can act as high-capacity, low-affinity acceptors of intracellular cholesterol[30,31].

Nanomedicine-based delivery represents a new paradigm in the treatment of atherosclerotic disease[5,32]. In a first-in-human anti-atherosclerosis nanotherapy trial we demonstrated that long-circulating liposomal nanoparticles accumulate in plaque macrophages of patients. This phenomenon likely also holds true for other long-circulating nanoparticle platforms, such as micellar[33] or polymeric nanoparticles[34]. Future efforts should be aimed at the non-invasive and quantitative assessment of nanoparticle plaque targeting by imaging. This will also enable studying cardiovascular patients' heterogeneity in plaque permeability, and consequently the ability of nanoparticles to accumulate in plaques. Existing experience in rheumatoid arthritis patients with the current LN-PLP nanotherapy allowed us to accelerate its translation into cardiovascular disease. However, the GC drug payload may not have been ideal for atherosclerotic disease. Therefore, to further develop cardiovascular nanomedicine, an important focus should be on identifying suitable drug candidates for targeted treatment of human atherosclerotic plaques with a complex inflammatory, lipid-rich micro milieu.

In conclusion, we present evidence of local delivery of intravenously administered LN-PLP into macrophages isolated from human atherosclerotic plaques. In patients with atherosclerosis, however, short-term LN-PLP administration did not achieve a significant anti-inflammatory effect in atherosclerotic lesions. Nonetheless, we emphasize the potential of nanomedicine as a novel treatment paradigm for patients with atherosclerotic disease. Our work may serve as a guide for both the development as well as efficacy readout of future anti-atherosclerotic nanotherapies using imaging-assisted efficacy measures in relatively small-scaled studies.

Disclosures and funding: This work was supported by a European Framework Program 7 grant (ESS, GS: FP7-Health 309820: Nano-Athero); the Dutch network for Nanotechnology NanoNext NL, in the subprogram "Drug Delivery"; the National Heart, Lung, and Blood Institute, National Institutes of Health, as a Program of Excellence in Nanotechnology (PEN) Award, Contract #HHSN268201000045C (Z.A.F.); and NIH grants R01 HL118440 (W.J.M.M.), R01 HL125703 (W.J.M.M.), R01 EB009638 (Z.A.F.), andNWOVidi 91713324 (W.J.M.M.). Additionally, this work was supported by a grant from Enceladus Pharmaceuticals (Amsterdam, The Netherlands). M.E.L was partially supported by the International Atherosclerosis Society (USA) and by the Foundation "De Drie Lichten" (The Netherlands). J.M.M. is affiliated with the company Enceladus Pharmaceuticals (Amsterdam, The Netherlands), and G.S. is an advisor for the company Enceladus Pharmaceuticals (Amsterdam, The Netherlands). These other authors declare that they have no competing interests. All other authors declare that they have no conflict of interest and no relationships with industry relevant to this study.

REFERENCES

1. Libby P et al. Progress and challenges in translating the biology of atherosclerosis. Nature 2011:473;317–25.
2. Van der Valk FM et al. Novel anti-inflammatory strategies in atherosclerosis. Curr Opin Lipidol 2012:23;532–9.
3. Wagner, V et al. The emerging nanomedicine landscape. Nat Biotechnol 2006:24;1211–7.
4. Zhang L et al. Nanoparticles in Medicine : Therapeutic Applications and Developments. Transl Med 2008:83;761–769.
5. Lobatto ME et al. Perspectives and opportunities for nanomedicine in the management of atherosclerosis. Nat Rev Drug Discov 2011:10;835–52.
6. Czock D et al. Pharmacokinetics and pharmacodynamics of systemically administered glucocorticoids. Clin Pharmacokinet 2005:44;61–98.
7. Wei L. Taking Glucocorticoids by Prescription Is Associated with Subsequent Cardiovascular Disease. Ann Intern Med 2004:141;764.
8. Wang L et al. Stent-mediated methylprednisolone delivery reduces macrophage contents and in-stent neointimal formation. Coron Artery Dis 2005:16;237–43.
9. Lobatto ME et al. Multimodal Clinical Imaging To Longitudinally Assess a Nanomedical Anti-Inflammatory Treatment in Experimental Atherosclerosis. Mol Pharm 2010:7;2020–2029.
10. Reagan-Shaw S et al. Dose translation from animal to human studies revisited. FASEB J 2008:22;659–61.
11. Allen TM and Cullis PR. Drug delivery systems: entering the mainstream. Science 2004:303;1818–22.
12. Hak S et al. The effect of nanoparticle polyethylene glycol surface density on ligand-directed tumor targeting studied in vivo by dual modality imaging. ACS Nano 2012:6;5648–58.
13. Swirski FK and Nahrendorf M. Leukocyte behavior in atherosclerosis, myocardial infarction, and heart failure. Science 2013:339;161–6.
14. Flögel U et al. In vivo monitoring of inflammation after cardiac and cerebral ischemia by fluorine magnetic resonance imaging. Circulation 2008:118;140–8.
15. Davignon J and Ganz P. Role of endothelial dysfunction in atherosclerosis. Circulation 2004:109;III27–32.
16. Virmani R et al. Atherosclerotic plaque progression and vulnerability to rupture: angiogenesis as a source of intraplaque hemorrhage. Arterioscler Thromb Vasc Biol 2005:25;2054–61.
17. Ritman EL and Lerman A. The dynamic vasa vasorum. Cardiovasc Res 2007:75;649–58.
18. Lammers T et al. Drug targeting to tumors: principles, pitfalls and (pre-) clinical progress. J Control Release 2012:161;175–87.
19. Bartlett D et al. Impact of tumor-specific targeting on the biodistribution and efficacy of siRNA nanoparticles measured by multimodality in vivo imaging. Proc Natl Acad Sci U S A 2007:104;15549–54.
20. Liew YY et al. Effect of rapamycin and prednisolone in differentiated THP-1 and U937 cells. Transplant Proc 2002:34;2872–3.
21. Hu W et al. Statins synergize dexamethasone-induced adipocyte fatty acid binding protein expression in macrophages. Atherosclerosis 2012:222;434–43.
22. Spann NJ et al. Regulated accumulation of desmosterol integrates macrophage lipid metabolism and inflammatory responses. Cell 2012:151;138–52.
23. Luo MJ et al. 11 β-HSD1 inhibition reduces atherosclerosis in mice by altering pro-inflammatory gene expression in the vasculature. Physiol Genomics 2012:7;47:57.
24. Hadoke PWF et al. Modulation of 11β-hydroxysteroid dehydrogenase as a strategy to reduce vascular inflammation. Curr Atheroscler Rep 2013:15;320.
25. Alipour M et al. Safety and pharmacokinetic studies of liposomal antioxidant formulations containing N-acetylcysteine, α-tocopherol or γ-tocopherol in beagle dogs. Toxicol Mech Methods 2013:23;419–31.
26. Mamidi RN et al. Pharmacokinetics, efficacy and toxicity of different pegylated liposomal doxorubicin formulations in preclinical models. Cancer Chemother Pharmacol 2010:66;1173–84.
27. Musacchio T and Torchilin VP. Recent developments in lipid-based pharmaceutical nanocarriers. Front Biosc 2011:16;1388–412.

28. Torchilin VP. Recent advances with liposomes as pharmaceutical carriers. Nat Rev Drug Discov 2005:4;145–60.
29. Metselaar JM et al. Liposomal targeting of glucocorticoids to synovial lining cells strongly increases therapeutic benefit in collagen type II arthritis. Ann Rheum Dis 2004:63;348–353.
30. Dass CR and Jessup W. Apolipoprotein A-I, Cyclodextrins and Liposomes as Potential Drugs for the Reversal of Atherosclerosis. A Review. J Pharm Pharmacol 2000:52;731–761.
31. Rodrigueza WV et al. Cholesterol mobilization and regression of atheroma in cholesterol-fed rabbits induced by large unilamellar vesicles. Biochim Biophys Acta - Biomembr 1998:1368;306–320.
32. Mulder WJM et al. Imaging and nanomedicine in inflammatory atherosclerosis. Sci Transl Med 2014:6;239.
33. Torchilin VP. Micellar nanocarriers: pharmaceutical perspectives. Pharm Res 2007:24;1–16.
34. Pridgen EM et al. Biodegradable, polymeric nanoparticle delivery systems for cancer therapy. Nanomedicine 2007:2;669–80.

SUPPLEMENT

Formulation of liposomal prednisolone. The liposomal prednisolone formulation comprises the lipids dipalmitoyl phosphatidyl choline (DPPC), cholesterol and PEG 2000 distearoyl phosphatidylethanolamine (PEG-DSPE) in a molar ratio of 62%, 33% and 5%, respectively. Water-soluble PLP was encapsulated in the aqueous interior of the LN at a starting concentration of 100 mg/mL. In order to produce 1 liter of LN-PLP under GMP conditions, 62.5 g PLP was dissolved in 450 mL of sterile water for injection. The lipid components (45.0 g DPPC, 13.4 g PEG-DSPE and 12.6 g cholesterol) were dissolved in 50 mL ethanol by heating to 70°C and continuously stirring. Subsequently, the alcoholic lipid solution was injected into the aqueous prednisolone phosphate solution to create a coarse lipid dispersion. Downsizing towards the desired particle diameter occurred by high-sheer homogenization. Sterilization was achieved by continuously circulating 500 mL 1 M sodium hydroxide and rinsing with phosphate buffered water for injections until pH 7.4. To clear the formulation from free PLP and ethanol, the liposome dispersion was filtered using polysulfonate membrane capsules with a cutoff of 100 kD. A sterile phosphate buffered (pH 7.6) sucrose solution (10%) was added to compensate for the loss of filtrate from the unit. After the exchange of approximately 15 L of sucrose solution, the dispersion was shown to be devoid of free PLP (< 5% of to the encapsulated quantity). Finally, the liposome dispersion was filtered using a 0.2 µm filter unit connected to a membrane pump. Characterization assays were performed to determine particle size, polydisperisty, surface charge, sterility and endotoxin content, among other features. In brief, the particle size averaged 100 nm ± 10 nm, the polydispersity index was 0.04, the ζ-potential of our liposomal particle was *-2.7 ± 1.2 mV*, sterility was compliant and endotoxin testing was ≤ 1.8 EU/ml. Shelf life stability studies indicate that LN-PLP remains stable in storage for at least 2 years when kept between 2 and 8 degrees C.

Macrophage isolation and staining. Plaque tissue macrophages were isolated according to the methods described by Liu et al[10]. In brief, fresh plaques were washed, cut into small segments of approximately 1 mm^3, and incubated in a proteolytic solution containing 25 mg collagenase (Sigma, C2139, St. Louis, MO, USA), 25 mg trypsin inhibitor (Sigma, T6522, St. Louis, MO, USA) and 125 mg HEPES in 25 ml HBSS solution for 2 hours at 37°C. Free cells were collected every 5 minutes and kept in FBS. Using a lymph-prep (d=1.077 g/ml) centrifugation gradient, macrophages were isolated and suspended in PBS + 0.2% BSA.

(DCE-)MR imaging. DCE-MRI was performed according to previously published methods[11]. In brief, the change of signal intensity in a region of interest (ROI) during contrast agent injection was studied with a custom-made Matlab (The MathWorks, Inc., Natick, MA, USA) program. Contours were traced manually for AUC calculation. A modified Tofts model was used to calculate the exchange of contrast agent from the plasma to the tissue compartment

(K^{trans}). Quantitative MR image analysis was performed using semi-automated measurement software (VesselMass, Leiden, the Netherlands).

FDG-PET/CT imaging. FDG-PET/CT scans were performed on a Gemini time-of-flight multi-detector helical PET/CT scanner (4 min/bed position) (Philips, Best, The Netherlands) according to methods described previously[12]. In brief, after 90 minutes of circulation using 200 MBq of FDG (5.5 mCi), subjects underwent PET/CT imaging initiated with a non-contrast CT for attenuation correction and anatomic co-registration. For every arterial segment (ascending aorta, left and right carotid artery) at least 5 ROIs were drawn to delineate the arterial wall. Each arterial ROI provides a mean and maximum SUV. To correct for blood pool activity in the aorta and carotids, at least 5 ROIs were placed in either the superior vena cava or jugular vein. The TBR was calculated by the ratio of mean arterial SUV mean or maximum compared with venous background activity (SUV mean). For efficacy analysis, TBR of the carotid segments were used.

TABLE S1. Safety parameters in PK study in humans

Parameter	Baseline	Week 4	Week 8	Week 12
Glucose, mmol/L	6.0 ± 2.3	5.6 ± 1.1	5.4 ± 1.3	5.6 ± 1.8
Insulin, IU/L	16.9 ± 14.4	12.7 ± 5.9	10.1 ± 3.8	11.4 ± 4.3
Cholesterol, mmol/L	5.5 ± 0.9	5.4 ± 1.0	5.2 ± 1.4	5.2 ± 1.1
LCL-c, mmol/L	3.6 ± 0.7	3.6 ± 0.9	3.5 ± 1.2	3.5 ± 0.9
HDL-c, mmol/L	1.2 ± 0.3	1.2 ± 0.3	1.2 ± 0.3	1.2 ± 0.2
Osteocalcin, µg/L	8.2 ± 2.8	na	na	8.8 ± 5.6
AP, U/L	84.8 ± 29.1	83.7 ± 20.1	82.4 ± 28.1	79.6 ± 27.9
ALT, U/L	32.6 ± 12.4	36.1 ± 13.4	28.3 ± 10.6	36.7 ± 12.8
AST, U/L	24.4 ± 8.1	23.3 ± 8.0	22.3 ± 7.7	30.1 ± 10.7
Creatinine, µmol/L	72.1 ± 15.7	77.1 ± 13.5	79.4 ± 23.7	70.4 ± 18.4

Data are shown as mean ± SD for subjects (n=8) infused intravenously with a single dose of 150mg LN-PLP. *AP indicates alkaline phosphatase; ALT, alanine transaminase; AST, aspartate transaminase; HDL-c, high density lipid cholesterol; LDL-c, low density lipid cholesterol; LN-PLP, liposomal prednisolone; na, not assessed; PK, pharmacokinetic.*

TABLE S2. Safety analyses of LN-PLP

	LN-PLP (n = 20)		Placebo (n = 10)	
Vital signs	**Baseline**	**After LN-PLP**	**Baseline**	**After Placebo**
SBP, mm Hg	131 ± 13	134 ± 15	150 ± 13	146 ± 11
DBP, mm Hg	80 ± 6	82 ± 10	91 ± 6	89 ± 4
Pulse, beats/min	65 ± 8	62 ± 9	71 ± 8	62 ± 10
Body temperature, °C	36.7 ± 0.5	36.6 ± 0.51	36.8 ± 0.55	36.5 ± 0.6
Body weight, kg	92 ± 18.3	91 ± 18.4	89 ± 12.2	90 ± 11.9
Safety lab				
ALT, U/L	34 ± 14	34 ± 17	35 ± 12	36 ± 10
AST, U/L	29 ± 8	23 ± 6	31 ± 4	31 ± 5
GGT, IU/L	48 ± 38	45 ± 31	30 ± 13	33 ± 15
Creatinine, µmol/L	83 ± 12	82 ± 12	77 ± 9	78 ± 10
Leukocytes, 10^9/L	5.64 ± 1.74	4.80 ± 1.22	5.33 ± 0.61	5.03 ± 0.66
Monocytes, 10^9/L	0.41 ± 0.09	0.40 ± 0.05	0.44 ± 0.13	0.46 ± 0.12
CRP, mg/L	1.82 ± 2.55	1.81 ± 1.70	2.27 ± 1.90	1.68 ± 1.53
TChol, mmol/L	5.99 ± 2.31	6.02 ± 2.37	5.62 ± 1.67	5.97 ± 1.84
LDL-c, mmol/L	4.11 ± 2.24	3.96 ± 2.16	3.92 ± 1.49	4.31 ± 1.53
HDL-c, mmol/L	1.34 ± 0.51	1.35 ± 0.52	1.09 ± 0.43	1.12 ± 0.48
TG, mmol/L	1.49 ± 1.07	1.75 ± 2.05	1.56 ± 0.76	1.66 ± 0.76

Data are shown as mean ± SD. *ALT, alanine aminotransferase; AST, aspartate aminotransferase; CRP, C-reactive protein; DBP, diastolic blood pressure, GGT, gamma glutamyltransferase; HDL-c, high density lipid cholesterol; LDL-c, low density lipid cholesterol; LN-PLP, liposomal prednisolone; SBP, systolic blood pressure; TChol, total cholesterol; TG, triglycerides.*

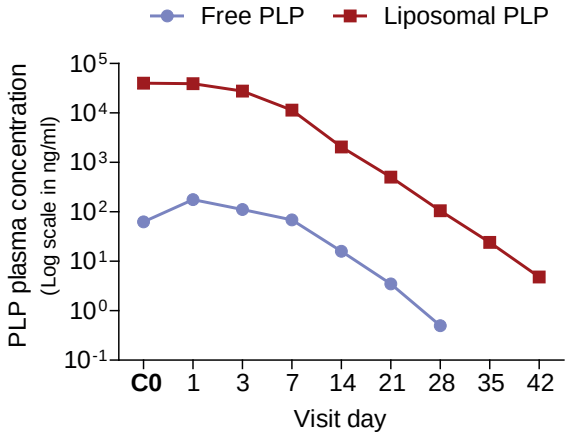

FIGURE S1. PK profile in humans

Line graphs showing the PLP/liposomal PLP ratio after 1.5mg/kg LN-PLP infusion, indicating that the peak plasma concentration of the free drug prednisolone (blue line) was on average 0.5% of the total liposomal PLP plasma concentration (red line), consistent throughout 28 days. *LN indicates liposomal nanoparticles; PLP, prednisolone phosphate.*

CHAPTER 10

LIPOSOMAL PREDNISOLONE AGGRAVATES ATHEROSCLEROSIS BY PROMOTING MACROPHAGE LIPOTOXICITY

Van der Valk FM*, Schulte DM*, Meiler S, Tang J, He Zheng K, van den Bossche J, Seijkens T, Laudes M, de Winther M, Lutgens E, Metselaar JM, Dallinga-Thie GM, Mulder WJM, Stroes ESG, Hamers AAJ

*Authors contributed equally

Nanomedicine. 2016;12:1463-70

ABSTRACT

Rationale: Atherosclerosis is a lipid-driven inflammatory disease, for which novel anti-inflammatory strategies are under evaluation. Prednisolone is a potent anti-inflammatory compound, yet, potential proatherogenic effects have been observed upon targeting of plaque macrophages using liposomal nanoparticles loaded with prednisolone phosphate (LN-PLP) in patients with atherosclerosis. We aimed to unravel the direct effects of LN-PLP on macrophages residing in the lipid-rich environment of atherosclerosis.

Methods and Results: In low-density lipoprotein receptor knockout ($LDLr^{-/-}$) mice fed a high fat diet, we show that LN-PLP accumulates in plaque macrophages. Biweekly injections of LN-PLP at 10mg/kg induces (i) enhanced monocyte recruitment to plaques after 2 weeks, followed by (ii) increased macrophage content, more advanced plaque stages, and larger necrotic core sizes after 6 weeks of LN-PLP administration. In vitro, we observed that both murine and human macrophages polarize into a lipid-avid phenotype after LN-PLP exposure, leading to increased lipid accumulation, endoplasmatic reticulum (ER) stress and late apoptosis.

Conclusion: These findings indicate that macrophage targeting in plaques with prednisolone may accelerate atherosclerosis by promoting macrophage lipotoxicity, thereby highlighting the challenges of anti-inflammatory therapy in atherosclerosis.

INTRODUCTION

Atherosclerosis is a chronic disease of the arterial wall, characterized by a lipid-rich, low-grade inflammatory milieu[1]. Despite the success of lifestyle changes and statins in cardiovascular prevention and treatment[2], disability and death from cardiovascular disease (CVD) is still increasing worldwide[3]. Consequently, novel anti-atherosclerotic strategies, amongst which anti-inflammatory compounds, are being assessed[4]. Glucocorticoids are potent anti-inflammatory agents, yet, long-term and systemic administration in CVD patients is considered undesirable due to systemic adverse effects[5].

Nanotechnology holds a promise by increasing drug accumulation in target tissues, while reducing systemic exposure[6,7]. In support of this concept, liposomal nanoparticles loaded with prednisolone phosphate (LN-PLP) were shown to accumulate in aortic lesions of rabbits, of which a high degree of LN-PLP co-localized with lesional macrophages[8]. Moreover, LN-PLP rapidly reduced the inflammatory activity of atherosclerotic lesions in rabbits[8]. In humans, the accumulation of LN-PLP in plaque macrophages isolated from patients after intravenous infusion was also found[9]. However, in patients with advanced atherosclerosis, LN-PLP treatment tended to increase the degree of arterial wall inflammation[9].

To elucidate the impact of LN-PLP on plaque macrophages in advanced atherosclerosis, we first addressed its effect in low-density lipoprotein receptor knockout (*LDLr*$^{-/-}$) mice, characterized by lipid-rich and macrophage-rich plaques. We found an increased number of inflammatory cells in the plaque after LN-PLP infusions for 2 weeks. In line with this initial proinflammatory effect, we next show that prolonged exposure to LN-PLP for 6 weeks induced more advanced plaque stages in this atherosclerotic mouse model. Subsequent *in vitro* studies in both murine and human macrophages corroborated that LN-PLP induced lipotoxic effects in macrophages residing in a lipid-rich environment.

METHODS

Nanoparticle formulations

The empty liposomal nanoparticles (LN) and liposomal prednisolone phosphate (LN-PLP) were formulated as previously described[10] and detailed in the Supplementary material.

LDLr$^{-/-}$ mice studies

In vivo studies, as illustrated in Figure S1, were performed in 8 weeks old *LDLr*$^{-/-}$ mice on a C57BL/6 background purchased from Jackson Laboratories, fed a high fat diet (HFD; Hope Farms) containing 0.15% (w/w) cholesterol, 16% fat (w/w) and no cholate for 6 weeks. All animal experiments were approved by the Committee for Animal Welfare of Amsterdam

Medical Centre or Mount Sinai New York and were carried out in compliance with guidelines issued by the local governments.

Biodistribution of LN-PLP: LDLr$^{-/-}$ mice were sacrificed 24 hours after tail vein injection of either PBS (n=4) or 10mg/kg cy5.5-labelled liposomal prednisolone (LN-PLP; n=4)[11]. LN-PLP uptake was assessed with near infrared fluorescence (NIRF) imaging and flow cytometric analysis of blood, spleen and aortic arches, as described in the Supplementary methods.

LN-PLP efficacy studies: Phosphate-buffered saline (PBS), free prednisolone (PLP, only in 6 weeks drug study), empty liposomes (LN) or LN-PLP tail vein injections of 10mg/kg were given twice a week for either 2 or 6 weeks (n=66 and n=64, respectively). Efficacy of LN-PLP was assessed using cytochemical and immunohistochemical stainings of aortic roots or arches, flow cytometric assays and mRNA expression in aortic arches.

In vitro macrophage assays

Bone marrow cells were isolated from both femurs and tibiae of wild-type mice (C57BL/6; n=2). Cells were cultured in RPMI-1640 with 100U/ml penicillin/streptomycin, 10% fetal bovine serum (FBS; all GIBCO Invitrogen) and 15% L929 conditioned medium (LCM) for 8 days to generate bone marrow-derived macrophages (BMDM) as previously described[12]. BMDM of two mice were pooled and seeded at a density of $0.15x10^6$ cells/cm^2 24 hours prior to stimulation. THP-1 monocytes (ATCC) were cultured in RPMI-1640 supplemented with 100U/ml penicillin/streptomycin and 10% FBS. Cells were differentiated into macrophages by adding 50ng/ml phorbol-12-myristate-13-acetate (PMA) for 24 hours. RAW264.7 stable cell line containing the 3x-NFκB-*luc* plasmid[13] was cultured in DMEM-high glucose (GIBCO Invitrogen) containing 100U/ml penicillin/streptomycin and 10% FBS. For each in vitro experiment, cells were stimulated with a low (20μM) and high (80μM) dose of PLP. LN-PLP was given at a concentration of 10μg/ml (equivalent to 20μM PLP) or 40μg/ml (equivalent to 80μM PLP). The empty liposomes (LN) were added in the same liposomal concentrations as LN-PLP. Macrophage assays comprised of immunostaining, NFκB transcriptional activity, mRNA gene expression, cholesterol efflux, oil-red-O staining and flow cytometric assays.

Statistical analysis

All experiments were at least performed in duplicate. Statistical analyses were performed using GraphPad Prism version 5 (San Diego, CA). An unpaired t-test (Welch corrected when necessary) or Mann Whitney test was used to define differences between 2 groups. For differences in plaque stage, the Chi2 test was used. Statistical significance between the 3 or 4 treatment groups was assessed using the 1-way ANOVA. Data are presented as mean ± SEM. The significance level was set at $p<0.05$.

RESULTS

LN-PLP accumulates in plaque macrophages

Near infrared fluorescence (NIRF) imaging substantiated accumulation of LN-PLP in the atherosclerotic plaques located in the aortas of *LDLr*$^{-/-}$ mice, 24 hours after tail vein injection (Figure 1A). In line with previous experiments[14], LN-PLP was also found in the liver, lung, spleen and kidney (Figure 1A). Flow cytometry assays showed that LN-PLP was predominantly taken up by myeloid cells, whereas not by non-myeloid cells (Figure 1B). In the circulating and splenic myeloid cells, the highest uptake was found in proinflammatory Ly6C^{+} monocytes and macrophages (Figure 1B). Also in the aortic arch, uptake of LN-PLP in macrophages and monocytes was demonstrated (Figure 1C).

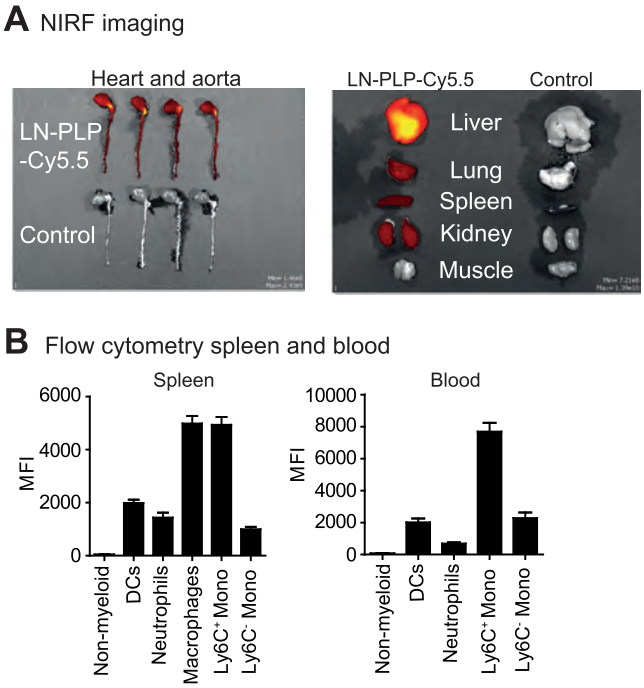

FIGURE 1. LN-PLP uptake in LDLr$^{-/-}$ mice

(**A**) NIRF images showing accumulation and distribution of Cy5.5-labelled LN-PLP (n=4) or PBS (n=4) 24 hours after tail vein injection (10mg/kg) in 8-week old *LDLr*$^{-/-}$ mice, 6 weeks on HFD. (**B,C**) Cellular distribution of LN-PLP in spleen, blood and aorta was assessed by flow cytometry. Data are presented as mean ± SEM. *HFD indicates high fat diet; LN-PLP, liposomal prednisolone; NIRF, near infrared fluorescence; PBS, phosphate-buffered saline.*

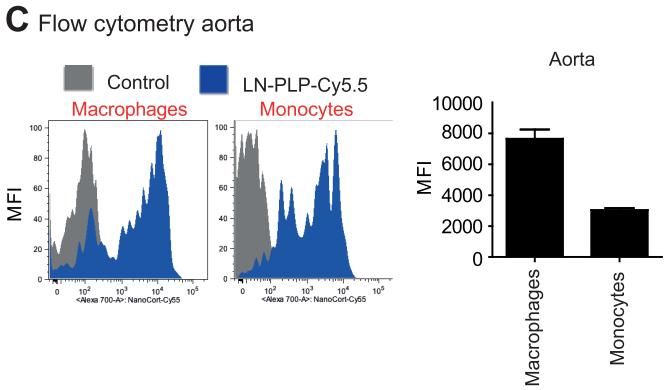

FIGURE 1. Continued

(**B,C**) Cellular distribution of LN-PLP in spleen, blood and aorta was assessed by flow cytometry. Data are presented as mean ± SEM. *HFD indicates high fat diet; LN-PLP, liposomal prednisolone; NIRF, near infrared fluorescence; PBS, phosphate-buffered saline.*

Two weeks LN-PLP induces monocyte recruitment

To evaluate drug effects in lipid-rich atherosclerotic plaques, we fed 8-week old *LDLr*$^{-/-}$ mice a high fat diet (HFD) for 6 weeks inducing substantial atherosclerosis in both the arches and roots (baseline; Figure 2A,B). Followed by 2 weeks administration of LN-PLP, empty liposomes (LN) or PBS (10 mg/kg, biweekly), no difference in plaque size was observed between the treatment groups (Figure 2A-B). However, the percentage of proinflammatory monocytes was significantly higher in aortic arches of the LN-PLP mice (11±6%) compared with LN (5±3%, $p<0.05$) and PBS (6±3%, $p<0.01$; Figure 2C). To analyse the recruitment of monocytes to the lesions, we assessed the expression of ER-MP58; a characteristic of circulating immature myeloid cells, which is lost upon differentiation into macrophages[15]. Immunostaining of the roots showed a significantly higher positivity for ER-MP58 after LN-PLP (24±11%) compared with LN (13±4%, $p<0.001$) and PBS (17±8%, $p<0.05$; Figure 2D), which indicates an increased presence of freshly influxed monocytes. No increase in the number of blood monocytes was observed after LN-PLP (Figure 2E). Of note, the body weight in LN-PLP treated mice was lower, whereas plasma cholesterol levels among the main lipoprotein classes were not different between groups (Figure S2A,B). Also, RBCs, platelets and haematocrit were similar between groups (Figure S2C).

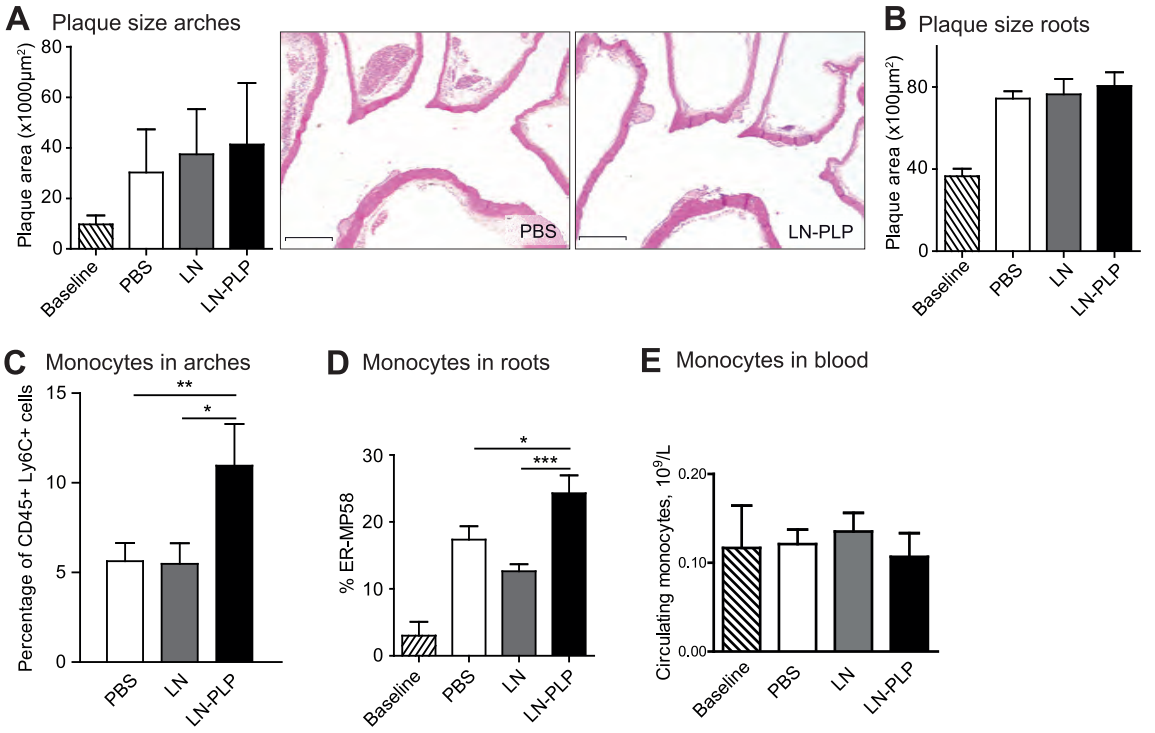

FIGURE 2. LN-PLP induces monocyte recruitment

(**A,B**) Plaque size was quantified in (**A**) the aortic arches (original magnification x25; scale bars represent 1mm) and (**B**) the roots using Hematoxylin-Eosin (HE) staining, 6 weeks after HFD (baseline, n=6) and an additional 2 weeks with PBS, LN or LN-PLP iv administration (n=20/group, 10mg/kg, biweekly). (**C**) Pro-inflammatory monocytes were assessed by flow cytometry of the arches, and (**D**) % of the lesion positive for ER-MP58 staining, indicative of freshly recruited monocytes in the roots, (**E**) the number of blood monocytes. Data are presented as mean ± SEM; *P<0.05, **P<0.01. *LN indicates empty liposomes; LN-PLP, liposomal prednisolone; PBS, phosphate-buffered saline.*

Six weeks LN-PLP aggravates atherosclerotic plaques

To assess whether increased monocyte influx after a 2-week LN-PLP administration translated into accelerated atherogenesis, we performed an additional experiment using a similar approach in 8-week old *LDLr*$^{-/-}$ mice fed a HFD for 6 weeks, yet, now receiving 6 weeks of intravenous LN-PLP, LN, PLP or PBS (10 mg/kg, biweekly). After the start of LN-PLP body weight decreased, whereas plasma cholesterol levels and circulating blood cells were not different between groups (Figure S3A-C). Plaque size was not different between groups (Figure 3A), yet, plaque stage was more advanced 6 weeks after LN-PLP (40% of plaques in stage V) compared with PLP, LN and PBS (for all <10% of plaques in stage V, $p<0.001$; Figure 3B). Immunohistochemical stainings revealed an increased macrophage content after LN-PLP (25±13%) compared with PLP (14±8%, $p<0.05$), LN (18±7%, $p<0.01$) or PBS (14±5%, $p<0.01$; Figure 3C). In addition, plaques had lower smooth muscle cell content in the LN-PLP mice (SMCs; 7±2%) compared with PLP (10±3%), LN (11±5%) and PBS (11±4%, for all $p<0.05$; Figure 3D). In agreement, less collagen was present in the LN-PLP group (43±11) compared with PLP (52±20%, $p<0.05$), LN (62±12%, $p<0.01$) and PBS (61±12%, $p<0.01$; Figure S3D). Finally, enlarged necrotic core areas were found after LN-PLP (68±4%) compared with PLP and LN (both 61±1%, both $p<0.05$), and PBS (52±3%, $p<0.01$; Figure 3E). In addition, the mRNA expression of chemokines *Mcp-1* and *Sdf-1*α in the aortic arches was higher after LN-PLP compared with control groups. In addition, the expression of *Chop*, a gene activated upon endoplasmic reticulum (ER) stress, was upregulated after LN-PLP in comparison to control groups (Figure 4).

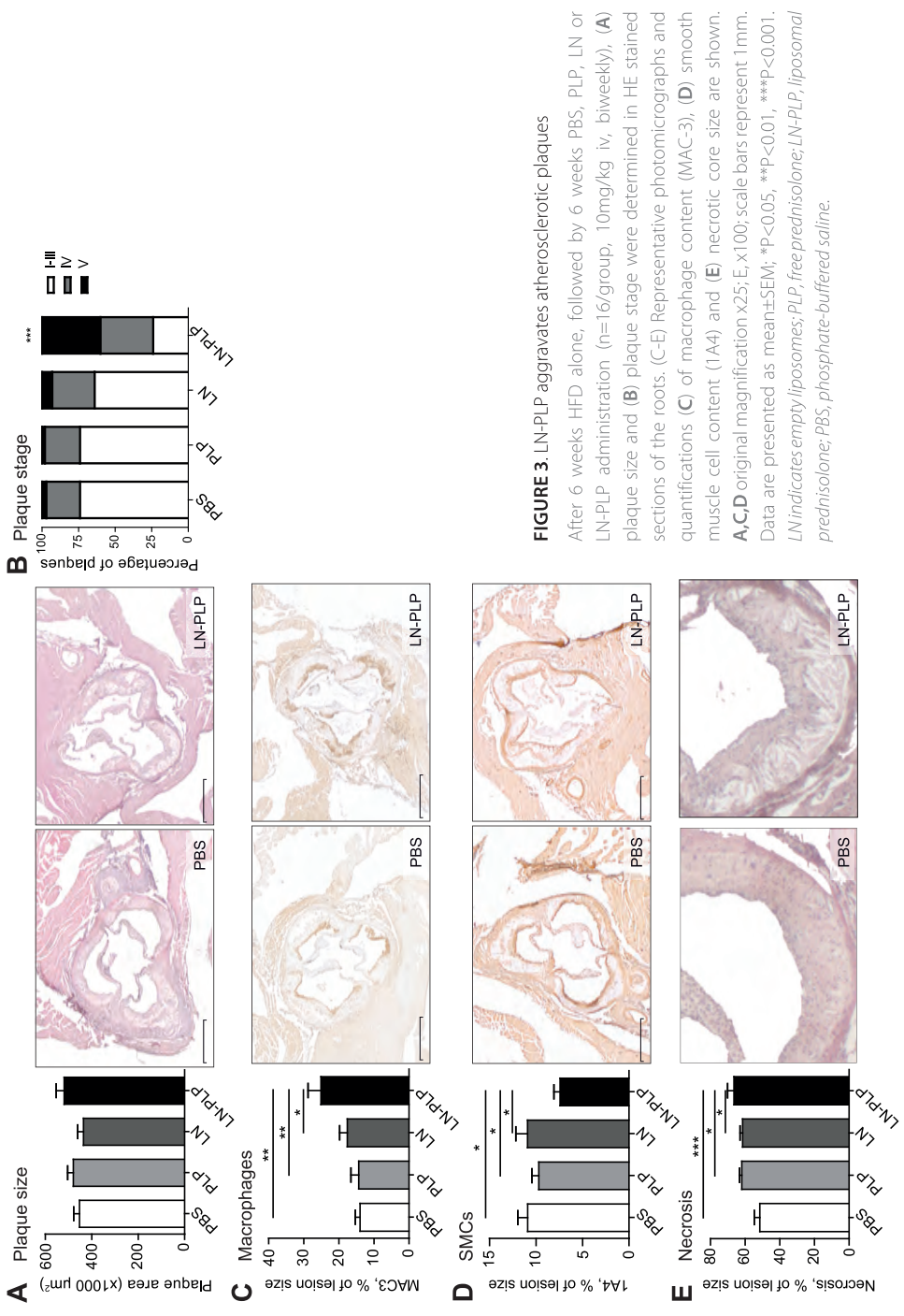

FIGURE 3. LN-PLP aggravates atherosclerotic plaques

After 6 weeks HFD alone, followed by 6 weeks PBS, PLP, LN or LN-PLP administration (n=16/group, 10mg/kg iv, biweekly). (**A**) plaque size and (**B**) plaque stage were determined in HE stained sections of the roots. (C-E) Representative photomicrographs and quantifications (**C**) of macrophage content (MAC-3), (**D**) smooth muscle cell content (1A4) and (**E**) necrotic core size are shown. **A,C,D** original magnification x25; E, x100; scale bars represent 1mm. Data are presented as mean±SEM; *P<0.05, **P<0.01, ***P<0.001. *LN indicates empty liposomes; PLP, free prednisolone; LN-PLP, liposomal prednisolone; PBS, phosphate-buffered saline.*

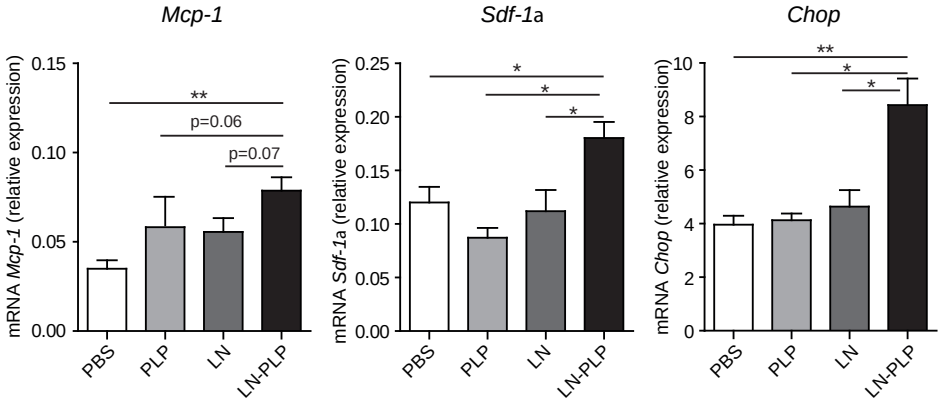

FIGURE 4. Gene expression in aortic arches

mRNA was isolated from aortic arches of *LDLr*$^{-/-}$ mice after 6 weeks administration of either PBS, PLP, LN or LN-PLP (n=16, 10mg/kg iv, biweekly) to analyse gene expression of monocyte migration factors, *Mcp-1* and *Sdf-1*α, and the endoplasmatic reticulum stress marker, *Chop*. Gene expression was normalized to *36B4* housekeeping gene. Data are presented as mean ± SEM; *P<0.05, **P<0.01. *Chop indicates C/EBP homologous protein; LN, empty liposomes; LN-PLP, liposomal prednisolone; Mcp-1, monocyte chemotactic protein-1; PBS, phosphate-buffered saline; PLP, free prednisolone; Sdf-1*α*, stromal cell-derived factor-1*α.

LN-PLP induces macrophage lipotoxicity in vitro

In vitro, RAW264.7 NFκB-*luc* cells were used to assess prednisolone's classical anti-inflammatory effect.(13) As expected, pretreatment of cells with either LN-PLP or PLP significantly decreased NFκB activity upon LPS challenge (8.6±0.8 and 9.8±0.4 for the highest dose, respectively) compared with control (23.8±3.8; for both p<0.001), whereas its activity was not influenced by empty LN (23.3±3.5; Figure 5A).

In view of the lipid-rich environment in atherosclerotic plaques, we addressed the effect of LN-PLP on lipid-handling pathways in BMDM. The expression of the major cholesterol efflux protein *Abca1* was significantly diminished after LN-PLP (0.007±0.001) or PLP (0.035±0.002) compared with control (0.013±0.002; p<0.001 and p<0.01, respectively; Figure 5B). In line, the cholesterol efflux capacity of macrophages reduced after LN-PLP and PLP (0.73±0.18% and 1.34±0.26%, respectively) compared with LN (1.65±0.45) or control (2.00±0.27, p<0.01; Figure 5B). Also, BMDM lipid content was higher after LN-PLP and free PLP compared with empty LN and control (Figure 5C).

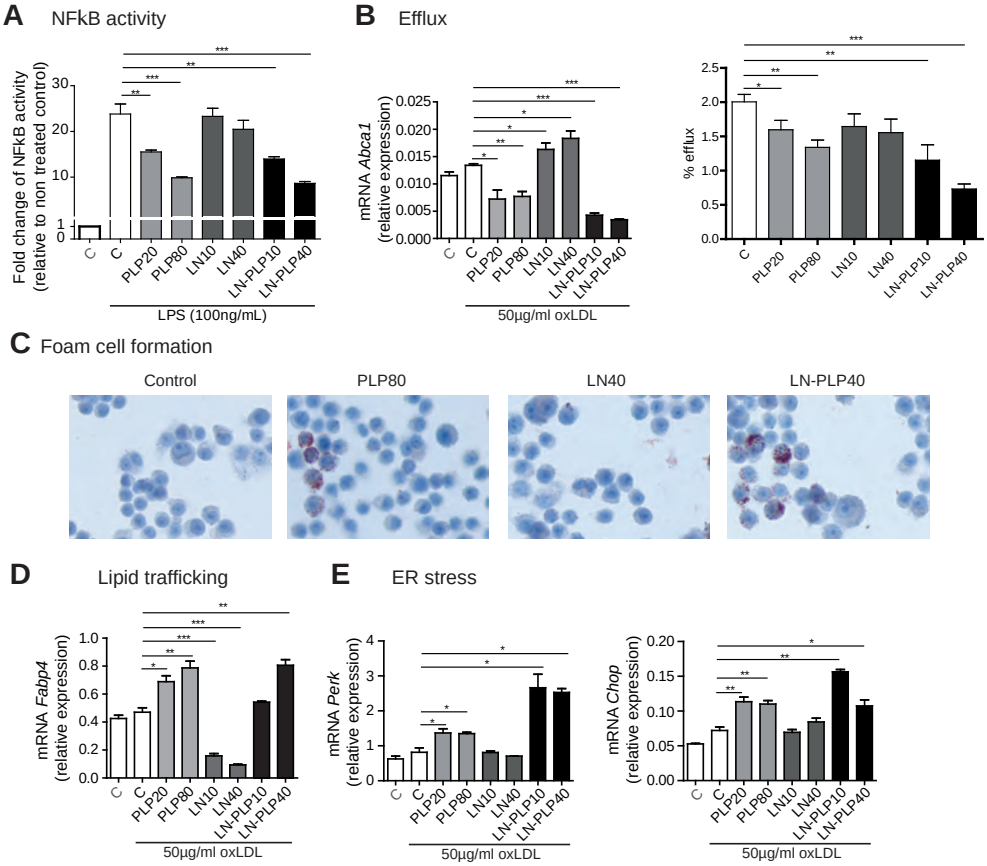

FIGURE 5. LN-PLP promotes macrophage lipotoxicity

(**A**) NFκB activity was determined in RAW267.4 NFκB-*luc* cells as the relative fold change to control without 100ng/ml LPS stimulation. (**B**) BMDM were isolated from C57BL/6 mice to study gene expression levels of ATP-binding cassette transporter A1 (*Abca1*) and cholesterol efflux towards the acceptor apo-A1. (**C**) BMDM lipid content after 48 hours oxLDL (50 ug/ml) using oil-red-O stain. (**D**) Gene expressions of the intracellular lipid transporter *Fabp4*, and (E) ER-stress markers *Perk* and *Chop* in BMDM exposed to oxLDL (50 ug/ml) for 24 hours.

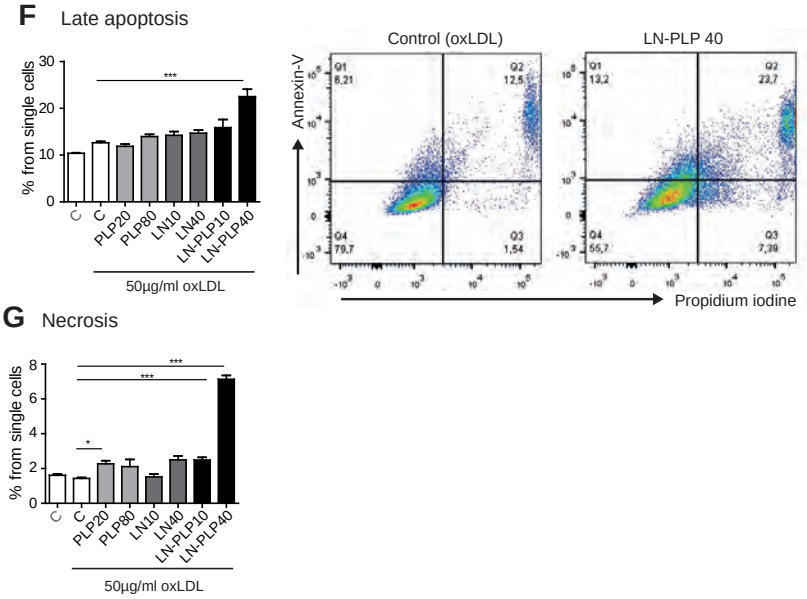

FIGURE 5. Continued

(**F-G**) Late apoptosis and necrosis following a 72-hour oxLDL (50 ug/ml) incubation were assessed by Annexin-V / propidium iodine flow cytometry. Gene expression was normalized to *36B4* and *18S* housekeeping genes. Oil-red-O photomicrographs were taken with a 400x magnification. Data are presented as mean ± SEM; *P<0.05, **P<0.01, ***P<0.001. *BMDM indicates bone marrow derived macrophages; Chop, C/EBP homologous protein; Fabp4, fatty acid binding protein 4; LN, empty liposomes; LN-PLP, liposomal prednisolone; PBS, phosphate-buffered saline; Perk, pancreatic endoplasmic reticulum kinase; PLP, free prednisolone.*

The expression of the intracellular lipid transporter *Fabp4* was also increased after both LN-PLP (0.81±0.07) and PLP (0.79±0.08), compared with control (0.47±0.05, both p<0.01), whereas after LN the *Fabp4* expression was decreased (0.09±0.01, p<0.001; Figure 5D). Increased levels of intracellular lipid trafficking by *Fabp4* have been shown to promote ER-stress and induce an unfolded protein response (UPR)[16]. Indeed, we observed that in lipid-rich macrophages LN-PLP markedly increased the mRNA expression of the ER-stress markers *Perk* (p<0.05 compared with either LN or PBS; Figure 4D) and *Chop* (p<0.05 compared with both control groups; Figure 5E). Activation of *Perk* and *Chop* are elementary in the switch from pro-survival to pro-death signalling; in line, 23% of the macrophages underwent late apoptosis and 7% necrosis after LN-PLP, as compared with<15% and <3% of the macrophages, respectively, in control conditions (Figure 5F-G).

Comparable results were observed using the human THP-1 cell line; a reduced cholesterol efflux towards apo-A1, increased *Fabp4* gene expression, and attenuated apoptosis in response to both PLP and LN-PLP (Figure S4).

DISCUSSION

In the present study, we show that LN-PLP administration for 2 weeks increases monocyte influx into the plaques of *LDLr*$^{-/-}$ mice. Following these early proinflammatory changes, administration of LN-PLP for 6 weeks results in an increased plaque macrophage content. In addition, prolonged LN-PLP administration aggravates plaque stage, characterized by a decreased collagen and smooth muscle cell content, as well as increased necrotic core area. Using an *in vitro* approach, we show that in a lipid-rich environment, LN-PLP decreases the macrophage cholesterol efflux capacity, driving lipid-induced ER-stress and subsequent apoptosis/necrosis. These findings indicate that local exposure to prednisolone elicits a proatherogenic, lipotoxic effect in plaque macrophages in *LDLr*$^{-/-}$ mice.

The early proinflammatory effect of LN-PLP in *LDLr*$^{-/-}$ mice is discordant with the previously observed reduction in inflammatory cell content in rabbit's atherosclerotic lesions only days after a single LN-PLP administration[8]. Explanations for this discrepancy may include differences in timing (2 days versus 2 weeks treatment), dosing (single versus multiple injections of LN-PLP) and differences in plaque composition between rabbits and mice[17]. The latter may be of particular relevance, since the acute inflammatory response following the double-balloon injury in the rabbit model more closely represents 'classical' inflammation[18], explaining the beneficial impact of glucocorticoids. Conversely, the lipid-driven inflammation in *LDLr*$^{-/-}$ mice, and for that matter also in patients, reflects a chronic inflammatory disease state[19].

The relevance of the early proinflammatory effect of LN-PLP is substantiated by the observation that after 6 weeks of LN-PLP administration, the number of macrophages, tissue descendants of monocytes, are higher in plaques compared with PLP, LN or PBS administration. In addition, mRNA expression of chemoattractants[20], *Mcp-1* and *Sdf-1*α, was upregulated in the aortic arches of the LN-PLP treated mice and may be an explanation for the observed increased monocyte influx and macrophage plaque content. This higher macrophage number after LN-PLP corresponds to our previous observation in patients treated with LN-PLP who exhibited a 7% increase in carotid ^{18}F-fluorodeoxyglucose (^{18}F-FDG) uptake[9], which is a marker of plaque macrophage content[21].

Since we have shown that LN-PLP is taken up by plaque macrophages in the atherosclerotic plaques, we focused on the direct effects of LN-PLP on plaque macrophages. It has been previously reported that glucocorticoids induce the repolarization of inflammatory (M1-like) macrophages towards reparative (M2-like) macrophages[22]. In support, we show that NFκB activity is decreased after (LN-)PLP. Interestingly, this reparative phenotype has also been reported to bear an increased vulnerability for lipid stress[23], as suggested by increased expression of the intracellular lipid chaperone *Fabp4*[24] and decreased expression of the major cholesterol efflux transporter *Abca1*[25]. Here, we report the consequences of these phenotypical changes in a lipid-rich environment, by showing that (LN-)PLP decreases the efflux capacity of lipid-laden macrophages, leading to accelerated foam cell formation.

Increased lipid burden in macrophages is known to promote cellular stress responses[16]. We show that exposure of lipid-rich macrophages to (LN-)PLP augments ER-stress and increases the number of macrophages undergoing late apoptosis and necrosis.

The finding of a direct proatherogenic effect adds to previous suggestions that prednisolone predominantly has indirect adverse effects on known cardiovascular risk factors such as glucose homeostasis, blood pressure and lipids[26]. Several observations strengthen the concept of an adverse effect of prednisolone itself on macrophages: (i) *in vitro* macrophages respond in a similar fashion to liposomal encapsulated PLP (LN-PLP) as to free PLP, and (ii) the lipotoxic effects of (LN-)PLP *in vitro* correspond to the observed proatherogenic changes *in vivo*, both in mice (higher number of monocytes/macrophages and more advanced plaque stages) as well as in patients with atherosclerotic plaques (increased ^{18}F-FDG uptake)[9].

Several limitations merit consideration. First, although we show local accumulation of LN-PLP in plaque macrophages in *LDLr*$^{-/-}$ mice, we cannot provide an absolute quantification of the drug concentration in the atherosclerotic plaques. With the advent of novel nanoparticle therapies for atherosclerosis[27,28], future studies need to address drug delivery efficiency. Second, whereas we have focused on the effects of LN-PLP on macrophages in a lipid-rich environment, we cannot exclude that other mechanisms of glucocorticoids may also have contributed to the observed proatherogenic effects. For instance, glucocorticoids have been shown to induce an upregulation of 11β-hydroxysteroid dehydrogenase type 1 (11β-Hsd1), which converts inactive glucocorticoids into active glucocorticoids. In line, 11β-Hsd1 inhibitors decrease the active intracellular glucocorticoids and attenuate atherosclerosis progression in *ApoE*$^{-/-}$ mice[29,30].

The present findings highlight the challenges of applying anti-inflammatory strategies in atherosclerosis. Thus, favourable effects of an anti-inflammatory compound in a classical inflammatory disease cannot be easily extrapolated to a comparable efficacy in the lipid-rich environment of an atherosclerotic plaque. Hence, future drug candidates need to undergo a multifaceted screening with careful consideration of the lipid-rich, atherosclerotic microenvironment.

Acknowledgements: We thank Alinda Schimmel, Stefan Havik and Linda Becker for their crucial support in experimental and lab work.

Disclosures and funding: This work was supported by a European Framework Program 7 grant (ESS: FP7-Health 309820: Nano-Athero); the Dutch network for Nanotechnology NanoNext NL, in the subprogram "Drug Delivery" and a NWO Vidi (W.J.M.M.). J.M.M. is affiliated with the company Enceladus Pharmaceuticals (Amsterdam, The Netherlands), declaring to have no competing interests. D.M.S. received support from the International Endocrine Scholars Program (IESP) by the European Society of Endocrinology (ESE) and the Endocrine

Society (ENDO) as well as from the "3E": Exchange in Endocrinology Expertise program by the European Union of Medical Specialists (U.E.M.S.). All other authors declare that they have no conflict of interest and no relationships with industry relevant to this study.

REFERENCES

1. Libby P et al. Progress and challenges in translating the biology of atherosclerosis. Nature. 2011;473:317–325.
2. Ford I et al. Long-term follow-up of the west of scotland coronary prevention study. N Engl J Med 2007;357:2373–2383.
3. Roth GA et al. Demographic and Epidemiologic Drivers of Global Cardiovascular Mortality. N Engl J Med 2015;372:1333–1341.
4. Van der Valk FM et al. Novel anti-inflammatory strategies in atherosclerosis. Curr Opin Lipidol 2012;23:532–539.
5. Wei L. Taking Glucocorticoids by Prescription Is Associated with Subsequent Cardiovascular Disease. Ann Intern Med; 2004;141:764.
6. Lobatto ME et al. Perspectives and opportunities for nanomedicine in the management of atherosclerosis. Nat Rev Drug Discov 2011;10:835–852.
7. Schiener M et al. Nanomedicine-based strategies for treatment of atherosclerosis. Trends Mol Med 2014;20:271–281.
8. Lobatto ME et al. Multimodal Clinical Imaging To Longitudinally Assess a Nanomedical Anti-Inflammatory Treatment in Experimental Atherosclerosis. Mol Pharm 2010;7:2020–2029.
9. Van der Valk FM et al. Prednisolone-containing liposomes accumulate in human atherosclerotic macrophages upon intravenous administration. Nanomedicine 2015;11:1039–1046.
10. Lobatto ME et al. Pharmaceutical development and preclinical evaluation of a GMP-grade anti-inflammatory nanotherapy. Nanomedicine 2015;11:1133–1140.
11. Tang J et al. Inhibiting macrophage proliferation suppresses atherosclerotic plaque inflammation. Sci Adv 2015;1:1400223.
12. Hamers AAJ et al. Bone marrow-specific deficiency of nuclear receptor Nur77 enhances atherosclerosis. Circ Res; 2012;110:428–438.
13. Carlsen H et al. In Vivo Imaging of NF- B Activity. J Immunol; 2002;168:1441–1446.
14. Metselaar JM and Storm G. Liposomes in the treatment of inflammatory disorders. Expert Opin Drug Deliv 2005;2:465–476.
15. Goossens P et al. Myeloid IκBα deficiency promotes atherogenesis by enhancing leukocyte recruitment to the plaques. PLoS One; 2011;6:22327.
16. Erbay E et al. Reducing endoplasmic reticulum stress through a macrophage lipid chaperone alleviates atherosclerosis. Nat Med 2009;15:1383–1391.
17. Getz GS and Reardon CA. Animal models of Atherosclerosis. Arterioscler Thromb Vasc Biol 2012;32:1104–1115.
18. Lobatto ME et al. Imaging the efficacy of anti-inflammatory liposomes in a rabbit model of atherosclerosis by non-invasive imaging. 1st ed. Methods Enzymol; 2012.
19. Viola J and Soehnlein O. Atherosclerosis – A matter of unresolved inflammation. Semin Immunol; 2015;1–10.
20. Bleul CC. A highly efficacious lymphocyte chemoattractant, stromal cell-derived factor 1 (SDF-1). J Exp Med; 1996;184:1101–1109.
21. Tarkin JM et al. PET imaging of inflammation in atherosclerosis. Nat Rev Cardiol; 2014;11:443–457.
22. Liu G and Yang H. Modulation of macrophage activation and programming in immunity. J Cell Physiol; 2013;228:502–512.
23. Isa SA et al. M2 macrophages exhibit higher sensitivity to oxLDL-induced lipotoxicity than other monocyte/macrophage subtypes. Lipids Health Dis; 2011;10:229.
24. Hu W et al. Statins synergize dexamethasone-induced adipocyte fatty acid binding protein expression in macrophages. Atherosclerosis; 2012;222:434–443.
25. Liew YY et al. Effect of rapamycin and prednisolone in differentiated THP-1 and U937 cells. Transplant Proc 2002;34:2872–2873.

26. Czock D et al. Pharmacokinetics and pharmacodynamics of systemically administered glucocorticoids. Clin Pharmacokinet 2005;44:61–98.
27. Fredman G et al. Targeted nanoparticles containing the proresolving peptide Ac2-26 protect against advanced atherosclerosis in hypercholesterolemic mice. Sci Transl Med; 2015;7:275ra20.
28. Zhang X-Q et al. Nanoparticles containing a liver X receptor agonist inhibit inflammation and atherosclerosis. Adv Healthc Mater 2015;4:228–236.
29. Luo MJ et al. 11 β-HSD1 inhibition reduces atherosclerosis in mice by altering pro-inflammatory gene expression in the vasculature. Physiol Genomics 2012;7:47:57.
30. Hadoke PWF et al. Modulation of 11β-hydroxysteroid dehydrogenase as a strategy to reduce vascular inflammation. Curr Atheroscler Rep; 2013;15:320.

SUPPLEMENT

LN-PLP formulation. The liposomal nanoparticles (LN) were composed of a hydrophilic core, either empty or encapsulating prednisolone phosphate (PLP), surrounded by a lipid bilayer of phospholipids and cholesterol, which was coated with polyethylene glycol (PEG) to increase plasma half-life and reduce rapid plasma clearance of the LN through the mononuclear phagocyte system.

In vivo mice studies:

Assays for LN-PLP uptake. Hearts, aortas, livers, lungs, spleens, kidneys, and femoral muscle were collected and imaged by near infrared fluorescence imaging (NIRF) using the IVIS200 spectrum optical imaging system (PerkinElmer). Overview of the whole aortic roots was taken with 20x magnification using digital stitching of Zeiss Axioplan2IE microscope. Spleens were homogenized using a 70μM cell strainer. Before flow cytometric analysis, blood and splenic erythrocytes were lysed. Aortas were diced into small pieces and digested with an enzyme cocktail containing 4U/ml liberase TH (Roche), 0.1mg/ml DNase I (Sigma-Aldrich), and 60U/ml hyaluronidase (Sigma-Aldrich) in PBS at 37°C for 60 minutes. The following antibodies were used: recognizing CD90 (clone 53.2.1), B220 (clone RA3-6B2), CD49b (clone DX5), NK1.1 (clone PK136), Ly-6G (clone 1A8), Ter-119 (clone TER-119), Ly-6C (clone AL21), CD11b (clone M1/70), CD11c (clone N418) and F4/80 (clone BM8). DAPI stain was used to exclude dead cells from analysis. All antibodies were either purchased from eBioscience, BD Biosciences, or Biolegend. Fluorescence was detected by flow cytometry (BD Biosciences LSR II), and the data were analyzed using FlowJo software (Tree Star).

Assays for LN-PLP efficacy. After sacrifice, blood was drawn from the mice after 4 hours fasting; and the hearts and aortic arches were taken out. The hearts were cut perpendicular to the heart axis just below the atrial tips. Tissue was embedded in paraffin and cut into sections, or cryosections were made (both 7μm). The lesions were visualized using hematoxylin-eosin (H&E) stain. The aortic arches were either embedded in paraffin, snap frozen, or processed for flow cytometry. Plaque size and necrotic core were quantified using Adobe photoshop CS5 software. Plaque stage was determined as previously described (de Waard et al, Current Protocols in Mouse Biology 2012).

Aorta flow cytometry. The aortic arches were dissected, put in 20mM HEPES in RPMI (GIBCO Invitrogen) and cut into small pieces. Digestion was performed by 30 minutes incubation at 37°C with a Collagenase I, XI, DnaseI and Hyaluronidase enzyme mix (all from Sigma). The lysate was transferred into a FACS tube with cell strainer (BD Biosciences) and centrifuged for 5 minutes at 1600 rpm. A live/dead stain was performed according to the manufacturer's protocol (Fixable Aqua Dead Cell Stain Kit; Life Technologies), Fc receptors were blocked

with an antibody against CD32/CD16 (eBioscience) and cells were labeled for analysis on the LSRFortessa (BD Biosciences) with the antibodies recognizing: CD45, Ly6C and CD11b (eBiosciences).

Mouse blood parameters. Red blood cells (RBC), platelets and hematocrit (Hct) were measured using a Coulter Counter. The total cholesterol distribution among the main lipoprotein classes of the plasma samples was measured using fast performance liquid chromatography (FPLC) analysis as described previously (Levels JHM et al. Crit Care Med. 2003). In brief, the system contained a PU-980 ternary pump with an LG-980-02 linear degasser and an UV-975 UV/VIS detector (Jasco, Tokyo, Japan). An extra PU 2080i-plus pump (Jasco, Tokyo, Japan) was used for in-line cholesterol RTU enzymatic reagent (Biomerieux, Marcy l'Etoile, France) addition at a flow rate of 0.1 mL/min respectively. EDTA plasma was diluted 1:1 with Tris buffered saline and 30 µL sample/buffer mixture was loaded on a Superose 6 HR 10/30 column (GE Health care, Life sciences division, Diegem, Belgium) for lipoprotein separation at a flow rate of 0.31 mL/min. Chromatographic profiles of commercially available plasma lipid standards (SKZL, Nijmegen, The Netherlands) served as a reference.

Cytochemical and immunohistological stainings. Cryosections (2 weeks study) were dried and subsequently fixed with dry acetone (Sigma). Newly influxed monocytes were shown using an antibody against ER-MP58 (Bioconnect) followed by detection with a biotin-labeled rabbit anti-rat antibody and staining with the ABC kit (Vector Labs). After counterstaining with hematoxylin sections were embedded with Vectamount (Vectashield). ER-MP58 positive cells were counted manually. Paraffin sections (6 weeks study) were deparaffinized and rehydrated. Aortic roots were stained for 60 minutes with a 0.2% Picro Sirius Red solution and incubated for 2 minutes in acidified water (0.01M HCl). The sections were dehydrated, embedded in pertex (Histolab) and collagen content was quantified using Adobe photoshop CS5 software. In addition, sections were incubated with antibodies detecting macrophages (MAC-3; Pharmingen) and smooth muscle cells (SMC; 1A4; Dako) followed by a horseradish peroxidase (HRP)-conjugated secondary antibody. DAB substrate (ImmunoLogic) was used for detection. After counterstaining with hematoxylin sections were embedded in pertex. Macrophage and smooth muscle cell area was quantified using Adobe photoshop CS5 software.

RNA isolation, cDNA synthesis and RT-qPCR. From snap frozen aortic arches, total RNA was extracted after crushing (under liquid nitrogen) using Trizol (Life technologies) and cDNA was synthesized from 300ng of total RNA using iScript cDNA Synthesis kit (BioRad). Semi-quantitative real-time PCR was performed using SensiFAST™ SYBR® (BC Biotech) and measured with the CFX384 system (Bio-Rad). Specific primers for monocyte chemotactic protein-1 (*Mcp-1*), stromal cell-derived factor-1α (*Sdf-1*α) and C/EBP homologous protein (*Chop*), and ribosomal protein *36B4* (to correct for cDNA content) were designed using Primer 3 software (see Table S1).

In vitro macrophage assays:

In vitro uptake of LN. Macrophages were seeded on Lab Tek chamber slides (Nunc), stimulated and incubated overnight. Cells were washed twice with PBS before a 20 minute fixation step with 100% methanol (Sigma) followed by a permeabilization/blocking step with 0.15% Triton 10% FBS in PBS for 1 hour at room temperature. Liposomes were detected with an antibody against polyethylene glycol (PEG;Epitomics) followed by an anti-Rabbit-FITC labelled secondary (Jackson Immuno Research). Slides were mounted using DAPI mounting media (Vectashield) and pictures were taken.

NFκB transcriptional activity. RAW267.4 NFκB-*luc* cells were cultured in a 96-well plate at a density of 70,000 cells/well. Cells were treated with compounds, stimulated with 100ng/ml LPS (Sigma) after 2 hours and luciferase activity was determined 22 hours later using the One-Glo reporter assay system (Promega) according to the manufacturer's instructions.

RNA isolation, cDNA synthesis and RT-qPCR. From cultured BMDM, total RNA was extracted using a similar approach, and cDNA made from 500ng RNA. Semi-quantitative real-time PCR was performed using SensiFAST™ SYBR® (BC Biotech) and measured with the CFX384 system (Bio-Rad). Specific primers for fatty acid binding protein 4 (*Fabp4*), ATP-binding cassette transporter A1 (*Abca1*), C/EBP homologous protein (*Chop*), pancreatic endoplasmic reticulum kinase (*Perk*), and ribosomal protein *36B4* and *18S* (to correct for cDNA content) were designed using Primer 3 software (see Table S1).

Cholesterol efflux (^{3}H cholesterol). BMDM or THP-1 macrophages were loaded with cholesterol for 24 hours using 30μg/ml cholesterol (Sigma) mixed with 0.5μCi/ml Tritium-labeled cholesterol (Amersham) and the compounds in RPMI supplemented with 100U/ml penicillin/streptomycin and 0.2% free fatty acid (FFA)-free bovine serum albumin (BSA; Sigma). After washing the cells with PBS containing 0.2% FFA-free BSA, they were incubated for 24 hours with 20μg/ml apolipoprotein A1 (apo-A1; Calbiochem) in RPMI containing 100U/ml penicillin/streptomycin and 0.2% FFA-free BSA. Both cell culture medium and the cells were harvested, and Tritium was measured using a Scintillation counter.

Oil-red-O. BMDM were cultured on a Lab Tek chamber slide, incubated with the compounds overnight and thereafter stimulated with 50μg/ml oxLDL (Alfa Aesar) for 48 hours. Cells were fixed with 3.5% formalfix and incubated with isopropanol for 10 minutes. Cellular lipids were stained with Oil-red-O (0.3g/100ml 60% isopropanol) for 30 minutes and briefly counterstained with hematoxylin. Slides were embedded in glycergel (Dako) and photomicrographs were taken with a 400x magnification.

Late apoptosis and necrosis (Annexin-V / propidium iodine). BMDM or THP-1 macrophages were stimulated with 50µg/ml oxLDL and the compounds for 72 hours. To determine late apoptosis and necrosis by Flow cytometry $5x10^5$ cells were suspended in 50µl Annexin-V binding buffer, and stained with 1:50 propidium iodine and 1:100 FITC-labelled Annexin-V (Life Technologies). Samples were measured on the FACS Canto II (BD Biosciences) and the data analysis was performed using FlowJo software (Tree Star).

TABLE S1. Primer sequences used for semi-quantitative real-time PCR

Gene	Forward primer sequence (5`-3`)	Reverse primer sequence (5`-3`)
36B4*	ACGGGTACAAACGAGTCCTG	GCCTTGACCTTTTCAGCAAG
36B4	GGACCCGAGAAGACCTCCTT	GCACATCACTCAGAATTTCAATGG
18S	AGGGTTCTGTTGGTCCTGTG	GCTTCAAGCCCAGAGATTTG
MCP-1	CCACTCACCTGCTGCTACTC	AGCTTGGTGACAAAAACTACAGC
SDF-1α	CCTCGGTGTCCTCTTGCT	GCCTCTGGCGATGTGGCTCTC
ABCA1*	ATGAGGACAACAACTACAAAGCC	GGGAAAGAGGACTAGACTCCAAA
ABCA1	GGTTTGGAGATGGTTATACAATAGTTGT	TTCCCGGAAACGCAAGTC
FABP4*	AGCACCATAACCTTAGATGGGG	CGTGGAAGTGACGCCTTTCA
FABP4	CATAACCCTAGATGGCGGGG	CGCCTTTCATAACACATTCCACC
CHOP*	TTGCCTTTCTCCTTCGGGAC	GATTCTTCCTCTTCATTTCCAGGAG
CHOP	CCCAGGAAACGAAGAGGAAGAA	CTGTCAGCCAAGCTAGGGAC
PERK*	GGATGAATGGACGATGTA	ATATGTTGGATGGCTTGA
PERK	GGACCTCAAGCCTTCCAACAT	CTACTTGTCCCGTGTGCGTA

* indicates human primers.

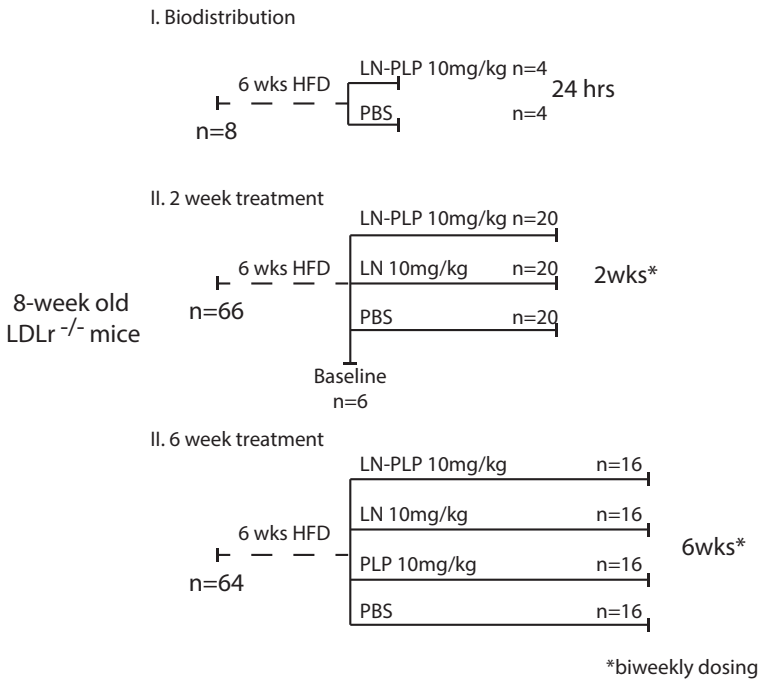

FIGURE S1. Schematic of *in vivo* studies in *LDLr*$^{-/-}$ mice

Eight-week old *LDLr*$^{-/-}$ mice were fed a HFD for 6 weeks, followed by (i) a single dose of LN-PLP 10mg/kg or PBS and sacrifice after 24 hours, (ii) 2 weeks administration of LN-PLP, LN or PBS (10mg/kg, biweekly) or (iii) 6 weeks of LN-PLP, LN, PLP or PBS (10mg/kg, biweekly). *LN indicates empty liposomes; LN-PLP, liposomal prednisolone; PBS, phosphate-buffered saline; PLP, free prednisolone.*

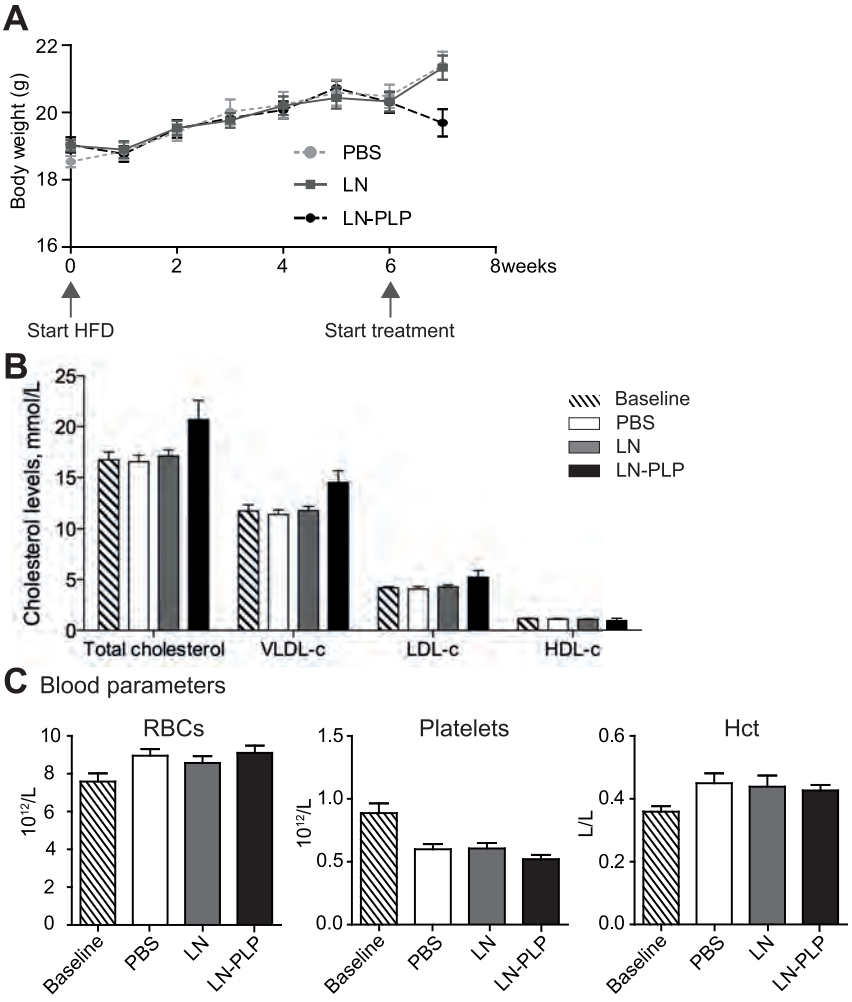

FIGURE S2. Safety parameters of *LDLr*$^{-/-}$ mice after 2 weeks treatment

(**A**) Body weight of the mice was monitored weekly. (**B**) After 6 weeks of HFD, followed by 2 weeks of drug administration, plasma cholesterol among the main lipoprotein classes were measured. (**C**) Red blood cells (RBC), platelets and hematocrit (Hct) was determined by Coulter Counter upon harvest. Data are presented as mean ± SEM; **P<0.01, ***P<0.001. *LN indicates empty liposomes; LN-PLP, liposomal prednisolone; PBS, phosphate-buffered saline.*

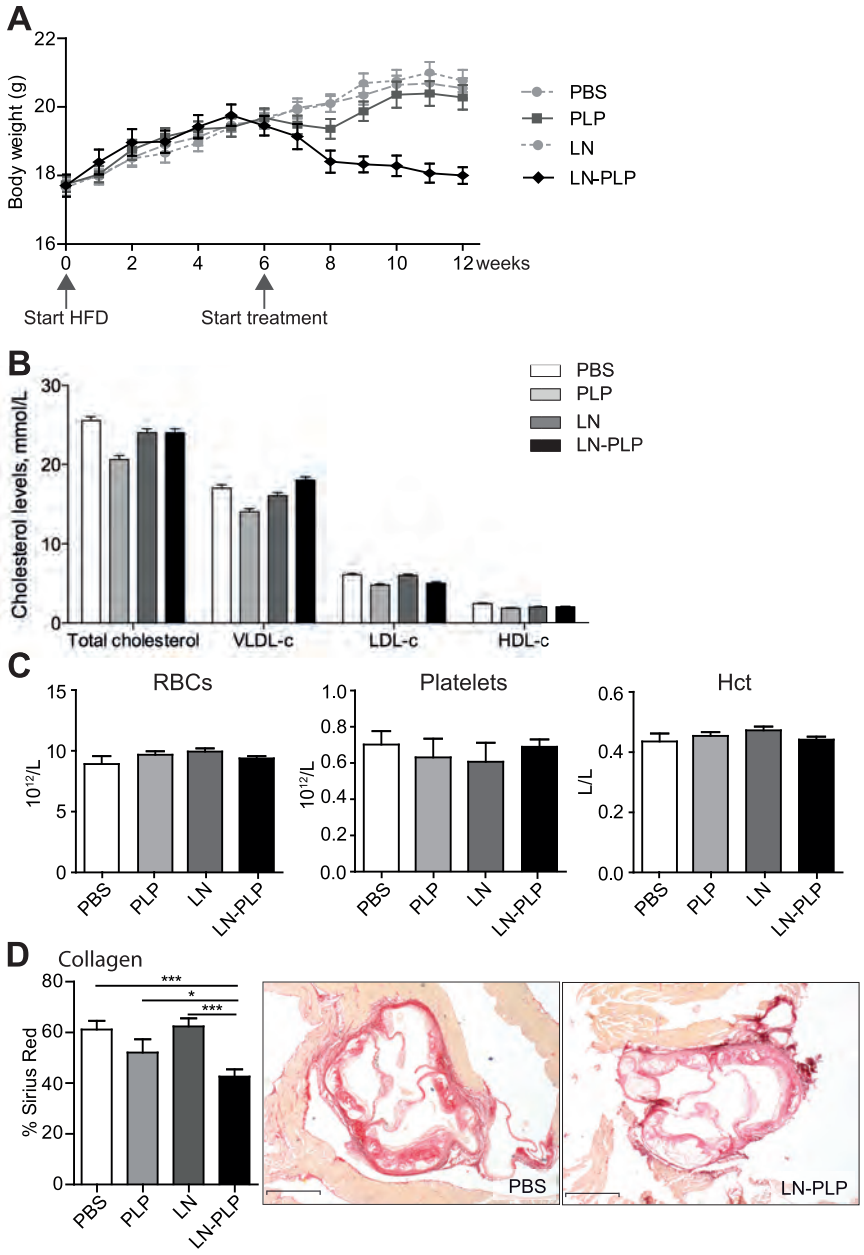

FIGURE S3. Safety parameters and plaque collagen content in *LDLr*$^{-/-}$ mice after 6 weeks treatment

(**A**) Body weight of the mice was monitored weekly. (**B**) After 6 weeks of HFD, followed by 6 weeks of drug administration, total cholesterol was measured in the main lipoprotein classes (**C**) Upon harvest red blood cells (RBC), platelets and hematocrit (Hct) was determined by Coulter Counter, (**D**) collagen content in the roots was assessed with sirius red staining (original magnification x25; scale bars represent 1mm). Data are presented as mean±SEM; *P<0.05, ***P<0.001. *LN indicates empty liposomes; LN-PLP, liposomal prednisolone; PBS, phosphate-buffered saline; PLP, free prednisolone.*

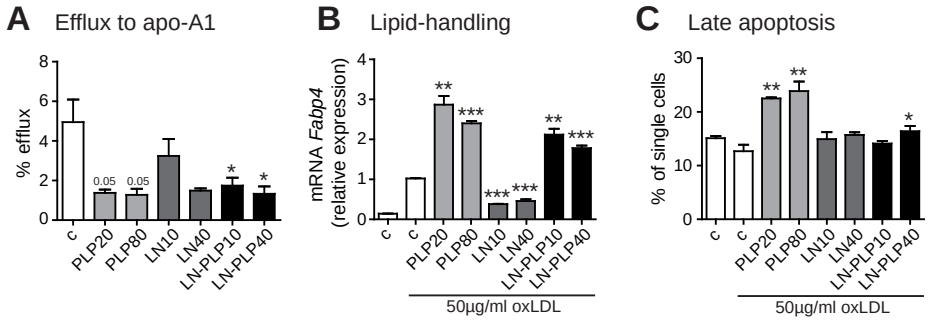

FIGURE S4. LN-PLP effects in human macrophages

THP-1 cells were differentiated into macrophages by PMA treatment and (**A**) cholesterol efflux towards apo-A1, (**B**) gene expression of intracellular lipid transporter *Fabp4* after 24 hours oxLDL (50 ug/ml), and (**C**) oxLDL-induced late apoptosis (50 ug/ml, 72 hours) were determined. Data are presented as mean±SEM; *P<0.05, **P<0.01, ***P<0.001. *LN indicates empty liposomes; LN-PLP, liposomal prednisolone; PBS, phosphate-buffered saline; PLP, free prednisolone.*

CHAPTER 11

MULTIPLE PATHWAY SCREENING TO PREDICT ANTI-ATHEROGENIC EFFICACY OF DRUGS TARGETING MACROPHAGES IN ATHEROSCLEROTIC PLAQUES

Alaarg A*, He Zheng K*, **van der Valk FM**, Eduardo da Silva A, Versloot M, Quarles van Ufford LC, Schulte DM, Storm G, Metselaar JM, Stroes ESG, Hamers AAJ

*Authors contributed equally

Vascul Pharmacol. 2016;82:51-9

ABSTRACT

Rationale: Macrophages play a central role in atherosclerosis development and progression, hence targeting macrophage activity is considered an attractive therapeutic. Recently, we documented nanomedicinal delivery of the anti-inflammatory compound prednisolone to atherosclerotic plaque macrophages in patients, which did however not translate into therapeutic efficacy. This unanticipated finding calls for in-depth screening of drugs intended for targeting plaque macrophages.

Methods and Results: We evaluated the effect of several candidate drugs on macrophage activity, rating overall performance with respect to changes in cytokine release, oxidative stress, lipid handling, endoplasmic reticulum (ER) stress, and proliferation of macrophages. Using this *in vitro* approach, we observed that the anti-inflammatory effect of prednisolone was counterbalanced by multiple adverse effects on other key pathways. Conversely, pterostilbene, T0901317 and simvastatin had an overall anti-atherogenic effect on multiple pathways, suggesting their potential for liposomal delivery.

Conclusion: This dedicated assay setup provides a framework for high-throughput screening. Further *in vivo* studies are warranted to determine the predictive value of this macrophage-based screening approach and its potential value in nanomedicinal drug development for cardiovascular patients.

INTRODUCTION

Atherosclerosis is a multifaceted disease of the arterial wall, underlying the vast majority of cardiovascular diseases[1]. Triggered by endothelial cell dysfunction, circulating lipids accumulate in the arterial wall and become modified through oxidation. Recruited macrophages become foam cells when taking up these oxidized lipids, which is a hallmark of initial atherosclerotic lesions. Over time, a complex interplay of maladaptive responses contributes to atherosclerosis progression, including, amongst others, chronic local inflammation, oxidative stress, impaired cholesterol efflux and excessive cell proliferation[2].

Past decades, the widespread use of statin-based lipid lowering strategies has revolutionized cardiovascular disease management, reducing the risk of an acute event by 25-35%[3]. Nonetheless, a considerable residual risk remains[4], driving the pursuit for novel anti-atherosclerotic strategies. Since plaque macrophages are crucial in atherogenesis, main mechanisms related to macrophage activity, including inflammation, oxidative stress, lipid metabolism and proliferation, are considered potential therapeutic targets[5]. Nanomedicine offers an attractive strategy to locally target macrophage activity within an atherosclerotic plaque[6]. In addition to promising results in experimental models[7,8], we recently reported successful targeting of plaque macrophages in patients with atherosclerosis using a liposomal delivery platform for prednisolone[9]. However, the unexpected lack of anti-inflammatory efficacy strongly argued for a more in-depth characterization of drug effects on plaque macrophages[9].

Therefore, we set up a dedicated series of *in vitro* assays to rapidly screen drug compounds for their effects on multiple key pathways of macrophage activity. Seven compounds recognized for their beneficial modulating effect on *one* of these pathways were selected to evaluate their effect on *all* other aforementioned macrophage pathways (Table 1). To facilitate potential nanomedicinal development, we aimed to screen drugs and compounds that have a good safety profile in humans and are suitable for liposomal encapsulation. We demonstrate here that we can rapidly assess overall performance of drug candidates to identify those likely to exert anti-atherogenic effects on lesional macrophages.

TABLE 1. Selected drug compounds for multi-pathway screening

Drug	Mode of action	Clinical use	Status for atherosclerosis
Prednisolone ***Anti-inflammatory***	Glucocorticoid receptor agonist	Inflammatory, oncological and hematological disorders	Phase I/II: Liposomal formulation of prednisolone phosphate showed no efficacy[9]
Methotrexate (MTX) ***Anti-inflammatory***	Folic acid antagonist	Neoplastic diseases, rheumatoid arthritis, psoriasis	Phase III: Systemic low dose MTX trial in progress (CIRT)[40]
T0901317 (T09) ***Cellular cholesterol efflux stimulator***	Liver X receptor (LXR) agonist	Only preclinical use	Preclinical: Systemic dosing reduces atherosclerosis in animal models, but promotes hepatic lipogenesis[24-29]
Pterostilbene ***Anti-oxidant***	Free radical scavenging	No clinical indications; available as dietary supplement	Preclinical: Long term oral dosing of resveratrol (analogue) reduces atherosclerosis in mice and rabbits[31-35]
Mercaptopurine (6-MP) ***Anti-proliferative***	Purine antagonist	Organ transplantation, leukemia, auto-immune disorders	Preclinical: Drug-eluting cuff reduces atherosclerosis in mice[36]
Simvastatin ***Lipid lowering*** ***Anti-inflammatory***	HMG-CoA reductase inhibitor	Primary and secondary prevention of atherosclerosis	Preclinical: rHDL-vehicle delivery reduced atherosclerosis in mice[7]
Rapamycin ***Anti-inflammatory***	mTOR inhibitor	Organ transplantation, drug-eluting stents	Preclinical: Oral dosing reduces atherosclerosis in mice[43-50]; local delivery strategies are being developed[41,42]

CIRT indicates cardiovascular inflammation reduction trial; MTX, methotrexate; HMG-CoA, 3-hydroxy-3-methyl-glutaryl-coenzyme A; rHDL, recombinant high-density lipoprotein; mTOR, mammalian target of rapamycin.

METHODS

Materials

All chemicals were purchased from Sigma unless mentioned otherwise. T0901317 (T09) was purchased from Cayman Chemical. The compounds were dissolved in dimethyl sulfoxide (DMSO), yet ensuring that in all experiments the final DMSO fraction in culture wells was below 0.05% (v/v). Lipoprotein depleted serum (LPDS) was prepared from fetal calve serum by ultracentrifugation in KBr at a density of 1.21 g/ml. After centrifugation at 50000 RPM and 4°C for 50000 RPM, the lipoprotein layer was removed by aspiration. The bottom fraction was dialysed against phosphate buffered saline (PBS) and sterile filtered. The purity is determined via HPLC.

Cell culture

Human monocytic THP-1 cells[10], and RAW264.7 murine macrophages[11] and murine bone marrow derived macrophages (BMDM) are widespread models to study macrophage function in atherosclerosis. THP-1 cells and RAW264.7 macrophages were obtained from the American Type Culture Collection. RAW264.7 cells stably transfected with the 3x-NF-κB-*luc* plasmid were kindly provided by Prof. M.P.J. de Winther[11].

THP-1 cells and RAW264.7 were cultured in RPMI-1640 and DMEM-high glucose, respectively. Both media were supplemented with penicillin (100 IU/ml), streptomycin (100 µg/ml) and 10% fetal bovine serum (FBS; GIBCO Invitrogen). THP-1 cells were differentiated into macrophages with 50ng/ml phorbol-12-myristate-13-acetate (PMA) for 24 hours, after which cells were washed and left in PMA-free medium for another 24 hours before adding the compounds. Bone marrow cells were isolated from both femurs and tibiae of wild-type mice (C57BL/6). Cells were cultured in RPMI-1640 with penicillin (100 U/ml), streptomycin (100 µg/ml) and 10% FBS and 15% L929 conditioned medium for 8 days to generate BMDM according to a method previously described[12]. For the oxidative burst assay, polymorph-nuclear neutrophils (PMNs) were isolated by Ficoll centrifugation of buffy coats purchased from Sanquin (Amsterdam) blood supply.

Cell viability

THP-1, and RAW264.7 and BMDM cells were seeded in 96-well plates (5 x 10^4 cells/well). The next day, cells were treated with the compounds in concentrations ranging from 0.3 to 30 µM for 24 hours. The toxicity of compounds was determined by colorimetric MTT cell viability assay as described previously[13].

NF-κB transcriptional activity

RAW264.7 NF-κB-*luc* macrophages were seeded in 96-well plates (7 x 10^4 cells/well). After 24 hours, cells were washed and treated with the compound for 2 hours after which cells were stimulated with lipopolysaccharide (LPS) (100 ng/ml) for another 18 hours. NF-κB luciferase activity was determined by the ONE-Glo™ Luciferase Assay System (Promega).

Pro-inflammatory cytokine production

Quantitation of secreted cytokine concentrations of tumor necrosis factor alpha (TNF-α) and interleukin(IL)-6 was performed by using the Cytometric Bead Array Human Inflammation Kit (BD Biosciences). THP-1 and BMDM cells were seeded in 96-well plates (5 x 10^4 cells/well). After differentiation with PMA, cells were treated with each compound for 2 hours. Thereafter, LPS was added at final concentration of 100 ng/ml for another 22 hours. Before analysis, cellular debris was removed from the supernatants of treated cells by centrifugation (400g 5'5 minutes at 500G).

RNA isolation, cDNA synthesis and qRT-PCR

THP-1 cells were seeded into 12-well plates (5 x 10^5 cells/well). After differentiation with PMA, cells were first incubated with oxidized low-density lipoprotein (oxLDL; 50 µg/ml; Alfa Aesar) for 24 hours, then treated with the compounds for an additional 18 hours. Total RNA was extracted using Trizol and cDNA was synthesized from 1µg RNA with the iScript cDNA Synthesis kit (BioRad). Semi-qQuantitative real-time PCR (qRT-PCR) was performed using SensiFAST™ SYBR® (BC Biotech) and measured with the CFX384 system (BioRad). Specific primers for human CD36, ATP-binding cassette transporter A1 (ABCA1), fatty acid binding protein 4 (FABP4), C/EBP homologous protein (CHOP), inositol-requiring transmembrane kinase/endonuclease 1 (IRE1) and ribosomal protein 36B4 were designed (Table S1).

Nitric oxide (NO) production

In vitro evaluation of NO production of THP-1 macrophages using the Griess assay is not achievable[14]. RAW264.7 macrophages and BMDM were seeded in 96-well plates (1 x 10^5 cells/well) and next day washed and pre-treated with each compound for 2 hours followed by 100 ng/ml LPS for another 22 hours. Nitrite (NO_2^-) concentrations in the supernatants were measured by adding 100 µl freshly made Griess reagent ((0.1% N-(1-Naphtyl)ethylenediamine dihydrochloride (Merck), 2,5% pPhosphoric acid (Merck), 1% sulfanilamide (Sigma))) to 100 µl culture supernatant. Serial dilutions of nitrite standard solution were used to generate a standard curve ranging from 0 to 100 µM of nitrite. The absorbance was measured at 550 nm with a microplate reader (SPECTROstar Nano).

Production Reactive Oxygen Species (ROS)

PMNs were suspended in Hank's' Buffered Saline Solution (HBSS) substituted with 1% gelatine solution in deionized H_2O (HBSS-gel.). Cells were counted and diluted in the HBSS-gel to a concentration of 1x10^6 cells/ml. Zymosan A from *Saccharomyces cerevisiae* was used as ROS inducer. Luminol, dissolved in DMSO and diluted in HBSS resulting in a final DMSO concentration lower than 0.1% (v/v), was used as luminescence enhancer and was added to the PMNs in a 1:1 volume ratio in white 96-well plates. Compounds were added to the previously indicated final concentrations and zZymosan was added to final concentration of 0.2 mg/ml. Luminescence was measured using Titertek Luminoskan (TechGen International). The assay was repeated using buffy coats from different donors.

OxLDL uptake

Human oxLDL (Alfa Aesar) was labelled with DyLight 488 NHS Ester (#46402 Thermo Scientific). The manufacturer has oxidized the LDL via copper sulphate oxidation and the degree of oxidation was 99% (determined via the TBARS assay). Briefly, 0.43 µL Dylight 488 was added

per 250 µL of 2 mg/ml oxLDL. The solution was protected from light and incubated on a shaker at RT for 1 hour. Subsequently, unbound dye was washed away by dialysis at 4°C overnight. THP-1 complete medium was replaced by medium containing 10% lipoprotein depleted serum (LPDS) and pre-treated overnight with each compound. Subsequently, 25 µg/ml oxLDL-Dylight 488 was added to treated or non-treated cells for 6 or 24 hours. Finally, cells were washed once with ice cold phosphate buffered saline (PBS) containing 5% FBS, twice with ice cold PBS and lysed using radio-immunoprecipitation assay buffer (TEKnova). Fluorescence was measured with a Typhoon scanner (GE Healthcare).

Cholesterol efflux

THP-1 cells were seeded in 24-wells plates at a density of 5 x 10^5 cells/ml. Macrophages were treated with compounds for 8 hours and loaded with cholesterol overnight using 30 µg/ml cholesterol mixed with 0.5 µCi/ml tTritium-labeled cholesterol (Amersham) in RPMI with 100 U/ml penicillin-/streptomycin (100 U/ml-100 µg/ml) and 0.2% free fatty acid (FFA)-free bovine serum albumin (BSA). After washing with PBS containing 0.2% FFA-free BSA, cells were incubated for 4 hours with 20 µg/ml apolipoprotein-A1 (apoA-1; Calbiochem) in RPMI (without FBS) containing 100U/ml penicillin/-streptomycin (100 U/ml - 100 µg/ml) and 0.2% FFA-free BSA (Sigma). Cells were lysed using isopropanol 100%. Tritium was measured for both cell culture medium and cell lysates using a scintillation counter.

BrdU incorporation

Proliferation was primarily evaluated in RAW264.7 cells, since differentiation of THP-1 cells with PMA is known to halts proliferation[15]. RAW264.7 and THP-1 cells were seeded in 96-well plates (3 x 10^3 cells/well), washed the next day with serum free medium and subsequently serum starved for 24 hours. Thereafter, serum free medium was replaced with complete medium reconstituted with each compound except for the control, in which only complete medium was added. After 24 hours, proliferation was measured using the 5-bromo-2'-deoxyuridine (BrdU) ELISA kit (Roche) according to the manufacturer's recommendations.

Overall performance score

The experiments provided outcomes known to have either an atheroprotective or atherogenic effect, which was expressed in fold change compared to the untreated control. A scoring system was applied where a statistical significant change compared to control was scored as +1 or -1 point depending on whether the effect was atheroprotective or atherogenic, respectively. A two-fold change or more was scored by adding or subtracting 2 points. The total score was tallied and compounds were ranked accordingly. Subsequently, a summarizing heatmap was generated in MultipleExperiment Viewer (MeV 4.9.0., Microarray Software Suite, www.tm4.org).

Statistical analysis

All experiments assays were at least performed in triplicatethree independent experiments. Statistical analysis was performed using GraphPad Prism 5 software. Statistical significance was calculated using the unpaired Student's T-test (Welch corrected when necessary). Values are represented as mean ± SEM. The significance level was set at $p<0.05$.

RESULTS

Cell viability

Prior to evaluating the chosen macrophage pathways relevant to atherosclerosis, cell viability was assessed after treatment with drug concentrations ranging from 0.3 μM to 30 μM to assess the non-toxic dose to be used for the other assays. MTT cell viability assays showed that none of the compounds affected THP-1 cell viability, apart from rapamycin, which was toxic at 30 μM. In addition to human cells, viability assays of murine RAW264.7 cells and BMDM showed comparable results (data not shown Figure S1). Thus, for each compound a concentration of 30 μM was applied, whereas for rapamycin a concentration of 3 μM was used in the screening assays.

Anti-inflammatory potency

Anti-inflammatory effects of the selected compounds were first evaluated with LPS-induced NF-κB activation in RAW264.7 NF-κB-*luc* macrophages (Figure 1A). A strong (>50%) inhibition of LPS-induced NF-κB activity was observed after prednisolone, T09 and 6-MP treatment compared to LPS stimulation only (all $p>0.001$). MTX, pterostilbene and simvastatin showed a modest (25%) reduction on NF-κB activity (all $p<0.01$), whereas rapamycin increased NF-κB activity ($p=0.006$). The subsequent release of pro-inflammatory cytokines following LPS was determined in THP-1 macrophages. Prednisolone, T09 and pterostilbene strongly (>50%) reduced the production of TNFα and IL-6. Simvastatin did repress TNFα, but had no statistically significant effect on IL-6 (Figure 1B&+C-E). MTX, 6-MP and rapamycin did not significantly influence cytokine release, apart from a strong reduction (>50%) in IL-6 by rapamycin ($p=0.046$). Generally similar effects for cytokine release were observed for BMDM (Figure S2A-B).

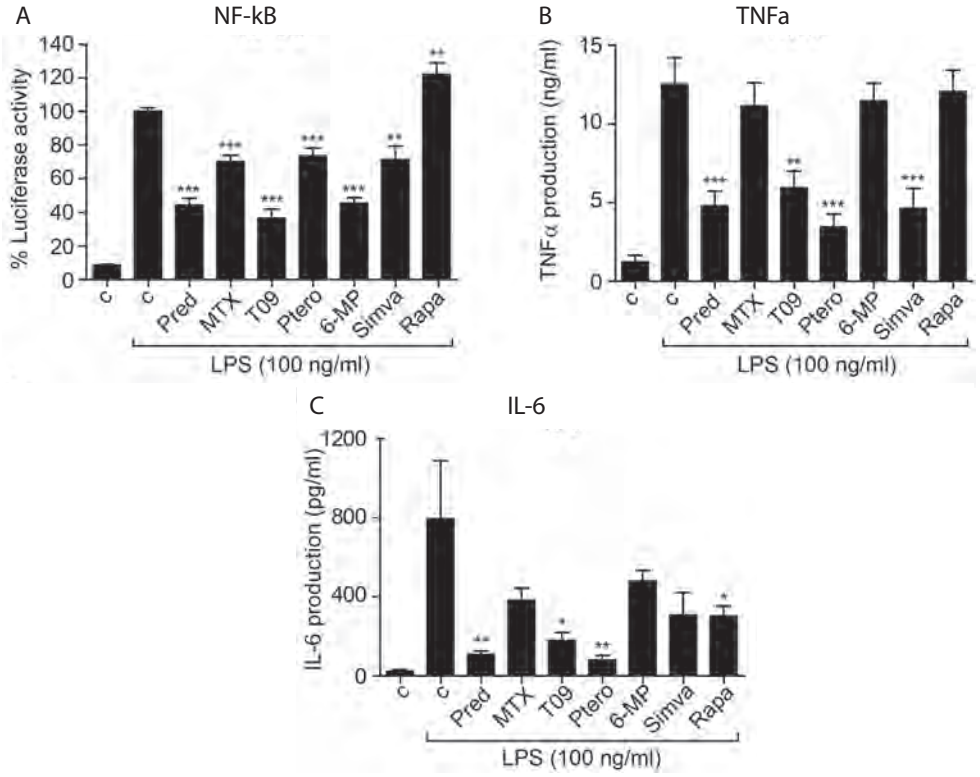

FIGURE 1. Inflammation

RAW264.7 NF-κB-*luc* cells (**A**) or THP-1 macrophages (**B,C**) were treated with the compounds and stimulated with LPS (100 ng/ml) for 24 hrs. (**A**) NF-κB activity was determined by luciferase assay and fold change was calculated relative to LPS stimulation only from three independent experiments (n=6). (**B,C**) TNF-α and IL-6 production was measured using a cytometric bead array. Data are presented as mean±SEM; *p<0.05, **p<0.01, ***p<0.001 compared to LPS stimulation only. *6-MP indicates 6-mercaptopurine; c, control; MTX, methotrexate; pred, prednisolone; ptero, pterostilbene; rapa, rapamycin; simva, simvastatin; T09, T0901317.*

Generation of reactive oxygen species

Potential anti-oxidative effects were studied using LPS-induced NO production and zymosan-induced PMN ROS generation. After treatment with prednisolone and rapamycin, a substantial reduction in NO production of more than 40% compared to LPS stimulation only (both p<0.001) was observed, while pterostilbene and T09 reduced NO production in the order of 25 to 30% (both p<0.001). MTX, simvastatin, and 6-MP did not affect NO production at all (Figure 2A). In BMDM, NO production was reduced the most (>50%) by prednisolone, pterostilbene and T09 (Figure S2C). With respect to ROS, pterostilbene was the strongest inhibitor of ROS production (8 fold change). T09, 6-MP and simvastatin diminished ROS production to a less extent, while prednisolone, MTX and rapamycin did not affect ROS production (Figure 2B).

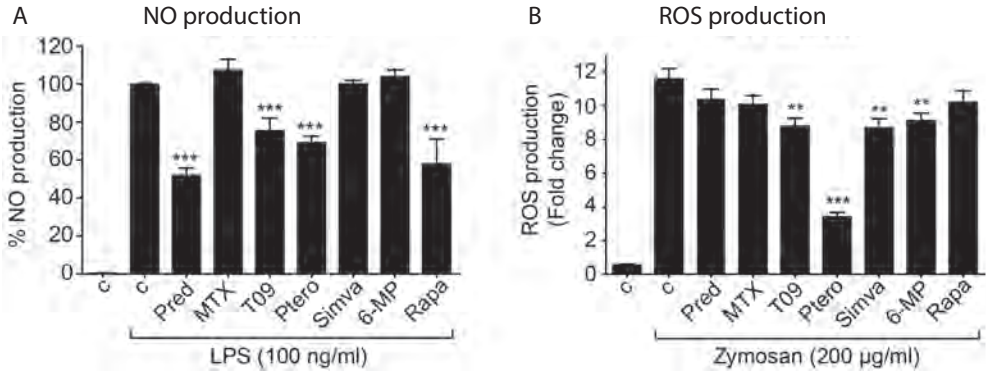

FIGURE 2. Anti-oxidant properties

RAW264.7 cells were treated with the compounds and stimulated with LPS (100 ng/ml) for 24 hrs after which nitric oxide (NO) production was determined with Griess reagent (**A**). PMNs were treated with the compounds and stimulated with zymosan to measure the inhibition of reactive oxygen species (**B**). Fold change was calculated relative to zymosan stimulation only (c) from three independent experiments (n=6). Data are presented as mean±SEM; *p<0.05, **p<0.01, ***p<0.001 compared to LPS or zymosan stimulation only. *6-MP indicates 6-mercaptopurine; c, control; MTX, methotrexate; pred, prednisolone; ptero, pterostilbene; rapa, rapamycin; simva, simvastatin; T09, T0901317.*

Lipid handling by macrophages

Important changes in macrophage lipid handling with regard to atherosclerosis comprise the uptake, efflux and intracellular trafficking of lipids. First, the uptake of fluorescently labelled oxLDL was assessed in THP-1 macrophages. Correcting for background fluorescence measured in control cells without oxLDL, T09 and pterostilbene modestly reduced oxLDL uptake by 2545% (both p<0.001) compared to oxLDL stimulation only (Figure 3A), whereas MTX, simvastatin and rapamycine decreased oxLDL uptake to a somewhat lesser extent (all p<0.001). Similar results were observed when oxLDL treatment was extended to 24 hours (Figure S2D). In line with the diminished oxLDL uptake, both T09 and pterostilbene markedly down-regulated the expression of the lipid uptake receptor CD36 (both p<0.001; Figure 3B).

Next, treatment effects on cholesterol efflux from THP-1 cells to apoA-1 were assessed. As expected, the LXR-agonist T09 greatly increased cholesterol efflux by 2.5-fold (p<0.001), in respect to untreated control cells. Simvastatin (p=0.005) and rapamycin (p=0.017) also strongly augmented cholesterol efflux, whereas the other compounds did not affect this process (Figure 3C). mRNA expression of the cholesterol efflux transporter ABCA1 was significantly (>2.5-fold) elevated by T09 and pterostilbene, while it was reduced in response to prednisolone (45%) and simvastatin (20%) (all p<0.001 compared to oxLDL stimulation only) (Figure 3D).

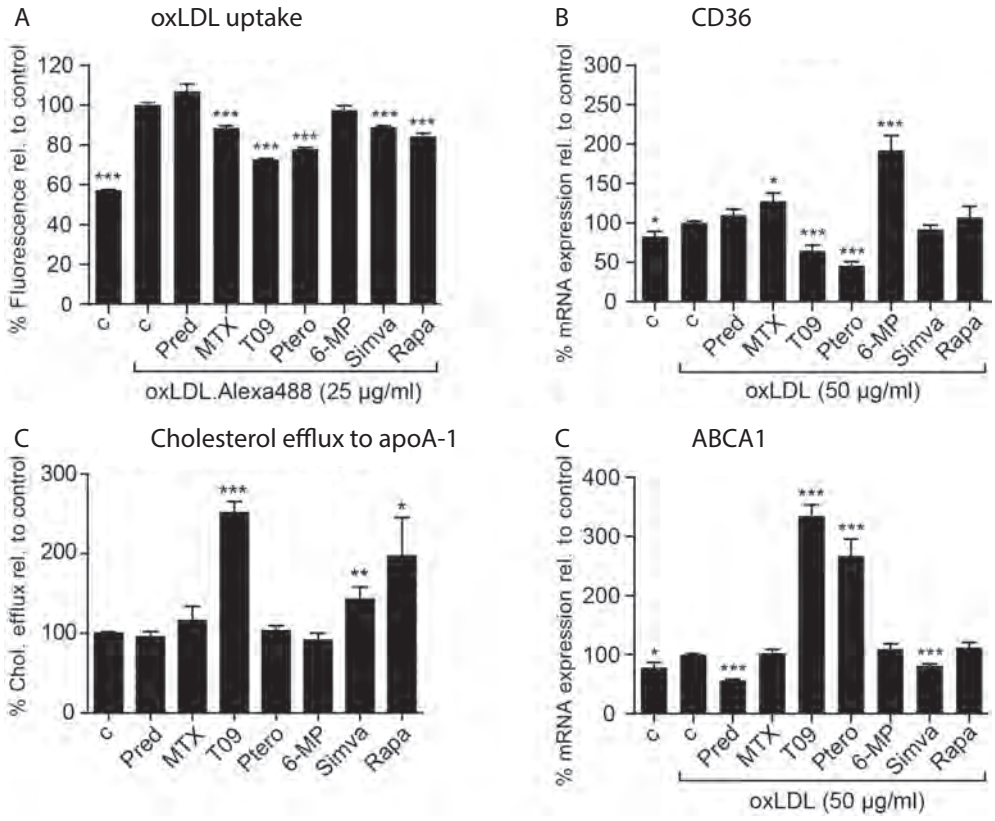

FIGURE 3. Macrophage lipid handling

THP-1 macrophages were treated with compounds and oxLDL-Alexa488 for 6 hrs (**A**) or oxLDL for 24 hrs (**B, D**). (**A**) OxLDL uptake was determined in protein lysates and by (**B**) mRNA expression of CD36 using qPCR. (**C**) Cholesterol efflux was measured by Tritium-labelled cholesterol loading and using ApoA1 as acceptor. (**D**) mRNA expression of ABCA1 was determined using qRT-PCR. Total mRNA input was corrected for the housekeeping gene 36B4. Fold change was calculated relative to oxLDL stimulation only from three independent experiments (n=3). Data are presented as mean±SEM; *p<0.05, **p<0.01, ***p<0.001 compared to oxLDL stimulation (**A, B, D**) or untreated cells (**C**). *6-MP indicates 6-mercaptopurine; c, control; MTX, methotrexate; pred, prednisolone; ptero, pterostilbene; rapa, rapamycin; simva, simvastatin; T09, T0901317.*

Endoplasmic reticulum (ER) stress

To examine whether the compounds affected macrophage ER stress, changes in mRNA expression of ER stress related proteins in THP-1 macrophages pre-exposed to oxLDL were assessed. As regulator of intracellular lipid trafficking[16-18] and lipid-induced ER stress[16-19], mRNA expression of lipid chaperone FABP4 was found to be significantly increased by 6-MP (p=0.002) and up to almost 2-fold by prednisolone (p<0.001) and 6-MP (p=0.002) treatment compared to oxLDL stimulation only, whereas T09 and pterostilbene markedly decreased FABP4 expression by 30-70% (both p<0.001) (Figure 4A).

Prolonged or unresolved ER stress can induce apoptosis mediated through CHOP and IRE1[20]. Compared to oxLDL treated control, mRNA expression of CHOP was most notably increased by treatment with T09 (>1000%), pterostilbene (>200%), 6-MP (75%) (all p<0.001); whereas prednisolone modestly decreased CHOP by 20% (p=0.002). MTX and simvastatin had no significant effects on CHOP expression (Figure 4B). IRE1 mRNA expression was strongly upregulated (50%) in response to prednisolone, T09, pterostilbene and rapamycin compared to oxLDL stimulation only, while modestly upregulated by MTX and 6-MP. Simvastatin treatment did not change IRE1 levels. (Figure 4C)

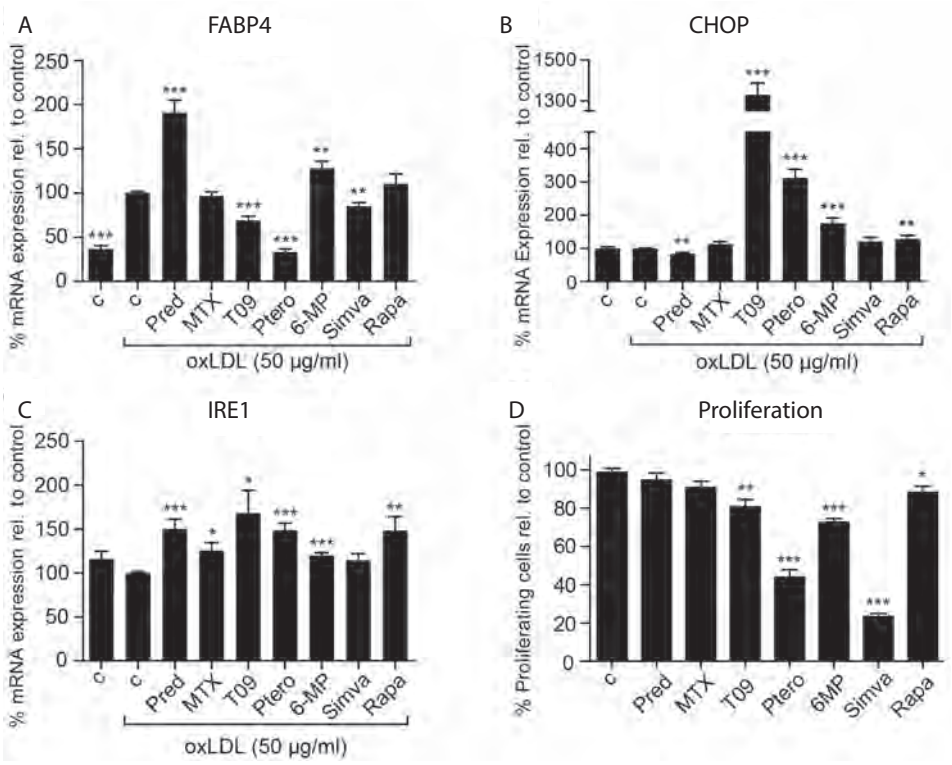

FIGURE 4. Macrophage oxLDL-induced ER-stress and macrophage proliferation

(**A-C**) To measure ER stress,THP-1 macrophages were treated with compounds and oxLDL for 24 hrs. mRNA was isolated, cDNA was made and qRT-PCR was performed for FABP4 (**A**), CHOP (**B**) and IRE1 (**C**). Total mRNA input was corrected for the housekeeping gene 36B4. (**D**) Macrophage proliferation was determined in RAW264.7 cells by BrdU-incorporation after an initial serum starvation. Proliferating cells were expressed as a percentage relative to untreated controls. Three independent experiments (each n=6) were performed. Data are presented as mean±SEM (**A-D**); *p<0.05, **p<0.01, ***p<0.001 compared to oxLDL stimulation (**A-C**) or untreated control (**D**). *6-MP indicates 6-mercaptopurine; c, control; MTX, methotrexate; pred, prednisolone; ptero, pterostilbene; rapa, rapamycin; simva, simvastatin; T09, T0901317.*

Macrophage proliferation

The proliferative capacity of macrophages after treatment was assessed using BrdU incorporation in RAW264.7 cells (Figure 4D). Simvastatin and pterostilbene demonstrated the strongest anti-proliferative effect by reducing the BrdU incorporation with 75% and 55% (both $p < 0.001$), respectively. T09, 6-MP and rapamycin also significantly inhibited cell proliferation, though to a less extent. MTX did not affect macrophage proliferation. In THP-1 cells fluorescence intensity was generally lower, as may be expected with this cell line. Still, a reduction pattern (≥50%) similar to RAW264.7 was observed for T09, pterostilbene and 6-MP (Figure S2E).

Overall drug performance

Finally, the outcomes of the assays were expressed in an atheroprotective or atherogenic score. The overall performance of each compound was assessed, with heterogeneous results between the different compounds and assays, largely in concordance with their mode of action. The constructed heatmap illustrates that T09, pterostilbene, and simvastatin were identified as highest scoring compounds for anti-atherosclerotic impact on plaque macrophages (Figure 5).

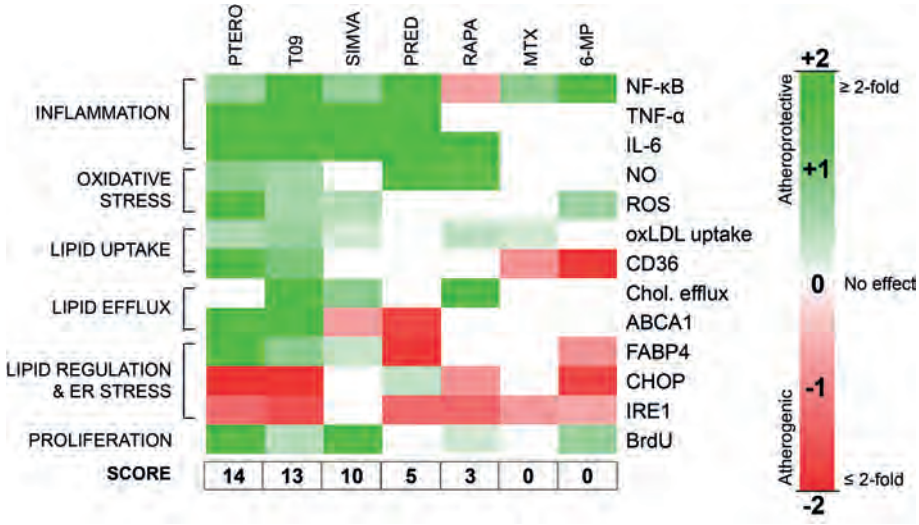

FIGURE 5. Summary

Results from each macrophage assay were expressed in fold change compared to stimulated controls to reflect an atheroprotective or atherogenic effect. A heatmap was generated in MultiArray viewer (MeV4.9.0). *6-MP indicates 6-mercaptopurine; MTX, methotrexate; pred, prednisolone; ptero, pterostilbene; rapa, rapamycin; simva, simvastatin; T09, T0901317.*

DISCUSSION

In this study, we assessed multiple macrophage-related pathways to evaluate the overall anti-atherogenic impact of several drug candidates. We focused on key mechanisms of macrophage activity in atherosclerotic plaques: inflammation, oxidative stress, lipid handling, ER stress and proliferation. Using a dedicated *in vitro* approach, we rated the overall performance of the 7 candidate drugs known to interfere in one or more of these pathways. The overall performance of the well-known anti-inflammatory corticosteroid prednisolone was found to be counterbalanced by pro-atherogenic effects, leading to a low anti-atherogenic score. Conversely, pterostilbene, T09 and simvastatin exhibited a strong overall anti-atherogenic performance in macrophages, exerting beneficial effects in multiple pathways at the same time, suggesting their potential for plaque macrophage-targeted liposomal delivery. *In vivo* validation studies are warranted to corroborate the predictive value of this macrophage-based screening approach and its potential value in compound selection for nanomedicinal delivery in cardiovascular patients.

We recently demonstrated successful liposomal delivery of prednisolone to plaque macrophages in patients with advanced atherosclerotic disease[9]. Prednisolone is a potent, anti-inflammatory compound, exerting pleiotropic effects on many signalling pathways via the glucocorticoid receptor, which is widely used to reduce inflammatory activity in both acute and chronic inflammatory diseases[21]. In patients with atherosclerosis we were, however, unable to show a reduction in overall plaque inflammatory activity with even a small increase in FDG-PET/CT signal, despite successful plaque delivery of the liposomal payload[9]. In our *in vitro* assays, we corroborate that prednisolone indeed potently inhibits inflammatory activity, including NF-κB activity and attenuation of inflammatory cytokines. Concomitantly, prednisolone has a strong adverse impact on lipid handling, as it reduced expression of ABCA1 and upregulated the lipotoxicity mediator FABP4. Moreover, prednisolone activated the ER stress pathways by increasing IRE1 levels. These findings imply unsuitability of prednisolone to exert an overall anti-atherogenic effects on macrophages in an atherosclerotic, lipid-rich environment.

From the selected variety of drug candidates, simvastatin, T09 and pterostilbene were identified to have a broad anti-atherogenic effect in our assays, attributed to their beneficial impact on inflammation, oxidative stress, lipid handling and proliferation.

Simvastatin has been widely acknowledged for its marked LDL-c lowering effect[22]. Previous studies have emphasized non-lipid *pleiotropic* effects of statins[23]. In the present study, we corroborate a spectrum of anti-atherogenic effects on macrophages. The potential relevance of these macrophage-related effects are supported by our recent findings using targeted delivery of statins to macrophages. Namely, statins packaged within reconstituted HDL were found to be delivered effectively to plaque macrophages[7], where statins were shown to exert potent anti-inflammatory[7] as well as anti-proliferative effects[24].

The LXR-agonist T09 has been previously shown to have strong anti-atherogenic effects mediated by both enhanced cholesterol efflux and suppression of inflammation[25-30]. Here, we

indeed establish these beneficial effects on both lipid handling and inflammation, as attested by the decrease in NF-κB activity, reduction of inflammatory cytokines, decrease in oxLDL uptake and increase in cholesterol efflux. The anti-atherogenic effect of T09 is further favoured by the observed reduction of oxidative stress and decrease in macrophage proliferation. However, clinical development has been hampered by adverse effects on hepatic lipogenesis, leading to hepatic steatosis and dyslipidemia. Local delivery to macrophages and/or development of novel LXR-agonists may overcome these drawbacks.

The evaluation of pterostilbene (and its analogue resveratrol) in atherogenesis has so far been limited. Pterostilbene has been attributed a wide range of beneficial effects in various medical settings, including cancer prevention and therapy, neurological decline, and metabolic syndrome[31]. We here show the anti-atherogenic potential of pterostilbene on several macrophage activities. Pterostilbene suppresses inflammation by decreasing NF-κB activity strongly inhibiting the release of inflammatory cytokines, decreases oxidative stress by potently lowering NO and ROS production, beneficially affects lipid handling, and decreases macrophage proliferation. Together with some preliminary experimental studies showing that oral supplementation of resveratrol may reduce atherosclerosis[32-36], this favourable *in vitro* profile paves the way for further exploration of pterostilbene in a macrophage-targeted therapy approach.

Remarkably, we observed discrepancies between ABCA1 expression and cholesterol efflux after simvastatin and pterostilbene treatment. Although reduced ABCA1 expression may be expected based on statin-mediated inhibitory effects on LXR and SREBP-2 pathways[37], the increase in cholesterol efflux to apoA-1 was not expected. Previous studies do not corroborate such a divergent effect[37-39]. These results underline the complexities of lipid metabolism in macrophages and that mRNA expression does not equal downstream functionality. In addition, pterostilbene treatment resulted in up regulation of ABCA1, although the cholesterol efflux assay unexpectedly did not show an increase. While data on pterostilbene in current literature is lacking, its analogue resveratrol has shown similar effects on ABCA1 expression[40], however this was indeed coupled with an increase in cholesterol efflux[41-42]. Further investigations are warranted to assess whether pterostilbene has inherently different effects on cholesterol efflux than resveratrol, or that this is due to differences in experimental setup.

Despite demonstrating clear *prednisolone-like* anti-inflammatory effects, we find that 6-MP and MTX fail to convince in our *in vitro* screening as anti-atherogenic compounds, considering their lack of efficacy in non-inflammatory pathways. Preclinical work for 6-MP in atherosclerosis has so far been scarce[43] and reports from clinical use in inflammatory disorders lean towards an increased cardiovascular risk[44-46]. In contrast, MTX is seen as a viable compound for atherosclerosis. Currently, a low-dose of MTX is being evaluated as add-on therapy in cardiovascular patients in the Cardiovascular Inflammation Reduction Trial (CIRT)[47]. Even though MTX did not cumulate any points in our heatmap, overall it appears to be a relatively neutral compound without any excessive atherogenic pathway effects. With this

in mind, we await with interest the results of CIRT; although not specifically plaque targeted, these results will add to our understanding of the value and relative contribution of the separate pathways in our assays.

Similar to MTX, rapamycin also exhibited a generally neutral effect in our assays with a low total score. While already applied for over a decade in drug eluting coronary stents, targeted delivery strategies seem to be underway[48-49] following anti-atherogenic efficacy in mice models of atherosclerosis[50-57.]

Our study has several limitations. First, we assess the effects of the compounds only on macrophage activity, thereby disregarding potentially beneficial or harmful effects on other relevant plaque cell types, such as endothelial cells, smooth muscle cells and immune cells other than macrophages[2]. However, since we intend to employ a targeted drug delivery system based on endothelial permeability and phagocytosis, it is reasonable to expect the largest and most relevant impact on plaque macrophages. In addition, we used compounds in their free (unencapsulated) form in our macrophage assays. As a next step, experiments using encapsulated formulations of promising compounds are to be performed to assess any additional effects of the delivery vehicle itself. Lastly, we use only *in vitro* tests, mimicking an atherogenic environment by adding atherogenic factors such as oxLDL to monocyte/macrophage cell lines. However, the extrapolation of *in vitro* tests towards clinical impact remains to be established. Hence, *in vivo* validation testing is warranted to determine the value of our screening assays as a translational tool in atherosclerotic disease. Thus far, earlier *in vivo* experiments with nanodelivery of simvastatin[7] and prednisolone[9] appear to be in agreement with our *in vitro* data, hinting at the feasibility of the currently employed *in vitro* testing strategy.

Nanomedicinal drug delivery has the potential to take cardiovascular disease management to the next level. Transitioning from previous work in which we focused on targeting inflammation as the main driver behind atherosclerosis, the current study clearly underlines the need to broaden our focus and take a wide array of macrophage-related processes into account for nanomedicinal drug development. Out of a variety of drug candidates, we identified T09, pterostilbene and simvastatin as potential anti-atherogenic compounds for plaque macrophage targeted therapy. Our current assay setup provides a promising framework for high-throughput screening, as it offers a rapid and comprehensive method to simultaneously screen multiple drug candidates for their anti-atherogenic potency. We envision our work will facilitate the process of bringing novel cardiovascular treatment strategies from bench to bedside.

Acknowledgements: We like to thank Alinda Schimmel for her assistance in the efflux experiments.

Disclosures and funding: This work was supported by a European Framework Program 7 grant (ESS, GS: FP7-Health 309820: Nano-Athero); the Dutch network for Nanotechnology NanoNext NL, in the subprogram "Drug Delivery". All other authors declare that they have no conflict of interest and no relationships with industry relevant to this study.

REFERENCES

1. Mozaffarian D et al. Heart Disease and Stroke Statistics-2015 Update: A Report From the American Heart Association. Circulation 2014;131:29–322.
2. Libby P. Inflammation in atherosclerosis. Nature 420:868–74.
3. Fulcher J et al. Efficacy and safety of LDL-lowering therapy among men and women: meta-analysis of individual data from 174 000 participants in 27 randomised trials. Lancet 2015;385:1397-405.
4. Libby P. The forgotten majority: unfinished business in cardiovascular risk reduction. J Am Coll Cardiol 2005;46:1225–8.
5. Tiwari RL et al. Macrophages: an elusive yet emerging therapeutic target of atherosclerosis. Med Res Rev 2008;28:483–544.
6. Lobatto ME et al. Perspectives and opportunities for nanomedicine in the management of atherosclerosis. Nat Rev Drug Discov 2011;10:835–52.
7. Duivenvoorden R et al. A statin-loaded reconstituted high-density lipoprotein nanoparticle inhibits atherosclerotic plaque inflammation. Nat Commun 2014;5:3065.
8. Lobatto ME et al. Multimodal clinical imaging to longitudinally assess a nanomedical anti-inflammatory treatment in experimental atherosclerosis. Mol Pharm 2010;7:2020–9.
9. Van der Valk FM et al. Prednisolone-containing liposomes accumulate in human atherosclerotic macrophages upon intravenous administration. Nanomedicine 2015;11:1039-1046.
10. Qin Z et al. The use of THP-1 cells as a model for mimicking the function and regulation of monocytes and macrophages in the vasculature. Atherosclerosis 2012;221:2–11.
11. Groeneweg M et al. Lipopolysaccharide-induced gene expression in murine macrophages is enhanced by prior exposure to oxLDL. J Lipid Res 2006;47:2259–67.
12. Hamers AAJ et al. Bone marrow-specific deficiency of nuclear receptor Nur77 enhances atherosclerosis. Circ Res 2012;110:428–38.
13. Sylvester PW et al. Optimization of the tetrazolium dye (MTT) colorimetric assay for cellular growth and viability. Methods Mol Biol 2011;716:157–68.
14. Fang FC andVazquez-Torres A. Nitric oxide production by human macrophages: there's NO doubt about it. Am J Physiol Lung Cell Mol Physiol 2002;282:941–3.
15. Auwerx J et al. Changes in IgG Fc receptor expression induced by phorbol 12-myristate 13-acetate treatment of THP-1 monocytic leukemia cells. Leuk Res 1992;16:317–27.
16. Saksi J et al. Low-expression variant of fatty acid-binding protein 4 favors reduced manifestations of atherosclerotic disease and increased plaque stability. Circ Cardiovasc Genet 2014;7:588–98.
17. Makowski L et al. Lack of macrophage fatty-acid-binding protein aP2 protects mice deficient in apolipoprotein E against atherosclerosis. Nat Med 2001;7:699–705.
18. Layne MD et al. Role of macrophage-expressed adipocyte fatty acid binding protein in the development of accelerated atherosclerosis in hypercholesterolemic mice. FASEB J 2001;15:2733–5.
19. Erbay E et al. Reducing endoplasmic reticulum stress through a macrophage lipid chaperone alleviates atherosclerosis. Nat Med 2009;15:1383–91.
20. Scull CM and Tabas I. Mechanisms of ER stress-induced apoptosis in atherosclerosis. Arterioscler Thromb Vasc Biol 2011;31:2792–7.
21. Rhen T and Cidlowski JA. Anti-inflammatory action of glucocorticoids--new mechanisms for old drugs. N Engl J Med 2005;353:1711–23.
22. Baigent C et al. Efficacy and safety of cholesterol-lowering treatment: prospective meta-analysis of data from 90,056 participants in 14 randomised trials of statins. Lancet 2005;366:1267–78.

23. Liao JK and Laufs U. Pleiotropic effects of statins. Annu Rev Pharmacol Toxicol 2005;45:89–118.
24. Tang J et al. Inhibiting macrophage proliferation suppresses atherosclerotic plaque inflammation. Sci Adv 2015;1:1400223.
25. Grefhorst A et al. Stimulation of lipogenesis by pharmacological activation of the liver X receptor leads to production of large, triglyceride-rich very low density lipoprotein particles. J Biol Chem 2002;277:34182–90.
26. Terasaka N et al. T-0901317, a synthetic liver X receptor ligand, inhibits development of atherosclerosis in LDL receptor-deficient mice. FEBS 2003;536:6–11.
27. Verschuren L et al. LXR agonist suppresses atherosclerotic lesion growth and promotes lesion regression in apoE*3Leiden mice: time course and mechanisms. J Lipid Res 2009;50:301–11.
28. Honzumi S et al. Synthetic LXR agonist inhibits the development of atherosclerosis in New Zealand White rabbits. Biochim Biophys Acta 2011;1811:1136–45.
29. Chen J et al. Liver X receptor activation attenuates plaque formation and improves vasomotor function of the aortic artery in atherosclerotic ApoE(-/-) mice. Inflamm Res 2012;61:1299–307.
30. Srivastava RAK et al. Evaluation of anti-atherosclerotic activities of PPAR-α, PPAR-γ, and LXR agonists in hyperlipidemic atherosclerosis-susceptible F(1)B hamsters. Atherosclerosis 2011;214:86–93.
31. Estrela JM et al. Pterostilbene: Biomedical applications. Crit Rev Clin Lab Sci 2013;50:65–78.
32. Wang Z et al. Dealcoholized red wine containing known amounts of resveratrol suppresses atherosclerosis in hypercholesterolemic rabbits without affecting plasma lipid levels. Int J Mol Med 2005;16:533–40.
33. Do G-M et al. Long-term effects of resveratrol supplementation on suppression of atherogenic lesion formation and cholesterol synthesis in apo E-deficient mice. Biochem Biophys Res Commun 2008;374:55–9.
34. Matos RS et al. Resveratrol causes antiatherogenic effects in an animal model of atherosclerosis. Arq Bras Cardiol 2012;98:136–42.
35. Berbée JFP et al. Resveratrol protects against atherosclerosis, but does not add to the antiatherogenic effect of atorvastatin, in APOE*3-Leiden.CETP mice. J Nutr Biochem 2013;24:1423–30.
36. Tomayko EJ et al. Resveratrol supplementation reduces aortic atherosclerosis and calcification and attenuates loss of aerobic capacity in a mouse model of uremia. J Med Food 2014;17:278–83.
37. Niesor EJ et al. Statin-induced decrease in ATP-binding cassette transporter A1 expression via microRNA33 induction may counteract cholesterol efflux to high-density lipoprotein. Cardiovasc Drugs Ther 2015;29:7–14.
38. Qiu G et al.Atorvastatin inhibits ABCA1 expression and cholesterol efflux in THP-1 macrophages by an LXR-dependent pathway. J Cardiovasc Pharmacol 2008;51:388–95.
39. Wong J et al. Statins inhibit synthesis of an oxysterol ligand for the liver x receptor in human macrophages with consequences for cholesterol flux. Arterioscler Thromb Vasc Biol 2004;24:2365–71.
40. Sevov M et al. Resveratrol regulates the expression of LXR-alpha in human macrophages. Biochem Biophys Res Commun 2006;348:1047–54.
41. Allen AM et al. Mitochondrial function is involved in regulation of cholesterol efflux to apolipoprotein (apo)A-I from murine RAW 264.7 macrophages. Lipids Health Dis 2012;11:169.
42. Voloshyna I et al. Resveratrol mediates anti-atherogenic effects on cholesterol flux in human macrophages and endothelium via PPARγ and adenosine. Eur J Pharmacol 2013;698:299–309.
43. Pols TWH et al. 6-mercaptopurine inhibits atherosclerosis in apolipoprotein e*3-leiden transgenic mice through atheroprotective actions on monocytes and macrophages. Arterioscler Thromb Vasc Biol 2010;30:1591–7.
44. Solomon DH et al. Immunosuppressive medications and hospitalization for cardiovascular events in patients with rheumatoid arthritis. Arthritis Rheum 2006;54:3790–8.
45. Vanrenterghem YFC et al. Risk factors for cardiovascular events after successful renal transplantation. Transplantation 2008;85:209–16.
46. Haque S et al. Risk factors for clinical coronary heart disease in systemic lupus erythematosus: the lupus and atherosclerosis evaluation of risk (LASER) study. J Rheumatol 2010;37:322–9.
47. Everett BM et al. Rationale and design of the Cardiovascular Inflammation Reduction Trial: a test of the inflammatory hypothesis of atherothrombosis. Am Heart J 2013;166:199–207.

48. Miao Z-L et al. Preparation of a liposomal delivery system and its in vitro release of rapamycin. Exp Ther Med 2015;9:941–6.
49. Kilroy JP et al. Reducing Neointima Formation in a Swine Model with IVUS and Sirolimus Microbubbles. Ann Biomed Eng 2015.
50. Beutner F et al. Effect of everolimus on pre-existing atherosclerosis in LDL-receptor deficient mice. Atherosclerosis 2012;222:337–43.
51. Waksman R et al. Oral rapamycin inhibits growth of atherosclerotic plaque in apoE knock-out mice. Cardiovasc Radiat Med 4:34–8.
52. Zhao L et al. Low-dose oral sirolimus reduces atherogenesis, vascular inflammation and modulates plaque composition in mice lacking the LDL receptor. Br J Pharmacol 2009;156:774–85.
53. Mueller MA et al. Prevention of atherosclerosis by the mTOR inhibitor everolimus in LDLR-/- mice despite severe hypercholesterolemia. Atherosclerosis 2008;198:39–48.
54. Pakala R et al. Rapamycin attenuates atherosclerotic plaque progression in apolipoprotein E knockout mice: inhibitory effect on monocyte chemotaxis. J Cardiovasc Pharmacol 2005;46:481–6.
55. Castro C et al. Rapamycin attenuates atherosclerosis induced by dietary cholesterol in apolipoprotein-deficient mice through a p27 Kip1 -independent pathway. Atherosclerosis 2004;172:31–8.
56. Basso MD et al. Effect of sirolimus on the cholesterol content of aortic arch in ApoE knockout mice. Transplant Proc 2003;35:3136–8.
57. Elloso MM et al. Protective effect of the immunosuppressant sirolimus against aortic atherosclerosis in apo E-deficient mice. Am J Transplant 2003;3:562–9.

SUPPLEMENT

TABLE S1. Human primer sequences for semi-quantitative real-time PCR

Gene	Forward primer sequence (5′-3′)	Reverse primer sequence (5′-3′)
36B4	ACGGGTACAAACGAGTCCTG	GCCTTGACCTTTTCAGCAAG
CD36	TGCAAAATCCACAGGAAGTG	CAGCGTCCTGGGTTACATTT
ABCA1	ATGAGGACAACAACTACAAAGCC	GGGAAAGAGGACTAGACTCCAAA
FABP4	AGCACCATAACCTTAGATGGGG	CGTGGAAGTGACGCCTTTCA
CHOP	TTGCCTTTCTCCTTCGGGAC	GATTCTTCCTCTTCATTTCCAGGAG
IRE1	GAAGCATGTGCTCAAACACC	TCTGTCGCTCACGTCCTG

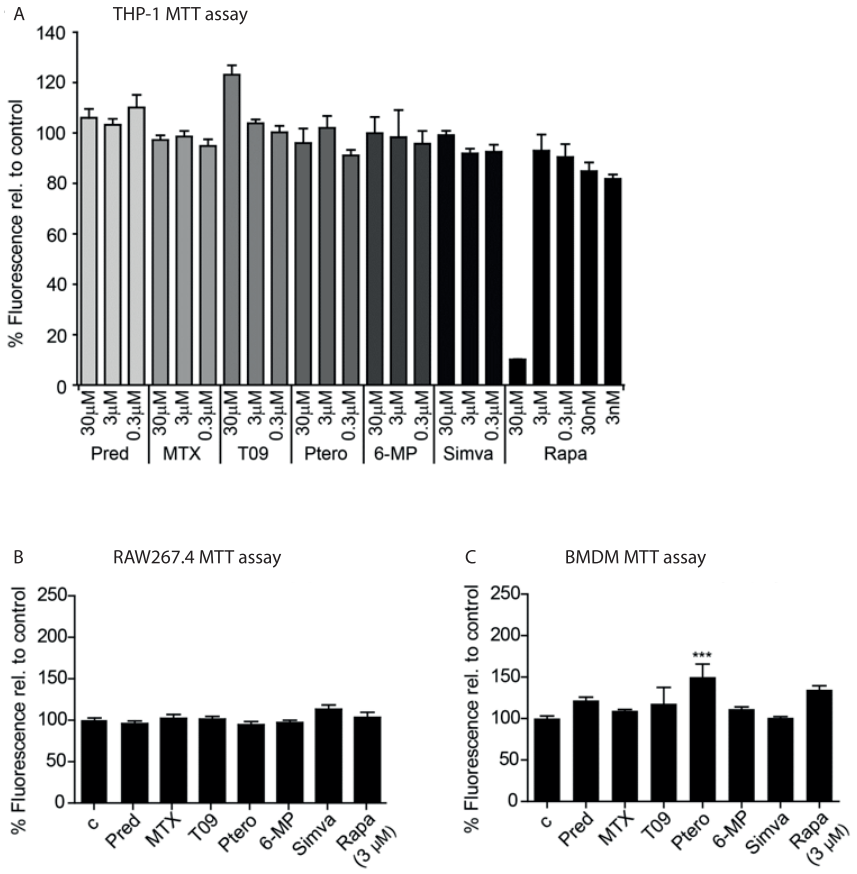

FIGURE S1. Cell viability

Cell viability for (**A**) THP-1, (**B**) RAW cells and (**C**) BMDM was determined by measuring active mitochondria using MTT. Cell viability was calculated as a percentage from untreated cells. A 50% decrease in fluorescence was considered toxic. Data was combined from two independent experiments (n=5) and are presented as mean±SEM; *p<0.05, **p<0.01, ***p<0.001 compared to control. *c = control; Pred = prednisolone; MTX = methotrexate; T09 = T0901317; Ptero = pterostilbene; 6-MP = 6-mercaptopurine; Simva = simvastatin; Rapa = rapamycin.*

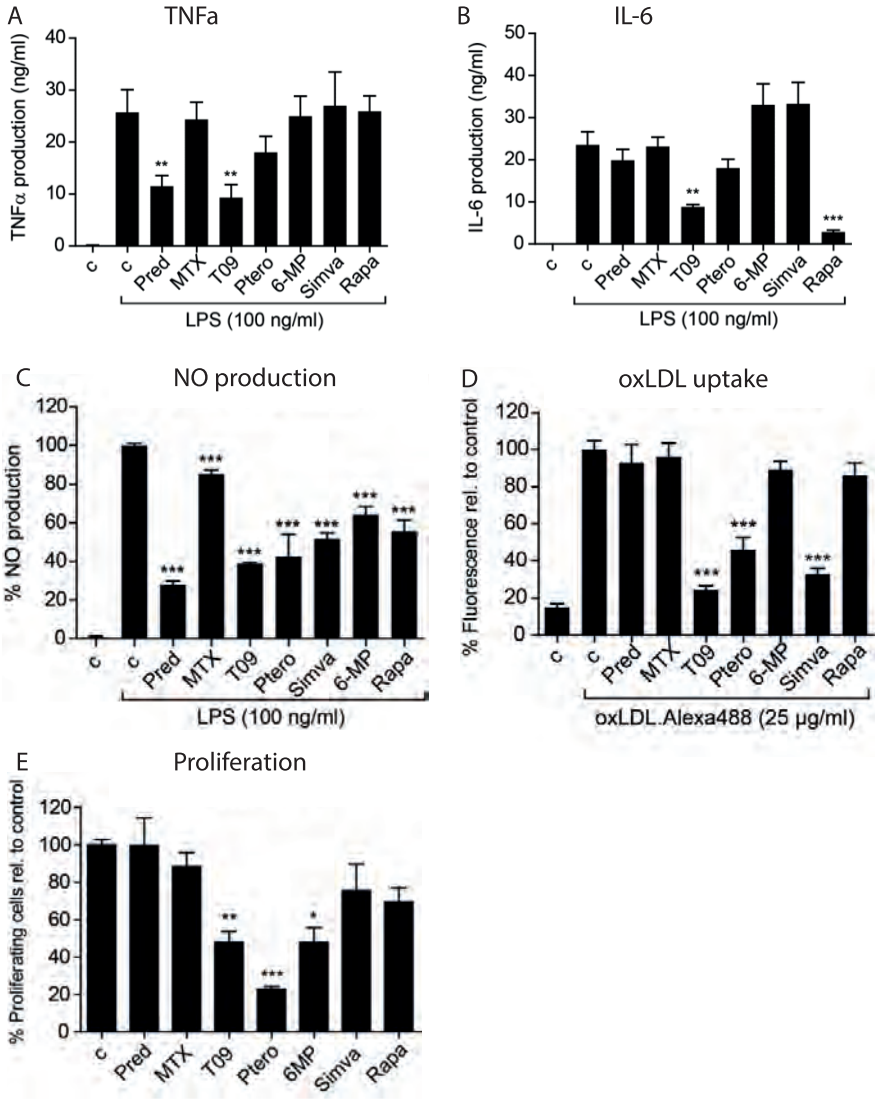

FIGURE S2. Pro-inflammatory cytokines

(**A-B**) Bone marrow derived macrophages (BMDM) were treated with the compounds and stimulated with LPS (100 ng/ml) for 24 hrs. TNF-α and IL-6 production was measured using a cytometric bead array, compared to LPS stimulation only. (**C**) BMDM were treated with the compounds and stimulated with LPS (100 ng/ml) for 24 hrs after which nitric oxide (NO) production was determined with Griess reagent, fold change was calculated relative to LPS stimulation. (**D**) THP-1 macrophages were treated with compounds and oxLDL-DyLight488 for 24 hrs and oxLDL uptake was determined in protein lysates, fold change was calculated relative to oxLDL stimulation only. (**E**) Macrophage proliferation was determined in THP-1 cells by BrdU-incorporation after an initial serum starvation. Proliferating cells were expressed as a percentage relative to untreated controls. Data are presented as mean±SEM. $p<0.05$, $^{**}p<0.01$, $^{***}p<0.001$. *c = control; Pred = prednisolone; MTX = methotrexate; T09 = T0901317; Ptero = pterostilbene; 6-MP = 6-mercaptopurine; Simva = simvastatin; Rapa = rapamycin.*

CHAPTER 12

SUMMARY, INTERPRETATION AND FUTURE PERSPECTIVES

Van der Valk FM

SUMMARY AND INTERPRETATION

The translation of lipid-driven inflammation in atherosclerosis is the central theme of this thesis. **Chapter 1** provides the general introduction by pointing out the clinical and societal need for an improved understanding on atherosclerosis. Whereas in the 20th century atherosclerosis research mainly focuses on lipoproteins and cholesterol, today we recognize the elementary contribution of inflammatory processes throughout all stages of atherogenesis. Yet, most advances on inflammation's role in atherosclerosis have been made in the preclinical realm. In three parts, this thesis aims to translate the systemic increased inflammatory activity, its response to atherogenic lipoproteins, and the potential of targeted anti-inflammatory therapies in patients with atherosclerosis.

Part I - Imaging inflammatory network in atherosclerosis

The first part of this thesis illustrates the increased inflammatory activity present in multiple compartments in patients with atherosclerosis, visualized with functional imaging. Positron emission tomography with computed tomography (PET/CT) is a nuclear technique that employs radioactive tracers, such as the glucose analogue ^{18}F-fluorodeoxyglucose (^{18}F-FDG). Uptake of this tracer marks cellular glucose consumption, and as such, the metabolic need of a cell. Several cell types are known for their high metabolic demands, including proliferative and inflammatory cells. Considering the large number of inflammatory cells in plaques, predominantly macrophages, ^{18}F-FDG PET/CT is also an attractive strategy in atherosclerosis. In fact, several histological, plaque gene expression and biomarker studies have validated arterial ^{18}F-FDG uptake as a surrogate for (macrophage-driven) inflammation[1].

In **chapter 2** we question whether and to what extent PET can be used as a reliable method to non-invasively assess arterial wall inflammation in humans. To this end, we include 83 individuals comprising of 25 healthy subjects, 23 patients at risk and 35 patients with atherosclerosis. First, we show that ^{18}F-FDG uptake metrics (expressed as the target to background ratio, TBR) gradually increase from healthy to diseased subjects. This indicates that arterial wall inflammation can serve both as an early indicator (patients at risk) and as an advanced indicator (patients with atherosclerotic events) of disease severity. Second, we determine what degree of ^{18}F-FDG uptake in the arterial wall is to be considered pathological. Assuming ^{18}F-FDG uptake in the arterial wall of healthy subjects to represent normal, physiological uptake, we determine thresholds to identify inflamed arterial walls. Of note, these thresholds are exceeded by the vast majority of patients with atherosclerosis (>86%), or only risk factors for it (>78%), despite the standard of care. These data exemplify the therapeutic window for anti-inflammatory strategies in atherosclerosis. Hence, this chapter also emphasizes the opportunities for ^{18}F-FDG PET/CT to select patients suitable for future interventions and provide reproducible readout metrics in relative small-scaled studies.

Next to arterial wall inflammation, **chapter 3** describes the continuous accumulation of circulating immune cells, peripheral blood mononuclear cells (PBMCs), to atherosclerotic plaques in patients. For this purpose, PBMCs are isolated from the blood, labelled with the radiolabel ^{99m}technetium (^{99m}Tc), re-infused into the subject and trafficked using single photon emission computed tomography co-registered with computed tomography (SPECT/CT). As a validation step, we first confirm that the isolation and labelling procedures not significantly affect the migratory and adhesive capacity of PBMCs via flow cytometric and migration assays. Subsequently, SPECT/CT imaging is performed in 5 healthy controls and 10 patients with advanced atherosclerotic plaques, as evidenced by magnetic resonance imaging (MRI) and ^{18}F-FDG PET/CT imaging. In this chapter we objectify, for the first time, a rapid and marked accumulation of immune cells in atherosclerotic plaques of patients, expressed as the arterial-wall-to-blood-ratio (ABR). An important finding is that the rate of PBMCs accumulation does not correlate with arterial wall thickness, as assessed with MRI, whereas it does with arterial wall inflammation on PET (r=0.88). These observations emphasize the difference between plaque burden and plaque biology, also indicating the room for improvement of risk stratification when refining conventional imaging with functional techniques to detail plaque composition and function. Next to arterial wall metrics, the level of low density lipoprotein cholesterol (LDL-c) correlates with PBMCs accumulation (r=0.77); an interaction that is further examined in the second part of this thesis. Taken together, we here show that also beyond the initiation phase, circulating immune cells are involved in much more advanced stages of atherogenesis. Whether these freshly influxed contribute to the plaque cell content (macrophages) or only serve as signaling molecules warrants further cell-trafficking studies[2].

In **chapter 4** we subsequently set out to evaluate whether the production sites of immune cells, comprising bone marrow and spleen, are also affected in atherosclerosis. In this translational work, we first visualize the increased uptake of ^{18}F-FDG in not just the arterial wall, but also in bone marrow and spleen as assessed with PET/CT imaging in 26 atherosclerosis patients compared with 25 controls. Whereas previously an increased activity of the hematopoietic system has been described in the setting of an acute myocardial infarction[3], these findings indicate that, in patients with atherosclerosis, hematopoietic tissues are chronically active. To study this phenomenon at a cellular level, we screen a cohort of 953 cancer patients in whom hematopoietic stem and progenitor cells (HSPCs) have been harvested via granulocyte-colony stimulating factor (G-CSF) in the context of an autologous stem cell transplantation. In this cohort we identify 18 patients with atherosclerosis and 30 matched controls. Retrospectively, we find that the HSPCs of atherosclerosis patients have a 1.6-fold higher progenitor potential (expressed as the colony forming units-granulocyte/monocyte; CFU-GM capacity) compared with controls. Tentatively, this finding could imply that the enhanced hematopoietic ^{18}F-FDG uptake in patients represents an increased proliferative rate of HSPCs. Alternatively, when taking a closer look at the SPECT images of the previous chapter, one can observe an increased immune cell signal in the bone marrow of patients compared with controls, suggesting that

an increased presence of inflammatory cells might also explain the bone marrow ^{18}F-FDG signal.

Finally, this chapter describes an *in vitro* experiment studying the effect of (oxidized) lipids on healthy donor HSPCs. In line with the correlation between hematopoietic tissue ^{18}F-FDG uptake, LDL-c (r=0.72) and monocytes (r=0.18) in patients, we find that the CFU-GM capacity of healthy HSPCs is 1.5-fold higher after co-incubation with oxidized LDL (oxLDL), also obtaining a myeloid differentiation bias *in vitro*. These data support the concept that predominantly oxidized lipids transduce the broad range of inflammatory responses in atherogenesis[4]. To paraphrase the first part of this thesis, patients with atherosclerosis have an increased multilevel inflammatory strain proportional to their lipids levels; an interplay that is further explored in the succeeding part of this thesis.

Part II - The impact of lipids on atherosclerotic inflammation

Having witnessed the correlations between lipids and inflammation in plaque, plasma and progenitors, the second part of this thesis further investigates the direct impact of atherogenic lipoproteins on inflammation by integrating functional imaging with immunological assays. First, we focus our attention on LDL-c; the bad cholesterol.

Chapter 5 is a multi-center, intervention study demonstrating the direct contribution of LDL-c on arterial wall inflammation in patients suffering from familial hypercholesterolemia (FH). Baseline ^{18}F-FDG PET/CT imaging shows that FH patients (n=24) have increased arterial wall inflammation, correlating to their LDL-c levels (r=0.52), compared with control subjects (n=14). Subsequently, half of the FH patients undergoes lipoprotein-apheresis, on average reducing LDL-c levels by 51±23%. An important finding is that concomitantly arterial wall inflammation decreases with 11.8±14.2%. In other words, each 10% reduction in LDL-c via apheresis, induces a 2% reduction in arterial wall inflammation. Contrary to the concept of pleiotropic, anti-inflammatory effects induced by statins on top of lipid lowering[5], these data imply that LDL-c reduction directly affects arterial wall inflammation. Interestingly, we find that the decreased arterial wall inflammation does not translate into lower levels of C-reactive protein (CRP), indicating that this generalized marker of inflammation might fail to reflect the inflammatory activity at the level of the arterial wall[6]. The latter might even imply that the lack of CRP change following lipid lowering by proprotein convertase subtilisin/kexin type 9 (PCSK9) antibodies[7], does not mean that no improvement of arterial wall inflammation or eventually outcome of PCSK9 inhibition is to be expected. Finally, in view of the rapid reduction within just 5 days after lipid-apheresis, this study shows that arterial wall inflammation in patients is susceptible to improvement.

Supplementary to the increased (macrophage-driven) arterial inflammation, **chapter 6** studies monocytes (the precursors of macrophages) in FH patients. In this observational study we characterize the monocytes of 11 healthy controls and 38 FH patients, of whom 16 not

on therapy, 11 on statins and 12 receiving PCSK9 antibodies. First, we find a proinflammatory phenotype of monocytes harvested from FH patients compared with those from healthy controls, as evidenced by flow cytometric and gene expression assays. These data imply that indeed LDL-c has a direct inflammatory effect on immune cells, already in the plasma compartment. In addition, we show that monocytes of FH patients with reduced LDL-c levels show an improvement of their phenotype, independent of the drug inducing LDL-c lowering (e.g. statins or PCSK9 inhibition). Again these findings stress that lipid lowering itself, and not just a pleiotropic effect of statins, silences the inflammatory phenotype of immune cells in atherosclerosis. In addition, these findings give PCSK9 therapy the opportunity to counterbalance their lack of CRP reduction with decreased monocyte activation

Next to the well-described LDL particle, in **chapter 7** we propose a novel inflammatory route for lipoprotein (a) [Lp(a)], which is a plasma lipoprotein composed of apolipoprotein(a) [apo(a)] bound to apolipoprotein B-100 (apoB). Whereas Lp(a) is elevated in one-fifth of the general community and described as a causal atherosclerotic risk factor, its pathogenic mechanisms have remained unresolved. In this chapter we include 30 subjects with elevated Lp(a) and 30 matched controls with normal Lp(a) levels. Proportional to their Lp(a) levels, these subjects have increased arterial wall inflammation quadrated by an increased immune cell accumulation *in vivo*, as assessed with the functional imaging approaches described in Part I. Of note, functional inflammatory measures of the arterial wall did not correlate with structural arterial wall metrics, which might imply that Lp(a) increases cardiovascular event risk by enhancing plaque vulnerability rather than accelerating plaque burden. Moreover, monocytes isolated from subjects with high Lp(a) exhibit a long-lasting primed state, evidenced by an increased capacity to transmigrate endothelium, and to produce inflammatory cytokines. Further, *in vitro* studies unravel that oxidized phospholipids (OxPL), which are preferentially carried by Lp(a) in the plasma, are obligatory mediators in the increased monocyte responsiveness. These OxPL can be considered as danger signals recognized by multiple innate pattern recognition receptors (PRRs) on myeloid cells. In line with other pathogen- and danger-associated signals previously described to prime monocytes via epigenetic alterations[8], our findings suggest that a similar epigenetic phenomenon might transduce the effects of OxPL and Lp(a).

To summarize the major findings in part II, atherogenic lipids and its associated oxidized phospholipid content directly affect inflammation both at the level of the arterial wall as the circulating cells in the plasma compartment. Considering the increased inflammatory activity in patients, despite standard of care including lipid lowering, the final part of this thesis addresses inflammation as a potential additional target in atherosclerosis.

Part III - Therapeutic targeting of inflammation in atherosclerosis

Notwithstanding the spectacular success of statin therapy, even in the best of scenario - the controlled clinical trial - two thirds of the patients still experience major cardiovascular events[9]. In view of excess inflammation in the majority of patients, as described in this thesis, the final part discusses inflammation as therapeutic target in atherosclerosis.

Chapter 8 reviews anti-inflammatory therapies in atherosclerosis, discussing their potential benefits and drawbacks. Two of the most advanced strategies, currently in ongoing phase III trials, comprise the cardiovascular inflammation reduction trial (CIRT) using low-dose methotrexate and the canakinumab anti-inflammatory thrombosis outcomes study (CANTOS) addressing the impact of interleukin 1 inhibition. The outcome of these studies will color the horizon for anti-inflammatory strategies in cardiovascular patients (expected in 2017-2019). In addition, this review envisions non-invasive imaging modalities to aid future drug development studies by means of patient selection and surrogate endpoint studies. Long-term and systemic use of immunosuppressive drugs in patients with atherosclerosis, however, might be complicated by severe side effects. Hence, this chapter underscores the need for selective and targeted immunomodulation in atherosclerosis.

In pursuit of the latter, nanotechnology offers opportunities for targeted drug delivery in atherosclerosis[10]. In **chapter 9** we describe our efforts concerning the first anti-inflammatory nanomedicinal approach in patients with atherosclerosis, hypothesizing that local exposure to prednisolone will silence plaque inflammation. First, a pharmacokinetic study shows that liposomal encapsulation of prednisolone (in short LN-PLP) makes its plasma half-life 7 to 15-fold longer. The latter is a prerequisite for nonspecific drug targeting in atherosclerosis; long circulating particles eventually accumulate at sites of enhanced permeability in the arterial wall - typical of atherosclerosis[11]. Indeed, we find that the liposomal nanoparticles appear in 75% of plaque macrophages isolated from 7 patients, who received LN-PLP infusions twice. Strengthened by the confirmed macrophage targeting, we next question whether local exposure of prednisolone to plaque macrophages can decrease the inflammatory activity of atherosclerosis. Counter intuitively though, this randomized placebo-controlled efficacy study shows that LN-PLP is not suited for patients with atherosclerosis. After two LN-PLP infusions, the arterial wall permeability is unaltered, however, the arterial wall inflammation increases with 7% in just 12 days in 20 patients compared with 10 receiving placebo, as assessed with multimodal imaging. At that time, we are faced with the fact that the negative outcome in patients diametrically opposes previous LN-PLP work in an experimental model of atherosclerosis in rabbits[12].

Therefore, we aim to unravel why liposomal prednisolone increases arterial wall inflammation in patients in **chapter 10**. To this end, we first study the effect of LN-PLP in another experimental model of more chronically induced atherosclerosis; the low-density lipoprotein receptor knockout ($LDLr^{-/-}$) mice, characterized by lipid- and macrophage-rich plaques. Initially, we find an increased number of monocytes in the plaque after LN-PLP infusions for 2 weeks. In line

with these early proinflammatory effects, we subsequently show that prolonged exposure to LN-PLP for 6 weeks induces more advanced plaque stages; evidenced by a larger necrotic core size and macrophage number. The latter is of specific interest considering the observed increase in arterial ^{18}F-FDG uptake in patients (chapter 9), a marker of macrophage content[1]. Succeeding *in vitro* studies in both murine and human macrophages show that prednisolone polarizes inflammatory macrophages towards a reparative phenotype. However, the latter phenotype is also more prone to lipid loading, resulting in ER stress with subsequent apoptosis. Considering the high lipid-burden in atherosclerotic plaques, this prednisolone-induced macrophage phenotype might explain the proinflammatory changes observed after LN-PLP treatment in mice and men. Hence, these findings highlight the importance of taking the atherosclerotic micro-environment into account upon modulating inflammation.

Fuelled by our experience with liposomal prednisolone, we next propose a screening approach for drug candidates intended to target plaque macrophages in **chapter 11**. Drug effects on multiple key pathways of macrophage activity are assessed, comprising cytokine release, oxidative stress, lipid handling, ER stress and proliferation of macrophages. Seven compounds recognized for their beneficial impact on at least one of these pathways are selected to evaluate their overall performance. First, we confirm that a reduced cytokine release induced by prednisolone is counterbalanced by multiple adverse effects on lipid handling pathways, which is in line with the previous two chapters. In addition, we show that other candidates, comprising pterostilbene (anti-oxidant), T0901317 (liver X receptor agonist) and simvastatin, have an overall anti-atherogenic effect. In recognition of just *in vitro* data, *in vivo* validation is warranted to determine the value of our screening assays as a translational tool in atherosclerotic disease. Thus far, earlier *in vivo* experiments with nanodelivery of prednisolone (chapter 9 and 10; negative control) and simvastatin[13] (positive control) are in agreement. Ultimately, such approaches might provide a framework for high-throughput screening to facilitate drug development.

In aggregate, the studies in part III of this thesis illustrate the challenges and opportunities of anti-inflammatory drugs in atherosclerosis, in which nanotechnology might facilitate the pursuit for selective and targeted approaches.

As a summary to this thesis, this central illustration aims to capture the highlights.

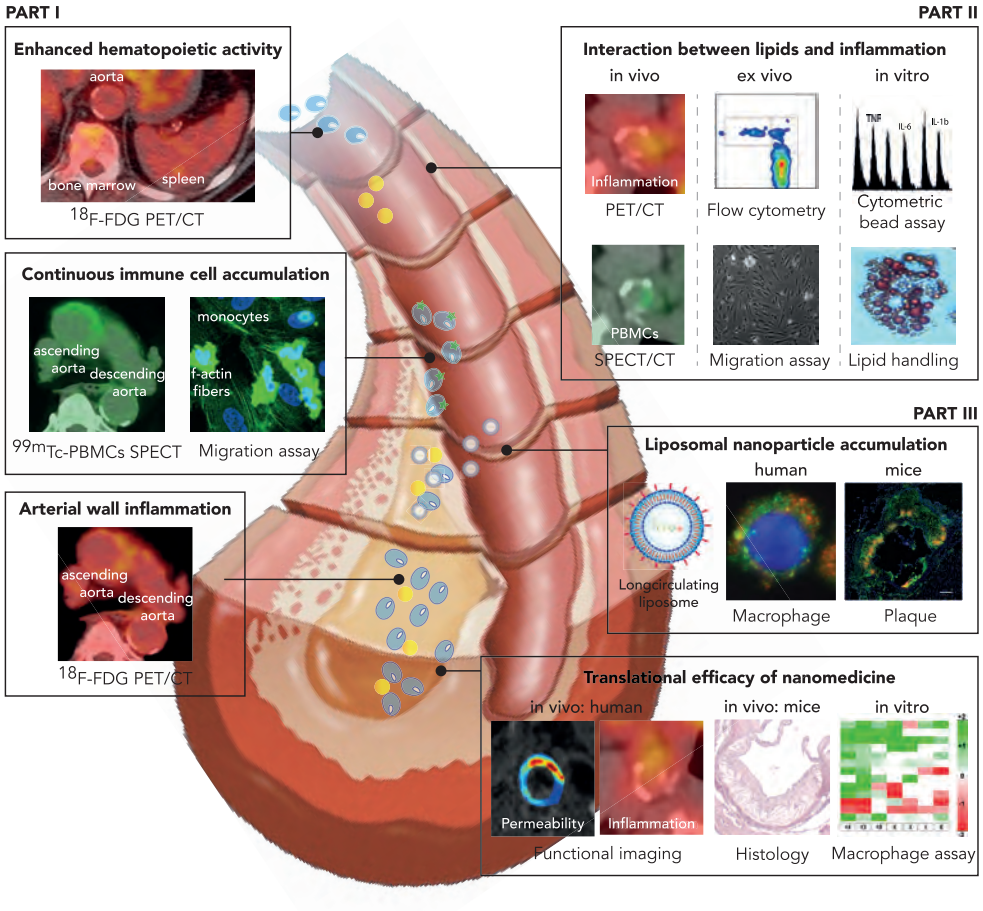

FUTURE PERSPECTIVES

From local anatomy to systemic inflammatory networks

This thesis illustrates that atherosclerosis imaging has advanced beyond its traditional anatomical metrics to a versatile tool that permits quantification of metabolic pathways or cellular behavior involved in atherogenesis. Several advances of this thesis include that both in early as advanced stages, independent of structural changes, arterial inflammatory measures are correlating to established atherogenic lipids, and amendable upon vascular interventions. These findings emphasize that imaging modalities have the capacity to shift focus from late-stage plaque burden to multiple-phase plaque biology. Moreover, when looking beyond the local changes in the arterial wall, we have demonstrated the involvement of circulating PBMCs, bone marrow and spleen in atherosclerosis. These findings further evidence that

atherosclerosis is a multi-compartment disease, and stress the need for whole body imaging to objective systemic inflammatory networks *in vivo*. Whereas this thesis mainly concerned observational studies, prospective approaches integrating whole body imaging with cellular assays of peripheral and stem cells are warranted to address (i) the nature of tracer uptake in various target cells and tissues, and (ii) the incremental value of inflammatory metrics in future risk stratification. With respect to the latter, the ongoing prospective BioImage[14] and PESA[15] studies are awaited to address the additional prognostic value of ^{18}F-FDG PET inflammation imaging in cardiovascular risk prediction. Future imaging studies are also challenged to dissect more specific inflammation-associated targets in multiple compartments involved in atherosclerosis. Alternative PET tracers have the opportunity to improve the specificity of ^{18}F-FDG, and facilitate cardiac and neurovascular imaging with decreased myocardial and cerebral uptake, respectively. In view of the key role of myeloid cells described in this thesis, selective ligands such as (i) the translocator protein (TSPO) with a higher affinity for myeloid cells and (ii) the folate receptor-β (FR-β) predominantly present on activated macrophages, are considered promising. Next to an improved understanding of plaque biology, such advances might aid in the identification of those at high risk for major cardiovascular events.

From count, to function and phenotype

Whereas lipids have a central role in atherogenesis, the mechanistic links between lipids and atherosclerosis have not yet been fully crystalized. Current concepts state that the oxidative modification of lipids induce a broad range inflammatory processes, eventually driving atherosclerosis. Indeed, we find that the carry load of oxidized phospholipids is elementary in changing cell behavior, driving monocyte-mediated arterial wall inflammation in humans. As such, this thesis underscores the need for an improved understanding of (i) not just lipid-driven inflammation within the plaque, but also in the plasma compartment, (ii) not just lipid particle numbers, but also their carry load, and (iii) not just inflammatory cell count, but also their functional features such as migratory and proliferative rate. In addition, future studies need to unravel the (epigenetic) mechanism responsible for the adaptive response of immune cells upon exposure to oxidized lipids. Moreover, in view of the prognostic value of OxPL associated to lipoproteins in the plasma[16], therapeutic lowering of the oxidized lipid burden in the plasma might bear potential. Whereas the observational studies per definition have a limited clinical relevance, the findings in chapter 7 have provoked the unique opportunity to assess the plasticity of monocytes in response to specific Lp(a) (and OxPL) lowering using an apo(a) antisense strategy (first data expected in 2016). This antisense-based approach has previously shown to specifically reduce Lp(a) levels, and its associated oxPL load, by ~80% in a phase I study[17,18]. Such strategies will not only facilitate studies on Lp(a)'s pathogenic mechanisms, but also address whether substantial and specific Lp(a) lowering will benefit cardiovascular outcome. Finally, in line with the transition in atherosclerosis imaging from anatomical to functional features, this thesis illustrates that we should look beyond "count" to "function and

phenotype" in the assessment of lipid-driven inflammation in atherosclerosis. Such progress might generate novel biomarkers better reflecting early, functional changes in atherosclerosis.

From systemic exposure to targeting therapies

Whereas expectations are high, it is fair to state that immunomodulation still remains to be proven beneficial in reducing cardiovascular disease risk in patients. To this end, we eagerly await the first data of two randomized clinical trials testing anti-inflammatory drugs on cardiovascular outcome, expected in 2017-2019. A general movement in medicine, is the tendency towards patient-tailored therapy of which targeted drug delivery is a fine example. In a first-in-human anti-atherosclerosis nanotherapy trial we demonstrate that long-circulating nanoparticles accumulate in human plaque macrophages. This phenomenon most likely holds true for other long-circulating platforms, such as micellar or polymeric nanoparticles. In addition, particles with a natural conduit to the plaque, like HDL mimetics, bear potential as drug carriers in atherosclerosis. Future efforts should be aimed at the non-invasive and quantitative assessment of nanoparticle targeting-efficacy (% injected dose) by imaging. Such approaches can also address the heterogeneity in arterial wall permeability, and consequently the ability of nanoparticles to accumulate in atherosclerotic lesions. Existing experience in rheumatoid arthritis has accelerated the translation of liposomal prednisolone (LN-PLP) into atherosclerosis. However, the prednisolone payload was not suited for patients with atherosclerosis. The LN-PLP work illustrates that the favorable effects of an anti-inflammatory compound in a classical inflammatory disease like rheumatoid arthritis cannot be extrapolated to a comparable efficacy in the lipid-rich environment of an atherosclerotic plaque. Hence, future drug candidates need to undergo a multifaceted screening with careful consideration of its effect on the target cells and tissues, as well as its microenvironment. In addition, preclinical validation should preferably be addressed in a model closely resembling the chronic, lipid-driven inflammatory burden in human atherosclerosis. This thesis may provide guidance for future development of anti-atherosclerotic (nano)therapies using imaging-assisted readouts of efficacy in small-scaled studies.

CONCLUSION

This thesis illustrates that inflammation is involved throughout all stages of human atherogenesis, exceeding physiological levels in the vast majority of patients with atherosclerosis, or only risk factors for it. In addition, this multilevel inflammatory burden is directly linked to circulating atherogenic lipids and their contents. Now the most LDL-c lowering seems achieved with statins and PSCK9 inhibition, and even Lp(a) lowering is within reach with the advent of anti-sense based strategies, future efforts should pursuit the therapeutic targeting of inflammatory pathways in atherosclerosis. Finally, in view of the previous stated "*who, what and how*" issues, we envision an important role for inflammatory pathways in atherosclerosis.

REFERENCES

1. Tarkin et al. PET imaging of inflammation in atherosclerosis. Nat Rev Cardiol 2014;11:443–457.
2. Randolph GJ. Proliferating macrophages prevail in atherosclerosis. Nat Med 2013;19:1094–5.
3. Emami H et al. Splenic Metabolic Activity Predicts Risk of Future Cardiovascular Events. JACC Cardiovasc Imaging 2015;8:121–130.
4. Steinberg D. Atherogenesis in perspective: hypercholesterolemia and inflammation as partners in crime. Nat Med 2002;8:1211–1217.
5. Zhou Q and Liao JK. Pleiotropic effects of statins. Circ J 2010;74:818–26.
6. Duivenvoorden R et al. Relationship of serum inflammatory biomarkers with plaque inflammation assessed by FDG PET/CT: the dal-PLAQUE study. JACC Cardiovasc Imaging 2013;6:1087–94.
7. Raal FJ et al. PCSK9 inhibition with evolocumab in heterozygous familial hypercholesterolaemia: a randomised, double-blind, placebo-controlled trial. Lancet 2015;385:331–340.
8. Saeed S et al. Epigenetic programming of monocyte-to-macrophage differentiation and trained innate immunity. Science 2014;345:1251086–1251086.
9. Libby P. The forgotten majority: unfinished business in cardiovascular risk reduction. J Am Coll Cardiol 2005;46:1225–8.
10. Lobatto ME et al. Perspectives and opportunities for nanomedicine in the management of atherosclerosis. Nat Rev Drug Discov 2011;10:835–52.
11. Prabhakar U et al. Challenges and key considerations of the enhanced permeability and retention effect (EPR) for nanomedicine drug delivery in oncology. Cancer Res 2013;
12. Lobatto ME et al. Multimodal Clinical Imaging To Longitudinally Assess a Nanomedical Anti-Inflammatory Treatment in Experimental Atherosclerosis. Mol Pharm 2010;7:2020–2029.
13. Duivenvoorden R et al. A statin-loaded reconstituted high-density lipoprotein nanoparticle inhibits atherosclerotic plaque inflammation. Nat Commun 2014;5:3065.
14. Muntendam P et al. The BioImage Study: novel approaches to risk assessment in the primary prevention of atherosclerotic cardiovascular disease--study design and objectives. Am Heart J 2010;160:49–57.e1.
15. Fernández-Ortiz A et al. The Progression and Early detection of Subclinical Atherosclerosis (PESA) study: rationale and design. Am Heart J 2013;166:990–8.
16. Tsimikas S et al. Oxidized phospholipids, Lp(a) lipoprotein and coronary artery disease. NEJM 2015;353:46-57.
17. Tsimikas S et al. Antisense therapy targeting apolipoprotein(a): a randomised, double-blind, placebo-controlled phase 1 study. Lancet 2015;6736:61252–61.
18. Van der Valk et al. A sense of excitement for a specific Lp(a) lowering strategy. Stroes ESG, van der Valk FM. The Lancet. 2015.

APPENDICES

NEDERLANDSE SAMENVATTING

Achtergrond

Tijdens mijn medicijnen studie was het woordenboek Pinkhof een belangrijke leidraad om de medische taal eigen te maken. Ik moet dan ook glimlachen als ik een aantal jaar later haar verklaring voor de term "aderverkalking" nog eens opzoek. Het is vrij kort; "onjuiste term, zie atherosclerose".

Drijfveren voor atherosclerose-onderzoek

Atherosclerose is een aandoening van de vaatwand, zich manifesterend in hart- en vaatziekten zoals een hartinfarct of beroerte. Hart- en vaatziekten ten gevolgen van atherosclerose vormen de belangrijkste oorzaak van ziekte en sterfte wereldwijd. Ook dichter bij huis, in Nederland, sterven er elke dag 100 mensen aan de gevolgen van atherosclerose. Hoewel het sterftecijfer gestaag blijft dalen, zal het voorkomen (de prevalentie) van atherosclerose blijven stijgen. In 2030 zullen we naar verwachting 840.000 patiënten voor hart- en vaatziekten behandelen in Nederland, onder meer als gevolg van de bevolkingsgroei als door onze langere levensverwachting. Daarom zijn de maatschappelijke en economische lasten van deze aandoening ook enorm; in Nederland is atherosclerose één van de duurste medische aandoeningen, met een kostenpost van 8.3 miljard euro in 2011.

Primaire preventie van atherosclerose richt zich vrijwel uitsluitend op het opsporen en behandelen van traditionele risicofactoren, zoals geslacht, leeftijd, rookgedrag, bloeddruk en vetwaardes in het bloed. Echter, deze risico-inschatting heeft slechts een matig voorspellende waarde; meer dan 75% van de klinische manifestaties van atherosclerose treedt op bij individuen die met de huidige benadering worden geclassificeerd als hebbende een laag of intermediair risico. Ook in de secundaire preventie (dus bij patiënten die reeds de ziekte hebben) blijkt deze strategie niet afdoende, aangezien meer dan 1 op de 5 patiënten na een doorgemaakt hartinfarct of beroerte binnen 30 maanden opnieuw klachten zal krijgen.

Kortom, wij moeten beter begrijpen *wie* er risico loopt, *wat* dit risico bepaalt en *hoe* we dit risico kunnen verminderen.

De evolutie van atherosclerose en de rol van ontsteking

Onderzoek naar de ontstaanswijze van atherosclerose reikt al ver terug. In 1913 ontdekt Anitschkow dat konijnen door middel van een hoog vet dieet atherosclerose ontwikkelen. Zijn experimenten luiden een eeuw in waarin de atherogene rol van vetrijke eiwitten (lipoproteïnen) verder wordt belicht. Epidemiologisch onderzoek toont dat mensen met een hoog low-density lipoproteïne cholesterol (LDL-c; het "slechte" cholesterol) meer risico hebben op hart- en vaatziekten. Daarnaast bevestigen interventie studies het gunstige effect

van vetverlaging (LDL-c) door middel van statines.

Dat ontsteking een rol speelt in atherosclerose wordt al vroeg onderkent; in de 19e eeuw beschrijft Virchow de atherosclerotische plaque als een actief ontstekingsproduct. Echter, onderzoek naar de rol van ontsteking in atherosclerose neemt pas echt een vlucht vanaf 1999, na het verschijnen van het baanbrekende artikel van Russel Ross getiteld "Atherosclerosis is an inflammatory disease".

Het huidige concept van atherogenese stelt dat verscheidende irriterende factoren, zoals hoge waardes van lipoproteïnen (zoals LDL-c en Lp(a)), de binnenkant van de vaatwand (de endotheelcel laag) kunnen beschadigen. Als gevolg van deze endotheelschade, kunnen vetten die in de bloedbaan circuleren zich ophopen in de vaatwand. Aldaar nemen deze vetten een geoxideerde vorm aan (zoals oxLDL of OxPL). Als een natuurlijke reactie op dit proces gaan ook ontstekingscellen (zoals monocyten) de vaatwand in; eenmaal in de wand transformeren deze cellen tot macrofagen. In lijn met haar letterlijke vertaling, namelijk *veelvraat*, proberen deze macrofagen de geoxideerde producten op te ruimen. Echter, macrofagen kunnen het vet niet kwijt en vormen schadelijke schuimcellen (foam cells). Wat in wezen dus begint als een herstelpoging leidt uiteindelijk tot een vetrijke ontsteking; kenmerkend voor de vroege atherosclerotische laesie, de zogenaamde *fatty streak*. Gedurende vele jaren ontwikkelt deze fatty streak zich uiteindelijk tot een kwetsbare atherosclerotische plaque, voornamelijk gedreven door ontstekingsreacties.

DOEL VAN DIT PROEFSCHRIFT

De afgelopen 15 jaar is er ontzettend veel gepubliceerd over de rol van ontsteking in atherosclerose. Echter, het merendeel van deze studies behelst cel- en dieren-onderzoek, zoals geïllustreerd in Figuur 1 in **Hoofdstuk 1**. Dit proefschrift beoogt om juist in mensen de relevantie van ontsteking in atherosclerose te bestuderen aan de hand van de volgende thema's:

1. De mate van (vaatwand)ontsteking in mensen, in het spectrum van gezond tot ziek;
2. Het stimulerende effect van atherogene lipoproteïnen (LDL en Lp(a)) op deze ontstekingslast; en
3. De therapeutische waarde van ontstekingsremmers in patiënten met atherosclerose.

Terugkomend op de eerder gestelde *wie-wat-hoe* kwesties, stelt dit proefschrift een belangrijke rol voor vetgedreven ontsteking in atherosclerose.

INHOUD

Hoofdstuk 1 onderstreept de klinische en maatschappelijke relevantie van atherosclerose onderzoek, en beschrijft de behoefte aan klinische vertaalslag van de rol van ontsteking in atherosclerose. In de drie delen behandelt dit proefschrift: de systemische verhoogde ontstekingsactiviteit in patiënten met atherosclerose, het stimulerende effect van atherogene lipoproteïnen op ontsteking, en tot slot, ontstekingsremmers als therapie voor patiënten met atherosclerose.

Deel I - Systemisch verhoogde ontsteking in atherosclerose in beeld

Het eerste deel van dit proefschrift beschrijft de verhoogde ontstekingsgraad in patiënten met atherosclerose, onder andere geobjectiveerd door beeldvormende technieken (imaging). Een veelgebruikte methode is positronemissietomografie gecombineerd met computertomografie (PET/CT); een nucleaire techniek die gebruik maakt van radioactieve tracers, zoals fluor-18-deoxyglucose (^{18}F-FDG). Deze tracer heeft dezelfde biologische eigenschappen als glucose (suiker), maar kan niet worden afgebroken en stapelt zich in de cel; genaamd "metabolic trapping". Hierdoor kan de glucosestofwisseling van een cel, wat dient als maat voor de metabole activiteit, worden gekwantificeerd. Verschillende celtypes staan bekend om hun hoge metabole behoefte, zoals snel delende cellen (proliferatie) maar ook ontstekingscellen.

De grote hoeveelheid ontstekingscellen, met name macrofagen, in plaques maakte ^{18}F-FDG PET/CT imaging ook interessant voor atherosclerose. Sinds haar eerste toepassing in 2002, hebben verschillende histologische, gen expressie en biomarker studies ^{18}F-FDG opname gevalideerd als een marker voor (macrofaag gedreven) vaatwandontsteking. In **hoofdstuk 2** vragen we ons af welke mate ^{18}F-FDG opname (uitgedrukt als de *target-to-bloodpool ratio*, TBR) als pathologisch (als teveel) kan worden beschouwd. Hiertoe hebben we in drie verschillende groepen mensen de ^{18}F-FDG opname in de wand van de hoofdslagader (de aorta) en de halsslagaderen (de carotiden) gemeten. Door ^{18}F-FDG opname in de vaatwand van gezonde mensen als fysiologisch te beschouwen, worden afkapwaarden voor vaatwand ^{18}F-FDG opname bepaald. Dit hoofdstuk toont dat de overgrote meerderheid van patiënten met (risicofactoren voor) hart- en vaatziekten deze afkapwaarden overschrijden. Met andere woorden, de meeste patiënten hebben, ondanks de huidige medicijnen en behandelingen, teveel ontsteking in hun vaatwand. Deze bevinding benadrukt de ruimte voor aanvullende strategieën om vaatwandontsteking in patiënten met atherosclerose te verminderen. Dit hoofdstuk schetst ook het perspectief van ^{18}F-FDG PET/CT om in toekomstige studies geschikte kandidaten voor nieuwe therapieën te selecteren, als ook op een reproduceerbare wijze haar effect te meten in relatief kleinschalige studies.

Naast de lokale ontsteking in de vaatwand, beschrijven we in **hoofdstuk 3** de continue toestroom van circulerende ontstekingscellen naar atherosclerotische plaques in patiënten. Om dit te onderzoeken worden ontstekingscellen (perifere mononucleaire bloedcellen, PBMCs, waaronder monocyten) geïsoleerd uit het bloed, gelabeld met een radiolabel (^{99m}technetium, ^{99m}Tc) en teruggegeven aan de deelnemer. Eenmaal terug in het bloed volgen we deze gelabelde ontstekingscellen middels single photon emission computertomografie gecombineerd met computertomografie (SPECT/CT). Als een soort tussenstop, verzekeren we eerst dat de isolatie en labeling procedures het gedrag van deze ontstekingscellen niet significant beïnvloeden. Vervolgens wordt beeldvorming verricht in 10 patiënten met gevorderde atherosclerotische plaques - aangetoond door magnetische resonantie beeldvorming (MRI, kernspinresonantie) en ^{18}F-FDG PET/CT - als ook 5 gezonde individuen. In dit hoofdstuk objectiveren we de snelle influx van ontstekingscellen in atherosclerotische plaques van patiënten, uitgedrukt als de *arterial wall-to-bloodpool ratio*, ABR. Ook opvallend is dat de stapeling van ontstekingscellen (een functioneel verschil) niet in verband staat met de dikte van de vaatwand op de MRI (een anatomisch verschil), maar wel met vaatwandontsteking (r=0.88) gemeten met PET (ook een functioneel verschil). Dit onderschrijft het verschil tussen plaque grootte en plaque functie, als ook de ruimte voor verfijning van conventionele beeldvorming door functionele applicaties, uiteindelijk bedoelt om de risico inschatting van de patiënt de verbeteren. Naast vaatwand karakteristieken correleert de ontstekingscel stapeling in de vaatwand ook met plasma LDL-c (r=0.77) in patiënten; een verband wat verder wordt belicht in het tweede deel van dit proefschrift. Waar de rol van ontstekingscellen in de initiatie van atherosclerose buiten kijf staat, laat deze studie voor het eerst in mensen zien dat ontstekingscellen ook in een vergevorderd stadium van atherosclerose continu migreren naar ontstoken plaques.

In **hoofdstuk 4** beschrijven we vervolgens dat ook de productie organen van ontstekingscellen, namelijk beenmerg en milt, zijn aangedaan in atherosclerose. Eerder is aangetoond dat de activiteit van deze hematopoïetische organen tijdelijk toeneemt in de (semi-) acute fase van een hartinfarct. Echter hier brengen wij in beeld, middels ^{18}F-FDG PET/CT, dat de hematopoïetische activiteit in beenmerg en milt waarschijnlijk chronisch is verhoogd in patiënten met atherosclerose (n=26) in vergelijking met controles (n=25). Om dit verschil verder op celniveau te bestuderen, hebben we een cohort van 953 kankerpatiënten bestudeerd, van wie hematopoïetische stam en voorloper (progenitor) cellen (afgekort HSPCs) waren geïsoleerd in het kader van een autologe stamceltransplantatie. In dit cohort identificeren we 18 patiënten met hart- en vaatziekten, als ook 30 controles. In retrospect vinden we dat de HSPCs van patiënten met atherosclerose meer celkolonies kunnen vormen (de CFU-GM capaciteit). Dit zou kunnen impliceren dat de verhoogde ^{18}F-FDG opname in hematopoïetische weefsels een reflectie is van verhoogde proliferatie van HSPCs. Als alternatieve verklaring, wanneer we terugbladeren naar hoofdstuk 3 en de SPECT plaatjes bekijken, zien we een verhoogd PBMCs signaal in het beenmerg van patiënten in vergelijking

met controles. Dit suggereert dat eventueel een groter aantal ontstekingscellen het verhoogde ^{18}F-FDG signaal in het beenmerg verklaart.

Als besluit beschrijft dit hoofdstuk een *in vitro* experiment waarbij de HSPCs van gezonde donoren worden blootgesteld aan geoxideerd LDL (oxLDL). In lijn met de associatie tussen hematopoïetische ^{18}F-FDG opname, LDL-c (r=0.72) en monocyten (r=0.18) *in vivo*, vinden we in dit *in vitro* experiment een toename van de CFU-GM capaciteit na stimulatie met oxLDL, gepaard gaande met een neiging tot myeloïde cel differentiatie (monocyten/macrofagen). Deze data ondersteunen het concept dat voornamelijk geoxideerde vetten ontsteking veroorzaken in atherosclerose.

Om het eerste deel van dit proefschrift te parafraseren, brengen we in patiënten met atherosclerose een verhoogde ontstekingsactiviteit in beeld van beenmerg tot vaatwand. De correlatie tussen ontstekingsparameters en vetwaardes in het bloed in deel I van dit proefschrift, is een interactie die in het volgende deel verder wordt besproken.

Deel II - De interactie tussen vetten en ontsteking in atherosclerose

Het tweede deel van dit proefschrift schetst de verwevenheid van vetten en ontsteking in atherosclerose. De eerste twee hoofdstukken richten zich op de relatie tussen ontsteking en LDL-c; het *slechte* cholesterol, het laatste hoofdstuk op de interactie met lipoproteine (a) (spreek uit als *l-p-kleine-a*).

Hoofdstuk 5 is een multicenter, interventie studie in patiënten met familiaire hypercholesterolemie (FH), genetisch belast met verhoogde LDL-c waarden. In patiënten met FH (n=24) wordt een verhoogde vaatwandontsteking waargenomen, die correleert met LDL-c (r=0.52), in vergelijking met een controle groep (n=14). Vervolgens ondergaat de helft van de FH-patiënten behandeling(en) met lipoproteïne-aferese (een soort dialyse voor teveel vet); resulterend in een LDL-c verlaging van gemiddeld 51±23%. Een belangrijke bevinding is dat tegelijkertijd de vaatwandontsteking afneemt met 11.8±14.2%, gemeten met ^{18}F-FDG PET/CT. Dus, elke 10% LDL-c daling via aferese, veroorzaakt ook een daling van ongeveer 2% in vaatwandontsteking. In tegenstelling tot het concept dat statines ontstekingsremmende effecten hebben, pleiten deze bevindingen voor een direct effect van LDL-c verlaging op vaatwandontsteking. Opvallend is dat de reductie in vaatwandontsteking niet hand in hand gaat met een verlaging in C-reactive protein (CRP, een ontstekingsmarker in het bloed), wat impliceert dat de systemische CRP waarde misschien geen goede reflectie is van de lokale veranderingen in de vaatwand. Wanneer we deze bevinding extrapoleren naar een nieuw middel om LDL-c te verlagen, namelijk proprotein convertase subtilisin/kexin type 9 (PCSK9) inhibitie, dan wordt het gebrek aan CRP verlaging door PCSK9 inhibitie klinisch misschien minder relevant. Tot slot, dit hoofdstuk illustreert dat vaatwandontsteking gevoelig is voor verbetering, gezien de snelle afname in slechts 5 dagen na behandeling.

In aanvulling op de (macrofaag-gedreven) vaatwandontsteking, karakteriseert **hoofdstuk 6** het fenotype van de monocyten (de voorlopers van macrofagen) in FH patiënten. In deze observationele studie worden monocyten geïsoleerd uit het bloed van 11 gezonde controles en 38 FH patiënten. Van deze patiënten gebruiken 16 geen medicijnen, worden 11 behandeld met statines en 12 met PCSK9 inhibitie. Door middel van flowcytometrie en transendotheliale migratie proeven tonen we aan dat de ontstekings- en migratie- capaciteit van monocyten in FH patiënten groter is dan die van controles. Dit laat zien dat niet alleen in de vaatwand, maar al in het plasma vetten en ontstekingscellen met elkaar interacteren. Daarnaast laten we zien dat een daling in LDL-c leidt tot een verbetering van dit monocyte fenotype, onafhankelijk van het type medicijn. Dit is een interessante bevinding, aangezien het opnieuw suggereert dat vetverlaging op zichzelf ontstekingsremmend is, en dus niet enkel een pleiotroop effect van statines. Ook voor de klinische toepassing van PSCK9 inhibitie is deze bevinding relevant, aangezien hun gebrek aan CRP verlaging nu geschermd kan worden met de inductie van minder monocyte activatie.

Hoewel LDL een van de bekendste cholesterol deeltjes is, benadrukken we in **hoofdstuk 7** het belang van hernieuwde aandacht voor lipoproteïne (a) [Lp (a)]; een vetdeeltje bestaande uit apolipoproteïne (a) [apo (a)] gebonden aan apolipoproteïne B-100 (apoB). Lp(a) is sterk genetisch bepaald, verhoogd in 20% van de bevolking en beschreven als een causale risicofactor voor atherosclerose, echter haar pathogene mechanismen zijn nog niet verhelderd. In dit hoofdstuk laten we zien dat mensen met een hoog Lp(a) (n=30) meer ontsteking, als ook meer rekrutering van ontstekingscellen naar de vaatwand hebben, in vergelijking met diegene met een normaal Lp(a) (n=30). Een belangrijke bevinding is dat deze ontstekingsparameters niet in verband staan met de vaatwand dikte gemeten met MRI. Dit suggereert dat in Lp(a) de functie van atherosclerotische laesies (vaak in verband staand tot de kwetsbaarheid) een betere reflectie is van het risico op hart- en vaatziekten dan de grootte van de laesie. Aanvullend celwerk laat zien dat monocyten geïsoleerd van mensen met een hoog Lp(a) in een geactiveerde staat zijn; deze cellen produceren meer ontsteking en kunnen sneller transmigreren over endotheel (de binnenste cellaag van de vaatwand). Deze bevindingen kunnen worden nagebootst in vervolgexperimenten, aangezien monocyten van gezonde donoren ook geactiveerd worden door Lp(a) en haar lading van OxPL. Tot nu toe hebben we het mechanisme van monocyte activatie door OxPL nog niet ontrafeld. Een belangrijke veronderstelling is dat deze OxPL behoren tot de categorie van "danger-associated-molecular patterns", welke kunnen fungeren als gevaarsignalen voor ontstekingscellen. Eerder is beschreven dat dit soort signalen (afgegeven door pathogenen of geoxideerde vetten) monocyten langdurig kunnen activeren door middel van epigenetische veranderingen. Dit in achtnemend, zou een soortgelijk fenomeen kunnen plaatsvinden in patiënten met een hoog Lp(a), en hoog OxPL.

Om de belangrijkste bevindingen van het tweede deel samen te vatten beschrijven we dat atherogene vetten en hun geassocieerde geoxideerde producten direct ontsteking induceren, zowel op het niveau van de vaatwand als in het plasma compartment. Gezien de verhoogde ontstekingsgraad in patiënten ondanks de huidige richtlijnen, besteed het laatste deel van dit proefschrift aandacht aan ontsteking als therapeutische target in atherosclerose.

Deel III - Atherosclerotische ontsteking als therapeutische target

Ondanks het enorme succes van statine therapie, krijgt nog steeds (zelfs in de gecontroleerde setting van een medicijnonderzoek) twee derde van de patiënten een hartinfarct of beroerte. Het laatste deel van dit proefschrift bespreekt ontsteking als 'therapeutische target' in atherosclerose, waarvoor de indicatie herhaaldelijk naar voren is gekomen in de eerste twee delen.

Hoofdstuk 8 is een review waarin ontstekingsremmende middelen ter behandeling van atherosclerose de revue passeren. Aangezien het nut van ontstekingsremmers in atherosclerose nog aangetoond dient te worden, kijken we uit naar de eerste resultaten van twee grootschalige gerandomiseerde cardiovasculaire uitkomst studies, naar verwachting in 2017-2019. Ook benadrukken we in dit review het risico op bijwerkingen van systemische en langdurige blootstelling aan ontstekingsremmers, zoals opportunistische infecties. Om dit te omzeilen is een specifieke en gerichte behandeling geïndiceerd, bij uitstek in het geval van een chronische en systemische ziekte als atherosclerose.

Nanotechnologie biedt mogelijkheden om lokale, gecontroleerde medicijnafgifte na te streven. In **hoofdstuk 9** beschrijven wij onze inspanningen voor de eerste nanomedicatie in patiënten met atherosclerose; met als hypothese dat lokale afgifte van de ontstekingsremmer prednisolon in plaques gunstig zou zijn. Allereerst toont farmacokinetisch onderzoek in 13 vrijwilligers dat de liposomale nanodeeltjes geladen met prednisolon (afgekort LN-PLP) lang circuleren in het bloed. Dit is een voorwaarde voor targeting van atherosclerotische plaques; lang circulerende deeltjes stapelen zich op plekken in de vaatwand met verhoogde doorlaatbaarheid (permeabiliteit), kenmerkend voor atherosclerotische plaques. Deze lokale stapeling kan inderdaad worden bevestigd in 7 patiënten die twee keer worden behandeld met deze nanomedicatie, toegediend via een infuus. In gemiddeld genomen 75% van de macrofagen (geïsoleerd uit de plaques van deze patiënten) meten we de aanwezigheid van liposomen. Echter, liposomaal prednisolon blijkt niet geschikt voor patiënten met atherosclerose. Na twee infusies met liposomaal prednisolon, neemt de vaatwandontsteking in 20 patiënten toe met gemiddeld 7% in slechts 12 dagen, terwijl patiënten behandeld met placebo geen veranderingen laten zien. Op dat moment worden we geconfronteerd met een negatieve uitkomst-studie in patiënten die in schril contrast staat met een eerdere positieve studie in konijnen met acuut-geïnduceerde atherosclerose.

Daarom trachten we in **hoofdstuk 10** te begrijpen waarom prednisolon vaatwandontsteking heeft doen toenemen in patiënten. Hiertoe bestuderen we eerst het effect van LN-PLP in een ander diermodel met meer chronisch-geïnduceerde atherosclerose; muizen zonder de LDL receptor (de LDL receptor knockout, $LDLr^{-/-}$) behandeld met een hoog vet dieet, waardoor vet- en macrofaag-rijke atherosclerotische laesies ontstaan. In dit muis model vinden we na 2 weken behandeling met LN-PLP meer ontstekingscellen in de atherosclerotische laesies. Sterker nog, na 6 weken behandeling met liposomaal prednisolon zijn de laesies verergerd; ze bevatten namelijk meer necrose en meer macrofagen. Dit laatste is ook interessante aangezien we eerder in patiënten hadden waargenomen dat de vaatwand ^{18}F-FDG opname, een marker van macrofagen, was toegenomen. Aanvullende *in vitro* experimenten laten zien dat macrofagen door prednisolon een "beter" vermogen tot opruimen (fagocyteren) krijgen. Echter, dit type macrofaag kan ook meer vet opnemen, wat ze paradoxaal genoeg juist weer ziek maakt. Er ontstaan meer schuimcellen, meer (ER) stress en meer celdood (necrose); een proces wat ook wel lipotoxisch wordt genoemd. Al met al benadrukken deze bevindingen het belang van de micro-omgeving van het ontstekingsproces wat wordt getarget door een medicijn, welke in atherosclerose erg vetrijk is.

Ingegeven door onze ervaringen met liposomaal prednisolon, bespreken we vervolgens in **hoofdstuk 11** een screeningsmethode voor medicijnen in atherosclerose om in een vroeger stadium het verwachte effect in te schatten. Het medicijn-effect wordt getoetst op een aantal belangrijke macrofaag processen; namelijk cytokine productie, oxidatieve stress, lipiden verwerking, cell stress, en proliferatie. Zeven medicijnen worden geselecteerd op basis van een beschreven positief effect op ten minste één van deze processen. In lijn met de voorgaande hoofdstukken komt prednisolon slecht uit de test (wel minder cytokine productie, maar slechte vetverwerking), terwijl pterostilbeen, T0901317 en simvastatine een goede algehele prestatie leveren *in vitro*. Twee eerdere *in vivo* studies met de nanodelivery van prednisolon (dit proefschrift, negatieve controle) en simvastatine (positieve controle) sterken onze bevindingen. Dit hoofdstuk biedt daarmee een raamwerk voor de high-throughput screening van medicijnen, bedoelt om de klinische translatie van nieuwe cardiovasculaire behandelingsstrategieën te optimaliseren.

Samenvattend zijn de studies in het derde deel van dit proefschrift illustratief voor de uitdagingen en mogelijkheden van ontstekingsremmende middelen in atherosclerose, waarin nanotechnologische benaderingen eventueel ons streven naar selectieve en gerichte behandelingen kunnen faciliteren.

De centrale illustratie in **hoofdstuk 12** tracht de belangrijkste bevindingen van dit proefschrift in één beeld te vangen.

CONCLUSIE

Dit proefschrift illustreert de betrokkenheid van ontstekingsprocessen in zowel de initiatie als progressie van de ziekte atherosclerose. Opvallend is dat de meerderheid van patiënten met (risico factoren voor) atherosclerose last heeft van teveel vaatwandontsteking. Daarnaast verbindt dit proefschrift twee scholen in atherosclerose-onderzoek door het directe effect van vetten op ontsteking in atherosclerose te onderstrepen. Waar het *punctum maximum* lijkt te zijn bereikt voor LDL-c verlagende strategieën met statines en PCSK9 inhibitie, en nieuwe middelen voor Lp(a) verlaging dichter bij zijn dan ooit, is het nu de tijd om onze aandacht te richten op het klinische toepasbaarheid maken van ontstekingsremmende middelen in atherosclerose. Tot slot, met het oog op de eerder gestelde "wie, wat en hoe" kwesties, lijkt er een belangrijke rol weggelegd voor vetgedreven ontsteking in atherosclerose.

AUTHORS AND AFFILIATIONS

Siroon Bekkering
Department of Experimental Internal Medicine, Radboud University Medical Center, Nijmegen, The Netherlands.

Roelof J. Bennink
Department of Nuclear Medicine, Academic Medical Center, Amsterdam, the Netherlands.

Jan van den Bossche
Experimental Vascular Biology, Department of Medical Biochemistry, Academic Medical Center, Amsterdam, The Netherlands.

Jaap D. van Buul
Department of Molecular Cell Biology, Sanquin Research and Landsteiner Laboratory, Academic Medical Center, Amsterdam, the Netherlands.

Acarilia Eduardo da Silva
Department of Biomaterials Science and Technology, University of Twente, Enschede, The Netherlands.

Claudia Calcagno
Translational and Molecular Imaging Institute, Icahn School of Medicine at Mount Sinai, New York, USA.

Geesje M. Dallinga-Thie
Department of Experimental Vascular Medicine, Academic Medical Center, Amsterdam, The Netherlands.

Hamed Emami
Cardiac MR PET CT Program and Division of Cardiology, Massachusetts General Hospital and Harvard Medical School, Boston, USA.

Zahi A. Fayad
Translational and Molecular Imaging Institute, Icahn School of Medicine at Mount Sinai, New York, USA.

Amparo Figueroa
Cardiac MR PET CT Program and Division of Cardiology, Massachusetts General Hospital and Harvard Medical School, Boston, USA.

Anouk A.J. Hamers
Department of Experimental Vascular Medicine, Academic Medical Center, Amsterdam, The Netherlands.

Linda C. Hemphill
Cardiac MR PET CT Program and Division of Cardiology, Massachusetts General Hospital and Harvard Medical School, Boston, USA.

Martin A. Hoeksema
Experimental Vascular Biology, Department of Medical Biochemistry, Academic Medical Center, Amsterdam, The Netherlands.

G. Kees Hovingh
Department of Vascular Medicine, Academic Medical Center, Amsterdam, the Netherlands.

Leo A.B. Joosten
Department of Experimental Internal Medicine, Radboud University Medical Center, Nijmegen, The Netherlands.

Yannick Kaiser
Department of Vascular Medicine, Academic Medical Center, Amsterdam, the Netherlands.

John J.P. Kastelein
Department of Vascular Medicine, Academic Medical Center, Amsterdam, the Netherlands.

Marion G. Koopman
Department of Nephrology, Academic Medical Center, Amsterdam, the Netherlands.

Marlys L. Koschinksy
Department of Chemistry, Biochemistry and Pharmacology, University of Windsor, Ontario, Canada.

Jeffrey Kroon
Department of Molecular Cell Biology, Sanquin Research and Landsteiner Laboratory, Academic Medical Center, Amsterdam, the Netherlands.

Carlijn Kuijk
Department of Hematopoiesis, Sanquin Research and Landsteiner Laboratory, Academic Medical Center, Amsterdam, The Netherlands.

Matthias Laudes
Department of Internal Medicine I, University of Schleswig Holstein, Kiel, Germany.

Dink A. Legemate
Department of Vascular Surgery, Academic Medical Center, Amsterdam, The Netherlands.

Mark Lobatto
Translational and Molecular Imaging Institute, Icahn School of Medicine at Mount Sinai, New York, USA.

Esther Lutgens
Experimental Vascular Biology, Department of Medical Biochemistry, Academic Medical Center, Amsterdam, The Netherlands.

Megan H. MacNabb
Cardiac MR PET CT Program and Division of Cardiology, Massachusetts General Hospital and Harvard Medical School, Boston, USA.

Henk A. Marquering
Department of Biomedical Engineering and Physics, Academic Medical Center, Amsterdam, the Netherlands.

Svenja Meiler
Experimental Vascular Biology, Department of Medical Biochemistry, Academic Medical Center, Amsterdam, The Netherlands.

Josbert M. Metselaar
Department of Targeted Therapeutics, University of Twente, Enschede, The Netherlands.

Willem J.M. Mulder
Translational and Molecular Imaging Institute, Icahn School of Medicine at Mount Sinai, New York, USA.

Matthias Nahrendorf
Center for Systems Biology, Massachusetts General Hospital and Harvard Medical School, Boston, USA.

Aart J. Nederveen
Department of Radiology, Academic Medical Center, Amsterdam, the Netherlands.

Annet E. Neele
Experimental Vascular Biology, Department of Medical Biochemistry, Academic Medical Center, Amsterdam, The Netherlands.

Mihai G. Netea
Department of Experimental Internal Medicine, Radboud University Medical Center, Nijmegen, The Netherlands.

Max Nieuwdorp
Department of Vascular Medicine, Academic Medical Center, Amsterdam, the Netherlands.

Maarten J. Otten
Translational and Molecular Imaging Institute, Icahn School of Medicine at Mount Sinai, New York, USA.

Maarten P.M. Paridaans
Translational and Molecular Imaging Institute, Icahn School of Medicine at Mount Sinai, New York, USA.

Wouter V. Potters
Department of Radiology, Academic Medical Center, Amsterdam, the Netherlands.

Linda C. Quarles van Ufford
Medicinal Chemistry & Chemical Biology, Department of Pharmaceutical Sciences, Utrecht University, The Netherlands.

Sarayu Ramachandran
Translational and Molecular Imaging Institute, Icahn School of Medicine at Mount Sinai, New York, USA.

Amir Ravandi
Division of Cardiovascular Medicine, University California, San Diego, La Jolla, California, USA.

Niels P. Riksen
Department of Experimental Internal Medicine, Radboud University Medical Center, Nijmegen, The Netherlands.

James H.F. Rudd
Division of Cardiovascular Medicine, University of Cambridge, Cambridge, United Kingdom.

Dominik M. Schulte
Department of Internal Medicine I, University of Schleswig Holstein, Kiel, Germany.

Jan G. Schnitzler
Experimental Vascular Biology, Department of Medical Biochemistry, Academic Medical Center, Amsterdam, The Netherlands.

Corey Scipione
Department of Chemistry, Biochemistry and Pharmacology, University of Windsor, Ontario, Canada.

Tom Seijkens
Experimental Vascular Biology, Department of Medical Biochemistry, Academic Medical Center, Amsterdam, The Netherlands.

Barbara Sjouke
Department of Vascular Medicine, Academic Medical Center, Amsterdam, the Netherlands.

Gert Storm
Institute for Pharmaceutical Sciences, University of Utrecht, Utrecht, The Netherlands.

Aart C. Strang
Department of Vascular Medicine, Academic Medical Center, Amsterdam, the Netherlands.

Erik S.G. Stroes
Department of Vascular Medicine, Academic Medical Center, Amsterdam, the Netherlands.

Jun Tang
Translational and Molecular Imaging Institute, Icahn School of Medicine at Mount Sinai, New York, USA.

Ahmed Tawakol
Cardiac MR PET CT Program and Division of Cardiology, Massachusetts General Hospital and Harvard Medical School, Boston, USA.

Rogier M. Thurlings
Department of Internal Medicine, Academic Medical Center, Amsterdam, the Netherlands.

Sam Tsimikas
Division of Cardiovascular Medicine, University California, San Diego, La Jolla, California, USA.

Hein J. Verberne
Department of Nuclear Medicine, Academic Medical Center, Amsterdam, the Netherlands.

Miranda Versloot
Department of Experimental Vascular Medicine, Academic Medical Center, Amsterdam, The Netherlands.

Simone L. Verweij
Department of Vascular Medicine, Academic Medical Center, Amsterdam, the Netherlands.

Mani Venkatesh
Translational and Molecular Imaging Institute, Icahn School of Medicine at Mount Sinai, New York, USA.

Carlijn Voermans
Department of Hematopoiesis, Sanquin Research and Landsteiner Laboratory, Academic Medical Center, Amsterdam, The Netherlands.

Diederik F. van Wijk
Department of Vascular Medicine, Academic Medical Center, Amsterdam, the Netherlands.

Martine C.M. Willems
Department of Vascular Surgery, Academic Medical Center, Amsterdam, The Netherlands.

Menno de Winther
Experimental Vascular Biology, Department of Medical Biochemistry, Academic Medical Center, Amsterdam, The Netherlands.

Joseph L. Witztum
Division of Endocrinology and Metabolism, University California, San Diego, La Jolla, California, USA.

Sacha Zeerleder
Department of Hematology, Academic Medical Center, Amsterdam, The Netherlands.

Kang H. Zheng
Department of Vascular Medicine, Academic Medical Center, Amsterdam, the Netherlands.

Koos A.H. Zwinderman
Department of Clinical Epidemiology, Academic Medical Center, Amsterdam, the Netherlands.

PORTFOLIO

Naam PhD student: F.M. van der Valk

PhD period: November 2011 – October 2016

Name PhD supervisor: Prof. dr. E.S.G. Stroes

	Year	ECTs
1. PhD training		
General Courses		
Good clinical practice (GCP)	2011	0.10
Good Clinical Practice (BROK)	2012	0.90
Practical Biostatistics	2012	1.10
Specific Courses		
Advanced Immunology	2015	2.80
Seminars, Workshops and Master classes		
Weekly journal club, dept of Vascular Medicine, AMC.	2011-2015	4.00
Weekly clinical education, dept of Vascular Medicine, AMC.	2011-2015	4.00
Two-weekly scientific meeting, dept of Radiology, AMC.	2011-2015	4.00
Cardiovascular Masterclass in Amsterdam, The Netherlands.	2012	0.20
Oral presentations (first author only)		
Liposomal prednisolone aggravates atherosclerosis by macrophage lipotoxicity, American Heart Association, Orlando, USA.	2015	0.50
Hematopoietic activity is increased in patients with atherosclerosis, Annual Cardio Vascular Conference, Amersfoort, The Netherlands.	2015	0.50
Oxidized phospholipids on Lp(a) induce inflammation in patients, Rembrandt symposium, Noordwijkerhout, The Netherlands.	2014	0.50
Lp(a) induces epigenetic reprogramming in innate immune cells, Russell Ross Lectureship, American Heart Association, Chicago, USA.	2014	0.50
In vivo imaging of leukocyte accumulation in atherosclerosis, European Atherosclerosis Society, Madrid, Spain.	2014	0.50
In vivo imaging of leukocyte accumulation in atherosclerosis, Annual Cardio Vascular Conference, Ermelo, The Netherlands.	2014	0.50
Lipoprotein(a) elicits inflammation in atherosclerosis, Annual Cardio Vascular Conference, Ermelo, The Netherlands.	2014	0.50
Nanoparticles loaded with prednisolone in patients with in atherosclerosis, American Heart Association, Dallas, USA.	2013	0.50

Local delivery of liposomal prednisolone in atherosclerosis, Annual Cardio Vascular Conference, Noordwijkerhout, The Netherlands.	2013	0.50
Poster presentations (first author only)		
Sketching a new horizon for Lp(a), Internistendagen, Maastricht, The Netherlands	2016	0.50
Stem cells in atherosclerosis, International Atherosclerosis Society, Amsterdam, The Netherlands.	2015	0.50
References ranges for arterial inflammation using FDG PET/CT imaging, International Atherosclerosis Society, Amsterdam, The Netherlands.	2015	0.50
Lp(a) in atherosclerosis, Keystone on Innate Immunity, Whistler, Canada.	2014	0.50
Imaging leukocytes in atherosclerosis, American Heart Association, Dallas, USA.	2013	0.50
Thyroid hormone mimetics in metabolic syndrome, EASD, Barcelona, Spain.	2013	0.50
Conferences		
ISA, Sydney, Australia, and Amsterdam, The Netherlands.	2012, 2015	0.50
Rembrandt symposium, Noordwijkerhout, The Netherlands.	2014	0.25
European Atherosclerosis Society, Madrid, Spain.	2014	0.25
Keystone on Innate Immunity, Whistler, Canada.	2014	1.00
American Heart Association, Dallas and Chicago, USA.	2013, 2014	0.50
EASD, Barcelona, Spain.	2013	0.25
Annual Amstelsymposium, Amsterdam, The Netherlands.	2013	0.25
Annual Cardio Vascular Conference, The Netherlands.	2013-2015	0.75

2. Teaching

Lecturing

Nanomedicine in atherosclerosis, Cardiovascular Masterclass, Amsterdam, The Netherlands.	2012	0.50

Supervising

Yannick Kaiser, internship and bachelor thesis, University of Amsterdam.	2014/15	1.00
Quinten Dusoswa, master thesis, University of Amsterdam.	2015	1.00
Kayleigh Dukker, scientific internship, University Twente.	2015	1.00
Bram Bakhuizen, scientific internship, University Twente.	2014	1.00
Daphne Huizing, scientific internship, University of Twente.	2014	1.00
Kilian Kappert, scientific internship, University Twente.	2014	1.00
Thijs Vernooij, master thesis, University of Amsterdam.	2014	1.00
Bas Pattynama, scientific internship, University of Leiden.	2013	1.00
Lisa Alma, master thesis, University of Amsterdam.	2013	1.00
Timen ten Harkel, scientific internship, University of Twente.	2013	1.00
Ilse Kant, scientific internship, University of Twente.	2013	1.00
Margot van Remmerden, master thesis, University of Amsterdam.	2013	1.00

Wouter Nijhof, master thesis, University of Twente.	2013	1.00
Clif Wierink, master thesis, University of Amsterdam.	2013	1.00
Huguette Brink, master thesis, University of Maastricht.	2012	1.00
Bram Schermers, scientific internship, University of Twente.	2012	1.00
Anne Cappon, bachelor thesis, University of Amsterdam.	2012	1.00
Sandra Lammertse, bachelor thesis, University of Amsterdam.	2012	1.00

Other

Initiator WIT (wetenschap-inspiratie-talent) festival, Amsterdam.	2014,2015
Initiator and chair of PhDs Vascular Medicine.	2013,2014
Quality Management Imaging Core Lab, AMC.	2014

3. Parameters of esteem

Grants, awards and prizes

Award for best abstract and oral plenary presentation, Rembrandt symposium, Noordwijkerhout, The Netherlands.	2014
Nomination ATVB early career award, American Heart Association, Dallas, USA.	2014
CVC award best oral presentation, National Cardiovascular Conference, Ermelo, The Netherlands.	2014
CVC award best oral presentation, National Cardiovascular Conference, Noordwijkerhout, The Netherlands.	2013

PUBLICATIONS

1. Arterial wall inflammation in peripheral artery disease is augmented in type 2 diabetes. Bernelot Moens SJ, Verweij SL, van der Valk FM, Koelemay MJW, Verberne HJ, Nieuwdorp M, Stroes ESG. *Submitted.*
2. Increased arterial wall and cellular inflammation in patient with early stages of chronic kidney disease. Bernelot Moens SJ, Verweij SL, van der Valk FM, van Capelleveen JC, Kroon J, Versloot M, Verberne HJ, Duivenvoorden R, Vogt L, Stroes ESG. *Submitted.*
3. Anti-inflammatory effects of lipid lowering in patients with familial hypercholesterolemia: beyond statins and C-reactive protein. Bernelot Moens SJ*, Neele AE* Kroon J, van der Valk FM, van den Bossche J, Hoeksema MA, Schnitzler JG, Baccara-Dinet MT, Manvelian G, de Winther MPJ, Stroes ESG. *Submitted.*
4. Oxidized phospholipids on lipoprotein(a) elicit arterial wall inflammation and an atherogenic monocyte respons in humans. Van der Valk FM, Bekkering S, Kroon J, van den Bossche J, van Buul JD, Nederveen AJ, Verberne HJ, Scipione C, Nieuwdorp M, Joosten LAB, Netea MG, Koschinksy ML, Witztum JL, Tsimikas S, Riksen N, Stroes ESG. *Accepted in Circulation, 2016.*
5. Enhanced hematopoietic activity in patients with atherosclerosis. Van der Valk FM, Kuijk C, Verweij SL, Kaiser Y, Zeerleder S, Nahrendorf M, Voermans S, Stroes ESG. *Accepted in European Heart Journal, 2016.*
6. Thresholds for arterial wall inflammation quantified by (18)fluorodeoxyglucose positron emission tomographic imaging: implications for vascular intervention studies. Van der Valk FM, Verweij SL, Strang AC, Kaiser Y, Nederveen AJ, Stroes ESG, Verberne HJ, Rudd JHF. *Accepted in JACC Cardiovasc Imaging, 2016.*
7. Infused recombinant human apolipoprotein A-I HDL mimetic CER-001 preferentially targets atherosclerotic plaques in patients: the LOCATION study. Zheng KH, van der Valk FM, Smits LP, Sandberg M, Dasseux JL, Baron R, Barbaras R, Keyserling C, Coolen BF, Nederveen AJ, Verberne HJ, Nell T, Vugts D, Duivenvoorden R, Mulder WJM, van Dongen GAMS, Stroes ESG. *Accepted in Atherosclerosis, 2016.*
8. Unexpected arterial wall and cellular inflammation in patients with rheumatoid arthritis in remission using biological therapy: a cross-sectional study. Bernelot Moens SJ, van der Valk FM, Strang AC, Kroon J, Smits LP, Kneepens EL, Verberne HJ, van Buul JD, Nurmohamed MT, Stroes ESG. *Accepted in arthritis research & therapy, 2016.*
9. Multiple pathway screening to predict anti-atherogenic efficacy of drugs targeting macrophages in atherosclerotic plaques. Alaarg A*, He Zheng K*, van der Valk FM, Eduardo da Silva A, Versloot M, Quarles van Ufford LC, Schulte DM, Storm G, Metselaar JM, Stroes ESG, Hamers AAJ. *Accepted in Vascular Pharmacology, 2016.*

10. Increased arterial wall inflammation in patients with ankylosing spondylitis is reduced by statin therapy. Van der Valk FM, Bernelot Moens SJ, Strang AC, van Leuven S, Baeten D, Stroes ESG. Annals of the Rheumatic Diseases, 2016;Epub ahead of print.
11. Current therapies for lowering lipoprotein(a). Van Capelleveen JC, van der Valk FM, Stroes ESG. J Lipid Res. 2015;Epub ahead of print.
12. Systemic glucocorticoids are associated with mortality following carotid endarterectomy. Siemelink M, den Ruijter H, van der Valk FM, de Vries JP, de Borst GJ, Moll F, Stroes ESG, Pasterkamp G. J Cardiovasc Pharmacol. 2015;66:392-8.
13. Liposomal prednisolone aggravates atherosclerosis by promoting macrophage lipotoxicity. Van der Valk FM*, Schulte DM*, Meiler S, Tang J, He Zheng K, van den Bossche J, Seijkens T, Laudes M, de Winther M, Lutgens E, Metselaar JM, Dallinga-Thie GM, Mulder WJM, Stroes ESG, Hamers AAJ. Nanomedicine, 201*6*; Epub ahead of print.
14. Novel directions for targeting inflammation in atherosclerosis. Verweij SL, van der Valk FM, Stroes ESG. Curr Opin Lipidol. 2015;26:580-5.
15. A sense of excitement for a specific Lp(a) lowering strategy. Stroes ESG, van der Valk FM. The Lancet. 2015;10:1427-9.
16. Increased systemic and plaque inflammation in ABCA1 mutation carriers with attenuation by statins. Bochem AE, van der Valk FM, Tolani S, Stroes ESG, Westerterp M, Tall AR. Arterioscler Thromb Vasc Biol 2015;35:1663-9.
17. Pharmaceutical development and preclinical evaluation of a GMP-grade anti-inflammatory nanotherapy. Lobatto ME, Calcagno C, Otten MJ, Millon A, Ramachandran S, Paridaans MP, van der Valk FM, Storm GJ, Stroes ES, Fayad ZA, Mulder WJ, Metselaar JM. Nanomedicine. 2015;11:1133-40.
18. Prednisolone-containing liposomes accumulate in human atherosclerotic macrophages upon intravenous administration. Van der Valk FM, van Wijk DF, Lobatto M, Verberne HJ, Storm G, Willems MCM, Legemate DA, Nederveen AJ, Calcagno C, Venkatesh M, Ramachandran S, Paridaans MPM, Otten MJ, Dallinga GM, Fayad ZA, Nieuwdorp M, Schulte DM, Metselaar JM, Mulder WJM, Stroes ESG. Nanomedicine. 2015;11:1039-46.
19. Effect of open-label infusion of an apoA-I-containing particle (CER-001) on RCT and artery wall thickness in patients with FHA. Kootte RS, Smits LP, van der Valk FM, Dasseux JL, Keyserling CH, Barbaras R, Paolini JF, Santos RD, van Dijk TH, Dallinga-van Thie GM, Nederveen AJ, Mulder WJ, Hovingh GK, Kastelein JJ, Groen AK, Stroes ES. J Lipid Res. 2015;56:703-12.
20. In vivo imaging of hypoxia in atherosclerotic plaques in humans. Van der Valk FM, Sluimer JC, Vöö S, Verberne HJ, Nederveen AJ, Windhorst A, Stroes SG, Lambin P, Daemen MAP. JACC Cardiovasc Imaging. 2015;15:S1936-878.

21. In vivo imaging of enhanced leukocyte accumulation in atherosclerotic lesions in humans. Van der Valk FM, Kroon J, Potters WV, Thurlings RM, Bennink RJ, Verberne HJ, Nederveen AJ, Nieuwdorp M, Mulder WJ, Fayad ZA, van Buul JD, Stroes ES. J Am Coll Cardiol. 2014;64:1019-29.
22. Nonpharmacological lipoprotein apheresis reduces arterial inflammation in familial hypercholesterolemia. Van Wijk DF, Sjouke B, Figueroa A, Emami H, van der Valk FM, MacNabb MH, Hemphill LC, Schulte DM, Koopman MG, Lobatto ME, Verberne HJ, Fayad ZA, Kastelein JJ, Mulder WJ, Hovingh GK, Tawakol A, Stroes ES. J Am Coll Cardiol. 2014;64:1418-26.
23. The effect of a diiodothyronine mimetic on insulin sensitivity in male cardiometabolic patients: a double-blind randomized controlled trial. van der Valk F, Hassing C, Visser M, Thakkar P, Mohanan A, Pathak K, Dutt C, Chauthaiwale V, Ackermans M, Nederveen A, Serlie M, Nieuwdorp M, Stroes E. PLoS One.2014;9:e86890.
24. Atherosclerosis: dyslipidemia, inflammation and lipoapoptosis. FM van der Valk, DM Schulte, WJM Mulder, ESG Stroes. Advances in Dyslipidemia (Bookchapter in Future Medicine Ltd) 2013; 6-17.
25. Serendipity of post-hoc surrogate marker research. van der Valk FM, van Wijk DF, Stroes ES. Eur Heart J. 2012;33:2897-8
26. Novel anti-inflammatory strategies in atherosclerosis. Van der Valk FM, van Wijk DF, Stroes ES. Curr Opin Lipidol. 2012;23:532-9.

ABOUT THE AUTHOR

Fleurtje Marieke van der Valk werd op 16 december 1985 geboren in Dinxperlo. Opgroeien in dit grensdorp maakte dat Fleur zich al op jonge leeftijd realiseerde dat de wereld letterlijk aan haar voeten ligt en dat er grenzen te verleggen zijn. In 2004 behaalde zij haar gymnasiumdiploma aan het Isala college in Silvolde. In datzelfde jaar startte zij, in de voetsporen van haar vader en zussen (je vraagt je af wat deed de broer, die bleef helaas uitgeloot), met de opleiding Geneeskunde aan de Rijksuniversiteit Groningen. Aansluitend aan haar bachelor diploma in 2008 liep Fleur de coschappen van de masterfase in het UMC Groningen en Medisch Centrum Leeuwarden. In deze periode ontpopte zij zich als een intelligente, gedreven maar bovenal betrokken en echt menselijke dokter. In haar afstudeerstage en -onderzoek richtte Fleur haar pijlen al op de Interne Geneeskunde. Na haar afstuderen in 2011 werd Fleur aangesteld als arts-onderzoeker op de afdeling Vasculaire Geneeskunde van het Academisch Medisch Centrum in Amsterdam. Hier werkte zij onder de leiding van prof. dr. Erik Stroes, prof. dr. Max Nieuwdorp en dr. ir. Aart Nederveen en heeft zij onder andere onderzoek gedaan naar de rol van inflammatie in atherosclerose, wat heeft geresulteerd in dit proefschrift. Naast het feit dat Fleur een grote affiniteit met wetenschap bleek te hebben was er ook de wens om onderzoek meer toegankelijk te maken en mensen te inspireren om jong wetenschappelijk talent te steunen. Vanuit deze gedachte heeft zij daarom in 2015 het WIT festival georganiseerd, wat met veel enthousiasme is ontvangen en een jaarlijks evenement is geworden. Aansluitend op haar onderzoek is zij eind 2015 gestart met de opleiding Interne Geneeskunde in het Onze Lieve Vrouwe Gasthuis te Amsterdam onder supervisor van haar opleider dr. Yves Smets. Fleur woont samen met Hendrik in Amsterdam.

Namens de paranimfen

DANKWOORD

Het meest spannende hoofdstuk van dit boek! Ik beloof u, vol lof, clichés, maar niets is minder waar. Ook hetgene waar je misschien wel het meest op afgerekend kan worden (sta ik erin?!), toewerkend na de grote liefde als climax (hij heet hendrik); lees en huiver.

Allereerst veel dank aan allen die hebben deelgenomen aan de vaak intensieve onderzoeken. Met het ziekenhuis nog in sluimerstand, waren zij al op het lab of in de scan. Ik heb en zal altijd genieten van de bijzondere openheid die je in wit wordt toevertrouwd.

Professor dr. E.S.G. Stroes, promotor. Lieve Erik, initiator, inspirator, katalysator, groot van vertrouwen, niet van slag door een puberende promovenda, trots. Professor dr. M. Nieuwdorp, promotor. Lieve Max, your first! Dokkersbroek (…), extreem slim, vooral soepel, kritisch, echte borrelaar, zorg voor de groep. Dr. Ir. A.J. Nederveen, co-promotor. Lieve Aart, bijzonder, integer, altijd tijd, komt tot de kern, kunnen we wapenveld weer thuis laten bezorgen?, verzoek van mijn vader. Als een soort Earth, Wind & Fire (maar dan fire-wind-earth) boden jullie mij the mighty elements of wetenschap. Ik hoop dat ik nog lang met jullie mag samen werken.

Beste prof. dr. J. Booij, prof. dr. H.R. Büller, prof. dr. M.M. Levi, prof. dr. M.G. Netea, prof. dr. T. van der Poll en dr. J.H.F. Rudd, u wil ik bedanken voor het kritisch doornemen van dit proefschrift.

Lief F4, een begrip. Hoe kan groen linoleum toch zoveel warmte uitstralen? En nog zoveel meer mensen om mij heen; de mensen op het lab, de PET en MRI, het trialbureau (niet het trouw-bureau, blijft verwarrend), de vele studenten in het hartoor.

Lief OLVG. Wat een jaar. Beste opleiders en supervisoren, dank voor de fijne start. Lieve collega's, ik ga onze mini-ochtend overdracht (meer richting patiënt-cabaret) missen.

In het bijzonder Kristien, lieve paranimf, je bent een verademing. Lieve Rosie, wervelwind, als ik een zusje had gehad, dan was jij het. Lieve Lotte, zo bijzonder dat kleine Hazel er is, ik ben trots op je (ook op jou Nanne!). Fijn om te weten dat internistendagen altijd gezellig zullen zijn. Lieve Veer, lieve paranimf, de woongroep blijft een goed concept, wat vindt Juul? Misschien moeten we het evolueren tot gezamenlijke vakantie inclusief Joe Cocker (god, bless).

Mijn lieve familie, onze Franse tak (ciao ciao, bisou bisou), de Amelanders en ook schoonfamilie. Vooral lieve papa en mama, opgroeien met "me number two, you number one", "het liefste meisje van spanje" en "antifragile!", wat een luxe om met zoveel (on)zin te mogen opgroeien. Ik realiseer met steeds meer hoe bijzonder dat is. Lieve grote broer Willem, Fem, mijn petekind Julie en Boris, lieve Judith, jij schrijft de liefste kaartjes, Paul, Hanna en Pijke, lieve tomeloze Mirth en Gijs, capetown slowdown!

Lieve Hendrik (spreek uit als: Hendríque), met jou leef ik in superlatieven, niemand kan mij zo hard aan het lachen maken.

Veel liefs!

Fleur

omslag ontwerp:
KK
koopmaninvorm.nl